NORTHWESTERN UNIVERSITY

The Effect of Nanoconfinement on the Glass Transition Temperature (Tg) and Mobility Associated with Diffusion in Polymer Films: A Fluorescence Study

A DISSERTATION

SUBMITTED TO THE GRADUATE SCHOOL
IN PARTIAL FULFILLMENT OF THE REQUIREMENTS

for the degree
DOCTOR OF PHILOSOPHY
Field of Materials Science and Engineering

By
Manish Kumar Mundra

EVANSTON, ILLINOIS
December 2007

ABSTRACT

The Effect of Nanoconfinement on the Glass Transition Temperature (Tg) and Mobility Associated with Diffusion in Polymer Films: A Fluorescence Study

Manish Kumar Mundra

In this dissertation, the *Tg* behavior of nanoconfined polymer films and 1-dimensional (1-D) patterned polymer nanostructures was studied. Using a novel fluorescence method, a reduction in *Tg* was observed upon confinement in PS films supported on silica, where free-surface (polymer-air interface) effects are dominant in modifying *Tg*. In contrast, *Tg* was observed to increase upon nanoconfinement in poly(methyl methacrylate) (PMMA) films supported on silica, where moderate attractive polymer-substrate interactions are present. By placing dye-labeled polymer films in a multilayer geometry with unlabeled polymer films, unique information was obtained on the effect of interfaces in modifying *Tg* upon confinement and the distribution of *Tg*s across the multilayer film thickness. In particular, with nanoscale confinement of PMMA films it was shown how the free-surface effect competes with and is overwhelmed by the substrate effect. In a first ever measurement, it was demonstrated that this competition leads to a free-surface layer *Tg* exceeding the bulk polymer *Tg*. This research also led to the first study of *Tg*-nanoconfinement effects in 1-D polymer nanostructures. As with films, interfacial interactions dictate the ultimate *Tg* behavior of nanostructures.

This research has contributed in other ways to understanding the effects of nanoscale confinement on polymer properties. Using small variations in the repeat unit structure and backbone rigidity or addition of low molecular weight diluents, it was demonstrated that the magnitude of the *Tg*-nanoconfinement effect is strongly tunable in

polymers and can result in deviations from bulk *Tg* of about 45-50 K. Furthermore, this tunability can be understood qualitatively based on fundamental polymer physics related to cooperative segmental mobility.

In this dissertation a new method was also developed based on simple fluorescence to determine the effect of confinement on the diffusion coefficients of small dye molecules and found that diffusion coefficients can differ by as much as an order of magnitude in 125-nm-thick films as compared with bulk films. Finally, a novel technique that uses intrinsic fluorescence to characterize the effect of confinement on *Tg* in thin and ultrathin films of styrene containing copolymers as well as the effect of stress relaxation on local chain conformations was also developed.

ACKNOWLEDGEMENTS

First I would like to thank my thesis advisor John M. Torkelson. I could not have imagined having a better advisor and mentor for my PhD, and without his unwavering guidance and support this work would not be possible.

I would like to thank my father and mother, Surendra and Kalpana, for their love, support, encouragement and constant motivation. I express my sincere thanks to my sisters Sangita and Ankita, my brother-in-law Praveen Bajaj and his family and to my loving friends and their families. I thank them for their support and understanding at the mostly happy, but sometimes heavy moments during these years. I dedicate this work to my parents, my family and friends who taught me in so many different ways, from where I have drawn my strength during these years of the doctoral project.

I would like to thank my current group members: Jungki, Perla, Rodney, Connie, Katsuyuki, Cynthia, Soyoung, Sheldon, Amanda, Laura, Jun'ichi, Michelle, Robert, and Chris Wong. I thank you for your friendship and help during these wonderful years of my life.

I would also like to thank my past group members: Ying, Chris Ellison, Maisha, Brian, and Ross. I learned so many wonderful things from you. Your successful work encouraged me to follow your footsteps.

I would like to thank my colleagues with whom I have worked closely on many projects that constitute part of this current thesis research: Chris, Ross, Rodney, Suresh, Perla, Nina, and Soyoung.

Finally, I thank to Saswati Pujari. You have filled my life with cheerful happiness. I thank your for your encouragement and love.

TABLE OF CONTENTS

LIST OF TABLES

LIST OF FIGURES

CHAPTER 1

INTRODUCTION

The emerging field of nanotechnology is largely predicated by the ability to construct mechanical, electrical, and optical devices with nanometer dimensions. Working with materials at nanometer length scales can be challenging because many material properties deviate from their bulk-like behavior when the materials are confined to extremely small structures and geometries. Therefore, research focused on understanding the properties of materials on the nanoscale has gained significant impetus during the last decade or so. This interest is wide ranging including studies of the properties of metals, ceramics, and polymers at the nanoscale (Quake 2000).

As in many dimensionally constrained material systems, the physical properties of polymers confined to nanometer length scales can deviate significantly from those measured in the bulk state. For example, properties of thin polymer films such as the glass transition temperature (*Tg*) (Forrest 2001; Kawana 2001), physical aging (Priestley 2005b), modulus (Van Workum 2003), compliance (O'Connell 2006), crystallization behavior (Frank 1996b), relaxation dynamics (Hall 1997b), viscosity (Höhne 2003), and diffusion coefficients (Frank 1996a) are seen to deviate from bulk values.

Nanotechnology has also led to an array of emerging applications that require confined polymer structures on the nanoscale for diverse disciplines ranging from tissue engineering (Griffith 2002), molecular electronics (Huang 2001a), and microfluidic devices (Therriault 2003) to sacrificial templates (Xia 1999) and photonic materials (Lin 1998). The crucial role played by polymer resists for generating sub-100 nm features during the lithographic process in the microelectronics industry is another strong motivating factor for evaluating the properties of polymer on nanometer length scales (Bratton 2006). While the potential benefit of miniaturization is one of the drivers for

fabrication of confined polymer structures, the size-dependent properties observed in several material systems necessitates a thorough evaluation of the physical properties of polymeric structures confined to nanometer length scales.

An understanding of how confinement leads to a deviation from bulk properties is therefore significant from both basic scientific and technological standpoints. From a basic scientific standpoint, the research discussed in this study will both address the question as to why the properties deviate from bulk behavior upon confinement and simultaneously characterize the impact of different parameters that can be altered to control these confinement effects. This interest is also driven by many key technological applications as it is becoming ever more important to employ glass-forming polymeric materials with confined geometries. As a result, the research discussed in this dissertation is significant to fields ranging from now-conventional technologies (diffusion-controlled separation via membranes (Pfromm 1995; McCaig 2000a, 2000b)) to high-value nanotechnologies such as photoresists in microelectronics (Wallraff 1999), nanocomposites materials (Anastasiadis 2000; Ash 2004), disk drive lubricants (Tyndall 1998), and sensors (Agbor 1995, 1997), among others.

The research discussed in this dissertation is focused specifically on understanding the impact of various parameters that can affect the glass transition temperature (*Tg*) in confined thin and ultrathin films and 1-dimensional polymer nanostructures. In particular, this research uses fluorescence techniques to characterize the impact of various factors that can be altered to control or "tune" the effect of confinement on *Tg*. Besides determining how various parameters impact the value of *Tg* in confined systems, the research is also focused on issues such as the variation in the strength and the breadth of *Tg* with confinement, development of a novel intrinsic fluorescence technique for characterizing *Tg* in confined systems, as well as characterizing the relaxation of residual stresses associated with local chain

conformations in thin and ultrathin films of polystyrene and styrene-containing random copolymers. The research is also focused on polymer multilayer studies using fluorescence labels at specific locations to measure the distribution of *Tg*s and characterize the impacts of free surfaces and polymer-substrate interfaces on this distribution. The impact of the fundamental length scale underlying the *Tg* is investigated to determine whether there is any correlation between this fundamental length scale and the effect of confinement on *Tg*. Finally, the research is also focused on developing a novel fluorescence technique that takes advantage of recent group experience in trilayer fluorescence studies to develop a simplified experimental procedure to characterize the effect of confinement on mobility associated with diffusion in thin and ultrathin polymer films.

The first direct evidence regarding confinement-induced deviations in *Tg* was provided in 1991 by Jackson and McKenna (Jackson 1991), who found that the *Tg* values of confined glass forming liquids in nano-pores of Vycor glass were reduced as compared to the bulk values, with a maximum 18 K reduction for o-terphenyl in a 4 nm diameter porous glass. In 1993, Reiter (Reiter 1993) provided the first indication of enhanced mobility related to polymer chain motion in films by his dewetting experiments. Ultrathin films were seen to dewet at temperatures below the bulk *Tg*. In 1994, Keddie *et al.* (Keddie 1994b) used ellipsometry to provide direct evidence of a reduction of *Tg* relative to its bulk value in ultrathin polymer films. Later, Frank *et al.* (Frank 1996) provided the first direct evidence that polymer diffusion in thin polymer films may be impacted by the size of the confinement geometry. Since these influential studies, a number of research studies have followed with focus on understanding the effect of confinement on the deviation in thermophysical properties from bulk behavior. The several hundred research articles that followed the seminal studies answered a number of fundamental questions as well as raised many more new and challenging questions that

are still unanswered. Many reviews have since captured the recent state of this field and provided clarity to many issues (Forrest 2001; Kawana 2001; Alcoutlabi 2005; Roth 2005; Merabia 2004).

Various methods have been employed for measuring *Tg* in thin films. Most methods characterize *Tg* by probing the changes in thermal expansion of a sample (Jones 1999a). Ellipsometry (Keddie 1994b) is the most common technique, where the changes in the measured quantities are related to changes in thickness or refractive index of a sample with temperature. The intersection of the linear temperature dependences in the rubbery and glassy states is identified as the *Tg*. Other techniques that have been used to measure *Tg* in thin films include dielectric relaxation spectroscopy (Fukao 1999), x-ray reflectivity (Fryer 2001), fluorescence spectroscopy (Ellison 2002a, 2002b), nonlinear optics (Hall 1997a), Brillouin light scattering (Forrest 1997), positron annihilation lifetime spectroscopy (Soles 2004a), incoherent neutron scattering (Soles 2004a), atomic force microscopy (Ge 2000), and optical wave-guide spectroscopy (Prucker 1998).

The technique of fluorescence spectroscopy has an advantage over other techniques employed to measure *Tg* in thin films. Using fluorescence, Ellison and Torkelson (Ellison 2003) provided the first direct evidence of the distribution of *Tg*s in a polymer film; they showed that fluorescence can be used to characterize the distribution of *Tg*s by placing labels that are covalently attached to polymer at particular locations in a multilayer film. These experiments are important because one can directly measure the impact of various interfaces on the *Tg* as well as quantify how far these effects can penetrate away from the interface.

In a recent monograph by Breslow and coworkers (Breslow 2003), it has been stressed that the most significant future advancements in this field will come only with the development of new and innovative techniques capable of measuring properties of nanoscale films in confined geometries, which cannot be measured by the use of

conventional techniques. In this context, the work in this dissertation describes the use of fluorescence methods to answer questions that no other currently available experimental method has been able to address. A major outcome from this dissertation is work that stands as the first determination of the effect of nanoconfinement on *Tg* in 1-dimensional patterned polymer nanostructures (Mundra 2007a). Another key outcome from this dissertation involves the use of fluorescence multilayer method to provide the first determination of the distribution of *Tg*s in a polymeric system with attractive interactions with the substrate (Priestley 2007a). This research also describes the development of novel fluorescence techniques that can be used to characterize *Tg* of styrene-containing random copolymers and mobility associated with diffusion in confined geometries.

Prior to discussing details regarding the use of the fluorescence technique for characterizing *Tg* in confined geometries, an overview of the glass transition and related relaxation behavior in polymeric materials is presented in Chapter 2. That chapter describes basic polymer relaxation behavior in the rubbery and glass regimes. It also includes important concepts related to *Tg* and polymer relaxation dynamics such as the alpha relaxation, and the concepts of heterogeneity, cooperativity, cooperatively rearranging regions (CRR's), fragility, and physical aging.

A review of the impact of confinement on polymer properties confined to nanoscale dimension is also presented in Chapter 2. The effect of confinement on *Tg* and related relaxation behavior is discussed in the context of thin and ultrathin films, either substrate supported/grafted or freely standing films. Simulation studies of *Tg* in polymeric systems confined to nanometer length scales are discussed within the same framework. The effect of confinement on mobility related to diffusion and other physical properties is also discussed. Finally, a description of the current, incomplete understanding of the origins of the effect of nanoconfinement is discussed.

Chapter 3 introduces the use of the fluorescence method for characterizing *Tg* in thin and ultrathin polymer films. The general phenomenon of fluorescence is discussed followed by the use of fluorescence for characterizing *Tg* in thin and ultrathin films and the origin of the sensitivity of fluorescence to *Tg*. It is shown that *Tg* may be identified by a change in the temperature dependence of fluorescence between the rubbery and glassy states using a variety of chromophores both as dopants and covalently attached to the polymer chain as a label. It is also shown that *Tg* may be identified by a change in the temperature dependence of intrinsic fluorescence between the rubbery and glassy states that originate from phenyl rings which are a part of the polymer repeat unit structure, as in polystyrene (PS).

As a result of a recent disagreement in the literature regarding the impact of molecular weight (*MW*) on the *Tg*-nanoconfinement effect in supported PS films, this system is studied in the largest range of *MW*s examined to date in a single study of supported PS films and is discussed in Chapter 4. The effects of changes in *MW* as well as slight modification to the repeat unit structure of PS on the length scale of cooperatively rearranging regions (CRRs) at *Tg* are also discussed in detail in this chapter.

Chapter 5 addresses an important scientific and key technological question regarding the impact of interfaces and nanoconfinement on *Tg* of polymeric glass formers. It describes the use of the fluorescence multilayer film method to measure directly the impact of interfaces and nanoconfinement on *Tg*. These types of measurements reveal that interfacial effects can almost entirely explain the average *Tg* deviations observed in ultrathin polymer films. This chapter also shows that substrate effects in poly(methyl methacrylate) (PMMA) begin to perturb *Tg* dynamics at the free surface when the overall film thickness is greater than 200-nm-thick, indicating that substrate effects on polymer dynamics can, in certain instances, be very long range.

Results of this PMMA study are compared with those of a previous PS study to show that interfacial and nanoconfinement effects on *Tg* dynamics are strongly dependent on the repeat unit structure of the polymer.

Chapter 6 introduces the development of a novel method that uses intrinsic fluorescence for characterizing *Tg* in thin and ultrathin films of PS and styrene-methyl methacrylate (S/MMA) random copolymers. The *Tg* may be identified by a change in the temperature dependence of intrinsic fluorescence between the rubbery and glassy states that originate from phenyl rings, which are a part of the polymer repeat unit structure. It is shown that intrinsic fluorescence can be used to characterize *Tg* as a function of copolymer composition, which stands as the first determination of *Tg* in ultrathin films using intrinsic fluorescence. It is also shown that intrinsic fluorescence is a powerful technique not only to characterize *Tg* in thin and ultrathin films of styrene containing random copolymers but also to determine the effect of process conditions and the relative state of relaxation of the residual stresses associated with local chain conformations present in the system (for details, see Chapter 11). Intrinsic fluorescence can also be used as an efficient technique for characterizing the effect of nanoconfinement on *Tg* in systems with very high *Tg* values, which is difficult to do using fluorescence technique described in Chapter 3.

Chapter 7 describes studies of systems of technological importance, systems that otherwise have been overlooked by the research community. Chapter 7 explores in detail the impact of various parameters, which are directly related to the polymer itself, in modifying the *Tg* upon nanoconfinement. In particular, the focus is to study various parameters, such as polymer *MW*, composition of a random copolymer, slight modification to the repeat unit structure, changes in polymer chain stiffness or backbone rigidity, and addition of low *MW* diluents, that can be altered to “tune” the effect of

nanoconfinement on *Tg*. Study of systems other than PS helps to provide new insight into the origin of the *Tg*-nanoconfinement effects and a better understanding of *Tg* itself.

Chapter 8 explores in detail how modification of sample geometry or spatial confinement, which is not directly related to the polymer, can affect the *Tg* upon nanoconfinement. In this chapter, poly(methyl methacrylate) (PMMA) nanostructures which are fabricated using electron beam lithography are studied in detail. The *Tg*s of these one-dimensional (1-D) nanostructures (parallel lines) supported on oxidized silicon substrates are measured by monitoring their temperature-dependent fluorescence intensities, revealing substantial differences between the *Tg*s of the nanostructures and the thin films from which they were fabricated. For example, the *Tg* of 50-nm-wide PMMA nanolines on silica is ~ 15 K lower than that of a PMMA film on silica of the same 18 nm thickness. Attractive PMMA-silica interfacial interactions increase the *Tg*, while free surfaces decrease the *Tg* of PMMA in ultrathin films relative to bulk PMMA. It is shown that the significant differences between the *Tg*s of the 1-D and two-dimensional (2-D) forms of PMMA on silica are the result of a substantial increase in the ratio of free-surface area to interfacial area in the PMMA nanolines relative to ultrathin films.

Chapter 9 explores in detail the strength of *Tg* (related to the difference in the rubbery and glassy state measurables defining *Tg*) as a function of PS *MW* in thin and ultrathin films. It also describes the changes in the strength of *Tg* with slight modification to the PS repeat unit structure in confined geometry.

Chapter 10 introduces a simple, yet extremely powerful method, based on fluorescence multilayer measurements, to quantify changes in diffusion coefficients of small dye molecules a function of confinement, in polymer films near *Tg*. This technique involves a multilayer study, with the bottom layer consisting of a polymer doped with a fluorescent non-radiative energy transfer (NRET) type small molecule, which acts as an

acceptor probe. A neat layer of a polymer is placed on top of this layer. Another layer consisting of a polymer with a NRET-type small molecule donor dye covalently attached to the polymer chain is then placed on top of the neat polymer layer. The steady-state fluorescence intensity of the donor molecule attached to the polymer is then measured as a function of time. As the donor probe is attached to a polymer of substantial *MW*, the diffusion of donor is negligible in comparison to that of a small-molecule acceptor dye doped in a polymer of substantial *MW*. As the acceptor comes within several nanometers of the donor label, NRET will take place from the donor to the acceptor (Hall 1997c, 1998c). Consequently, a drop in donor fluorescence intensity is observed. The time required by the first acceptor molecule to travel the distance equal to the thickness of the middle layer or the neat polymer layer (called the "break-through" time) can be directly related to the diffusion coefficient. Using this technique, the translational diffusion coefficient of decacyclene and Disperse Red 1 (DR1) in PS thin and ultrathin films is characterized. This study reveals that the DR1 diffusion coefficients can undergo a factor of ten reduction in diffusivity with decreasing PS film thickness.

Chapter 11 shows that intrinsic fluorescence of styrene-containing polymer and copolymers can be used to characterize the relative state of stress relaxation associated with local chain conformations resulting from the processing conditions such as spin coating. Intrinsic fluorescence is revealed to be a powerful technique not only to characterize the effect of processing conditions and the relative state of relaxation of the residual stresses present in the system but also to help understand the conditions required to relax stresses that can be characterized via local chain conformations

Chapter 12 provides the first direct quantitative analysis of the impact of small-molecule diluent content in modifying the distribution of relaxation times, fragility and the cooperative length scale dynamics in various systems and the correlation between the size scale of CRRs to the width or distribution in the relaxation spectrum and fragility.

This chapter connects the important concepts related to *Tg* and polymer relaxation dynamics such as the alpha relaxation, the concept of heterogeneity and cooperativity, size scale of CRRs, and fragility.

Lastly, Chapter 13 summarizes the work related to the investigation of the effect of nanoconfinement on *Tg* and mobility related to diffusion in thin and ultrathin films using novel fluorescence techniques. In addition, Chapter 13 also provides recommendations for future work.

CHAPTER 2

BACKGROUND

This chapter provides an overview of the glass transition temperature (*Tg*) and related relaxation behavior in polymeric glass formers. It describes basic polymer relaxation behavior in the rubbery and glass regime. It also includes important concepts related to *Tg* and polymer relaxation dynamics such as alpha relaxation dynamics, dynamic heterogeneity, cooperativity, cooperatively rearranging regions (CRRs), fragility, and physical aging.

This chapter also provides a detailed review of the impact of confinement on properties in polymer confined to nanoscale dimension. The effect of confinement on *Tg* and related relaxation behavior is discussed in the context of both experimental studies of thin and ultrathin films (substrate supported/grafted or freely standing films) and simulation studies of *Tg* in polymeric systems confined to nanometer length scales. Finally, the effect of confinement on mobility associated with diffusion in polymeric glass formers is provided along with description of the current explanation of the effect of nanoconfinement and its origin in polymeric glass formers.

2.1 Glass Transition and Related Relaxation Behavior in Bulk Polymers

2.1.1 Glass Transition Temperature

Upon cooling a glass-forming liquid to lower temperature, eventually the system reaches a temperature at which it is no longer able to maintain its thermodynamic equilibrium state. The temperature at which the experimental time scale associated with a particular temperature becomes equal to the dominant relaxation time scale is defined as *Tg*. The glass transition temperature can also be described simply as the transition from liquid-like rubbery equilibrium state to solid-like glassy non-equilibrium state. The *Tg* is typically identified as the temperature at which a change in the slope of the

temperature dependence of specific volume or enthalpy is observed in going from rubbery to glassy state as shown in Figure 2-1. Typically, a sample that is cooled faster falls out of the equilibrium at a higher temperature, resulting in a *Tg* value higher than that observed for a slower cooling rate (Figure 2-1).

As the *Tg* depends upon the cooling rate, it does not fall into the category of well-defined thermodynamic transitions such as melting temperature, which is a true first order thermodynamic phase transition. Rather, *Tg* is a kinetic transition which is sometimes arbitrarily defined as the temperature at which the viscosity reaches 10^{12} Pa.s in simple liquid, or at which the dominant relaxation time becomes larger than about ~ 100 s (Ediger 1996; Angell 1995b). Typically, the viscosity or the dominant relaxation time increases by 12 orders of magnitude between *Tg* + 100 K and *Tg*, and over this range the evolution of both viscosity and the relaxation time is described by the WLF (Williams-Landel-Ferry) or VTF (Vogel-Tamman-Fulcher) equations (Ferry 1980).

The glass transition of glass-forming materials, including amorphous polymers, has been well characterized but is still poorly understood. At present, no single theory or model exists that can describe all aspects of the glass transition. The free volume model (Cohen 1959), mode-coupling theory (Gotze 1992) and thermodynamic theories (Gibbs 1958) fail to explain the underlying transition phenomena accurately. Adam and Gibbs (Adam 1965) proposed a kinetic theory coupled with the idea of the probabilities of cooperative rearrangements. This theory is frequently used to explain glass transition dynamics. Adam and Gibbs correlated the temperature dependent relaxation times to the probabilities of cooperative rearrangements; they defined rearranging regions as a subsystem of the sample, which can relax cooperatively upon sufficient fluctuations in energy. In other words, the mobility of molecules in low molecular weight glass formers or of segments in a polymer is tied to the mobility of other molecules or chain segments in a cooperative way.

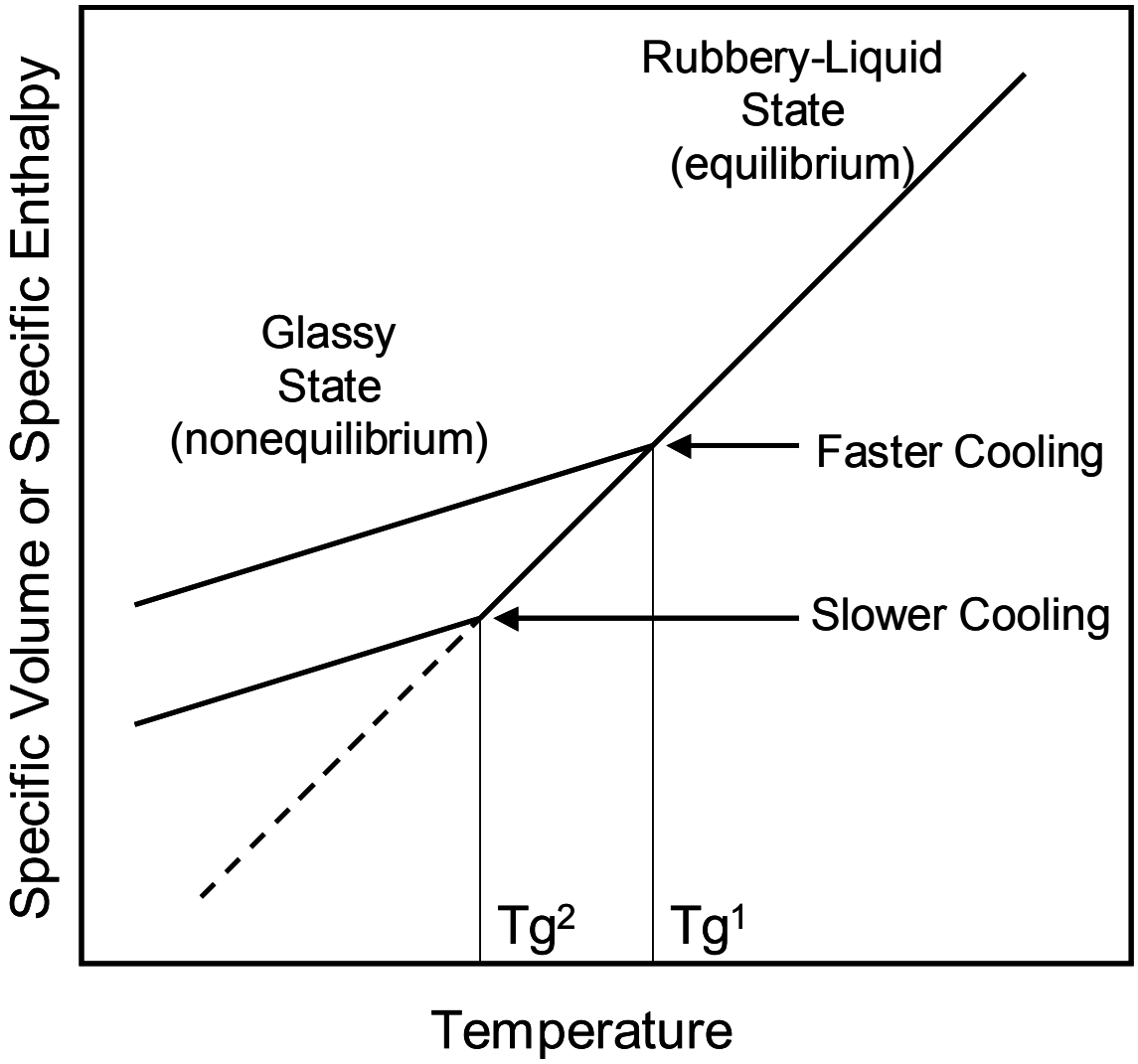

Figure 2-1: The temperature dependence of specific volume or specific enthalpy for a general amorphous polymer. The vertical lines denote Tg^1 determined at a faster cooling rate and Tg^2 determined at a slower cooling rate.

In polymeric systems, a large variety of relaxation processes are observed, which are a result of molecular relaxation processes that occur across a broad range in time and length scales. The molecular relaxation processes include motion of the primary backbone chain, motion of side groups, whole chain motions, motion of end groups, etc., and are highly dependent on the structure of the polymer repeat unit. In this chapter, concepts that will be discussed include the alpha relaxation, fragility, dynamic heterogeneity or cooperativity, size scale of cooperatively rearranging regions, and physical aging.

2.1.2 Alpha Relaxation Dynamics

The alpha relaxation (α-relaxation) is a relaxation process that is associated with cooperative segmental motion of repeat units along the chain backbone. The α-relaxation is the dominant relaxation process observed in polymers, and it is therefore termed as the primary relaxation. Near *Tg*, the α-relaxation processes are believed to be caused by the cooperative segmental motion of ~ 30-300 chain segments (both intrachain and interchain) (Sperling 1992; Schmidt-Rohr 1991; Reinsberg 2001; Hempel 2000; Merabia 2004; Ellison 2005a). In contrast, secondary molecular relaxation processes such as the beta- (β), gamma- (γ) and delta (δ) relaxations are caused by localized relaxations, typically associated with the motion of a side group attached to a single repeat unit or even more localized relaxation associated with rotation of a portion of a side group such as methyl unit (Mark 2004). It is also important to note that low molecular weight glass formers exhibit both primary as well as secondary relaxation processes which occur at the molecular level (Gotze 1992), indicating that these processes constitute the fundamental relaxation processes underlying the molecular physics seen in various glass formers.

Free volume arguments (Cohen 1959) as well as the cooperative segmental dynamic theory proposed by Adam and Gibbs (Adam 1965, Roland 1992) have been used to explain the temperature dependence of the α-relaxation process as a glass former

approaches *Tg* from the rubbery state (Cohen 1959; Kovacs 1958; Roland 1992). The free volume (V_f) results from the inefficient packing of the disordered chain segments in the amorphous regions of the material and is defined as the difference between the actual volume (V) and the theoretical volume (V_0), based on actual chemical structure and van der Waals radii shown pictorially in Figure 2-2. The mobility in a polymeric system is facilitated by the unoccupied free volume that allows the configurational or structural reorientation of un-equilibrated chain segments towards equilibrium state. As the free volume of the system decreases, i.e., with decreasing temperature, the mobility of the chain segments reduces until the relaxation time becomes increasingly long and the system can no longer achieve its thermodynamic equilibrium state.

Doolittle (Doolittle 1957) was the first to observe an empirical relation between the viscosity of low molecular fluids and microscopic free volume of the system. Doolittle found that the logarithmic change in the viscosity is inversely proportional fractional free volume (V_f/V) available to the system and is given by the following relationship:

$$\log\left(\frac{\eta}{\eta_{Tg}}\right) = \log\left(\frac{\tau_T}{\tau_{Tg}}\right) = \frac{B}{2.303}\left(\frac{1}{f} - \frac{1}{f_g}\right) \qquad 2.1$$

where f_g is the fraction free volume at *Tg*, τ_T and τ_{Tg} are relaxation times at temperatures *T* and *Tg*, and *B* is a constant also known as Doolittle's constant. The definition of volume thermal expansion coefficient in the liquid or rubbery state (α_r), we have

$$\alpha_r = \frac{1}{V}\frac{dV}{dT} \qquad 2.2$$

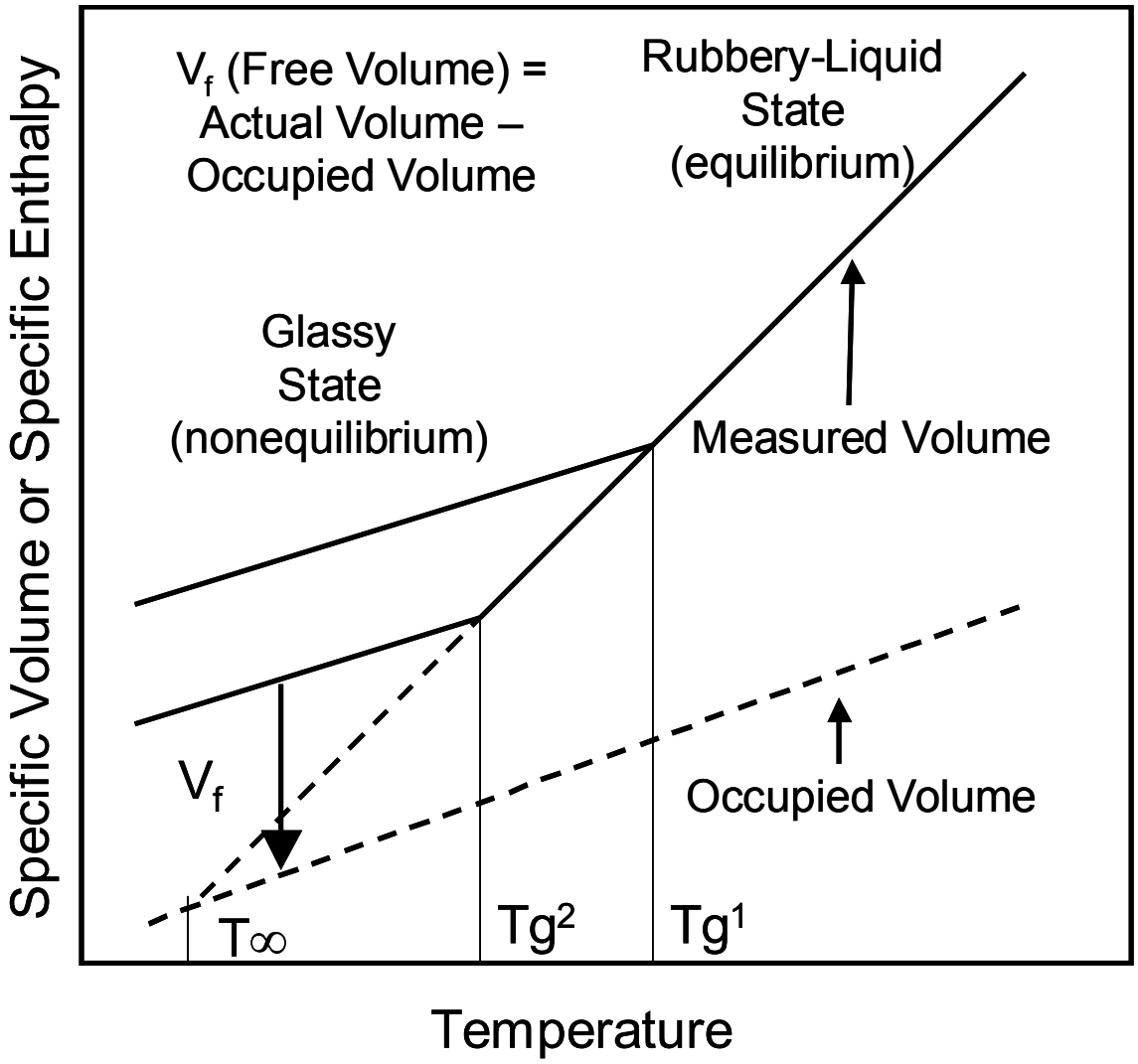

Figure 2-2: The temperature dependence of specific volume or specific enthalpy for a general amorphous polymer. The vertical lines denote Tg^1 determined at a faster cooling rate and Tg^2 determined at a slower cooling rate. Another vertical line denoting $T\infty$, which is underlying thermodynamic glass transition temperature where the free volume vanishes as the sample is cooled infinitely slowly. Free volume, denoted by V_f, is the difference between the actual volume and occupied volume denoted by dashed line.

Substituting equation 2.2 in equation 2.1 yields

$$\log\left(\frac{\tau_T}{\tau_{Tg}}\right) = \frac{-(B/2.303 f_g)(T-T_g)}{f_g/\alpha_r + T + T_g} = \frac{-C_1(T-T_g)}{C_2 + T - T_g} \qquad 2.3$$

Equation 2.3 is known as the Williams-Landel-Ferry or WLF equation (Williams 1955). The WLF equation is able to describe the temperature dependence of α-relaxation dynamics of not only low molecular fluids but also that of polymeric glass formers for $Tg < T < Tg + 100$ K. Here, C_1 and C_2 are constants, and α_r is thermal expansion coefficient in the liquid or rubbery state.

Equation 2.3 is usually used to describe the dramatic change in viscosity or relaxation times as a function of temperature in the rubbery regime, typically in the range of *Tg* to *Tg* + 100 K (Ferry 1980). From equation 2.3, the fractional free volume at *Tg* is equal to $B/2.303\ C_1$. However, since *B* is undefined parameter, usually it is taken as unity in estimates of the fractional free volume of polymer at *Tg* (Ferry 1980). For polymers, the so called "universal" values of the WLF constants are $C_1 = \sim 17.4$ while $C_2 = \sim 51.6$ K (Angell 1997; Williams 1955; Bower 2002; Ferry 1980).

The WLF equation can also be expressed in the form known as the Vogel-Fulcher-Tammann (Vogel 1921; Fulcher 1923) or VFT equation, shown below:

$$\frac{<\tau(T)>}{\tau_0} = \exp\left(\frac{C}{T - T_0}\right) \qquad 2.4$$

where T_o is a standard temperature, and τ_o and *C* are constants. Equation 2.4 is also used to describe the temperature dependence of $<\tau>$ above *Tg* in the rubbery state. This equation approximately fits the behavior of a number of polymers with values of $C = 2.1 \times 10^3$ K and $T_o = Tg - 52$ K (Bower 2002). The parameters in the WLF and VFT

equations are related by $T_o = Tg - C_2$, $C = C_1C_2/\log_{10} e$ and $\tau_o = <\tau(Tg)> \exp(-C_1/\log_{10} e)$ (Bower 2002). One can show that the cooperative segmental dynamic theory proposed by Adam and Gibbs (Adam 1965) based on configurational entropy argument can be reduced to the WLF or VFT type relationship (Donth 1979; Roland 1992,), which is otherwise derived from the free volume argument (Cohen 1959).

In the glassy state, a modified WLF type equation was developed by Vrentas and Duda (Vrentas 1977) taking into account the variation of the thermal expansion coefficient in the glassy state as compared to the thermal expansion coefficient in the rubbery state used in the derivation of WLF equation. However, most commonly, in the glassy state, the temperature dependence of the average alpha relaxation time is best fit by an Arrhenius expression as shown in equation 2.5:

$$\frac{<\tau>}{<\tau_g>} = A\exp\left[\frac{E_A}{kT}\right] \qquad 2.5$$

where A is a pre-exponential factor, k is the Boltzmann constant and E_A is the apparent activation energy. E_A typically falls in the range of 20-60 kcal/mol for a number of polymeric systems and it depend on chain aromaticity and chain rigidity (Hamilton 1996; Solunov 1999).

As the α-relaxation does not conform to a single exponential decay in either the rubbery or glassy regions, it is common to use a stretched exponential expression to fit α-relaxation data. This relaxation function ($\varphi(t)$) is known as the Kohlrausch (Kohlrausch 1847)-Williams-Watts (1970;1971) (KWW) "stretched exponential" function:

$$\varphi(t) = \exp\left[-\left(\frac{t}{\tau}\right)^{\beta_W}\right] \qquad 2.6$$

where τ is the characteristic time constant and β_W is the stretched exponent which (with $0 < \beta_W < 1$) is related to the width of the relaxation spectrum. The value of $\beta_W = 1.0$ corresponds to a single exponential decay; as β_W decrease toward 0, the distribution of relaxation times becomes increasingly broad.

Even though the KWW equation is an empirical equation, the form of the KWW equation has been said to be "a consequence of cooperative motion" (Williams 1970, 1971). The intermolecular chain coupling theory by Roland and Ngai has illustrated how the value of β_W directly reflects the extent of cooperative segmental dynamics of the alpha relaxation process (Roland 1992; Ngai 1993, 1998a, 1998b, 2000).

Liquids of all classes, including even liquid metals, have been extensively studied with respect to the temperature dependence of transport properties such as viscosity and diffusivity and relaxation times. Different techniques have been used to characterize the distribution of relaxation times by fitting various parameters in the relaxation function to data taken by dielectric relaxation spectroscopy (Stickel 1996; McCrum 1991; Dixon 1990), light scattering (Sidebottom 1993; Li 1992), neutron spin-echo measurements (Mezei 1987), probe molecule excitation methods (Wendt 1998), shear mechanical relaxations (Torell 1983; Menon 1994; Plazek 1994), electron spin correlation (Stebbins 1992; Andreozzi 1996, 1999), enthalpy relaxation measurements (Birge 1985; Bauer 1999), nuclear magnetic resonance (NMR) (Spiess 1983) and second harmonic generation (SHG) (Dhinojwala 1994a, 1994b; Hamilton 1996). From the distribution in alpha relaxation times fit to the KWW expression, an average alpha relaxation time ($<\tau>$) may be calculated by the equation:

$$< \tau >= \int \exp\left(-\left(\frac{t}{\tau} \right)^{\beta_W} \right) dt = \left(\frac{\tau}{\beta_W} \right) \Gamma\left(\frac{\tau}{\beta_W} \right) \qquad 2.7$$

where Γ is the gamma function (Williams 1970, 1971).

The stretching exponent (β_W) has a strong temperature dependence in the rubbery or equilibrium state and a much weaker dependence below *Tg* in the glassy state (Hamilton 1996). Upon cooling towards *Tg* from elevated temperatures, the width of the α-relaxation distribution broadens and β_W decreases. For instance, based on SHG measurements for polystyrene (PS), β_W is reduced by a factor of 2 from 0.51 at *Tg* + 34°C to 0.24 at *Tg* + 1°C (Dhinojwala 1994b). Even though there are large changes in relaxation times or viscosity as a function of temperature, the effect on other thermophysical properties such as density or specific volume is rather small. For instance, for a temperature range of 80°C around *Tg*, change of 2 to 5 % is typically observed in density or specific volume (Greiner 1984; Richardson 1977).

2.1.3 Fragility

Fragility is a scaling formalism that was introduced by Angell in 1991 for comparison of temperature-dependent viscosity data of low molecular weight glass formers (Angell 1991). This concept is important as it provides a fair comparison of the different systems with widely varying *Tg*s and temperature dependencies of relaxation dynamics. Since the idea was proposed by Angell, a number of studies (Erwin 2002; Saiter 2004; Solunov 1999; Huang 2002; Hodge 1996, 1997; Roland 1997, 2003; Duvvuri 2002, 2004; Fitz 1999; McKenna 2003; Angell 2000; Bohmer 1993a; Plazek 1991; Pissis 1994; Bartos 1998) have used this concept to understand the critical length scales necessary for understanding the mechanisms of α-relaxations on a molecular scale, i.e., the critical size scale of the cooperative dynamics that is actually involved in the α-relaxation process.

Figure 2-3 shows the temperature dependence of $<\tau>$ that is observed for PS. It can be seen that heating in the rubbery state from *Tg* results in a change in $<\tau>$ by many more orders in magnitude as compared to cooling from *Tg* in the glassy state. The slope

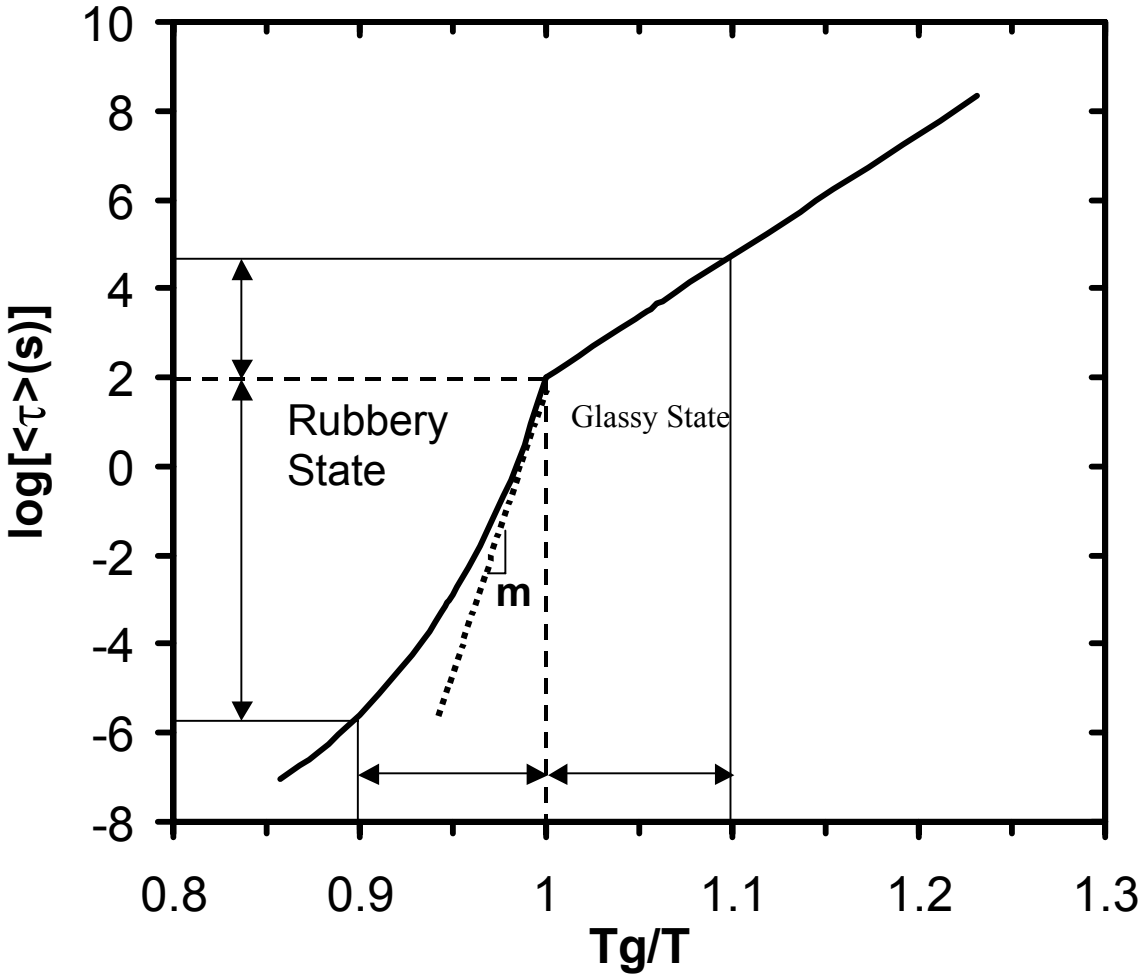

Figure 2-3: The temperature dependence of the average α-relaxation time (< τ>) for PS. Following Dhinojwala *et al.* (Dhinojwala1994b), WLF parameters of C_1 = 15, C_2 = 40 and <τ(*Tg*)> = 100s were used for the rubbery-liquid state while an activation of 46 kcal/mol was used for the glassy state. The arrows and lines shows that for the same deviation in temperature around *Tg*, huge differences in relaxation dynamics are seen in the rubbery and the glassy state. Fragility index (*m*) is defined as the slope of WLF curve at *Tg*, which is depicted as the dotted line in the plot above).

of the curve in Figure 2-3 or d(log<τ(T)>)/d(Tg/T) as $T \rightarrow Tg$ from elevated temperature is known as the fragility or steepness index (m) (Bohmer 1993a; Bohmer 1993b; Angell 1991, 1995, 1997). This defines the steepness with which the average alpha relaxation dynamics transition from WLF or VFT temperature dependence in the rubbery state to Arrhenius temperature dependence in the glassy state.

One can also define the fragility index, m, or simply fragility in an alternate manner, which allows for a simple comparison of fragility when the WLF parameters are known. Here the fragility is determined solely from the Tg and WLF parameters, C_1 and C_2 on a Tg/T scale. We start with the WLF temperature dependence:

$$\log(a_T) = \log\left(\frac{<\tau>}{<\tau>_{T_g}}\right) = \frac{-C_1(T - T_g)}{C_2 + T - T_g} \qquad 2.8$$

Dividing the numerator and denominator in the final term by T, we obtain

$$\log(<\tau>) - \log(<\tau> T_g) = \frac{-C_1\left(\frac{T_g}{T} - 1\right)}{\frac{C_2}{T_g}\left(\frac{T_g}{T}\right) + 1 - \frac{T_g}{T}} \qquad 2.9$$

Since, log $<\tau>_{Tg}$ is constant, we can write the following expression by taking the first derivative with respect to Tg/T:

$$\left(\frac{d\log<\tau>}{dT_g/T}\right) = \frac{C_1\left(\frac{T_g}{T} - 1\right)}{\frac{C_2}{T_g}\left(\frac{T_g}{T}\right) + 1 - \frac{T_g}{T}} + \frac{1 - \frac{T_g}{T}}{\left[\frac{C_2}{T_g} - 1\right]^2} \qquad 2.10$$

By evaluating this expression at $T = Tg$, equation 2.10 simplifies to an expression that is equivalent to the fragility index:

$$m \equiv \left(\frac{d \log < \tau >}{dT_g / T} \right) @ T = T_g = \frac{C_1 T_g}{C_2} \qquad 2.11$$

With this alternate definition of fragility, the relationship between m and the breadth of the distribution of relaxation times, which is associated with βw, can be analyzed. This is due to the fact that both m and βw are correlated to polymer chain cooperativity (Sauer 1992; Bohmer 1993a). This also allows us to directly compare the fragility (Roland 2003) and the βw parameter of the KWW expression (Bohmer 1993a) to the length scale of CRRs. A βw parameter closer to zero correlates to a more cooperative motion or a larger length scale of CRRs and a larger m.

With this classification, both low molecular weight glass formers and polymeric glass formers are classified into either "fragile" glass formers which have a strong temperature dependence of the α-relaxation dynamics just above Tg in the rubbery regime and "strong" glass formers which have a weaker, nearly Arrhenius temperature dependence just above Tg in the rubbery regime. Hence, fragile glass formers have larger m value than stronger glass formers. See Figure 2-4 (Bohmer 1993a, 1993b; Angell 1991, 1995, 1997). This fragility concept is obviously intimately connected to WLF and VFT type descriptions as shown above. For the VFT equation, the fragility index may be calculated by $m = (1/\ln 10)(C\,Tg)/(Tg - T_o)^2$ (Gapinski 2002; Bohmer 1993b).

2.1.4 Dynamic Heterogeneity or Cooperativity

It is believed that the cooperative rearrangements, a concept proposed by Adams and Gibbs (Adam 1965), may lead to heterogeneity in relaxation dynamics close to Tg. This has been demonstrated experimentally over the past several decades using

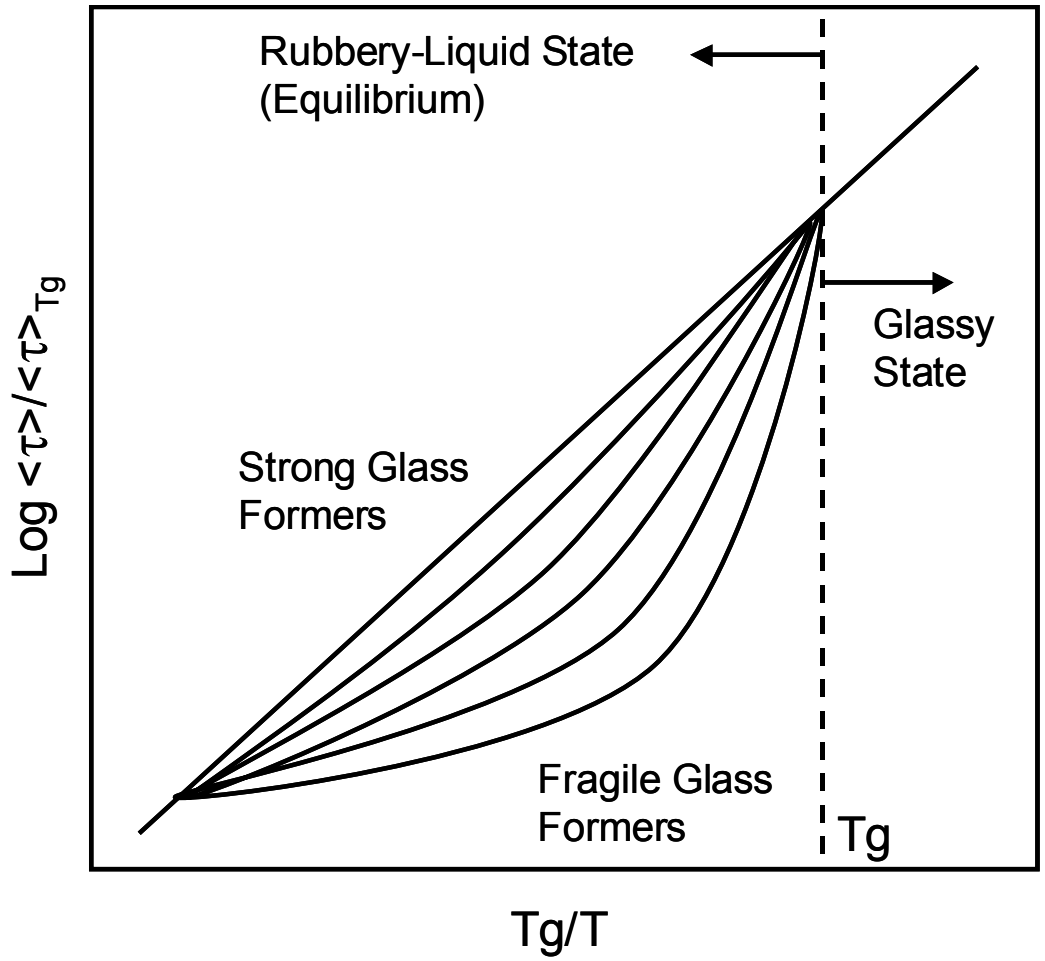

Figure 2-4: An example of a fragility plot used to compare the temperature dependence of the primary relaxation process in the rubbery regime of polymeric or low molecular glass formers (Angell 1991, 1995). As the temperature dependence of the relaxation times increases in the rubbery regime, the glass formers are seen as more "fragile" with higher fragility index (*m*, which is the slope of WLF equation at *Tg*) as shown in the plot.

techniques such as differential scanning calorimetry (DSC) (Donth 1982, 1984, 1996, 1999, 2000, 2001; Hempel 2000; Vyazovkin 2004; Tran 2004, Robertson 2004; Mundra 2005; Korus 1997; Mitteilungen 1982; Khale 1999), NMR (Schmidt-Rohr 1991; Barut 1998; Tracht 1998; Reinsberg 2001; Qin 2003), fluorescence recovery after photo-bleaching (FRAP) (Cicerone 1995, 1997; Wang 1997, 1999, 2000; Hwang 2000), translational and rotational probe diffusion (Cicerone 1995, Wang 1997, 2000; Chang 1994), dielectric hole-burning (Schiener 1996) or solvation dynamics (Richert 2000), etc. (Deschenes 2001; Arndt 1996, 1997; Hong 2002; Erwin 2002; Richert 1996). It has also been studied computationally/theoretically (Merabia 2004; Glotzer 2000; Jain 2004; Baljon 2004). A detailed description of this issue has been captured by a number of excellent reviews published recently (Sillescu 1999; Ediger 2000; Richert 2002).

These studies have demonstrated the coexistence of domains with relaxation time distributions spread over more than 4 decades in time at temperatures typically 20 K above *Tg*. These cooperatively rearranging regions (CRRs), which increase in size with decreasing temperature near *Tg* (Rizos 1999; Greiner 1984, Erwin 2002), have been found to lie in the range of 1-5 nm for small molecules and polymeric glass formers (Schmidt-Rohr 1991; Reinsberg 2001; Hempel 2000; Merabia 2004; Sillescu 1999; Ediger 2000; Richert 2002). Recent studies have found the spatial arrangement of the cooperative segments to be stringlike as compared to spherical geometry, which was originally proposed by Adam and Gibbs (Glotzer 2000; Merbia 2004; Weeks 2000).

There is some evidence that this length scale is temperature dependent, increasing in size as temperature is decreased (Reinsberg 2001; Viot 2000; Merabia 2004; Ray 1994). According to the random walk model proposed by Arkhipov and Bassler (Arkhipov 1994a, 1994b), the transition from a non-cooperative relaxation process to a cooperative relaxation process occurs at a critical temperature, *Tc*. The more the temperature decreases, the greater is the size scale of CRRs, i.e., the size scale varies

inversely to drop in the temperature from the critical temperature. Based on this theory, a number of researchers have tried to model the temperature dependence of the average size of a CRR (Erwin 2002; Solunov 1999). Even though no single model has come close to capturing the physics, such connections can lead to better understanding of correlations between the value of cooperativity and the other relaxation parameters such as fragility index and stretched exponent. More significantly, the length scales to which these homogeneities may impact the relaxation dynamics have been studied using various techniques. Dielectric noise experiments in polyvinylacetate (PVAc) (Russell 2000) and single molecule diffusion experiments in poly(isobutyl methacrylate) (PiBMA) (Quirin 2001) have shown that this length scale is greater than several tens of nanometers.

The origin of the spatial and dynamic heterogeneities is incompletely understood, and much research remains focused on understanding this phenomenon (Ediger 2000) due to the fact that spatially heterogeneous dynamics can potentially impact a wide range of polymer properties at the nanoscale. It has been hypothesized (Keddie 1994b) that as the size scale of the sample becomes comparable to the length scale of CRR, the system dynamics and physical properties differ from the bulk. As the length scale of a CRR is on the order of a few nanometers, the ideal geometry to study these nanoconfinement effects is in thin films due to the fact that the thickness can be controlled easily and uniform. Defect free samples of polymer films can be made simply by means of spin coating in a wide thickness range from nanometers to micrometers.

2.1.5 Physical Aging of Amorphous Polymers

The time dependent process by which an amorphous glassy material spontaneously evolves from a non-equilibrium glassy state towards thermodynamic and structural equilibrium is known as physical aging (Struik 1978). This relaxation process leads to sample densification, which is easily observable on laboratory time scales. This densification occurs because the material relaxes in the glassy state towards its

thermodynamic and structural equilibrium state. Figure 2-5 shows the graphical description of the densification process associated with physical aging. This relaxation process also results in many time dependent properties, e.g. volume recovery, enthalpy, entropy, yield stress, modulus, fracture energy, and ultimate elongation at break (Struik 1978; Kovacs 1981; Tant 1981; McKenna 1989; Hutchinson 1995; Hodge 1995; Greiner 1984).

Physical aging is a result of the kinetic nature of the glass transition. Upon cooling the molecules lose the ability to reach their equilibrium conformational state due to substantial reduction in their mobility and are semi-frozen into a non-equilibrium glassy state. Properties such as specific volume decrease roughly linearly with logarithmic aging time (Kovacs 1981). The slope of the specific volume versus logarithmic aging time curve defines the volume relaxation rate, r_v:

$$r_v = -\frac{1}{v} \cdot \frac{dv}{d \log t_a} \qquad 2.12$$

where r_v is the volume relaxation aging rate, v is the specific volume, and t_a is aging time (Kovacs 1981; McKenna 1989; Hutchinson 1995; Greiner 1984). The volume relaxation rate is temperature dependent and generally increases with decreasing temperature, passes through a maximum, and then decreases. The reason for the existence of the maximum in aging rate is the competition between the thermodynamic driving forces which promote physical aging and the molecular mobility which allows volume relaxations to occur. Therefore, any changes in local heterogeneities may result in different aging characteristics due to the change in local molecular mobility which is dependent on spatially heterogeneous dynamics (Thurau 2002).

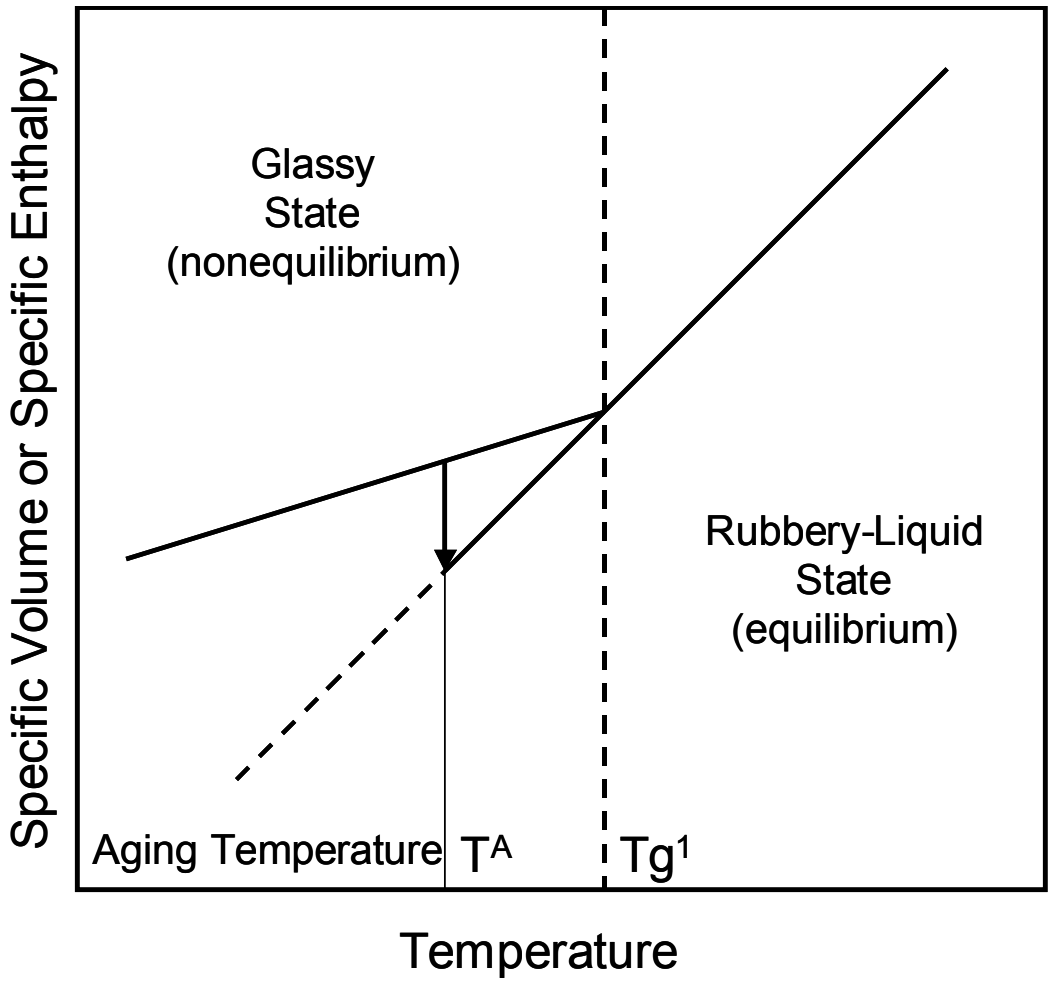

Figure 2-5: The vertical arrow denotes the physical aging process at an aging temperature T^A as the non-equilibrium glass densifies as it attempts to achieve its equilibrium state. The vertical lines denote Tg^1 determined at a particular cooling rate.

2.2 Polymer Confinement

Deviations from bulk properties are seen when polymers are confined to the extent that the interface (or surface) to volume ratio becomes increasingly important. The first direct evidence regarding deviations in *Tg* was provided in 1991 by Jackson and McKenna (Jackson 1991), who found that the *Tg* values of confined glass forming liquids in nano-pores of Vycor glass were reduced as compared to the bulk values, with a maximum 18 K reduction for o-terphenyl in a 4 nm diameter porous glass. In 1994, Keddie *et al.* (Keddie 1994a, 1994b), using ellipsometry, provided direct evidence of a reduction relative to bulk in the *Tg* of ultrathin polymer films.

In 1993, Reiter (Reiter 1993) provided the first indication of enhanced mobility related to polymer chain motion in films by his dewetting experiments. Ultrathin films were seen to dewet at temperatures below the bulk *Tg*. Later Frank *et al.* (Frank 1996a) provided the first direct evidence that polymer diffusion in thin polymer films may be impacted by the size of the confinement geometry.

In general, deviations from bulk polymer properties are seen if the polymer is confined by interfaces whose separation length scale approaches some characteristic length scale associated with polymer dynamics. As the confining dimension is decreased, a higher proportion of material is in immediate contact with an interface, suggesting that interfacial interactions might play a significant role in the observed properties of confined polymer. This work will focus on *Tg* and related relaxation behavior and mobility associated with diffusion in thin and ultrathin films. Even though this work will focus on confined polymers, it is important to note that because confinement effects have also been observed for low molecular weight or monomeric glass formers (Jackson 1991; Arndt 1997; Barut 1998; Melnichenko 1995; Schonals 2002; Wang 2004), such effects are a universal phenomenon for all glass formers.

Most of the measurements quantifying the effect of confinement on *Tg* make use of

a thin film geometry, involving either substrate-supported thin films or freely standing thin films. Freely standing films have a symmetric geometry with a polymer-air interface on both sides. Substrate supported films are very important in characterizing the impact of a solid-polymer interface on the *Tg* in confined films. They also represent a pragmatic case, as many thin film applications are substrate based. An assessment of the effect of confinement on *Tg* for each type of geometry is given below followed by a comprehensive review on mobility associated with diffusion in thin and ultrathin polymer films.

2.2.1 Effect of Polymer Confinement on Tg and Related Relaxation Behavior

A variety of methods have been used to characterize *Tg* and related relaxation behavior including dielectric relaxation spectroscopy (Wubbenhorst 2003; Sharp 2003a, 2003b, 2003c), fluorescence spectroscopy (Mundra 2006, 2007a, 2007b; Priestley 2005a,; Rittigstein 2007; Roth 2007a, 2007b; van den Berg 2004, 2006; White 2001), Brillouin scattering (Forrest 1996), ellipsometry (Beaucage 1993; Keddie 1994b; Kawana 2001, 2003; Forrest 1997; Dalnoki-Veress 2001; D'Amour 2004; Pham 2003; Fryer 2001) , X-ray reflectivity (van Zanten 1996; Miyazaki 2004; Fryer 2001; Soles 2004a), positron annihilation spectroscopy (DeMaggio 1997; Jean 1997) and nonlinear optics (Hall 1997a). These methods identify *Tg* either by following the temperature dependence of specific volume, density, film thickness, or by characterizing the relaxation dynamics directly. Most reports in this area involve investigations of linear polymers, but several studies (Lenhart 2002, 2003; Grohens 2001) have considered cross-linked or network thin and ultrathin polymer films.

2.2.1.1 Tg in Supported Polymer Films

The first systematic study of the effect of confinement on *Tg* of thin polymer films was offered by Keddie *et al.* (Keddie 1994a, 1994b). It involved the ellipsometric study of confined films of PS spin coated onto silicon (111) wafers. They observed a

reduction in *Tg* with a decrease in film thickness. Relative to bulk PS, a 25 K reduction in *Tg* was observed for a 10-nm-thick film. Three *MW*s were investigated ranging from 120,000 g/mol to 2,900,000 g/mol, and no impact of *MW* was observed on the thickness dependence of *Tg*. Their results were fitted to the following empirical relation:

$$T_g(d) = T_g(\infty)\left[1 - \left(\frac{A}{d}\right)^{\delta}\right] \qquad 2.13$$

where, A and δ are fitting parameters, d is the thickness of the film, and $Tg(\infty)$ is the bulk *Tg*. The onset of the deviation of the bulk *Tg* was seen at a thickness of ~ 40 nm. This effect was explained by suggesting the presence of a liquid-like layer at the free surface of high mobility and reduced *Tg*. Many later studies have confirmed this trend in PS films using a variety of techniques (Ellison 2002a, 2002b, 2003, 2005a; Fukao 1999, 2000; Kawana 2001; Forrest 1997, 2001; DeMaggio 1997). Similar although not identical trends were also reported for systems other than PS, for example, *Tg* decreases with decreasing film thickness have been reported for bisphenol-A-polysulfone (BPAPS) (Kim 2000), poly(alpha-methylstyrene) (PAMS) (Kim 2000, 2001), poly(4-methyl styrene) (P4MS) (Ellison 2005a), poly(tert-butyl styrene) (PTBS) (Ellison 2005a), bisphenol-A-polycarbonate (BPAPC) (Soles 2004a), poly(methyl methacrylate) (PMMA) (Grohens 2002; Yamamoto 2002; Prucker 1998; Sharp 2003b; Keddie 1994a; Fryer 2001), poly(2,6-dimethyl-1,4-phenyleneoxide) (PPO)/PS blends (Kim 2002a), and polycarbonate/PS blends (Pham 2002). The total number of studies for PS alone outnumbers the collective studies for other systems; consequently, there is a great need for studies of systems other than PS.

Thus, it is clear that the impact of nanoconfinement is not restricted to a particular system. It was apparent that the systems listed immediately above, which exhibit a *Tg*

reduction with confinement, had no particular interaction with the substrate. Thus, the effect of confinement on *Tg* in these polymers originates at the free surface. The direct proof came from the study by Forrest *et al.* (Forrest 1997) where a supported PS thin film was capped with a 7-nm-thick silicon oxide layer, changing the free surface to a solid-polymer interface (similar to that of the polymer-substrate interface). Upon replacing the free surface with the solid-polymer interface, Forrest *et al.* (Forrest 1997) observed a *Tg* value invariant with film thickness, indicating that PS has no attractive interaction with silicon oxide and also that the *Tg* reduction in ultrathin supported PS films is due to the presence of the free surface.

In contrast to systems with no interaction with the substrate, for instance PS, systems such as PMMA and poly(2-vinyl pyridine) (P2VP) may have attractive polymer-substrate interactions (due to presence of hydrogen bonding) with a native oxide substrate. (The surface of ordinary unmodified silicon or glass is comprised of silicon oxide and an equilibrium level of hydroxyl units at room temperature and ambient conditions which lie in the concentration range of 7-9 OH/nm^2 (McCafferty 1998) and an adsorbed layer of water 1-2 monolayers in thickness (Weldon 1996).) Keddie *et al.* (Keddie 1994a) showed that PMMA on a gold substrate, with no potential for hydrogen bonding, yielded a decrease in *Tg* with decreasing film thickness, qualitatively similar to that seen with PS films. In contrast, PMMA on silicon (containing native oxide and hydroxyl groups at the surface) exhibited an increase in *Tg* with decreasing thickness; the onset of the increase in *Tg* with nanoconfinement was observed at a thickness of ~ 80 nm. Prucker *et al.* (Prucker 1998) carried out similar studies on PMMA and measured *Tg* reductions in thin films supported on a hydrophobic glass substrate. Grohens *et al.* (2002) studied the effects of tacticity on the *Tg* of thin films of isotactic, syndiotactic and atactic PMMA on silicon substrates with native oxide and determined that there are significant differences in the observed *Tg* of films of similar thickness but different

tacticity. Isotactic PMMA exhibited the most extreme *Tg* increases with decreasing thickness (~ 39 K increase from bulk in a 20 nm film) on substrates where an attractive interaction exists between the substrate and polymer in agreement with the study of isotactic PMMA of Sharp *et al.* (2003b). In contrast, atactic PMMA exhibited no change (within error) for nearly identical films. Interestingly, syndiotactic PMMA exhibited decreases in *Tg* with decreasing thickness, even though there is the potential for an attractive interaction with the substrate. These results were explained in terms of a correlation that was found between the tacticity and the density of repeat unit/substrate interactions and the observed *Tg*. These studies showed that the response of *Tg* to thickness could be tuned to various degrees by changing the polymer-substrate interaction. In another study where the polymer-substrate interactions are highly attractive, van Zanten *et al.* (van Zanten 1996) reported an increase in *Tg* relative to bulk of ~ 50 K for a 7.7-nm-thick film of P2VP on a silicon substrate. More recently, Pham and Green (Pham 2002) have investigated tetramethylbisphenol-A polycarbonate (TMPC) thin films on silicon substrates containing native oxide with ellipsometry and found a 30 K increase in *Tg* for a 20-nm-thick film, consistent with the fact that TMPC interacts strongly with the substrate. Other polymers that have exhibited *Tg* increases with decreasing film thickness include tetramethylbisphenol-A polycarbonate (TMPC) (Soles 2004a; Pham 2002) and polyhydroxystyrene (Tate 2001).

Separately, there have been studies of the thickness dependence of *Tg* in thin polymer blend films which found that the *Tg*-nanoconfinement effects are tunable by simply varying the blend composition (Kim 2002a; Pham 2002). Tsui *et al.* (Tsui 2001a) also showed with a random copolymer of poly(styrene-co-methyl methacrylate) (PS-co-PMMA) that a small change in the interfacial energy noticeably influenced *Tg* in thin films. The interfacial energy was tuned by varying the styrene mole fraction in a random copolymer. Park *et al.* (Park 2004) studied the impact of confinement on *Tg* of random

copolymer thin films of PS-co-PMMA and poly(2-vinyl pyridine-co-styrene) (P2VP-co-PS). The choice of the two systems was supported by the fact that one system was moderately attractive to the substrate while other was strongly attractive. In a few cases involving copolymers with comonomer units that exhibit attractive and neutral or repulsive substrate interactions, *Tg* has been observed to be nearly invariant with film thickness (Park 2004; Hall 1997a) or tunable between *Tg* increases and *Tg* decreases with decreasing film thickness, depending on copolymer composition (Park 2004).

Ellison *et al.* (Ellison 2004a) discovered a tunable impact of plasticizer on the *Tg*-nanoconfinement effect. In case of PS films, they found that the *Tg*-nanoconfinement effect was eliminated down to a thickness of 13 nm upon the addition of either 9 wt % pyrene or 4 wt % dioctyl phthalate (DOP) to the polymer. They also found that a 14-nm-thick film with 4 wt % DOP can have a *Tg* that is ~ 27 K higher than that of a neat PS film of identical thickness.

Few other studies have been done on thin films produced by directly grafting the polymer onto the surface of the substrate. Keddie *et al.* made some preliminary attempts (Keddie 1995) to study PS grafted onto a native oxide substrate by reacting a monocarboxy-terminated PS chain with the native oxide of silicon producing a covalently bound film of PS. Down to an 8 nm thickness, a similar response of *Tg* reduction was seen as for a PS film spin coated onto a substrate. Prucker *et al.* (1998) investigated surface grafted PMMA made by conducting interfacial free radical polymerizations from azo-initiator functionalized silanes that were covalently attached to silicon dioxide substrates. Their results indicated a decrease in *Tg* with decreasing thickness that is quantitatively the same as PMMA films formed by spin coating on silanized silicon wafers. Yamamoto *et al.* (2002) studied high-density surface grafted PMMA where the chains were packed at such high grafting density (0.5-0.9 chains/nm^2) that they were highly extended and resembled a molecular “brush” structure on the substrate. Their

ellipsometry studies revealed a decrease in *Tg* with decreasing film thickness for PMMA spin coated onto silane-treated silicon wafers. However, the PMMA brush exhibited an increasing *Tg* with decreasing brush thickness. They rationalized this by hypothesizing that the surface grafted PMMA chains experience a more restricted mobility as the brush thickness is decreased resulting in limited cooperative segmental mobility.

2.2.1.2 Tg in Freely Standing/Unsupported Polymer Films

As compared to substrate-supported films, few studies have been reported on the *Tg*-nanoconfinement effect of freely standing films, likely because sample preparation and handling are tedious and problematic (Forrest 1996, 1997, 1998; Dalnoki-Veress 2001; Mattsson 2000; Roth 2003, 2005; Miyazaki 2007). The first *Tg* measurements for freely standing thin polymer films were provided by Forrest *et al.* (Forrest 1996, 1997, 1998). The *Tg* values were measured by Brillouin light scattering (Forrest 1996, 1997, 1998) and transmission ellipsometry (Forrest 1997). These measurements were later reproduced by Roth and Dutcher (Roth 2003) and are summarized in a recent review article (Roth 2005). A much greater reduction in *Tg* with confinement was observed in freely standing films as compared to substrate-supported films. Forrest and Mattsson (Mattsson 2000) reported an astonishing reduction of 70 K from bulk *Tg* in a freely standing 20-nm-thick PS film. Additionally, a strong effect of molecular weight (*MW*) at high *MW* on the *Tg*-nanoconfinement effect was found in freely standing films. Apparently there exist two *MW* regimes (Forrest 2001) for the thickness dependence of *Tg*. In the low *MW* regime ($Mn \leq \sim 378$ kg/mol), the thickness dependence of *Tg* is *MW* independent (Forrest 2001). In the high *MW* regime ($Mn \geq \sim 575$ kg/mol) there is substantial *MW* dependence, where higher *MW* samples exhibit a stronger *Tg* thickness dependence. It is not known at this time why this *MW* dependence is observed in freely standing PS films but no *MW* dependence is observed in the supported PS films.

Recently reported studies on PMMA (Roth 2003) showed the same qualitative dependence of *Tg* on thickness as PS, but the extent of *Tg* reduction was smaller in the PMMA films. Thus, it was suggested that the impact of the repeat unit structure or steric hindrance could be very crucial and needs further study. A study (Forrest 1998) examining the relaxation dynamics of freely standing PS films has confirmed that the relaxation dynamics are affected by nanoconfinement even at room temperature, supporting a strong reduction in *Tg* with confinement. In a recent DSC study of nanosized PS spheres dispersed in water (Sasaki 2003), no substantial impact on *Tg* was seen with a reduction in the size of the spheres. Equivalence can be drawn between this system and freely standing films as both have similar interfaces. However, the response was remarkably different as compared to freely standing PS films. Reasons for this could be the difference in the shape of nanoconfinement geometry, agglomeration of particles, and a possible reduction in the *Tg*-nanoconfinement effects due to the presence of surfactants acting as plasticizer. Recently, Miyazaki and coworkers (Miyazaki 2007) studied thermal expansion behavior of free standing polystyrene (PS) thin films using X-ray reflectivity for the first time to determine the glass transition temperature *Tg* and the thermal expansivity. They observed very large decrease in *Tg* with the film thickness in free standing films compared with the supported films on Si substrate and *MW* dependence was also observed. They argued that the result suggests that free surfaces on both sides activate some segmental motions in a free standing film different from in a supported film.

2.2.1.3 Alpha Relaxation Dynamics in Confined Polymer Films

One of the first measures of the impact of polymer confinement on the alpha relaxation time distribution came from the second harmonic generation (SHG) studies of Hall *et al.* (Hall 1997a). They revealed that there was a substantial broadening in the alpha relaxation distribution in confined polymer films of poly(isobutyl methacrylate)

(PiBMA) (at 98°C β_W = 0.59 for a 520-nm-thick film while β_W = 0.42 for a 23-nm-thick film). Later, a few other studies have shown faster dynamics and broader relaxation time distribution in confined films (Hartmann 2002; Fukao 2000, 2001). Studies of atactic and syndiotactic PMMA (Fukao 2003) have shown no change in relaxation dynamics in films down to 10 nm compared to bulk for atactic PMMA and faster relaxation dynamics for syndiotactic PMMA in films of similar thickness compared to bulk. These results are consistent with the tacticity effects observed for the thickness dependence of *Tg* reported by Grohens (Grohens 2002). In 2001, Lin *et al.* (Lin 2001) showed similar results in poly(methyl acrylate) (PMA) composites using NMR. As compared to bulk, a higher degree of segmental mobility was observed at the air-polymer interface while a lower degree of segmental mobility was observed at the silica-polymer interfaces where secondary bonding between silica and polymer may occur.

2.2.1.4 Physical Aging in Confined Polymer Films

The effect of confinement on the physical aging response of amorphous polymers has received relatively little attention in the research literature compared to the *Tg*-nanoconfinement effect. However, a small number of studies have been focused at understanding the effect of confinement on the physical aging response of polymers (Huang 2004; Kawana 2003; Priestley 2005a, 2005b; Rittigstein 2006, 2007; Fukao 2005; Ellison 2002a; Pfromm 1995; Dorkenoo 1999, 2000; Lu 2003; Zhou 2004).

Using permeability measurements, Pfromm and Koros (Pfromm 1995) reported an increase in the physical aging rate for free-standing polyimide and polysulfone films of thicknesses below 500 nm. Such a large length scale for a confinement effect had not been previously reported for either *Tg* or physical aging. Later, Dorkenoo and Pfromm (Dorkenoo 1999) used permeability measurements and reported accelerated physical aging for free-standing polynorbornene films of thicknesses less than 800 nm. Using permeability measurements (Huang 2004), Huang and Paul recently reported accelerated

physical aging for free-standing polysulfone, polyimide, and poly(phenylene oxide) (PPO) films for thicknesses below 900 nm. However, they found no change in *Tg* with film thickness down to 290 nm. These studies highlight the effect of film thickness on the physical aging behavior of free-standing polymer films studied by permeation measurements.

Ellison *et al.* (Ellison 2002a) conducted the first study to address the impact of confinement on physical aging of supported polymer films. Later in 2003, Kawana and Jones (Kawana 2003) studied the effect of confinement on the physical aging response of PS films with thicknesses between 10-200 nm. For a 10-nm-thick PS film aged at either 70^{o}C or 80^{o}C, no expansivity overshoot was detected upon heating the film above the bulk *Tg* (100^{o}C). The result suggested that the 10-nm-thick film was still in an equilibrium state at temperatures 30^{o}C below the bulk *Tg*, i.e., the *Tg* of confined film was reduced by at least 30^{o}C below the bulk *Tg*. A recent study by Priestley *et al.* (Priestley 2005b) answered some of the critical questions related to physical aging in confined films. By using novel fluorescence multilayer film approach, they analyzed the physical aging response near surfaces and interfaces in PMMA films. They found that relative to that of bulk, the rate of physical aging is reduced by a factor of 2 at a free surface and by a factor of 15 at a silica substrate interface with the latter exhibiting a nearly complete arresting of relaxation dynamics. Also, a distribution of relaxation rates extended more than 100 nanometers into the film interior.

2.2.2 Effect of Polymer Confinement on Mobility Associated with Diffusion

Besides *Tg*, other key polymer properties are affected by confinement. These include polymer chain diffusion (Frank 1996a; Pu 2001a, 2001b; Zheng 1997; Kuhlmann 1998; Kawaguchi 2003), probe diffusion (Hall 1998b), dewetting behavior (Reiter 1992, 1993, 2001a, 2001b, 2005), viscosity (Masson 2002), and hole growth (Dalnoki-Veress 1999; Masson 2002).

In spite of the efforts by various groups, the understanding of mobility associated with diffusion in confined geometry is very limited. The techniques used for diffusion studies in confined systems are often experimentally demanding. Also, results from the relatively few quantitative studies to date indicate an increase in, decrease in, or invariance of mobility related to diffusion with nanoconfinement, making it difficult to draw meaningful conclusions. A concise review of the work associated with diffusion in confined polymeric systems is given below.

Reiter (Reiter 1993) provided the first direct evidence of enhanced mobility in thin polymer films by optical microscopy studies of dewetting at temperatures below the bulk *Tg*. Films with thicknesses less than 100 nm were seen to dewet at temperatures even below bulk *Tg*. Using a fluorescence recovery after patterned photobleaching (FRAPP) technique, Frank *et al.* (Frank 1996a) found that the in-plane diffusion of PS labeled with a fluorescent dye decreased with decreasing film thickness below 150 nm. For example, the PS diffusion coefficient for a 60-nm-thick film was reduced by a factor of 2 as compared to the bulk value. They correlated the film thickness at which the onset of this behavior was first seen with the extended end-to-end length of the polymer chain; however, they did no study as a function of PS *MW*. In another study (Tseng 2000b) of in-plane diffusion of rubrene dye molecules in PS thin films, an enhancement in diffusion was seen with reduction in film thickness. The onset of this increase was seen at thickness close to 100 nm, and an increase of the diffusion coefficient by two orders of magnitude was reported. Fluorescence nonradiative energy transfer (NRET) studies by Hall *et al.* (Hall 1997b, 1998b) showed a small decrease in the out-of-plane dye diffusion in PS for films less than 150 nm. In contrast, no change in probe diffusion was found in poly(isobutyl methacrylate) (PiBMA) and poly(2-vinyl pyridine) (P2VP) films down to thicknesses of 50 nm and 88 nm, respectively. A detailed analysis of the fluorescence NRET technique and impact of probe size, shapes, and interactions on diffusion

coefficient can be found in references from the Torkelson research group (Hall 1997b, 1997c, 1998c, 1999; Dhinojwala 1994a; Deppe 1996a).

Rafailovich and coworkers (Zheng 1997; Pu 2001a) used dynamic secondary ion mass spectroscopy (SIMS) to measure the out-of-plane diffusion of deuterated PS (dPS) in a matrix of PS and found a decrease in the diffusion coefficient with reduction in thickness. The thickness at which the onset of the confinement effect was seen was correlated to the radius of gyration of the polymers. In another study from the same group (Pu 2001b), no change was seen in the out-of-plane diffusion coefficient of a small-molecule probe in a freely standing PS film. They used the WLF equation to describe the temperature dependence of diffusion and "back calculated" the *Tg* values, concluding that there was no change in *Tg* down to a thickness of 33 nm. This is in disagreement with direct study of *Tg* for freely standing films from many other studies (Forrest 1996, 1997, 1998; Dalnoki-Veress 2001; Mattsson 2000; Miyazaki 2007). In bilayer experiments on PS/dPS using neutron reflectivity experiments, Kuhlmann *et al.* (Kuhlmann 1998) showed that the out-of-plane diffusion coefficient in thin PS films was unchanged, except for a slight decrease when the bilayer interface was placed near the substrate. In a different study using neutron reflectivity and dynamic SIMS on a similar system (Kawaguchi 2003), enhanced mobility at the interface of a PS/dPS bilayer was seen. Lin *et al.* (Lin 1997) studied out-of-plane polymer interdiffusion using neutron reflectometry in bilayers of hydrogenated and deuterated PMMA. The diffusion near the attractive solid substrate was impacted by more than two orders of magnitude as thickness was reduced. Two other studies have also reported the impact of nanoconfinement on diffusion (Boiko 1998; Tseng 2000a). Apart from the experimental studies, a few simulation studies have also investigated the impact of confinement on mobility associated with diffusion. These studies have indicated that the effect of confinement on polymer diffusion should be asymmetric, with enhanced diffusion in the

plane of the film and suppressed diffusion out of the plane of the film for supported films (Baschnagel 1996; Mansfield 1989; Bitsanis 1990) and for freely standing films (Doruker 1999).

The lack of consensus among the studies cited above indicates that more work is required in order to make a just assessment of the impact of nanoconfinement on mobility associated with diffusion. In conjunction with this, it would be useful to develop a simplified, high-resolution technique in order to access changes in diffusion coefficients of small molecules and polymers as a function of confinement.

In addition to *Tg* and diffusion, other studies have revealed anomalous properties in confined geometries compared to bulk including phase separation behavior (Krausch 1993; Tanaka 1995; Sung 1996), crystallization (Despotopoulou 1996; Jackson 1996; Frank 1996b; Sutton 1997; Srinivas 1997; Reiter 2001; Loo 2000; Jones 2004), physical cross-linking in associative polymers (Kim 2002b), thermal expansion coefficients (Orts 1993; Oh 2004; Kanaya 2001, 2003; Soles 2004b; Beaucage 1993; Mukherjee 2002), chain conformations (Despotopoulou 1995; Grohens 1997; Jones 1999b; Kraus 2000; Muller 2002) and rheology (Hu 1992; Granick 1994).

2.3 Explanations of the Effect of Confinement on Tg

This section will provide a review and critical discussion of the explanations of the *Tg* nanoconfinement effect that have been offered in the literature.

2.3.1 Origin of Deviations from Bulk Tg in Confined Polymer

Many postulates have been offered regarding the origin of these effects (Forrest 2001) in systems lacking attractive polymer-substrate interactions: internal stresses caused by film preparation methods (e.g. spin coating) (McKenna 2000; Bernazzani 2002); a “finite size effect” due to the thickness approaching a fundamental length scale associated with glass formers (Keddie 1994b), e.g. the cooperatively rearranging region (CRR) introduced by Adam and Gibbs (Adam 1965); interfacial effects involving a

reduced entanglement concentration (Tsui 2001a; McKenna 2000; Bernazzani 2002; Brown 1996) or a segregation of chain ends to the free surface (air-polymer interface) (Tsui 2001a; Mayes 1994); and a radius of gyration (*Rg*) that is on the order or a small multiple of the film thickness, *h* (Singh 2004; Dalnoki-Veress 2001). With supported polystyrene (PS) films, two reviews (Kawana 2001; Forrest 2001) have found extensive agreement for the *Tg*-nanoconfinement effect across many measurement methods: when scaled according to the bulk *Tg* as *Tg*(*h*)/*Tg*,bulk, the thickness dependence of *Tg* has been found to be approximately independent of PS molecular weight (*MW*) (Kawana 2001; DeMaggio 1997; Fukao 2000; Forrest 2001; Tsui 2001a) over a *MW* range of 3,600-2,900,000 g/mol.

The notion that internal stresses cause the *Tg*-nanoconfinement effect may be refuted by the agreement among many studies of supported PS films (Kawana 2001; Forrest 2001) in which films of similar thickness were prepared using different solutions (solvent type and polymer concentration) and preparation conditions (spin coating speed). However, related studies of ultrathin PS (Kanaya 2003; Orts 1993) and polycarbonate (Soles 2004a) films have shown the existence of a negative thermal expansivity in the glassy state which has been attributed to a non-relaxed structure that is set in during spin coating (Miyazaki 2004; Kanaya 2003). This effect, which exhibits little impact on *Tg* (Kanaya 2003), can be removed by annealing at *Tg*,bulk + 50 K for 2 hr (Kanaya 2003; Miyazaki 2004).

There has been interest (Forrest 2001) in connecting the size scale at which nanoconfinement effects are observed to the size scale of a CRR. (Adam and Gibbs (Adam 1965) introduced the concept of a CRR in which local relaxation occurs by the collective motion of many molecules or polymer segments.) The length scale of a CRR near *Tg* has been investigated by differential scanning calorimetry (Donth 1982, 1984, 1996, 1999, 2000, 2001; Hempel 2000; Vyazovkin 2004; Tran 2004, Robertson 2004;

Mundra 2005; Korus 1997; Mitteilungen 1982; Khale 1999), 4D-NMR (Barut 1998; Tracht 1998; Reinsberg 2001; Qin 2003) and other techniques (Arndt 1996, 1997; Hong 2002; Erwin 2002; Richert 1996) and has been reported to lie in the range of ~ 1-4 nm for low *MW* and polymeric glass formers. However, the length scale at which nanoconfinement effects are observed is ~ 10 nm or less for low *MW* glass formers (Jackson 1991; Arndt 1997; Barut 1998; Melnichenko 1995; Schonals 2002; Wang 2004) and ranges from several tens to more than one hundred nanometers for polymers (Keddie 1994b; DeMaggio 1997; Dalnoki-Veress 1999, 2000, 2001; D'Amour 2004; Pham 2002, 2003; Fryer 1999, 2000, 2001; Soles 2004a, 2004b; Mundra 2006, 2007a, 2007b; Priestley 2007b, 2007c; Rittigstein 2006, 2007; Roth 2007a, 2007b). This indicates that the length scale of a single CRR is far less than the thickness at which *Tg*-nanoconfinement effects are observed and is therefore not the origin of the *Tg*-nanoconfinement effect.

Recent understanding gained from fluorescence experiments (Ellison 2003) has reiterated this point. These experiments have revealed via multi-layer PS films with fluorescent labels in only one layer that the free-surface effect causes a *Tg* reduction that persists several tens of nanometers into the film interior (much larger than a single CRR). Furthermore, it was observed (Ellison 2003) that a region of reduced *Tg* near the free surface exists as a continuous distribution of *Tg*s that depends on the degree of nanoconfinement. These results have shown directly that two-layer and three-layer models (van Zanten 1996; Kawana 2001; DeMaggio 1997; Fukao 2000; Forrest 2000, 2001; McCoy 2002) are inadequate to explain *Tg*-nanoconfinement behavior and that a model that incorporates a continuous distribution of *Tg*s across the thickness of a film is needed (Priestley 2005b, 2007a; Roth 2007a, 2007b). This picture is consistent with recent simulations (Jain 2004) and predictions from theoretical pictures (Herminghaus 2004; Merabia 2004; Berriot 2002, 2003).

Many other studies (Wang 2004; Keddie 1994b, Forrest 2001; Sharp 2003a; Schwab 2000; Jean 1997; Torres 2000; Pochan 2001; Kajiyama 1997) have indicated that interfacial effects are the most logical explanation for the underlying cause of the *Tg*-nanoconfinement effect. Numerous studies have concluded (Ellison 2003; Roth 2007a, 2007b; Jain 2004; Herminghaus 2004; Merabia 2004; Schwab 2000; Jean 1997; Torres 2000; Pochan 2001; Kajiyama 1997) that the free-surface *Tg* of bulk PS films is some tens of degrees lower than the bulk *Tg*. Supporting the importance of free-surface effects for PS, a recent study (Sharp 2003a) has shown that removing the free-surface interface by placement of aluminum (Al) or gold (Au) metal onto the film results in a *Tg* that is independent of thickness down to 10 nm or less. The key role of interfacial effects is also supported by studies of the thickness dependence of *Tg* for polymers with attractive substrate interactions (Keddie 1994a; van Zanten 1996; Forrest 2001; Grohens 2002; Pham 2002; Ellison 2002a, 2002b; Fryer 2001; Mundra 2006, 2007a, 2007b, Priestley 2005a, 2005b, Rittigstein 2007), e.g. poly(2-vinylpyridine) and poly(methyl methacrylate) on silicon (with native oxide) or glass substrates which exhibit increases in *Tg* with decreasing thickness due to the attractive substrate interactions. This point has been reiterated by simulation study confirming that changing the interaction potential between substrate and polymer results in *Tg* deviation (decrease or increase based on the nature of interaction between the substrate and the polymer) as a function of film thickness (Torres 2000).

Although there is substantial evidence supporting a free-surface effect as the origin of *Tg* reductions in nanoconfined PS films, there is not yet a detailed understanding of the free-surface effect. A simple explanation is that polymer segments that lie at the free surface possess fewer conformational restrictions than those in the bulk and thus have a higher degree of cooperative segmental mobility and an associated lower *Tg*. While this explanation is logical, it lacks details regarding the extent to which

interfaces may be expected to modify cooperative segmental mobility or *Tg* from that of bulk. Others have offered the explanation that the free surface results in a reduced entanglement concentration (Tsui 2001a; McKenna 2000; Bernazzani 2002; Brown 1996), which in turn yields enhanced mobility and reduced *Tg* near the free surface. However, this explanation can be criticized because a thickness dependent *Tg* has been observed for both entangled and unentangled PS (Kawana 2001; DeMaggio 1997; Fukao 2000; Forrest 2001; Tsui 2001a) (M_c, the critical entanglement *MW*, is ~ 35 000-38 000 g/mol (Sperling 1992; Majeste 1998) for PS) and because bulk *Tg* does not depend on chain entanglements (Sperling 1992).

Another potential explanation involves the segregation of chain ends to the free surface that would be expected to reduce the local *Tg* at the free surface (Tsui 2001a; Mayes 1994). However, if chain ends were the origin of this effect, it would be expected that the thickness dependence of *Tg* could be significantly altered by varying the surface chain-end concentration by modification of the polymer *MW* (Mayes 1994), which is not supported by experimental data. Variation of polymer *MW* also greatly alters the *Rg* of the bulk polymer, which in turn would significantly affect the film thickness at which overall chain conformation would be expected to differ substantially from bulk. For example, when PS *MW* is increased from 3,600 g/mol to 10,000,000 g/mol, the bulk *Rg* increases from ~ 2 nm to 87 nm (using a characteristic ratio of 10 to calculate *Rg*) (Sperling 1992; Flory 1989). (It is however important to note that the overall chain conformation is likely altered in nanoconfined films, adopting, on average, ellipsoidal conformation with a large aspect ratio as opposed to the random coil expected in bulk.) Some have argued that such an effect may yield a *MW* dependence of the *Tg*-nanoconfinement effect (Singh 2004; Fukao 1999). In opposition to this picture is a large body of evidence (Kawana 2001; DeMaggio 1997; Fukao 2000; Forrest 2001; Tsui 2001a) indicating that the *Tg*-nanoconfinement effect for supported PS films is

approximately independent of *MW* indicating that neither chain ends nor bulk *Rg* plays a significant role in defining this effect.

It is noteworthy that two recent studies (Singh 2004; Miyazaki 2004) of supported PS films have reported a *MW* dependence of the *Tg*-nanoconfinement effect in the range of 212,000-2,900,000 g/mol. Singh *et al.* (Singh 2004) reported that the thickness dependence of *Tg* for a variety of PS *MW*s can be collapsed onto a master curve when thickness is scaled as h/Rg(bulk) and *Tg* is scaled as $Tg(h)/Tg$,bulk. While the study by Miyazaki *et al.* (Miyazaki 2004) was largely focused on thermal expansion effects, it also reported a larger *Tg*-nanoconfinement in ultrathin films of higher *MW* (2,890,000 g/mol vs. 303,000 g/mol) PS down to ~ 10 nm in thickness. It should be noted that both studies (Singh 2004; Miyazaki 2004) have measured *Tg* upon heating from the glassy state after prior annealing at 408 K for 20-48 h or 423 K for 48 h. Further discussion on the effect of *MW* on *Tg*-nanoconfinement can be found in Chapter 4.

Several researchers have recently discovered (Efremov 2004a, 2004b; Fakhraai 2004) that the heating or cooling rate can also have dramatic impact on the thickness dependence of *Tg*. For instance, with cooling rates of 60,000-120,000 K/min, no thickness dependence to *Tg* was observed for PS, P2VP or PMMA films down to thicknesses of ~ 3 nm (Efremov 2004a, 2004b). Other explanations originating from the idea that deviation in *Tg* values in thin and ultrathin films is due to a reduced average density value in confined geometry have also been found incorrect experimentally (Forrest 1998; Wallace 1998).

2.3.2 Models and Hypotheses Explaining Tg-nanoconfinement Effects

The first model proposed to explain the *Tg*-nanoconfinement effect was an empirical bilayer film model by Keddie *et al.* (Keddie 1994b), who introduced the idea of a high mobility layer at the air-polymer interface with a reduced value of *Tg*. Further it was assumed that the substrate had little effect on the mobility of PS thin films consistent

with what had been seen in molecular dynamics simulations (Bitsanis 1990). As freely standing films have two air-polymer interfaces, they are expected to exhibit behavior similar to that of a supported film of half the thickness, which was later shown experimentally (Forrest 2000; Mattsson 2000). Later, more models were proposed that were in essence a modified version of the bilayer model (Kawana 2001; Park 2004; DeMaggio 1997). Another layer model (Forrest 2000), with dynamic heterogeneities at the free surface, was proposed to describe *Tg* in low to moderate *MW* polymeric freely standing films. It was suggested that the mobile surface layer had a width determined by the length scale of cooperative dynamics. The model incorporated the idea of Adam and Gibbs (Adam 1965) of a fundamental length scale coupled with the dynamics of the *Tg*. Later, Ellison and Torkelson (Ellison 2003) showed that bilayer and trilayer models are inadequate to explain *Tg*-nanoconfinement effects and that a model with gradients in dynamics accounting for a distribution of *Tg*s across the film thickness is required.

The presence of enhanced mobility at the air-polymer interface can be understood by a simple argument. The air-polymer interface is exposed to a free surface on one side causing less restriction to the motion of polymer chain segments. This leads to a higher degree of freedom as compared to the bulk and consequently to higher segmental mobility. Many attempts have been made to characterize this free surface layer using different techniques (Kajiyama 1997; Kerle 2001; Kawaguchi 2001; Schwab 2000; Liu 1997) as well as simulations (Torres 2000; Mansfield 1991).

Propositions were made related to the reduction of density near the surface due to segregation of chain ends at the surface. Later studies (Ellison 2005a; Tsui 2001b) have shown that neither chain-end segregation nor chain entanglement reduction is responsible for the enhanced *Tg*-dynamics of the surface layer. The first direct evidence of an enhanced mobility layer with a reduced *Tg* was provided by multilayer experiments characterizing the distribution of *Tg* at various depths (Ellison 2003). These fluorescence

measurements showed that the free surface of a sufficiently thick film having bulk *Tg* can have a surface *Tg* value several tens of degrees below the bulk value. In a recently published article, Zhang *et al.* (Zhang 2007) supported these results. Using positron annihilation spectroscopy to measure the ortho-positronium lifetime variation as a function of temperature, they showed that for an 80-nm polystyrene film on silicon substrate the surface and interface *Tg* were significantly suppressed by 18 and 12K at the depth of 5 and 70 nm from the surface, respectively.

Hypothesis-driven models have also been proposed to explain the effect of confinement on *Tg*. Ngai *et al.* (Ngai 1998b, 2000) proposed the coupling model, which is focused on the cooperative motions associated with *Tg* (Adam 1965). The model characterizes the impact of local structure on the steric constraints from the neighboring nonbonded segments or simply the intermolecular coupling. This intermolecular coupling is linked to the size scale of CRRs, which is believed by some to be connected to *Tg*-nanoconfinement effects. Supporting evidence came from a recent study (Ellison 2005a) in which the addition of a small amount of plasticizer in PS reduced the requirement for the intermolecular coupling and the size scale of CRRs at *Tg*. Nevertheless, a connection between the size scale of CRRs and the *Tg*-nanoconfinement effects was not established. Several other models have also been proposed to describe the effect of confinement on *Tg* in thin and ultrathin films (Jiang 1999; de Gennes 2000).

Long and Lequeux (Long 2001; Merabia 2004) proposed a model based on the idea that thermally induced density fluctuations play a critical role in determining *Tg* in bulk. These fluctuations lead to regions of faster and slower dynamics. The total number of regions with slower dynamics increases with decreasing in temperature. They defined the *Tg* as the temperature at which these slow moving regions are interconnected throughout the bulk of the sample. The deviation from bulk *Tg* in confined systems is explained by a shift in the percolation of regions of fast and slow dynamics from a 3-

dimensional (3-D) to a 2-dimensional (2-D) geometry. In the case of ultrathin supported films with little or no attractive substrate interaction, the *Tg* occurs when the slow regions percolate in the direction parallel to the film. This requires a larger fraction of slow domains and results in a decrease of *Tg* relative to ultrathin films with attractive substrate interactions.

In the case of substrate-supported films with strong attractive interactions with the substrate, the transition occurs when both interfaces are connected with continuous paths of slow regions. This requires that the correlation length of the 3-D percolation (ζ) is comparable to the thickness of the film, which in turn requires a smaller fraction of slow subunits as compared to the bulk glass transition. The *Tg*-nanoconfinement effects are seen when the thickness of the sample becomes comparable to ζ.

The model by Long and Lequeux (Long 2001; Merabia 2004) explains many attributes of the *Tg*-nanoconfinement effect satisfactorily as well as addresses the issues of interactions with the substrate. In addition, the model is free of any fitting parameters used in various other models to describe at least qualitatively the behavior in bulk and in thin films. However, it has only been applied to a couple of systems (Merabia 2004) so far and calls for further investigation.

Clearly, the models that have been developed to explain the *Tg*-nanoconfinement and that have not yet been discredited rely on the notion of cooperative motion. Thus, it is imperative to provide greater characterization of the size scale of CRRs near *Tg* in order to develop a better understanding of the phenomenon.

CHAPTER 3

NOVEL FLUORESCENCE TECHNIQUES FOR CHARACTERIZING THE GLASS TRANSITION TEMPERATURE (Tg) OF POLYMERS IN THIN AND ULTRATHIN FILMS

3.1 Introduction

Fluorescence techniques are used in a number of areas ranging from biochemistry to polymer physics. Fluorescence can be especially useful in characterizing physical properties of polymers. These fluorescence techniques use a probe, which is either doped into or covalently attached to the polymer, to serve as a tool for characterizing various properties. Five years ago, Ellison *et al.* (Ellison 2002a, 2002b) presented the first demonstration of the utility of fluorescence probe methods to characterize glass transition temperature (*Tg*) values in confined polymer films. Later, Ellison and Torkelson (Ellison 2003) demonstrated the applicability of fluorescence to obtain unique information, such as the nanoscale distribution of *Tg* values from the free surface to the polymer-substrate interface. Since then, Torkelson and coworkers have also exploited fluorescence as a simple method to explore the tunability of the *Tg*-nanoconfinement effect in PS via small molecule diluent addition (Ellison 2004a) and small changes in repeat unit structure (Ellison 2005a). Taking advantage of earlier studies employing fluorescence probes to characterize physical aging and complex relaxation behavior in bulk polymer films (Royal 1992a, 1992b, 1993), Priestley *et al.* (Priestley 2005a) have recently developed fluorescence methods which yield continuous measurements of physical aging in thin and ultrathin films as well as determine the nanoscale distribution of physical aging rates across polymer films (Priestley 2005b). Finally, Torkelson and coworkers have also exploited fluorescence methods to characterize the effects of nanoconfinement in ultrathin films on small molecule diffusion in polymers (Hall 1998b) as well as physical

crosslinking and gel formation in liquid-state polymers systems (Kim 2002b).

This chapter provides other examples in which simple fluorescence methods can be used to investigate the glass transition behavior in confined polymer systems. It is shown that *Tg* values can be determined by excited-state fluorescence lifetime measurements as well as by intensity measurements. While previous characterization of *Tg* values in thin and ultrathin films employed extrinsic fluorescence from pyrene dyes doped or covalently attached as labels at trace levels in polymers (Ellison 2005a), it is shown here that intrinsic fluorescence from polystyrene as well as extrinsic fluorescence from selected non-pyrenyl dyes can also be used to characterize the *Tg*-nanoconfinement effect. In addition, a brief review on the phenomenon of fluorescence and various fluorescence techniques used to measure *Tg* and other physical properties in polymers is also provided.

3.2 Background

3.2.1 Basic Fluorescence

Luminescence is the emission of light from an electron in an electronically excited state when it returns to the ground state (Lakowicz 1999; Guilbault 1973). It is of two types: 1) fluorescence and 2) phosphorescence. Fluorescence occurs when an excited electron in a singlet state (i.e., paired to the second electron in the ground state of opposite spin) returns to the ground state with an emission of a photon. As the return to the ground state is spin-allowed, the process occurs rapidly, typically on the time scale of 1-100 nsec. This process is illustrated pictorially in the Jablonski diagram shown in Figure 3-1 (Lakowicz 1999). In contrast, in the case of phosphorescence, the excited-state electron is in the triplet state (same spin as the ground state electron), making the emission rates much slower. The vibrational energy bands in each energy level result in a continuous emission spectrum.

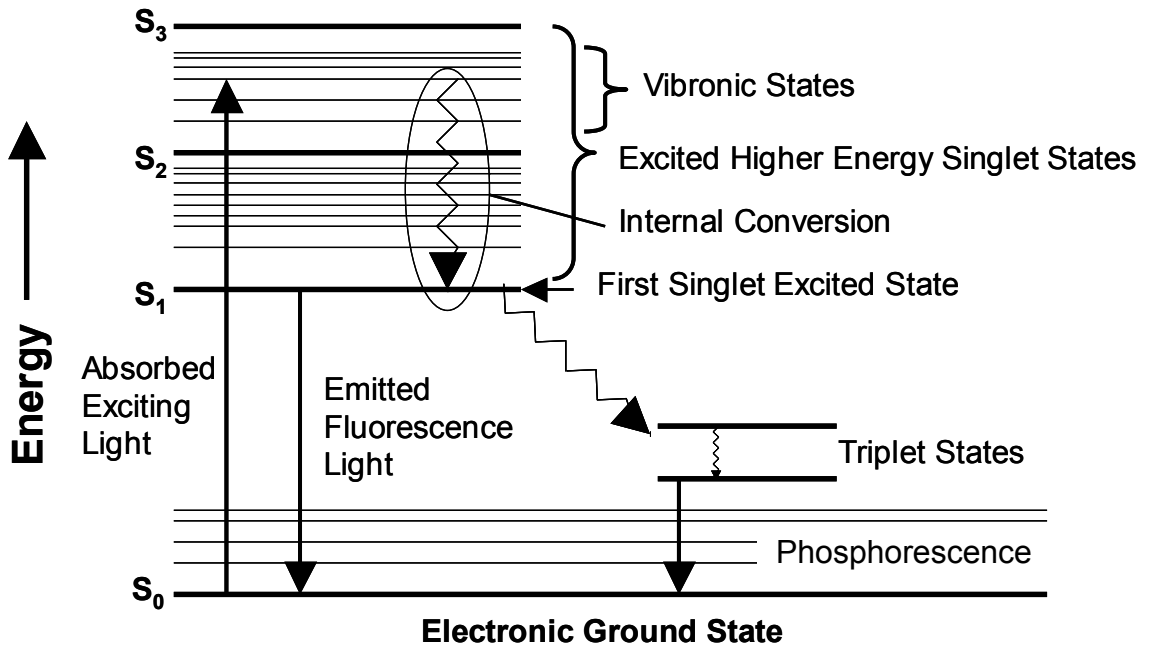

Figure 3-1: Jablonski diagram (Lakowicz 1999). The processes that lead to emission of fluorescence light include absorbance of a photon that promotes and electron to an excited singlet vibrational state, internal energy conversion (due to bond vibrations, collisions with environment/surroundings, etc.) and fluorescence emission.

The emission spectrum is obtained by exciting the probe by light of fixed wavelength and then measuring the emission intensity as a function of wavelength. The number of emitted photons is less than the number of absorbed photons as part of the energy is lost in nonradiative energy decay, e.g., that associated with thermal vibrational motions. Hence, the quantum yield for fluorescence (ratio of emitted photons to absorbed photons) is less than unity (Lakowicz 1999; Valeur 2002; Schulman 1977).

Experimentally, fluorescence can be classified into two types of measurements: steady state and time-resolved (Lakowicz 1999). Steady state measurements are performed under constant illumination. The chromophore is excited at an appropriate wavelength to efficiently promote the electrons to an excited electronic state. The fluorescence emission spectrum is recorded by monitoring the emission intensity as a function of wavelength. The excitation spectrum is obtained by monitoring the emission intensity at a single wavelength while scanning the excitation wavelength.

With time-resolved spectroscopy, it is possible to measure fluorescence intensity decays. Experimentally, the sample is exposed to a pulse of light that is shorter than the decay time. Intensity decay measurements are recorded with a rapid detection system. In general, time-resolved and steady state measurements are related by the following equation:

$$I_{SS} = \int_0^\infty Ao \exp\left(\frac{-t}{\tau}\right) dt = Ao\,\tau \qquad 3.1$$

where I_{SS} is the steady state emission intensity, Ao is a parameter that depends on the chromophore concentration and a number of instrument parameters, t is time, and τ is the relaxation time. The steady state emission intensity is simply an average of the time-resolved measurements. Time-resolved measurements are useful for systems that exhibit multiple relaxation times such as polymers. Also the measured decay is independent of

sample geometry, refractive index changes, and lamp fluctuations that may drastically affect a steady state emission measurement (Lakowicz 1999). The excited state lifetime of a chromophore, typically 1-100 ns, is the timescale the molecule is in the excited state. The lifetime determines the amount of time available for the excited state chromophore to interact with its environment (Lakowicz 1999).

3.2.2 Fluorescence Technique for Characterizing Tg and Related Relaxation Behavior in Polymer

The use of fluorescence to measure *Tg* and other physical properties of polymers was first suggested by Loutfy (Loutfy 1981, 1982, 1983a, 1983b, 1986; Law 1983). It was observed that the fluorescence intensity of a p-N,N-dialkylaminobenzylidene malononitrile rotor probe doped into poly(methyl methacrylate) (PMMA) decreased with increasing temperature and exhibited a transition occurring near the calorimetric *Tg*. Later, Royal and Torkelson (Royal 1992a, 1993) demonstrated that the use of fluorescence allows for the characterization of complex relaxation phenomena related to *Tg* such as physical aging (Royal 1992a; Royal 1993) and asymmetry and memory effects (Royal 1992a), due to the sensitivity of fluorescence to local density through the free volume required for the rotor motions of the probes.

Many research groups have since investigated *Tg* or issues closely related to *Tg* in bulk polymeric and monomeric glass formers with both steady state (Brady 1993; Hofstraat 1998; Lenhart 2000, 2001; Yilmaz 2004; de Deus 2004; Yamaki 2002; Albala 2004; Brown 2004; Schurr 2003; Hooker 1995; Anwand 1991; Corrales 2004; Thomas 2003; Martins 2003; van den Berg 2004; Meyer 1990; Schwab 1990) and time resolved (Yilmaz 2004; Martins 2003; Vallee 2004; Tomczak 2004; Serrano 2002; Ye 1996, 1997, 1998; Nakatsuka 1997; Przhonska 1996) fluorescence measurements as a function of temperature. In these studies, the temperature dependence of a wide variety of fluorescence parameters (e.g., lifetimes, intensity, peak intensity, peak wavelength, etc.)

has been reported to provide sensitivity to *Tg*.

Besides characterizing thermal transitions, fluorescence techniques have been used to monitor physical aging in glassy polymer (Royal 1990, 1992a, 1992b, 1993; Lamarre 1983; Sung 1981; Meyer 1990; Schwab 1990; van den Berg 2004b) and polymer degradation (Chipalkatti 1991; Jacques 1993; Remillard 1998). Royal and Torkelson used intramolecular charge transfer rotor fluorophores to monitor physical aging in PS, PMMA, poly(vinyl acetate), polycarbonate, and poly(isobutyl methacrylate) (Royal 1990, 1992a, 1992b, 1993). Using the probe julolidenemalononitrile in a series of amorphous polymers, Royal and Torkelson showed that the physical aging rates determined by fluorescence methods followed the same temperature dependence as the physical aging rates determined by volume relaxation measurements (Royal 1993). Recently, van den Berg *et al.* (van den Berg 2004b) have used wavelength shifting probes to monitor physical aging. Chipalkatti and Laski (Chipalkatti 1991) studied the degradation of polycarbonate by monitoring the emission spectrum of key byproducts such as phenyl o-phenoxybenzoate.

There are very few reports (White 2001; Ellison 2002a, 2002b, 2003, 2004a, 2004b, 2005a, 2005b; Priestley 2005a, 2005b, 2007a, 2007b, 2007c; Rittigstein 2006, 2007; Mundra 2006, 2007a, 2007b; Roth 2007a, 2007b) of fluorescence techniques being used to measure *Tg* and related relaxation processes in thin and ultrathin films. The recent work of Ellison and Torkelson has pioneered the use of fluorescence spectroscopy to monitor the glass transition temperature in ultrathin polymer films. Ellison and Torkelson (Ellison 2002a, 2002b, 2003, 2004a, 2004b, 2005a, 2005b) were able to characterize *Tg* in various systems and demonstrated that this technique was sensitive enough to measure the *Tg* values in extremely thin films with high precision. Using multilayer fluorescence measurements, Ellison and Torkelson (Ellison 2003) showed that this technique can be used to quantify the impact of various interfaces on the *Tg* as well

as provide the first direct evidence of how far these effects can penetrate away from a surface or interface.

3.2.3 Fluorescence Technique for Characterizing Mobility Associated with Diffusion in Polymer Thin and Ultrathin Films

Frank *et al.* (Frank 1996a) studied the in-plane diffusion of polymer in ultrathin films by using the fluorescence recovery after patterned photobleaching (FRAPP) technique. In this technique, dye-labeled polymers are bleached over a selected area, removing the chromophores locally, and then the diffusion of unbleached molecules into the bleached area is measured via fluorescence. Durning and coworkers (Tseng 2000a, 2000b) also used FRAPP to measure small-molecule dye diffusion in ultrathin PS films. Hall *et al.* (Hall 1997a, 1997b, 1998b) employed the non-radiative energy transfer (NRET) technique to study the out-of-plane diffusion in ultrathin polymer films. Using a bilayer sample geometry with one layer labeled with NRET donor chromophores and the other doped with NRET acceptors chromophores, they were able to measure the acceptor dye diffusion coefficient by measuring the changes in the intensity of the NRET donor chromophores as a function of interdiffusion time. The net decrease in the donor fluorescence intensity takes place due to the NRET between the donor and the acceptor. The decrease in steady-state donor fluorescence intensity or energy-transfer efficiency can be related to the diffusion coefficient. For detailed mathematical analysis, see the reference by Dhinojwala and Torkelson (Dhinojwala 1994a).

The reason that many diffusion studies in thin polymer films are based on fluorescence is because other methods, e.g. nuclear magnetic resonance and infrared spectroscopy, are not sufficiently distance-sensitive to measure the range of diffusion coefficients obtainable by fluorescence. Neutron reflectivity may be slightly more distance-sensitive than fluorescence. However, the facilities required for measurements are limited (Spangler 1992). (For further details on mobility associate with diffusion in

thin and ultrathin polymer films, refer to Chapter 10.)

3.3 Experimental

Polystyrene sample 1 (Pressure Chemical, reported values of Mn = 152,000 g/mol, Mw/Mn < 1.10) was used as received for intrinsic measurements; PS sample 2 (Pressure Chemical, reported values of Mn = 290,000 g/mol, Mw/Mn < 1.06) and PS sample 3 (Pressure Chemical, reported values of Mn = 200,000 g/mol, Mw/Mn < 1.08) were used as received for all the other measurements. The chromophore 4-tricyanovinyl-[N-(2-hydroxyethyl)-N-ethyl]aniline (TC1) was synthesized by reaction with tetracyanoethylene (TC1 America) and 2-(N-ethylaniline)ethanol (TC1 America) dissolved in dimethyl formamide (Fisher) at 55 ^{o}C for 15 min and then recrystallized from glacial acetic acid. TC1-labeled methacrylate monomer was synthesized through an esterification reaction with methacryloyl chloride (Aldrich) in the presence of triethylamine (Aldrich) and dichloromethane (Aldrich) at 0 ^{o}C for 2 hr. Labeled PMMA was synthesized by reaction of MMA monomer (Aldrich) in the presence of a trace amount of TC1-labeled methacrylate monomer. The TC1-labeled PMMA contained 1.37 mol% (1 in 73 repeat units) of the TC1-labeled monomer determined by UV-Vis absorbance spectroscopy (Perkin Elmer Lambda 35). For TC1-labeled PMMA, Mn = 509,000 g/mol, Mw/Mn = 1.67 measured by gel permeation chromatography using universal calibration with PS standards. All polymer was washed by dissolving in toluene (Fisher) and precipitating in methanol (Fisher) at least five times to remove residual solvent and then dried in a vacuum oven at Tg + 15 K for 24 hr.

Bulk Tg (Tg,bulk) values were measured by differential scanning calorimetry (DSC) (Mettler-Toledo DSC822, second heat, onset method, 10 K/min) and also via fluorescence methods and were found to agree within experimental error: PS sample 1 Tg,bulk = 105 ^{o}C by DSC and 105 ^{o}C by fluorescence; PS sample 2 Tg,bulk = 102 ^{o}C by

DSC and 101 ^{o}C by fluorescence; PS sample 3 *Tg*,bulk = 100 ^{o}C by DSC and 100 ^{o}C by fluorescence; PMMA *Tg*,bulk = 121 ^{o}C by DSC and 122 ^{o}C by fluorescence.

Thin films of polymers were prepared by spin coating (Hall 1998a) dilute solutions of polymer, with or without extrinsic dye, onto quartz slides. Film thicknesses were determined using a Tencor P10 profilometer. Films with thickness less than 500 nm were dried in a fume hood overnight, and films with thickness greater than 500 nm were dried for 48 h in vacuum at room temperature.

A Spex Fluorolog-2DM1B fluorimeter was used for extrinsic steady-state fluorescence measurements. Measurements employed a front-faced geometry. For thin and ultrathin films used for intrinsic measurements, fluorescence was measured using a PTI QM-2001 SE fluorimeter using front-face geometry. As the PTI fluorimeter has greater excitation intensity than the Spex fluorimeter, a smaller slit size was used with the PTI instrument to prevent films from photobleaching at high temperature. A clean quartz cover slide was placed on top of each film to reduce the potential for probe sublimation during the *Tg* measurement by fluorescence. (The film was adhered only to the glass substrate on which it was spin coated.) Film temperature was controlled by a microprocessor controller (Minco Products) with a Kapton ribbon heater attached to a flat aluminum plate that was also used as a clamping device to hold the sample. (For further details see Chapters 4 and 6.)

In fitting the temperature dependence of fluorescence in the rubbery and glassy states, only data points well outside *Tg* were used for the linear fits, and typical correlation coefficients (R^2) were better than 0.990. To initiate the fitting procedure, data points were added to the rubbery- and glassy-state linear regressions one-by-one at the extrema in the temperature range of the data. The correlation coefficient was monitored as more data points were added (approaching *Tg* from the extrema in the temperature range of the data) to each of the linear regressions. If the R^2 value began to steadily

decrease below a threshold value (i.e., < 0.990) as more data points were added, then these data points were removed to produce a value of R^2 higher than the threshold value and the linear regressions were considered acceptable. The linear fits in both the rubbery and glassy states included a minimum of four fluorescence data points (usually more), spanning a minimum of 15 K in temperature. This procedure was followed regardless of whether fitting linear functions to the fluorescence intensity data at particular emission wavelength(s) or the integrated intensity as a function of temperature. When using integrated intensities to identify *Tg*, spectra were taken over a sufficient range of wavelengths that integration could be done from instrument baseline at the lowest wavelengths to the same instrument baseline at the highest wavelengths. In all cases, regardless of using intensities or integrated intensities, the sample was reheated to the starting temperature following the measurements taken upon cooling to verify that the sample did not lose a substantial amount of fluorescence probe molecules due to photobleaching, sublimation, etc. Typically, the intensity after reheating the sample is within 10% of the original intensity before the measurements were taken upon cooling.

When fitting the temperature dependence of the fluorescence intensity data at the peaks in the emission spectra, the standard deviation in the determination of *Tg* at the various peaks in the emission spectra was typically less than 1.0 K for each sample. This is comparable to the estimated standard variation (or error) in *Tg* (+/- 1.0 K or less) from sample to sample (identified either using intensities or integrated intensities) for films of identical thickness on identical substrates when the film thickness is greater than ~ 25 nm. As film thickness is decreased below ~ 25 nm, the estimated standard variation (or error) is +/- 2 K. (Further details on measurement of *Tg* by fluorescence can be found in Chapters 4 and 6 in the references by Ellison *et al.* (Ellison 2002a, 2002b, 2005c).)

3.4 Novel Fluorescence Technique for Characterizing the Tg of Polymers in Thin and Ultrathin Films

Figure 3-2a shows the fluorescence emission spectrum of pyrene dopant in an 810-nm-thick PS film. There is a significant reduction in overall intensity with increasing temperature. Previous studies have shown (Ellison 2002a, 2002b, 2003, 2004a) that *Tg* values can be obtained by plotting the intensity near one or several of the peak wavelengths (~ 374, 385, and 395 nm) as a function of temperature. Over a 70-80 K temperature range roughly centered at *Tg*, two linear temperature dependences of intensity are observed, a stronger one in the rubbery state and a weaker one in the glassy state, with the intersection being identified as *Tg*. Careful inspection of Figure 3-2a reveals that the exact values of the two slopes in such a plot may depend on the emission wavelength selected, because the temperature dependence of intensity is stronger at the maxima (peaks) than at the minima (valleys) of the emission spectrum. Such effects have been observed by others (Vigil 1997; Brown 2004) studying the temperature dependence of pyrene fluorescence in various polymers and can be attributed to the temperature dependence of the different vibronic bands of pyrene. In addition to these effects, there are slight blue shifts in the emission spectrum of pyrene (1-2 nm) as temperature is decreased from 413 K to 333 K. In order to minimize these effects, integrated intensity is plotted as a function of temperature. Figure 3-2b compares the temperature dependence of integrated intensity to that of intensity at 400 nm; while the same *Tg* value (373 K) is determined from both plots, there is a discernable difference in the temperature dependences of intensity at 400 nm and the integrated intensity over a common temperature range. However, both the fluorescence intensity at a given wavelength or the integrated fluorescence intensity over the emission spectrum are extensive rather than intensive parameters, as they are a function of excitation intensity, sample geometry, and absorbance, along with sample refractive index.

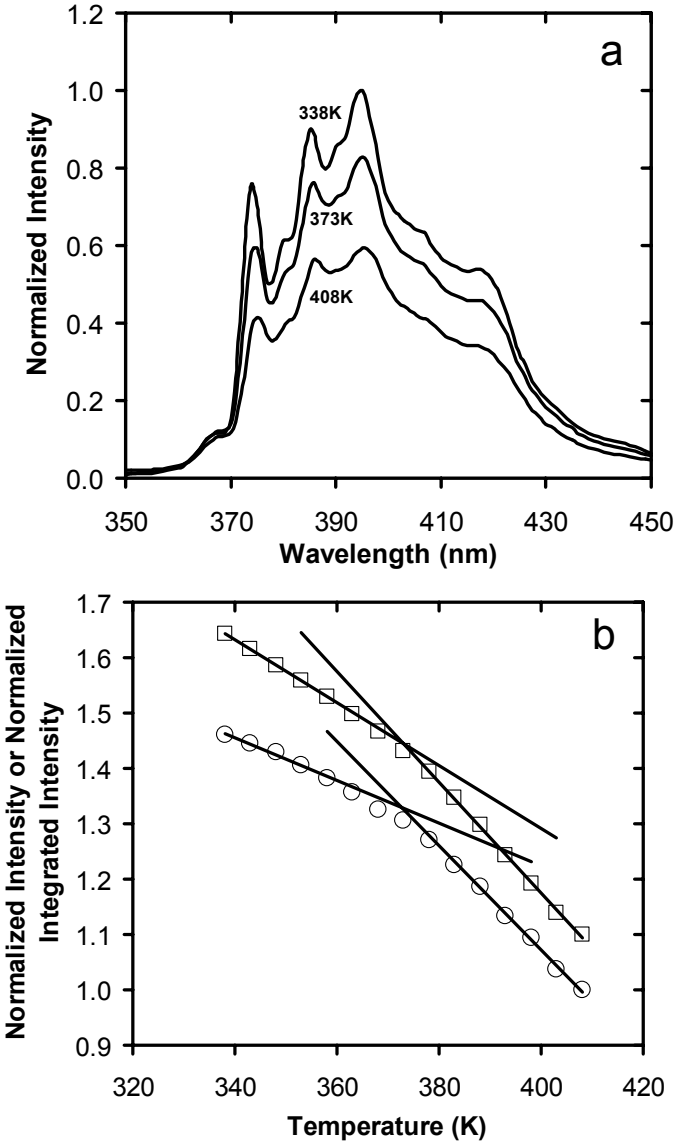

Figure 3-2: **(a)** Fluorescence emission spectra of pyrene dopant (< 0.2 wt%) in an 810-nm-thick PS (*Mn* = 200,000 g/mol) film taken at 338 K, 373 K and 408 K. The inset shows the structure of pyrene. **(b)** Temperature dependence of the fluorescence intensity (○) monitored at an emission wavelength of 400 nm and integrated intensity (□) of pyrene dopant in an 810-nm-thick PS film (*Mn* = 200,000 g/mol, $T_{g,bulk}$ = 373 K). The intensity and integrated intensity have been normalized to one at 408 K and arbitrarily shifted.

Another fluorescence measurable that should be useful in determining *Tg* is the excited-state fluorescence lifetime, an intensive parameter that does not depend on excitation source intensity, sample geometry, absorbance or refractive index. Excited-state lifetimes are obtained from excited-state decay measurements, in which excitation pulses (full width at half maximum is ~1–2 ns, in our case) generated by a laser allow for the collection of emitted photons as a function of time after excitation. Figure 3-3a shows the decay profiles for pyrene doped (0.2 wt% relative to polymer) in a 2150-nm-thick PS film at temperatures ranging from 333K to 413K (top to bottom). All decays are single exponential, allowing for simple determination of the characteristic fluorescence decay lifetime, τ, as a function of PS film temperature. At 333 K, τ = 235 ns. At 413 K, τ = 155.5ns.

Figure 3-3b compares the temperature dependence of τ to that of normalized integrated fluorescence intensity, demonstrating substantial agreement between the two. (Small differences may be associated with the temperature dependence of sample refractive index and absorbance, which impact fluorescence intensity and which exhibit small changes over the relevant temperature range (Beaucage 1993; Ellison 2005c).) The intersections of the rubbery- and glassy-state temperature dependences of τ and intensity yield *Tg* values of 374K and 375 K, respectively, identical within error. Thus, intensive fluorescence measurables can be used to obtain accurate *Tg* measurements. It should be noted that Jager *et al.* (Jager 2005) have recently reported similar ability to measure *Tg* using measurements of τ as a function of temperature. There was more noise in their data than indicated here in Figure 3-3b, presumably because of the much smaller τ values associated with their dye, limiting measurement accuracy.

Besides pyrene, other chromophores can provide sensitivity to the *Tg* of the polymer in which they are present. In some cases, the chromophore may naturally be a part of the polymer, such as the phenyl ring on each repeat unit of PS. (See Figure 3-4a.)

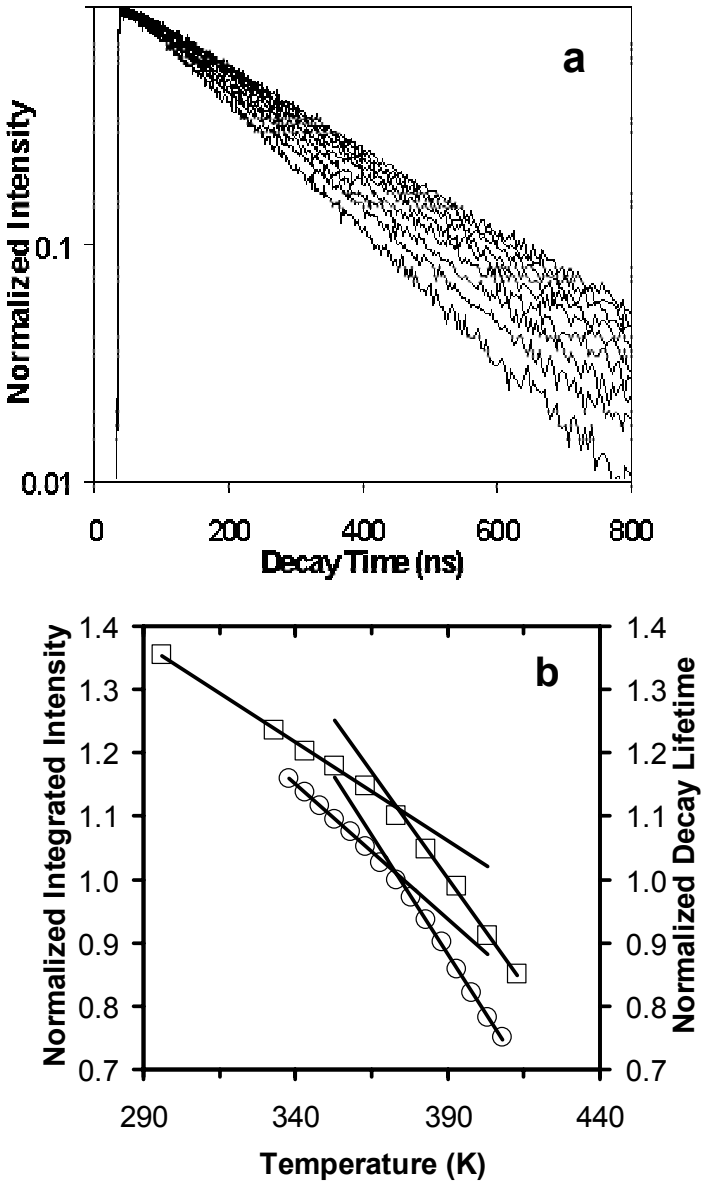

Figure 3-3: (a) Excited-state fluorescence decay profile for pyrene doped (0.2 wt %) into a 2150-nm-thick PS film at temperatures of 333, 343, 353, 363, 373, 383, 393, 403, 413 K (from top to bottom). **(b)** Comparison of the temperature dependence of the normalized decay lifetime (□) for the sample in Figure 3-3a with the temperature dependence of the integrated intensity (○) for an 810-nm-thick pyrene-doped PS film. All data in (b) have been normalized to one at 373 K and arbitrarily shifted vertically for clarity.

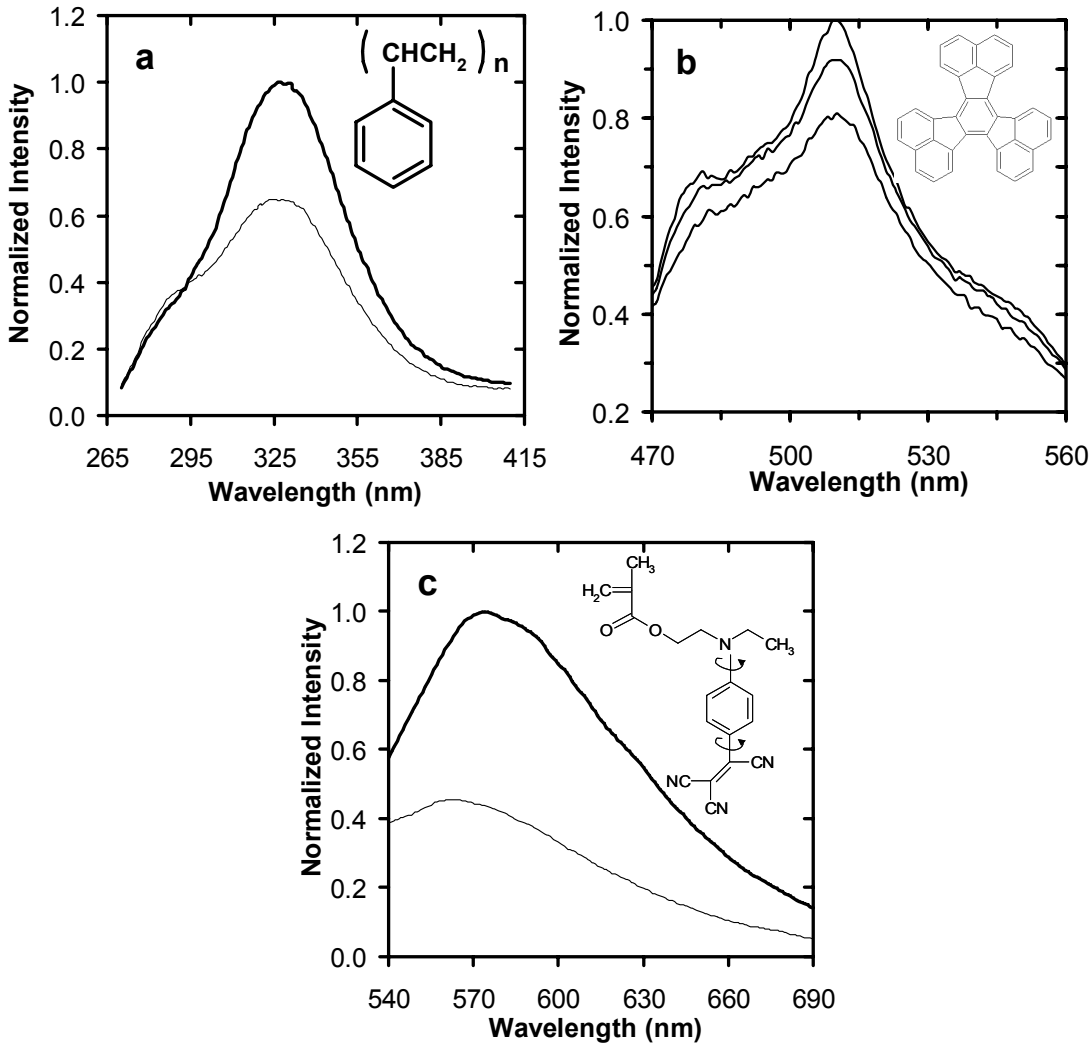

Figure 3-4: **(a)** Intrinsic fluorescence emission spectra for PS (4570-nm-thick film) at 343K (bold curve) and 403K (thin curve). Intensities normalized to one at the peak intensity at 343 K. Inset shows the repeat unit structure of PS. **(b)** Extrinsic fluorescence emission spectra for decacyclene-doped PS (370-nm-thick film) at 408K (bottom curve), 373 (middle curve) and 338K (top curve). Intensities normalized to one at the peak intensity at 338 K. Inset shows the structure of decacyclene. **(c)** Extrinsic fluorescence emission spectra for TC1-labeled-PMMA (200-nm-thick film) at 358K (bold curve) and 423K (thin curve). Intensities normalized to one at the peak intensity at 423 K. Inset shows the structure of TC1-labeled methacrylate monomer used in labeling PMMA.

In other cases, the dye may be an external dopant, as in the case of decacyclene. (See Figure 3-4b.) In yet other cases, the dye may be covalently attached at low levels to the polymer, as in the case of TC1-labeled PMMA. (See Figure 3-4c.) The temperature dependence of the intrinsic fluorescence spectrum of PS is given in Figure 3-4a while the temperature dependences of the extrinsic fluorescence spectra of decacyclene-doped PS and TC1-labeled PMMA are given in Figures 3-4b and 3-4c, respectively. In all cases, an increase in intensity is observed with a decrease in temperature. This is associated with a reduction in non-radiative decay from the excited state with decreasing temperature. The shape of the fluorescence spectrum is nearly invariant with temperature in the case of decacyclene, a situation also observed in the case of pyrene. However, the spectral shapes are significantly temperature dependent in the case of the intrinsic PS fluorescence and the extrinsic fluorescence from TC1-labeled PMMA. The former is due to the fact that PS has two forms of fluorescence, excimer (excited-state dimer) which is centered at ~ 330–335 nm and is associated with fluorescence from an excited-state complex in which two phenyl rings are in a sandwich-like configuration with a separation distance of several Angstroms, and monomer, which is centered at ~ 283 nm and is associated with fluorescence from a single excited-state phenyl ring (Vala 1965). With decreasing temperature, excimer fluorescence, which quenches monomer fluorescence, becomes more favorable. In the case of TC1-labeled polymer, the intramolecular charge transfer nature of the dye yields an excited state that is sensitive to local mobility, meaning that the emission energy and spectral shape are sensitive to temperature and local density (Jager 2005; Hooker 1995).

Figure 3-5 illustrates the temperature dependences of fluorescence intensity for PS and TC1-labeled PMMA for thin and ultrathin films supported on quartz. (While decacyclene doped in PS yields data similar to those of PS in Figure 3-5a for thin films, it has such a low efficiency of fluorescence that it yields insufficient fluorescence intensity

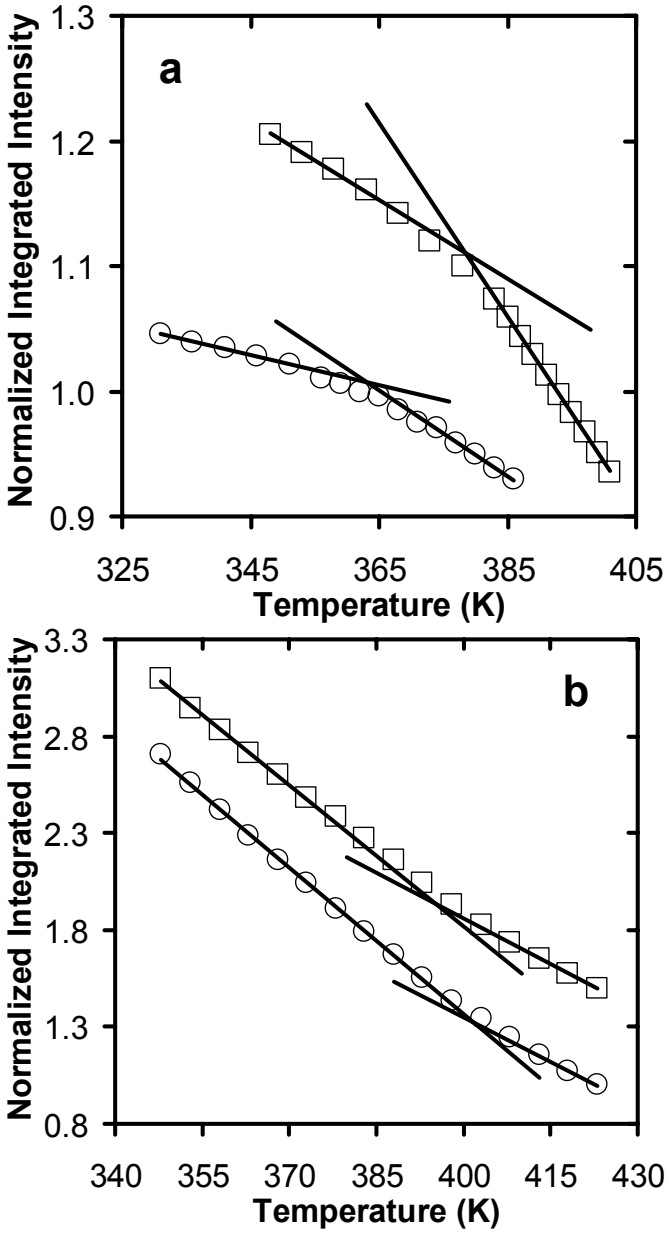

Figure 3-5: **(a)** Temperature dependence of the integrated intrinsic fluorescence intensity of PS in 4570-nm-thick films (□) and 22-nm-thick films (○). *Tg*,bulk = 378 K. (The integrated intensity has been normalized to one at the *Tg* of each film and arbitrarily shifted.) **(b)** Temperature dependence of the integrated fluorescence intensity of TC1-labeled PMMA in 200-nm-thick films (□) and 35-nm-thick films (○). *Tg*,bulk = 395 K. (The integrated intensity has been normalized to one at 423K for each film and arbitrarily shifted.)

in ultrathin films for reliable *Tg* measurements.) For PS, the *Tg* value decreases with decreasing film thickness for thicknesses less than ~ 60 nm; this is understood to originate from enhanced mobility at the free surface of the film which propagates several tens of nanometers into the film (Ellison 2003). In contrast, in the case of TC1-labeled PMMA, the *Tg* value increases with decreasing film thickness. This effect is due to the presence of hydrogen-bonding interactions between ester side groups in PMMA and hydroxyl groups naturally on the surface of the quartz. The hydrogen bonds at the PMMA-substrate interface reduce cooperative segmental mobility in the PMMA films and dominate free surface effects, yielding an increase in *Tg* (Priestley 2007a).

Figure 3-6 compares the film thickness dependence of *Tg* obtained from intrinsic fluorescence of PS to that obtained previously from the fluorescence of pyrene-doped and pyrene-labeled PS (Ellison 2003). Good agreement is observed at all film thicknesses. Furthermore, the *Tg*-nanoconfinement data by Ellison *et al.* (Ellison 2003) were shown to be in excellent agreement with other *Tg*-nanoconfinement data in the literature obtained by ellipsometry (Keddie 1994b). This makes clear that, in the case of *Tg* characterization, the presence of trace levels of pyrene dyes does not significantly perturb the behavior of the polymer.

3.5 Conclusions

Confinement effects in thin and ultrathin polymer films are studied by novel fluorescence techniques. The ability to employ an intensive measurable, the excited-state fluorescence lifetime, in defining the *Tg* of polymers is demonstrated and compared to the use of an extensive measurable, fluorescence intensity. Besides pyrene, other chromophores are also studied for their sensitivity to the *Tg* of the polymer in which they are present. In some cases, the chromophore may naturally be a part of the polymer, such as the phenyl ring on each repeat unit of PS. In other cases, the dye may be an external dopant, as in the case of decacyclene. In yet other cases, the dye may be covalently

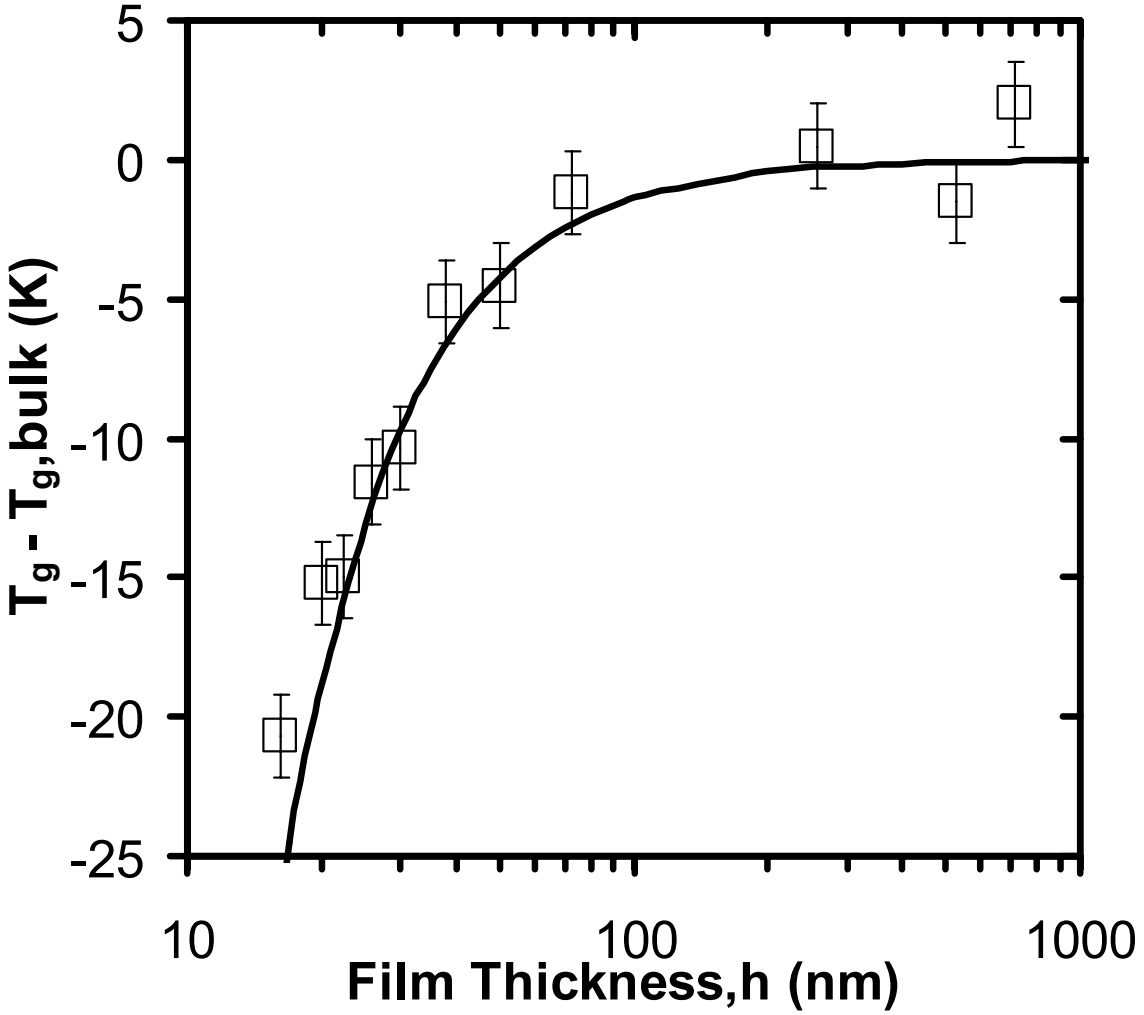

Figure 3-6: *Tg* – *Tg*,bulk (K) as a function of film thickness (*h*) for PS (□) measured by intrinsic fluorescence. The curve represents the best fit to the data published by Ellison *et al.* (Ellison 2005a) to the empirical relation original proposed by Keddie *et al.* (Keddie 1994b), yielding parameter values A = 3.2 nm and δ = 1.63.

attached at low levels to the polymer, as in the case of TC1-labeled PMMA. In addition, intrinsic fluorescence from the phenyl groups in PS is used to determine the *Tg*-nanoconfinement effect in films as thin as ~ 15 nm. The decrease in *Tg* with decreasing film thickness (below ~ 60 nm) agrees well with results obtained by extrinsic pyrene fluorescence (Ellison 2003).

CHAPTER 4

IMPACT OF MOLECULAR WEIGHT ON THE Tg-NANOCONFINEMENT EFFECTS IN SINGLE LAYER POLYSTYRENE (PS) FILMS AND THE STUDY OF COOPERATIVITY LENGTH SCALE

4.1 Introduction

When confined to nanoscale dimension, both low molecular weight (Jackson 1991, 1996; Arndt 1997; Barut 1998; Melnichenko 1995; Schonals 2002; Wang 2004) and polymeric (Keddie 1994a, 1994b, 1995; van Zanten 1996; Kawana 2001, 2003; DeMaggio 1997; Fukao 1999; Forrest 2002; Singh 2004; Miyazaki 2004; Ellison 2002a, 2002b; Tanaka 2004; Li 2004; Blum 2006; Bernazzani 2002; Pratt 2005; Baljon 2005; van den Berg 2004; Fakhraai 2004) glass formers have been widely observed to exhibit glass transition temperatures (*Tg*s) that deviate substantially from their bulk values. This behavior has implications in applications such as photoresists, disk drive lubricants, asymmetric membranes and nanocomposites, among others. This broadly based technological impact and the strong dependence of many key material properties (mechanical, viscoelastic, diffusive, etc.) on the proximity of temperature to *Tg* have driven research efforts in this area.

Thin and ultrathin films have dominated research into nanoconfined polymer behavior due to the ease with which the confining dimension, film thickness, can be varied. Polymer films may be supported by a substrate (Grohens 2002; Park 2004; Sharp 2003a, 2003b, 2003c; Tsui 2001a, 2001b; Kim 2000, 2001; D'Amour 2004; Pham 2002, 2003; Fryer 1999, 2000, 2001; Soles 2004a, 2004b; Hall 1997a; Miyazaki 2004) or freely standing (unsupported) (Forrest 1996, 1997, 1998, 2000, 2001, 2002; Dalnoki-Veress 1999, 2000, 2001; Roth 2003, 2005). For freely standing films, *Tg* decreases with decreasing film thickness. In contrast, for supported polymer films, increases in *Tg* for

polymers with strong attractive substrate interactions (Keddie 1994a; van Zanten 1996; Forrest 2001; Grohens 2002; Pham 2002; Ellison 2002a; Fryer 2001; Mundra 2006) and decreases in *Tg* for polymers with neutral or repulsive substrate interactions (Keddie 1994a, 1994b, 1995; Kawana 2001; DeMaggio 1997; Fukao 1999, 2000; Forrest 1997, 2001; Singh 2004; Miyazaki 2004; Ellison 2002a, 2002b, 2003, 2005a, 2005b; D'Amour 2004; Mundra 2006; Rittigstein 2007) have been observed with decreasing thickness. In a few cases involving copolymers with comonomer units that exhibit attractive and neutral or repulsive substrate interactions, *Tg* has been observed to be nearly invariant with film thickness (Park 2004; Hall 1997a; Mundra 2006). Various methods have been used to characterize *Tg* in polymer films including dielectric relaxation spectroscopy (Fukao 1999, 2000), fluorescence spectroscopy (Ellison 2003; Mundra 2007b; Priestley 2007b, 2007c; Rittigstein 2007; Roth 2007a, 2007b), Brillouin scattering (Forrest 1996, 1997, 1998, 2000), ellipsometry (Keddie 1994a, 1994b, 1995; D'Amour 2004; Park 2004; Pham 2003; Fryer 2001; Roth 2003, 2005), x-ray reflectivity (van Zanten 1996; Miyazaki 2004; Fryer 2001; Tsui 2001a, 2001b) and nonlinear optics (Hall 1997a).

Many postulates have been offered regarding the origin of these effects (Forrest 2001) in systems lacking attractive polymer-substrate interactions: internal stresses caused by film preparation methods (e.g. spin coating) (McKenna 2000; Bernazzani 2002); a "finite size effect" due to the thickness approaching a fundamental length scale associated with glass formers (Keddie 1994b), e.g. the cooperatively rearranging region (CRR) introduced by Adam and Gibbs (Adam 1965); interfacial effects involving a reduced entanglement concentration (Tsui 2001a; McKenna 2000; Bernazzani 2002; Brown 1996) or a segregation of chain ends to the free surface (air-polymer interface) (Tsui 2001a; Mayes 1994); and a radius of gyration (*Rg*) that is on the order or a small multiple of the film thickness, *h* (Singh 2004; Dalnoki-Veress 2001). With supported polystyrene (PS) films, two reviews (Kawana 2001; Forrest 2001) have found extensive

agreement for the *Tg*-nanoconfinement effect across many measurement methods: when scaled according to the bulk *Tg* as *Tg*(*h*)/*Tg*,bulk, the thickness dependence of *Tg* has been found to be approximately independent of PS molecular weight (*MW*) (Kawana 2001; DeMaggio 1997; Fukao 2000; Forrest 2001; Tsui 2001a) over a *MW* range of 3,600-2,900,000 g/mol. At this point, it should be noted that it is still unclear whether the appropriate *Tg* scaling is in terms of a departure from bulk *Tg* as *Tg*(*h*) - *Tg*,bulk or in terms of a reduced *Tg* as *Tg*(*h*)/*Tg*,bulk.

The notion that internal stresses cause the *Tg*-nanoconfinement effect may be refuted by the agreement among many studies of supported PS films (Kawana 2001; Forrest 2001) in which films of similar thickness were prepared using different solutions (solvent type and polymer concentration) and preparation conditions (spin coating speed). However, related studies of ultrathin PS (Kanaya 2003; Orts 1993) and polycarbonate (Soles 2004a) films have shown the existence of a negative thermal expansivity in the glassy state which has been attributed to a non-relaxed structure that is set in during spin coating (Miyazaki 2004; Kanaya 2003). This effect, which exhibits little impact on *Tg* (Kanaya 2003), can be removed by annealing at *Tg*,bulk + 50 K for 2 hr (Kanaya 2003; Miyazaki 2004).

There has been interest (Forrest 2001) in connecting the size scale at which nanoconfinement effects are observed to the size scale of a CRR. (Adam and Gibbs (Adam 1965) introduced the concept of a CRR in which local relaxation occurs by the collective motion of many molecules or polymer segments.) The length scale of a CRR near *Tg* has been investigated by differential scanning calorimetry (Donth 1982, 1984, 1996, 1999, 2000, 2001; Hempel 2000; Vyazovkin 2004; Tran 2004; Robertson 2004; Ellison 2005a; Korus 1997; Mitteilungen 1982; Khale 1999), 4D-NMR (Barut 1998; Tracht 1998; Reinsberg 2001; Qin 2003) and other techniques (Arndt 1996, 1997; Hong 2002; Erwin 2002; Richert 1996) and has been reported to lie in the range of ~ 1-4 nm for

low *MW* and polymeric glass formers. However, the length scale at which nanoconfinement effects are observed is ~ 10 nm or less for low *MW* glass formers (Jackson 1991; Arndt 1997; Barut 1998; Melnichenko 1995; Schonals 2002; Wang 2004) and ranges from several tens to more than one hundred nanometers for polymers (Keddie 1995; Fukao 2001, 2002, 2003; Ellison 2005a; Dalnoki-Veress 2001; D'Amour 2004; Pham 2002, 2003; Fryer 1999, 2000, 2001; Soles 2004a, 2004b). This indicates that the length scale of a single CRR is far less than the thickness at which *Tg*-nanoconfinement effects are observed.

Recent understanding gained from fluorescence experiments (Ellison 2003) has reiterated this point. These experiments have revealed via multilayer PS films with fluorescent labels in only one layer that the free-surface effect causes a *Tg* reduction that persists several tens of nanometers into the film interior (much larger than a single CRR). Furthermore, it was observed (Ellison 2003) that a region of reduced *Tg* near the free surface exists as a continuous distribution of *Tg*s that depends on the degree of nanoconfinement. These results have shown directly that two-layer and three-layer models (van Zanten 1996; Kawana 2001; DeMaggio 1997; Fukao 2000; Forrest 2000, 2001) are inadequate to explain *Tg*-nanoconfinement behavior and that a model that incorporates a continuous distribution of *Tg*s across the thickness of a film is needed (Priestley 2005b, 2007a; Roth 2007a, 2007b). This picture is consistent with recent simulations (Jain 2004) and predictions from theoretical pictures (Herminghaus 2004; Merabia 2004; Berriot 2002, 2003).

Many studies (Wang 2004; Keddie 1994b; Forrest 2001; Sharp 2003a; Schwab 2000; Jean 1997; Torres 2000; Pochan 2001; Kajiyama 1997) have indicated that interfacial effects are the most logical explanation for the underlying cause of the *Tg*-nanoconfinement effect. Numerous studies have concluded (Ellison 2003; Roth 2007a, 2007b; Jain 2004; Herminghaus 2004; Merabia 2004; Schwab 2000; Jean 1997; Torres

2000; Pochan 2001; Kajiyama 1997) that the free-surface *Tg* of bulk PS films is some tens of degrees lower than the bulk *Tg*. Supporting the importance of free-surface effects for PS, a recent study (Sharp 2003a) has shown that removing the free-surface interface by placement of aluminum (Al) or gold (Au) metal onto the film results in a *Tg* that is independent of thickness down to 10 nm or less. The key role of interfacial effects is also supported by studies of the thickness dependence of *Tg* for polymers with attractive substrate interactions (Keddie 1994a; van Zanten 1996; Forrest 2001; Grohens 2002; Pham 2002; Ellison 2002a, 2002b; Fryer 2001; Mundra 2006, 2007a, 2007b; Priestley 2005a, 2005b; Rittigstein 2007), e.g. poly(2-vinylpyridine) and poly(methyl methacrylate) on silicon (with native oxide) or glass substrates which exhibit increases in *Tg* with decreasing thickness due to the attractive substrate interactions.

Although there is substantial evidence supporting a free-surface effect as the origin of *Tg* reductions in nanoconfined PS films, there is not yet a detailed understanding of the free-surface effect. A simple explanation is that polymer segments that lie at the free surface possess fewer conformational restrictions than those in the bulk and thus have a higher degree of cooperative segmental mobility and an associated lower *Tg*. While this explanation is logical, it lacks details regarding the extent to which interfaces may be expected to modify cooperative segmental mobility or *Tg* from that of bulk. Others have offered the explanation that the free surface results in a reduced entanglement concentration (Tsui 2001a; McKenna 2000; Bernazzani 2002; Brown 1996), which in turn yields enhanced mobility and reduced *Tg* near the free surface. However, this explanation can be criticized because a thickness dependent *Tg* has been observed for both entangled and unentangled PS (Kawana 2001; DeMaggio 1997; Fukao 2000; Forrest 2001; Tsui 2001a) (*Mc*, the critical entanglement *MW*, is ~ 35,000-38,000 g/mol (Sperling 1992; Majeste 1998) for PS) and because bulk *Tg* does not depend on chain entanglements (Sperling 1992).

Another potential explanation involves the segregation of chain ends to the free surface that would be expected to reduce the local *Tg* at the free surface (Tsui 2001a; Mayes 1994). However, if chain ends were the origin of this effect, it would be expected that the thickness dependence of *Tg* could be significantly altered by varying the surface chain-end concentration by modification of the polymer *MW* (Mayes 1994), which is not supported by experimental data. Variation of polymer *MW* also greatly alters the *Rg* of the bulk polymer, which in turn would significantly affect the film thickness at which overall chain conformation would be expected to differ substantially from bulk. For example, when PS *MW* is increased from 3,600 g/mol to 10,000,000 g/mol, the bulk *Rg* increases from ~ 2 nm to 87 nm (using a characteristic ratio of 10 to calculate *Rg*) (Sperling 1992; Flory 1989). (It is important to note that the overall chain conformation is likely altered in nanoconfined films, adopting, on average, an ellipsoidal conformation with a large aspect ratio as opposed to the random coil expected in bulk.) Some have argued that such an effect may yield a *MW* dependence of the *Tg*-nanoconfinement effect (Singh 2004; Fukao 1999). In opposition to this picture is a large body of evidence (Kawana 2001; DeMaggio 1997; Fukao 2000; Forrest 2001; Tsui 2001a) indicating that the *Tg*-nanoconfinement effect for supported PS films is approximately independent of *MW* indicating that neither chain ends nor bulk *Rg* plays a significant role in defining this effect.

It is noteworthy that two very recent studies (Singh 2004; Miyazaki 2004) of supported PS films have reported a *MW* dependence of the *Tg*-nanoconfinement effect in the range of 212,000-2,900,000 g/mol. Singh *et al.* (Singh 2004) reported that the thickness dependence of *Tg* for a variety of PS *MW*s can be collapsed onto a master curve when thickness is scaled as $h/Rg(\text{bulk})$ and *Tg* is scaled as $Tg(h)/Tg,\text{bulk}$. While the study by Miyazaki *et al.* (Miyazaki 2004) was largely focused on thermal expansion effects, it also reported a larger *Tg*-nanoconfinement in ultrathin films of higher *MW*

(2,890,000 g/mol vs. 303,000 g/mol) PS down to ~ 10 nm in thickness. It should be noted that both (Singh 2004; Miyazaki 2004) have measured *Tg* upon heating from the glassy state after prior annealing at 408 K for 20-48 h or 423 K for 48 h.

Inspired by this recent disagreement regarding the impact of *MW* on the *Tg*-nanoconfinement effect in supported PS films, this chapter describes research on the *Tg*-nanoconfinement effect for the largest range of *MW*s examined to date in a single study of supported PS films. This chapter also details the effect of *MW* and slight modification to the repeat unit structure of PS on the cooperativity length scale at *Tg* as measured by differential scanning calorimetry methods.

4.2 Experimental

4.2.1 Materials and Methods

Polystyrene standards were purchased from Polysciences Inc. and Pressure Chemical Co. and used as received. Samples of PS films with *Mn* = 5,000 g/mol were prepared by co-dissolving a high *MW* PS standard (*Mn* = 200,000 g/mol) with a low *MW* PS standard (*Mn* = 1,850 g/mol) in toluene (99.9% purity) prior to film preparation. Pyrene-labeled PS was synthesized by copolymerizing a 1-pyrenyl butyl methacrylate with styrene resulting in a polymer with 1 in 170 repeat units being a pyrene-labeled methacrylate. (Further details of the synthesis of 1-pyrenyl butyl methacrylate are reported in Chapters 5, 10 and in references by Deppe *et al.* (Deppe 1996a, 1996b, 1996c) and by Ellison *et al.* (Ellison 2003, 2005c).) Poly(4-methylstyrene) (P4MS) was from Scientific Polymer Products and used as received. Poly(4-tert-butylstyrene) (PTBS) and glycerol (99.5+%) were from Aldrich. Due to the presence of 4-tert-butylstyrene monomer in the as-received polymer, the PTBS sample was dissolved in toluene (99.9% purity) and precipitated seven times in methanol (99.9% purity) to ensure monomer removal prior to use. The *Tg*,bulk values were measured as *Tg*,onset values by differential scanning calorimetry (DSC) (Mettler Toledo DSC822) on second heat at 10

K/min. For samples employed in the small molecules diluent addition studies for the estimation of size scale of cooperatively rearranging regions (CRRs), DSC samples were prepared by spin coating ~ 2 micron thick films and scraping them from a glass slide. Polymer *MW* was determined by gel permeation chromatography (GPC) (Waters) relative to a PS calibration. Table 4-1 provides details on values of *Mn*, *Mw*/*Mn*, *Tg*,bulk by DSC and *Tg*,bulk as determined by this fluorescence method for the neat polymer and other samples containing low molecular weight diluents. Pyrene (Aldrich Chemical, 99+% purity) and dioctylphthalate (DOP) (Aldrich, 99%) were used as received.

4.2.2 Thin and Ultrathin Film Synthesis

Thin films were prepared by spin coating (Hall 1998a) dilute solutions of polymer in toluene onto glass slides. Dioctyl phthalate used as low molecular weight diluent was introduced into the films by codissolving it with the polymer in toluene and then spin coating. The glass slides (VG9 ionically doped float glass filters (Schott Glass© 2007), 2"x2", 2 mm thick) were initially washed with a 10% sodium hydroxide/70% ethanol/20% water solution upon receipt and then solvent washed between experiments. Film thickness was measured with a Tencor P10 profilometer. Calibration of the profilometer was verified using a 14-nm-step-height standard (VLSI standards). At least ten measurements were taken in total at different locations close to the center of the film (where fluorescence was measured) and averaged with the typical standard deviation in these measurements being less than 1.5 nm for films thicker than ~ 20 nm and ~ 1.0 nm for films thinner than ~ 20 nm.

4.2.3 Instrumentation

A Spex Fluorolog-2DM1B fluorimeter was used for steady-state fluorescence measurements. Measurements employed a front-faced geometry with 2.5 mm excitation and emission slits (bandpass = 4.5 nm) for films with thickness less than 100 nm and 1.25 mm excitation and emission slits (bandpass = 2.25 nm) for films with thickness greater

Table 4-1: Molecular Weight and Bulk *Tg* for Materials Employed in this Study.

Material	*Mn* (g/mol)	*Mw*/*Mn*	*Tg*, bulk (K) (onset, DSC)	*Tg*, bulk (K) (fluor.)
PS	23,000,000	1.30	374	---
PS	3,000,000	1.05	374	373
PS	400,000	1.06	375	---
PS	263,000	1.10	373	373
PS	200,000	1.08	373	373
PS	13,500	1.06	368	---
PS	12,000	1.10	365	364
PS	5,000	bimodal[a]	358	358
PS	1,850	1.14	333	---
PS	800	1.11	269	---
PS	568	1.13	248	---
P4MS	279,000	1.57	376	376
PTBS	32,000	3.31	404	404
PS w/ pyrene label	440,000	1.73	369	371
glycerol	---	---	188	---
PS[b] + 4 wt% DOP	400,000[d]	1.06	361	---

[a] Blend of 1,850 g/mol and 200,000 g/mol PS
[b] PS with *Mn* = 400,000 g/mol was used for CRR measurements

than 100 nm. In the worst case, the signal-to-noise ratio exceeded 30. The probe (pyrene) content in each film was less than 0.2 wt% of dry polymer content. (At probe concentrations less than 0.2 wt%, the *Tg* of pyrene-doped polymer is the same within error as that of neat polymer) A clean quartz cover slide was placed on top of each film to reduce the potential for probe sublimation during the *Tg* measurement by fluorescence. (The film was adhered only to the glass substrate on which it was spin coated.) Film temperature was controlled by a microprocessor controller (Minco Products) with a Kapton ribbon heater attached to a flat aluminum plate that was also used as a clamping device to hold the sample. The excitation wavelength was 322 nm, and the emission spectrum was measured at 350 - 450 nm. Fluorescence spectra were recorded upon cooling after having annealed samples at ~ *Tg* + 40 K for 15 min. In the case of the PS with *Mn* = 3,000,000 g/mol, samples were annealed at ~ *Tg* + 40 K for 45 min; in the case of PS with *Mn* ≤ 12,000 g/mol, dewetting problems were reduced or eliminated by annealing for 15 min at ~ *Tg* + 35 K.

In fitting the temperature dependence of fluorescence in the rubbery and glassy states, only data points well outside *Tg* were used for the linear fits, and typical correlation coefficients (R^2) were better than 0.990. To initiate the fitting procedure, data points were added to the rubbery- and glassy-state linear regressions one-by-one at the extrema in the temperature range of the data. The correlation coefficient was monitored as more data points were added (approaching *Tg* from the extrema in the temperature range of the data) to each of the linear regressions. If the R^2 value began to steadily decrease below a threshold value (i.e., < 0.990) as more data points were added, then these data points were removed to produce a value of R^2 higher than the threshold value and the linear regressions were considered acceptable. The linear fits in both the rubbery and glassy states included a minimum of four fluorescence data points (usually more), spanning a minimum of 15 K in temperature. This procedure was followed regardless of

whether fitting linear functions to the fluorescence intensity data at particular emission wavelength(s) or the integrated intensity as a function of temperature. When using integrated intensities to identify *Tg*, spectra were taken over a sufficient range of wavelengths that integration could be done from instrument baseline at the lowest wavelengths to the same instrument baseline at the highest wavelengths. In all cases, regardless of using intensities or integrated intensities, the sample was reheated to the starting temperature following the measurements taken upon cooling to verify that the sample did not lose a substantial amount of fluorescence probe molecules due to photobleaching, sublimation, etc. Typically, the intensity after reheating the sample is within 10% of the original intensity before the measurements were taken upon cooling.

Fluorescence intensities were only used to identify *Tg* for pyrene-labeled PS samples. For pyrene-labeled PS, fluorescence was measured using an excitation of ~ 340 nm and monitoring emission intensity at the peaks of ~ 378 and 398 nm. When fitting the temperature dependence of the fluorescence intensity data at the peaks in the emission spectra, the standard deviation in the determination of *Tg* at the various peaks in the emission spectra was typically less than 1.0 K for each sample. This is comparable to the estimated standard variation (or error) in *Tg* (+/- 1.0 K or less) from sample to sample (identified either using intensities or integrated intensities) for films of identical thickness on identical substrates when the film thickness is greater than ~ 25 nm. For film thickness below ~ 25 nm, the estimated standard variation (or error) is +/- 2 K. (Further details on measurement of *Tg* by fluorescence can be found in Chapter 3 and in references by Ellison *et al.* (Ellison 2002a, 2002b, 2005c).)

4.2.4 Using the DSC Method by Donth to Characterize the Size of a CRR

Differential scanning calorimetry (Mettler Toledo DSC822) was used to measure the heat capacity for the determination of the size of the CRR (Donth 1982, 1984, 1996, 1999, 2000, 2001; Hempel 2000; Vyazovkin 2004; Tran 2004; Robertson 2004; Ellison

2005; Korus 1997; Mitteilungen 1982; Khale 1999). Initially, the furnace was heated to 973 K in the presence of oxygen to oxidize any impurity present from previous use. Specific heat capacities were measured against a sapphire standard. A blank pan was run followed by a sapphire standard immediately prior to characterization of each polymer sample. (Slight variation was observed in the blank sample curves over the course of multiple measurements. This variation is normal and was within the specification expected by the equipment manufacturer and was accounted for appropriately during the measurement of heat capacities). The calibration of the DSC instrument was regularly monitored via an indium standard. All DSC measurements were taken on the second heating cycle at the rate of 10 K/min after quenching from elevated temperature at the rate of 40 K/min. Approximately 10 milligram samples in 40 microliter aluminum pans were annealed for at least 45 min at the elevated temperature (353 K for PS *Mn* = 800 g/mol and PS *Mn* = 568 g/mol, and 473 K for the other samples) before quenching to erase prior thermal history and, even more importantly, to optimize sample-pan contact. Unless otherwise specified, all thermograms used in heat capacity measurements and thereby the determination of the size of the CRR were taken from *Tg*,bulk – 70 K to *Tg*,bulk + 70 K in order to measure baselines accurately. The reported heat capacity values are averages of a minimum of six runs.

Differential scanning calorimetry (DSC) thermograms were used to determine the unknown parameters from the fluctuation formula (Donth 1982, 1984, 1996, 1999, 2000, 2001; Hempel 2000):

$$V_{CRR} = \xi^3_{CRR} = k_B Tg(\text{mid})^2 \Delta(1/Cv)/(\rho \delta T^2) \qquad 4.1$$

where V_{CRR} is the volume of one CRR at *Tg*, ξ_{CRR} is the size of a single CRR at *Tg*, k_B is the Boltzmann constant, *Tg*(mid) is the Richardson (equal area construction) midpoint *Tg*, $\Delta(1/Cv)$ is the step change in $1/Cv$ at the dynamic *Tg*, ρ is density of bulk polymer at its *Tg*, δT is the mean-square temperature fluctuation of one average CRR, and *Cv* is the

constant volume heat capacity. The origin of this formula comes from the idea that there are thermal fluctuations in both time and space in a sample which results in associated fluctuations in local density and heat capacity and may be derived from the fluctuation dissipation theorem (Donth 1982, 1984, 1996). The calculation of the number of repeat units present in one CRR is given by the following equation:

$$N_{CRR} = (\rho\, V_{CRR}\, \mathrm{N_A})/Mo \qquad 4.2$$

where $\mathrm{N_A}$ is Avogadro's number and *Mo* is the single repeat unit molecular weight.

In Donth's construction, $\Delta(1/Cv)$ is estimated to be $\Delta(1/Cp)$ where *Cp* is the constant pressure heat capacity. The error in this estimation may be summarized by a parameter *S* where $S = \Delta(1/Cv)/\ \Delta(1/Cp)$ (Hempel 2000). Using data from O'Reilly (O'Reilly 1962; 1977a; 1977b), Hempel *et al.* (Hempel 2000) estimated that $S = 0.74 \pm 0.22$ for 14 different polymers and 4 different small molecule glass formers with the S value extrema at 1.07 and 0.26. Donth used the average *S* parameter to make corrections to all of his V_{CRR} and ξ_{CRR} data. No correction has been made to the V_{CRR} and ξ_{CRR} data to avoid overgeneralization of how *Cp* relates to *Cv* for all of the samples. However, this factor of *S* nearly exactly accounts for the difference between the ξ_{CRR} value of ~ 3.5 nm for PS obtained in this study and that measured by Hempel *et al.* (Hempel 2000) of ~ 3.0 nm.

For small heat capacity steps across *Tg*, $\Delta(1/Cp) \approx \Delta Cp/Cp^2$ where ΔCp is the difference between the rubbery and glassy state heat capacities at *Tg*(mid) and *Cp* is the average of the rubbery and glassy state heat capacities at *Tg*(mid). Figure 4-1 shows *Cp* as a function of temperature for a PS sample. The values of *Cp* in the rubbery and glassy regions are obtained by extending tangents of *Cp*(*T*) from deep in the rubbery and glassy states and are identified as the intersection points of the extrapolated lines with *Tg*(mid) as shown in Figure 4-1. The value of ΔCp is determined by ΔCp = *Cp*(rubbery) - *Cp*(glassy), while *Cp* is obtained by *Cp* = {*Cp*(rubbery) + *Cp*(glassy)}/2.

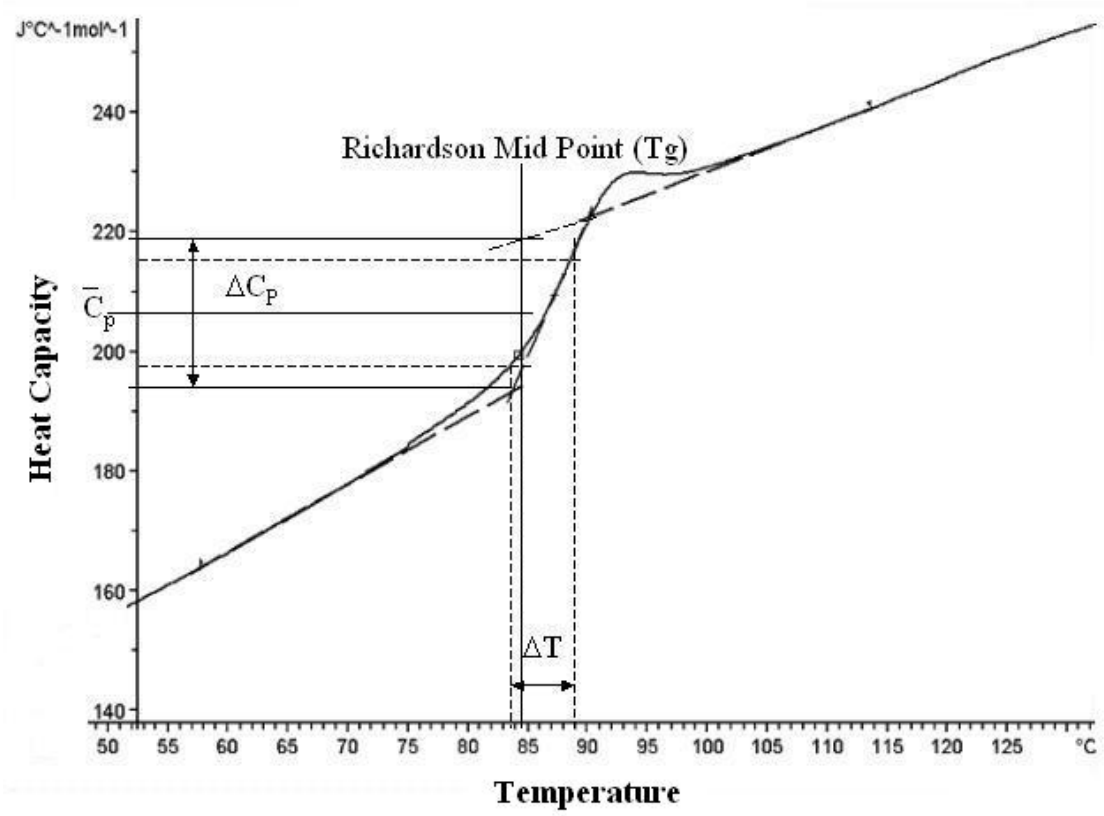

Figure 4-1: Sample *Cp* as a function of temperature for PS and the generalized construction of the method developed by Donth (Donth 1982) for determining the size of a CRR from ordinary DSC thermograms.

The experimental approach for determining the size of the CRR using a regular DSC method involves some "rules of thumb" for determining the δT parameter prescribed by Donth (rather than the more rigorous method by Donth involving determination of δT from the Kohlrausch-Williams-Watts exponent in conjunction with measurements by thermally modulated DSC); he has argued (Hempel 2000) that the accuracy of the characteristic size of a CRR determined using regular DSC is estimated to be within 85% and 125% of the calculated value. The "rule of thumb" for using DSC heating curves to obtain δT is that $\delta T = \Delta T / 2.5$, where ΔT is the temperature interval where the specific heat capacity thermogram varies between 16% and 84 % of the ΔCp step as shown in Figure 4-1. As described above, exactly the same procedure was applied to all the measurements. In all cases, the bulk polymer *Mo* and ρ values were used in the fluctuation formula. For all experiments in this study, the average standard deviations (expressed as a percentage of the average value) for ΔCp, Cp, δT, Tg(mid), ξ_{CRR}, N_{CRR} were 10.5, 9.9, 9.9, 0.27, 4.8 and 14.5 %, respectively. Table 4-2 shows the values for all the six measurements for PS (Mn = 800 gm/mol). A similar procedure was followed for the rest of the systems. Table 4-3 lists the average parameter values for all the systems while Table 4-4 shows the standard deviations for each of the variables of the various systems studied.

The density values used in the fluctuation formula were calculated from the volumetric parameters given by Richardson *et al.* (Richardson 1977). For each *MW* whose volumetric parameters were not known, two neighboring *MW*s were used, and then the value was obtained by linear interpolation. Densities were calculated at Tg – 15 K and Tg + 15K. Averages of these two values were used as the density value at Tg in all the calculations. For the Mn = 568 g/mol PS sample, the values for Mn = 580 g/mol were used for the density calculations.

Table 4-2: Parameter Values/Sample-to-Sample Reproducibility for the Calculation of ξ_{CRR} and N_{CRR}.

Samples (PS[a])	ΔCp[b] (J/gK)	Cp[b] (J/gK)	δT (K)	Tg(mid) (K)	ξ_{CRR}(nm)	N_{CRR}
1	0.408	1.558	2.64	268.19	2.85	138.7
2	0.395	1.414	2.56	270.50	3.09	176.0
3	0.383	1.288	2.92	270.90	2.99	158.8
4	0.423	1.365	2.88	270.99	3.00	160.6
5	0.386	1.229	3.04	271.63	3.01	162.8
6	0.471	1.399	3.00	270.72	2.97	156.7
Average	0.411	1.375	2.84	270.49	2.99	158.9
Std. Dev.	0.033	0.114	0.20	1.19	0.08	12.0

[a] Mn = 800 g/mol

[b] In Donth's method $\Delta(1/Cv)$ is approximated as $\Delta(1/Cp) \approx \Delta Cp/Cp^2$.

Table 4-3: Average Parameter Values for the Calculation of ξ_{CRR} and N_{CRR}.

Systems	ΔCp[h] (J/gK)	Cp[h] (J/gK)	δT (K)	Tg(mid) (K)	ρ (gm/cm^3)	ξ_{CRR}(nm)	N_{CRR}
PS[a]	0.372	1.147	2.93	250.86	1.04	3.03	170
PS[b]	0.411	1.375	2.84	270.49	1.03	2.99	159
PS[c]	0.258	1.732	2.11	358.25	1.03	3.20	198
PS[d]	0.322	1.838	2.05	368.47	1.03	3.46	248
PS[e]	0.261	1.741	1.98	377.18	1.03	3.47	249
PS[f]	0.277	1.873	1.90	377.19	1.03	3.48	253
PS[g]	0.262	1.804	1.86	377.14	1.03	3.55	269
P4MS	0.254	1.819	2.03	384.32	1.04	3.33	195
PTBS	0.226	2.119	2.61	405.03	0.95	2.61	64
PS[e] + 4wt% DOP	0.270	1.629	2.65	362.22	1.04	2.99	162
Glycerol	0.945	1.394	2.23	187.27	1.325	3.31	316

[a] Mn = 568 g/mol
[b] Mn = 800 g/mol
[c] Mn = 5,000 g/mol
[d] Mn = 13,500 g/mol
[e] Mn = 400,000 g/mol
[f] Mn = 3,000,000 g/mol
[g] Mn = 23,000,000 g/mol
[h] In Donth's method $\Delta(1/Cv)$ is approximated as $\Delta(1/Cp) \approx \Delta Cp/Cp^2$.

Table 4-4: Standard Deviation for the Average Parameter Values Used in the Calculation of ξ_{CRR} and N_{CRR} Given in Table 4-3.

Systems	ΔCp[h] (J/gK)	Cp[h] (J/gK)	δT (K)	Tg (mid) (K)	ρ (gm/cm$^{3)}$	ξ_{CRR} (nm)	N_{CRR}
PS[a]	0.042	0.134	0.18	1.52	NA[i]	0.17	28.10
PS[b]	0.033	0.114	0.20	1.19	NA	0.08	12.04
PS[c]	0.034	0.204	0.26	0.86	NA	0.20	36.18
PS[d]	0.022	0.092	0.10	0.42	NA	0.07	14.60
PS[e]	0.006	0.145	0.14	0.12	NA	0.11	24.14
PS[f]	0.023	0.139	0.22	0.11	NA	0.17	36.55
PS[g]	0.036	0.189	0.15	0.50	NA	0.21	49.80
P4MS	0.042	0.191	0.26	0.41	NA	0.14	24.77
PTBS	0.034	0.202	0.28	0.86	NA	0.17	12.73
PS[e] + 4wt% DOP	0.027	0.254	0.49	2.86	NA	0.21	33.81
Glycerol	0.048	0.116	0.12	0.53	NA	0.16	47.67

[a] Mn = 568 g/mol
[b] Mn = 800 g/mol
[c] Mn = 5,000 g/mol
[d] Mn = 13,500 g/mol
[e] Mn = 400,000 g/mol
[f] Mn = 3,000,000 g/mol
[g] Mn = 23,000,000 g/mol
[h] In Donth's method $\Delta(1/Cv)$ is approximated as $\Delta(1/Cp) \approx \Delta Cp/Cp^2$.
[i] NA = not applicable

4.3 Polystyrene Films

4.3.1 Comparison of Tg-Nanoconfinement Effects as a Function of PS Molecular Weight

Figure 4-2(a) shows the fluorescence emission spectrum of pyrene dopant in an 810-nm-thick PS film. There is a significant reduction in overall intensity with increasing temperature (*T*). Previous studies have shown (Ellison 2002a, 2002b, 2003, 2004a) that *Tg* values can be obtained by plotting the intensity near one or several of the peak wavelengths (~ 374, 385, and 395 nm) as a function of *T*. Over a 70-80 K *T*-range roughly centered at *Tg*, two linear *T*-dependences of intensity are observed, a stronger one in the rubbery state and a weaker one in the glassy state, with the intersection being identified as *Tg*. Careful inspection of Figure 4-2(a) reveals that the exact values of the two slopes in such a plot may depend on the emission wavelength selected, because the *T*-dependence of intensity is stronger at the maxima (peaks) than at the minima (valleys) of the emission spectrum. Such effects have been observed by others (Vigil 1997; Brown 2004) studying the *T*-dependence of pyrene fluorescence in various polymers and can be attributed to the *T*-dependence of the different vibronic bands of pyrene. In addition to these effects, there are slight blue shifts in the emission spectrum of pyrene (1-2 nm) as *T* is decreased from 413 K to 333 K. In order to minimize these effects, we have chosen to plot values of integrated intensity as a function of *T*. Figure 4-2(b) compares the *T*-dependence of integrated intensity to that of intensity at 400 nm; while the same *Tg* value (373 K) is determined from both plots, there is discernable difference in the *T*-dependences of intensity at 400 nm and the integrated intensity over a common *T* range.

Figure 4-3(a) shows the *T*-dependence of integrated intensity for PS with *Mn* = 5,000 g/mol at two thicknesses (500 nm and 29 nm, *Tg* = 356 K and 344 K, respectively). Similarly, Figure 4-3(b) shows a higher *MW* PS with *Mn* = 200,000 g/mol at two thicknesses (24 nm and 810 nm, *Tg* = 358 K and 373 K, respectively). In accord with

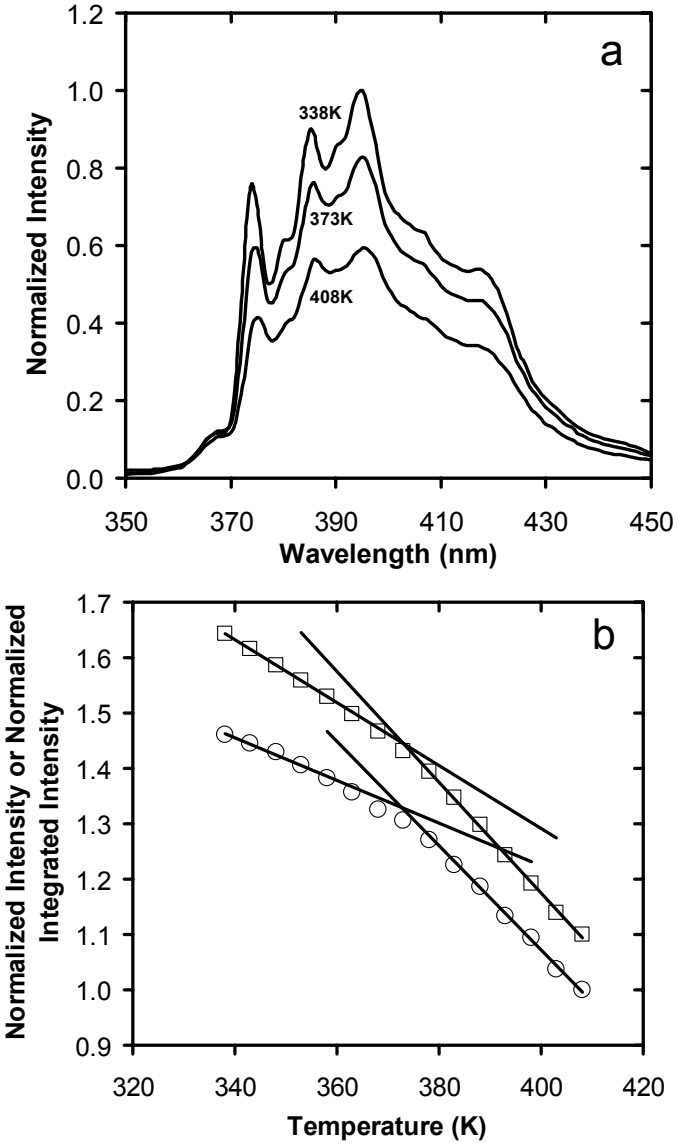

Figure 4-2: **(a)** Fluorescence emission spectra of pyrene dopant (< 0.2 wt%) in an 810-nm-thick PS (*Mn* = 200,000 g/mol) film taken at 338 K, 373 K and 408 K. The inset shows the structure of pyrene. **(b)** Temperature dependence of the fluorescence intensity (○) monitored at an emission wavelength of 400 nm and integrated intensity (□) of pyrene dopant in an 810-nm-thick PS film (*Mn* = 200,000 g/mol, $T_{g,bulk}$ = 373 K). The intensity and integrated intensity have been normalized to one at 408 K and arbitrarily shifted.

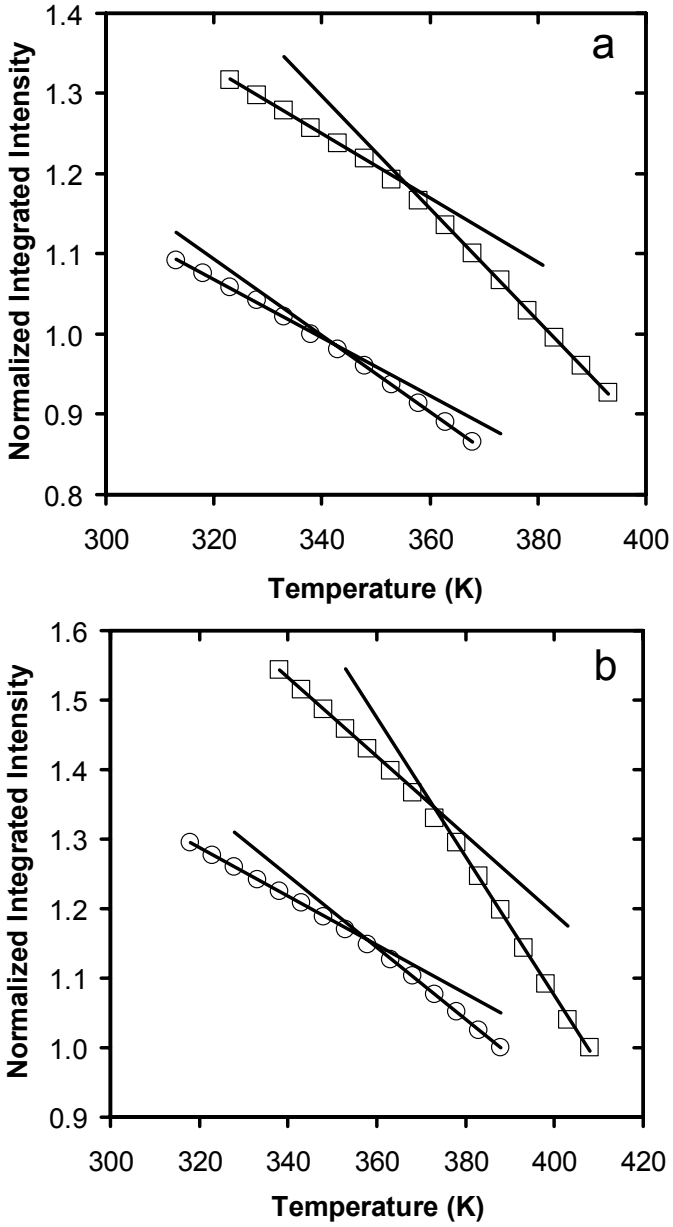

Figure 4-3: **(a)** Temperature dependence of the integrated intensity of pyrene dopant in 500-nm (□) and 29-nm (○) thick PS (*Mn* = 5,000 g/mol, *Tg*,bulk = 358 K) films (the integrated intensity has been normalized to one at 378 K and 338 K, respectively, and arbitrarily shifted). **(b)** Temperature dependence of the integrated intensity of pyrene dopant in 810-nm (□) and 24-nm (○) thick PS (*Mn* = 200,000 g/mol, *Tg*,bulk = 373 K) films (the integrated intensity has been normalized to one at 408 K and 388 K, respectively, and arbitrarily shifted).

earlier fluorescence studies (Ellison 2002a, 2002b, 2003, 2004a, 2005a) of the *Tg*-nanoconfinement effect as well as other studies (Kawana 2001), these figures demonstrate a weakening in the strength of *Tg* in highly nanoconfined PS films. In the studies conducted here, a weakening in the strength of *Tg* for PS is observed with decreasing thickness for films less than ~ 30-nm-thick, independent of PS *MW*. Associated with this strength of *Tg* effect, the error in estimating *Tg* values by the intersection of linear temperature dependences of integrated intensity in the rubbery and glassy states is ~ +/- 1 K when film thickness is greater than ~ 20-25 nm and ~ +/- 2 K when film thickness is less than ~ 20- 25 nm.

Figure 4-4 shows the thickness dependence of *Tg* for PS *Mn* values ranging from 5,000 to 3,000,000 g/mol, which is the broadest range of *MW* ever examined in a single *Tg*-nanoconfinement study. The data in Figure 4-4 indicate that there is no significant *MW* dependence over a broad range in PS *MW*s within the error of these measurements. The solid curve in Figure 4-4 represents a fit of all the PS data to the relation $Tg(h) = Tg,\text{bulk}(1 - (A/h)^{\delta})$ originally proposed by Keddie *et al.* (Keddie 1994b) with $A = 3.2$ nm and $\delta = 1.63$. (The apparent differences in the data for the thinnest films of the 5,000 and 3,000,000 g/mol samples should not be taken as significant. There is a ~ 1 nm uncertainty associated with those film thicknesses, and in the thinnest films this level of uncertainty has a very substantial effect in the extent of the *Tg* reduction relative to *Tg*,bulk. That factor, combined with the ~ 2 K uncertainty in assigning the *Tg* value in films less than 20 nm in thickness, is sufficient to indicate that any apparent difference of the *Tg*-nanoconfinement effect as a function of PS *MW* is not significant, given the inherent quality of the data.)

This demonstration of the independence of the *Tg*-nanoconfinement effect with respect to *MW* in supported PS films is consistent with many previous reports (Kawana 2001; DeMaggio 1997; Fukao 2000; Forrest 2001; Tsui 2001a) covering a *Mn* range of

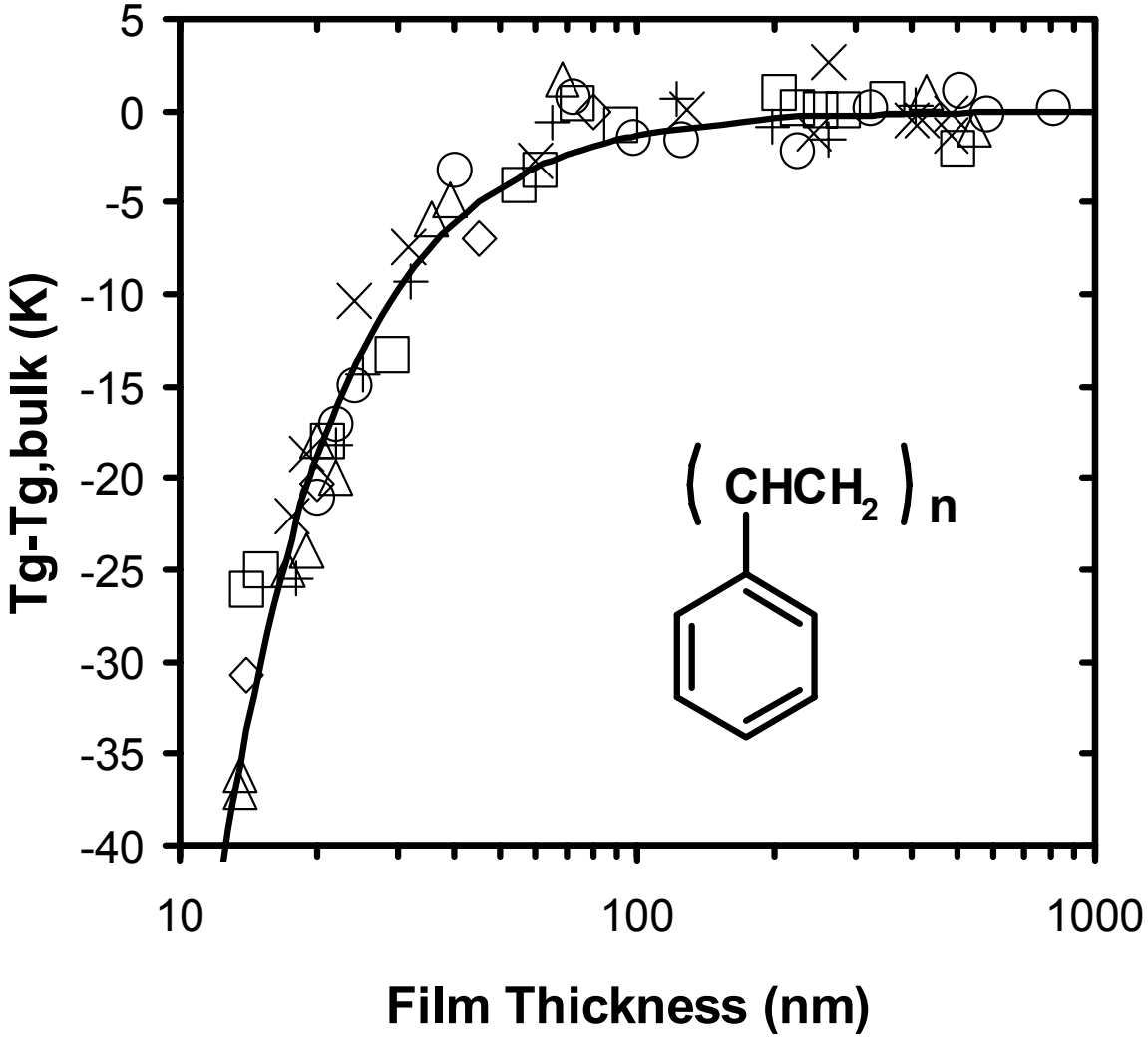

Figure 4-4: *Tg* – *Tg*,bulk as a function of film thickness for PS [*Mn* = 5,000 g/mol (□), *Mn* = 12,000 g/mol (+), *Mn* = 200,000 g/mol (○), *Mn* = 263,000 g/mol (×), *Mn* = 3,000,000 g/mol (◊)] films as measured by pyrene dopant fluorescence and PS [*Mn* = 440,000 g/mol (Δ)] as measured by pyrene label fluorescence. The curve represents a least squares fit of the data to the empirical relation originally proposed by Keddie *et al.* (Keddie 1994b) yielding parameter values A = 3.2 nm and δ = 1.63. The inset shows the structure of the PS repeat unit.

3,600-2,900,000 g/mol but is in contradiction with two very recent studies (Singh 2004; Miyazaki 2004) that have reported some *MW* dependence in the range of 212,000-2,900,000 g/mol. It is noteworthy that these two very recent studies are in some disagreement regarding how PS *MW* impacts the *Tg*-nanoconfinement effect. For example, Singh *et al.* (Singh 2004) reported a *Tg* for 100-nm-thick films that is 3 K lower for 1,600,000 g/mol PS than for 560,000 g/mol PS with a maximum difference of ~ 4 K between *Tg* values among PS *MW*s at any particular thickness. In contrast, Miyazaki *et al.* (Miyazaki 2004) reported no *Tg* difference (within error) between 303,000 and 2,890,000 g/mol PS in 100-nm-thick films but about a 7 K maximum difference for 20-nm-thick films. (Some of the *Tg* data from Miyazaki *et al.* (Miyazaki 2004) have large error bars, bringing into question the extent to which there is a true statistical difference in nanoconfined *Tg* values as a function of *MW*.)

At present, the cause for the disagreement between the many studies, including the present one, indicating that there is no significant *MW* dependence of the *Tg*-nanoconfinement effect in supported PS films and the two other recent studies indicating the opposite is not known. However, it is noteworthy that Fukao and coworkers (Fukao 1999, 2000) had concluded in 1999 and 2000 that there was some *MW* dependence to the *Tg*-nanoconfinement effect in supported PS films but later concluded (Fukao 2002) in 2002 that there was no *MW* dependence, which may be an indication of the difficulty in obtaining the highest quality data from what may be deceptively simple studies. Another factor that may contribute to the different results obtained by Singh *et al.* (Singh 2004) and by Miyazaki *et al.* (Miyazaki 2004) is that their studies reported *Tg* data taken upon heating from the glassy state after a 10 K/10 min step-and-hold method while most other studies, including the present one, have been taken upon cooling from the rubbery state. Measuring *Tg* upon cooling eliminates issues regarding how physical aging, which itself is a function of thickness in nanoconfined films (Priestley 2005a; Ellison 2002a; Kawana

2003; Richardson 2004) affects the measured *Tg*. In any case, we believe that the excellent agreement reported in Figure 4-4 among the many samples with *Mn* values over a broader range than in any previous single study provides ample evidence of the lack of a significant *MW* dependence to the *Tg*-nanoconfinement effect in supported PS films. As such, these results provide further evidence that neither a reduction in entanglement concentration with a reduction in film thickness nor a modification of *Rg* upon confinement plays a significant role in the thickness dependence of *Tg*. Furthermore, the fact that the results obtained with the PS sample with *Mn* = 5,000 g/mol, made from a blend of high and very low *MW* PS standards, agree with those of many nearly monodisperse PS standards effectively demonstrates that chain end segregation plays no significant role in the *Tg*-nanoconfinement effect. (It should be noted that the concentration of chain ends in a bulk system is only dependent on *Mn* (Sperling 1992). However, in a film made of a blend of very low *MW* and high *MW* polymer, it is possible (Mayes 1994) that the very low *MW* PS will segregate to the free surface or air-polymer interface, thereby dramatically increasing the chain end concentration near the surface beyond that expected in a monodisperse system with identical *Mn*.)

The results in Figure 4-4 reveal that even though bulk *Tg* decreases by ~ 16 K upon decreasing PS *Mn* from 3,000,000 to 5,000 g/mol, respectively, the thickness dependence of *Tg* is not tunable with *Mn*. This is consistent with the fact that studies (Roland 2003; Rizos 1998; Santangelo 1998; Robertson 2000) have shown that unless PS *MW* is reduced to that of oligomer, the fragility index or the degree of cooperativity near *Tg* remains essentially the same regardless of *MW*. In contrast to this, the addition of low molecular weight diluents and small modifications to the repeat unit structure of PS are observed to have a dramatic impact on the tunability of the *Tg*-nanoconfinement effect. Details on the tunability aspect of *Tg*-nanoconfinement can be found in Chapter 7.

4.3.2 Comparison of the Length Scale of Cooperative Dynamics for PS as a Function of MW and Repeat Unit Structure to the Tg-Nanoconfinement Behavior

In a recent study that discussed the determination of the distribution of *Tg* values in nanoconfined PS (Ellison 2003), it was shown that the free-surface effect results in a significantly reduced local *Tg* (by some tens of degrees) at the free surface and that the local *Tg* is perturbed from its bulk value in buried layers located several tens of nanometers into the film interior. From these results, it may be rationalized that the *Tg*-nanoconfinement effect in supported PS films results from two things: (1) a significant perturbation in local segmental dynamics at the free-surface interface, and (2) a mechanism by which these free-surface effects may propagate into the film interior. Ellison (Ellison 2003) indicated that there is not a one-to-one relationship between the length scale of a CRR at *Tg* and the length scale from the free surface over which *Tg* dynamics are modified, and thus not a one-to-one relationship between the length scale of a CRR and the onset thickness at which the *Tg*-nanoconfinement effect is observed. However, as yet unresolved is the issue of whether there is some even qualitatively definable relationship between the length scale of a CRR at *Tg* in the unperturbed bulk polymer and the other two length scales. (Furthermore, a recent perspective article (McKenna 2003) has indicated that cooperativity length scales have been insufficiently studied in regard to their potential connection to *Tg* dynamics in confinement.)

Here we address this issue by determining the size of a single CRR at *Tg*,bulk, ξ_{CRR}, using the thermal fluctuation theory and DSC method by developed by Donth (Donth 1982, 1984, 1996, 1999, 2000, 2001; Hempel 2000; Vyazovkin 2004; Tran 2004, Robertson 2004; Ellison 2005; Korus 1997; Mitteilungen 1982; Khale 1999). In this approach equation 4.1 and 4.2 are used to calculate V_{CRR} (the volume of one CRR), ξ_{CRR} (the size, or length scale, of one CRR) and N_{CRR} (the number of repeat units present in

one CRR). More details on the calculation can be found in the materials and methods section of this chapter.

Donth's approach has been described in the literature as being controversial (Erwin 2002) because the associated theoretical analysis "has not been verified." While acknowledging this point, we note that the experiments are straightforward and, when a reasonable temperature dependence for the cooperativity length scale is assumed, result in estimates of ξ_{CRR} that are consistent with the very few measurements of ξ_{CRR} obtained by 4D-NMR methods. For example, using equation 4.1 we have determined a value of ~ 3.3 nm (given the assumption employed in Donth's method, the associated error significantly exceeds +/- 0.1 nm) for the ξ_{CRR} for glycerol at *Tg*, allowing comparisons to results obtained for glycerol above *Tg* via 4D-NMR. (See Table 4-3 for the values of the parameters used in equation 4.1.) Using 4D-NMR (Tracht 1998; Reinsberg 2001) and their most recent analysis of the data, Speiss and co-workers (Reinsberg 2002) report ξ_{CRR} values for glycerol of 1.3 +/- 0.5 nm at *Tg* + 10 K, 1.1 +/- 0.5 nm at *Tg* + 14 K, and 1.0 +/- 0.5 nm at *Tg* + 18 K.

A direct comparison of ξ_{CRR} values obtained by Donth's approach and 4D-NMR cannot be made at the same temperature as the former method yields data at *Tg* while the latter method has been applied in a certain dynamic range associated with temperatures closer to *Tg* + 10 K. Employing a dynamic scaling approach and results from dielectric spectroscopy studies by others (Stickel 1995; Menon 1992), Erwin and Colby (Erwin 2002) provided data indicating that ξ_{CRR} for glycerol increases by ~ 80% as temperature is decreased from *Tg* + 10 K to *Tg*. Applying this factor to the data by Spiess and co-workers (Reinsberg 2002), a value of ξ_{CRR} of 1.44-3.24 nm for glycerol at *Tg* can be estimated. Given that there is a substantial uncertainty associated with the estimate of 3.3 nm using Donth's method (see Section 4.2.2), it is possible to conclude that, when the effects of temperature difference are taken into account, determinations of ξ_{CRR} by 4D-

NMR and Donth's approach are consistent with each other. (It is acknowledged that Reinsberg *et al.* (Reinsberg 2001) indicate there is inconsistency between ξ_{CRR} values for glycerol obtained by Donth (which are consistent with our data) and those obtained using 4D-NMR. However, that work invoked the use of a temperature dependence for the size scale or number of repeat units in a CRR that is different from that mentioned in this chapter from Erwin and Colby (Erwin 2002).)

Based on DSC measurements and equation 4.1, Figure 4-5 shows the effect of PS *MW* on the value of ξ_{CRR} over a *MW* range of 568 - 23,000,000 g/mol, an even broader *MW* range than employed in Section 4.3.1. This is also a broader *MW* range than that investigated more than twenty years ago by Donth (Donth 1984) in the only other study of the *MW* dependence of ξ_{CRR} for PS at *Tg*. (While Donth reported in 1984 (Donth 1984) on the *MW* dependence of the size of a CRR in PS at *Tg*, there are several reasons for believing that it is important to perform a separate investigation of this issue. First, there is a need to establish credibility for experiments described here, which also included the effects of diluent addition to PS and modification of repeat unit structure. Second, the 1984 reference by (Donth 1984) has been virtually ignored or forgotten in the research literature, even by Donth himself who has not cited this reference in his later studies. This leads to some concerns regarding the reference; those concerns were allayed by the measurements done in the present study.)

Figure 4-5 also includes the first determinations of the ξ_{CRR} values for P4MS, PTBS, and PS containing 4 wt % dioctyl phthalate (DOP) plasticizer. The latter system is identical to one studied by Ellison *et al.* (Ellison 2004a) that revealed that the *Tg*-nanoconfinement effect can be essentially eliminated down to film thicknesses of 14 nm by diluent addition to PS. Within the range of experimental error, the size of the CRR for PS is ~ 3.5 nm, invariant with *MW* from 23,000,000 g/mol at least down to *Mn* values of 13,500 g/mol. (See Table 4-3 for examples of parameter values that are required to

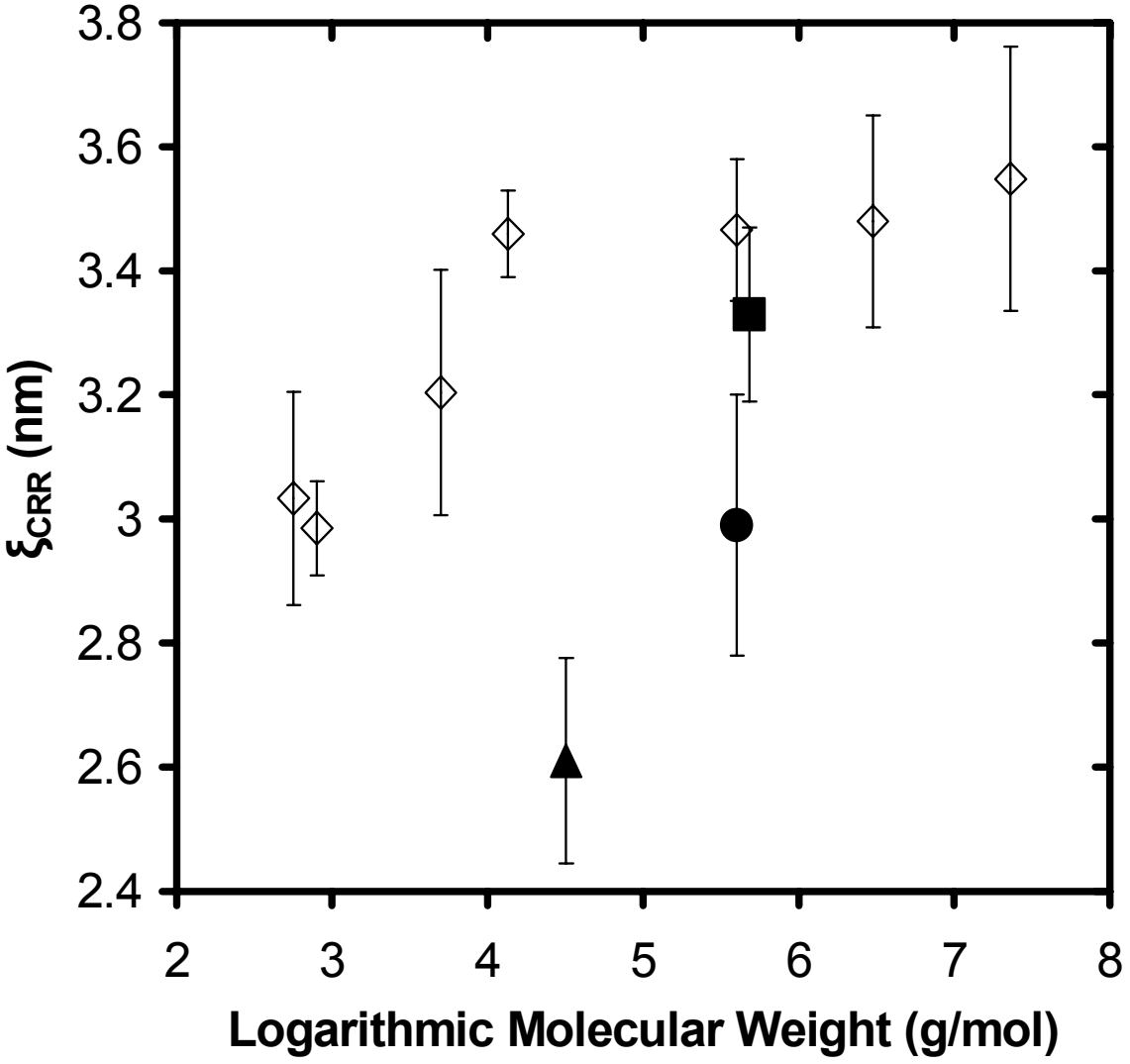

Figure 4-5: ξ_{CRR} values as a function of logarithmic molecular weight for PS (◊), P4MS (■), PtBS (▲) and PS (*Mn* = 400,000 g/mol) doped with 4 wt% dioctyl phthalate (●). Error bars indicate the standard deviation about the mean of measured ξ_{CRR} values for that *MW* of PS or other polymer.

determine ξ_{CRR} using equation 4.1.) Given the sizes of error bars in Figure 4-5, a case may even be made that within experimental error the size of the CRR is invariant with PS *MW* down to *Mn* values of 5,000 g/mol. This value of the CRR size in PS at *Tg*,bulk is slightly larger than the value of 3.0 nm recently reported by Donth and co-workers (Hempel 2000) using regular DSC methods similar to those employed in our study. Most of this difference is due to the level of inaccuracy of the assumption that $\Delta(1/Cv) = \Delta(1/Cp)$, where *Cp* is measured by DSC. Donth and co-workers (Hempel 2000) "corrected" the ξ_{CRR} data for this inaccuracy by a common factor of $S = 0.7479$ across all data (both low *MW* and polymeric glass formers). A similar adjustment to the data has not been made here in order to avoid overgeneralization, especially as the correction factor for each system is not known. However, if Donth's correction factor had been used, it would have resulted in a value of $\xi_{CRR} \sim 3.1\text{-}3.2$ nm for the PS data, almost in exact agreement with Donth's value of 3.0 nm (Hempel 2000).

In addition, the approach for determining the size of the CRR using a regular DSC method involves some "rules of thumb" for determining the δT parameter prescribed by Donth (rather than the more rigorous method by Donth involving determination of δT from the Kohlrausch-Williams-Watts exponent in conjunction with measurements by thermally modulated DSC). With the application of these rules of thumb, Donth has argued (Hempel 2000) that the accuracy of the characteristic size of a CRR is within 85% and 125% of the calculated value. (See section 4.2.1 for more details.) Thus, according to Donth's expectations for accuracy of the method, it can be argued that for nonoligomeric PS the value of ξ_{CRR} is between 3.0 and 4.4 nm. (These values do not include Donth's factor correcting for the average inaccuracy of the assumption that $\Delta(1/Cv) = \Delta(1/Cp)$.) While this range of values for ξ_{CRR} may seem large, it is less than that estimated from 4D-NMR determinations of the size of a CRR for PVAc (3.7 +/- 1 nm) (Reinsberg 2002).

Figure 4-5 also illustrates that when the PS *MW* is reduced to oligomeric systems with *MW*s 568 or 800 g/mol, the experimentally determined ξ_{CRR} value is, outside of the experimental uncertainty as described by the error bars, reduced from that of our higher *MW* PS samples, taking on a value of ~ 3.0 nm (not corrected with Donth's *S* parameter). The fact that the size of a CRR is, within experimental error, invariant with PS *MW* until the *MW* is sufficiently reduced to yield an oligomer (or nearly an oligomer) is reasonably consistent with studies (Roland 2003; Santangelo 1998; Robertson 2000) on the *MW* dependence of the fragility index or related behavior for PS. The fragility index *m* can defined by the value of d log(τ)/d(Tg/T) evaluated in the equilibrium rubbery or liquid state in the limit of $T = Tg$, where τ is the average α-relaxation time or the average relaxation time of the cooperative segmental dynamics associated with *Tg* (Angell 1991). Often the value of *m* is determined at a fixed value of τ associated with *Tg*, e.g., 100 s. The fragility index may be regarded as another measure of the nature of the cooperative motion and has been described (Roland 2003) as being a "...reflection of the effect intermolecular cooperativity has on the (segmental) dynamics." A couple of studies concerning the *MW* dependence of the fragility index for PS have yielded the following picture: oligomeric PS (e.g., 590 (Roland 2003) and 1,100 g/mol (Rizos 1998)) exhibits a major reduction in the fragility index (or related parameters such as Ngai's coupling parameter (Rizos 1998)) relative to high *MW* PS although some *MW* dependence to the fragility index is exhibited at *MW*s as high as 6,400 g/mol (Roland 2003).

Given the definitions of the size of an average CRR at *Tg* and the fragility index, for a particular glass forming system both values are expected to decrease with a decrease in the number of units involved in cooperative segmental mobility at *Tg*. In the case of PS, oligomers are expected to have a reduced requirement for cooperative segmental mobility at *Tg* because of the dramatically reduced connectivity between repeat units and increase in free volume that are manifested in large reductions of *Tg* relative to high *MW*

PS. However, the extent to which the values of ξ_{CRR} and m are reduced with reductions in the cooperativity of a particular system may differ substantially. It has been suggested (Solunov 1999; Hodge 1996) that a value such as m reflects the apparent activation energy associated with cooperative segmental mobility in the rubbery state in the limit of $T = Tg$. This is expected to be related to the number of units involved in cooperative segmental mobility and thereby the volume of the CRR rather than the size of the CRR. Thus, m is expected to exhibit a greater change than ξ_{CRR} with cooperativity requirements at Tg.

The experimentally measured reduction in the value of ξ_{CRR} from ~ 3.5 to ~ 3.0 nm upon addition of 4 wt% DOP to PS is also consistent with experimental observation of a reduction in fragility with diluent addition (Rizos 1998). (In calculating the value of N_{CRR} for the PS + 4 wt % DOP sample, the assumption was made that the density of the system was unaffected by the small amount of DOP diluent. Furthermore, the calculation of N_{CRR} assumed that all units were PS repeat units.) The reduction in the size of the CRR with diluent addition is expected based on the fact that the presence of diluent reduces constraints associated with cooperative segmental motion.

In contrast to the easily explained result for diluent addition, the effect of small changes to the repeat unit structure of PS on the size of the CRR is not as easily rationalized. The value of ξ_{CRR} obtained for P4MS is ~ 3.4 nm (not corrected with Donth's S parameter), within experimental error the same as that of PS. It is possible that the difference in repeat unit structure between PS and P4MS results in a small enough perturbation to cooperative segmental mobility that it is not evident in measurements of ξ_{CRR}. In contrast, the value of ξ_{CRR} obtained for PTBS is ~ 2.6 nm (not corrected with Donth's S parameter) which, outside of experimental error, is even smaller than that observed for oligomeric PS. From inspection of the structures of PS and P4MS, it would be logical to assume that, other things being equal, the presence of the tert-butyl group in

PTBS would greatly increase the cooperativity requirements relative to PS. However, other things are not equal in these two systems, as the 10% reduction in density of PTBS relative to PS easily attests. Thus, the tert-butyl groups in PTBS greatly reduce the packing efficiency of the repeat units relative to PS, and it is surmised that this packing effect may overcome the expectation of increased cooperativity (in the absence of free volume effects) and result in a net major reduction in the size of an average cooperatively rearranging region at *Tg*. (It is highly unlikely that the reductions in N_{CRR} and ξ_{CRR} for PTBS relative to PS have their origins in the values of the *S* parameter (see Hempel 2000) for PTBS and PS. In order for the values of N_{CRR} and ξ_{CRR} to be approximately the same in the two polymers, the value of the *S* parameter for PTBS would need to be about 4 times that of PS. This much variation in the *S* parameter is not observed across a wide variety of monomeric and polymeric glass formers.) Further study of these issues in related systems is warranted.

To better appreciate the importance of packing efficiency relative to that of polymer *MW* in dictating the cooperativity required at *Tg*, Figure 4-6 plots the number of repeat units associated with an average CRR, N_{CRR}, as a function of polymer *MW*. The value of N_{CRR} was calculated making the assumption that the volume of a CRR is cubic in nature (which oversimplifies the shape of a CRR) and taking into account the exact density of the polymers involved; thus, the important quantitative information in Figure 4-6 relates to how the N_{CRR} values depend on a particular parameter instead of the exact values of the N_{CRR}. The oligomeric PS samples have N_{CRR} values that are ~ 60- 70% that of higher *MW* PS, in reasonable agreement with 20-year-old data of Donth (Donth 1984), who found a *MW* dependence of N_{CRR} for PS at *Tg* similar to that shown in Figure 4-6. (Donth actually reported *MW* per CRR rather than N_{CRR}.) Most striking in Figure 4-6 is the fact that the PTBS sample has an N_{CRR} value that is 20-30% that of high *MW* PS. Similarly large differences among different polymers have been observed by Donth and

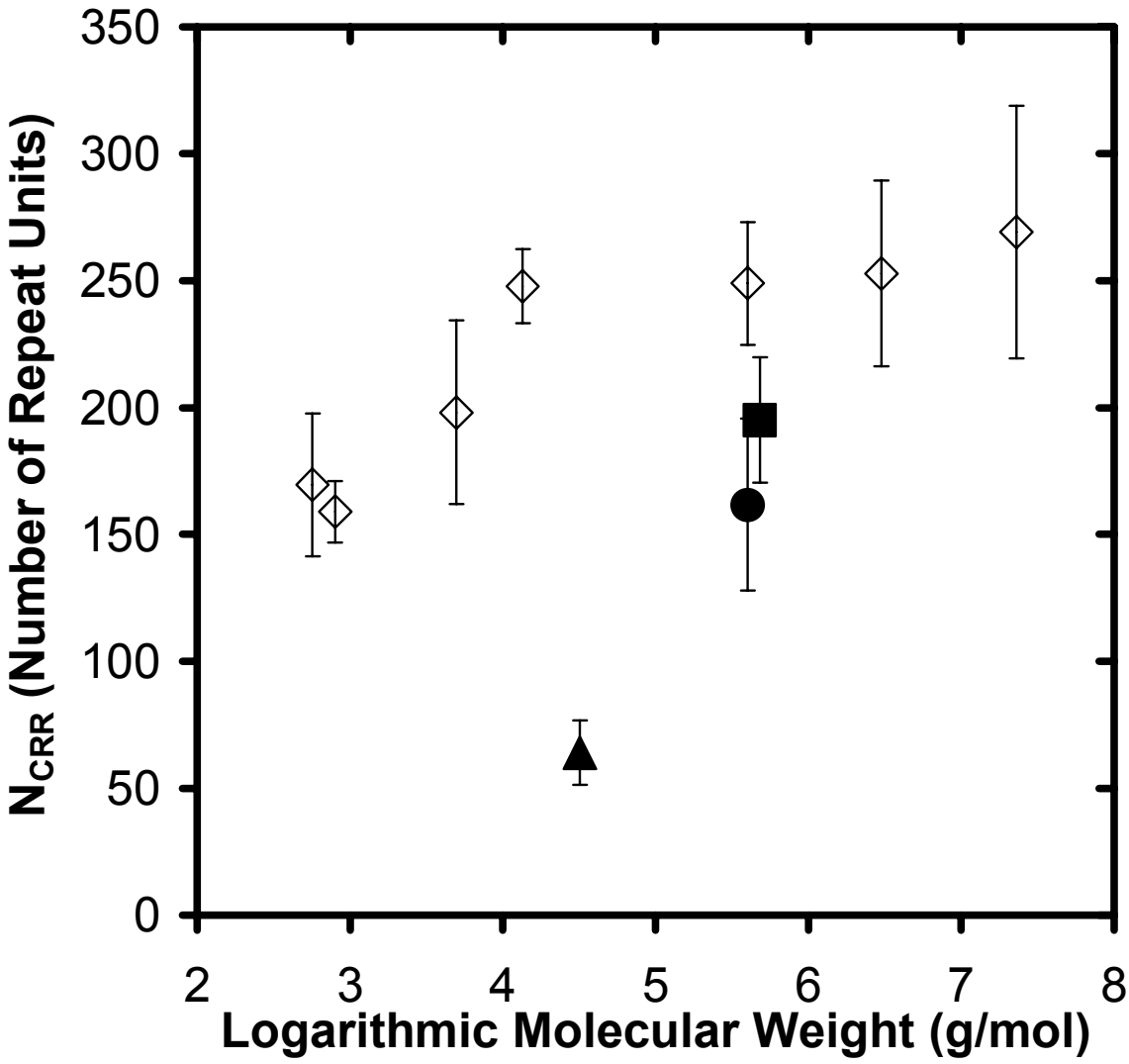

Figure 4-6: N_{CRR} values as a function of logarithmic molecular weight for PS (◊), P4MS (■), PtBS (▲) and PS (*Mn* = 400,000 g/mol) doped with 4 wt% dioctyl phthalate (●). Error bars indicate the standard deviation about the mean of measured N_{CRR} values for that *MW* of PS or other polymer.

co-workers (Hempel 2000), who reported that poly(n-alkyl methacrylates) have dramatically reduced values of N_{CRR} relative to other polymers including PS.

It is also important to note that two recent studies have employed the DSC method of Donth to investigate the values of ξ_{CRR} and N_{CRR} or V_{CRR} for PS (Vyazovkin 2004) and poly(methyl methacrylate) (PMMA) (Tran 2004) as a function of confinement in clay nanocomposites. Both studies reported an increase of *Tg* in the nanocomposite relative to neat polymer. However, the PS study reported a 75% increase in V_{CRR}, equivalent to about a 20% increase in ξ_{CRR}, upon confinement in the nanocomposite while the PMMA study reported about a 20% decrease in ξ_{CRR} upon confinement in the nanocomposite. The different trends in these two studies suggest that at present there is not a qualitative correlation between ξ_{CRR} and modification of *Tg* in nanocomposites.

With the results provided in Figures 4-5 and 4-6, it is possible to address the issue of whether a simple qualitative relationship exists between the size of a CRR at *Tg*,bulk and the *Tg*-nanoconfinement effect. At one level, the invariance of ξ_{CRR} and N_{CRR} with PS *MW* (except for oligomeric PS) is in accord with absence of a *MW* effect to the *Tg*-nanoconfinement effect in supported PS films. However, while large reductions in the values of ξ_{CRR} and N_{CRR} are observed in PTBS and PS with 4 wt% DOP relative to the values observed in neat PS, PTBS exhibits a major enhancement of the *Tg*-nanoconfinement effect relative to PS (Ellison 2005a) while the PS with 4 wt% DOP exhibits an elimination of the effect down to a film thickness of 14 nm (Ellison 2004a). Thus, the present results do not allow for a description of a "rule of thumb" regarding how a change in the size of the CRR in bulk polymer relates to the tunability of the *Tg*-nanoconfinement effect. However, it is believed that the impact of modifications to the repeat unit structure on the nature of the polymer dynamics at the air-polymer interface as well as how such modifications impact the manner in which the perturbation to dynamics at the free surface propagate into the film interior may hold the answer. Studies of such

issues as well as novel investigations to determine the general impact of interfaces on the cooperative segmental mobility (e.g., the full α-relaxation time distribution) in conjunction with repeat unit structural modifications may be key in gaining a better understanding of the *Tg*-nanoconfinement effect.

4.4 Conclusions

The effect of confinement on the *Tg* of PS films is investigated in neat PS over the broadest *MW* range ever reported in a single study (5,000-3,000,000 g/mol). In contrast to two recent reports (Singh 2004; Miyazaki 2004), here it is observed that PS *MW* has no significant impact on the film thickness dependence of *Tg* - *Tg*,bulk. This result is consistent with the substantial evidence in the literature, indicating that *Tg*-nanoconfinement effects originate from interfaces and surfaces which impact the cooperative segmental mobility associated with *Tg* and are not due to other factors which may depend on *MW* such as degree of chain end segregation, entanglement density, etc.

The characteristic dynamics of the cooperative motion associated with *Tg* is examined via the size of a CRR at *Tg*, ξ_{CRR}. The value of ξ_{CRR} is approximately independent of PS *MW* over the same range of *MW*s for which the *Tg*-nanoconfinement effect is *MW* invariant. However, other system variations such as modification of repeat unit structure yield changes in ξ_{CRR} values of bulk polymer systems that do not correlate in an obvious manner with the strength of the *Tg*-nanoconfinement effect. Future studies related to how free surfaces and interfaces impact cooperative segmental dynamics as a function of polymer repeat unit structure and diluent addition are warranted.

CHAPTER 5

DISTRIBUTION OF Tgs IN THIN AND ULTRATHIN FILMS

5.1 Introduction

The achievement of a complete understanding of the nature of the glass transition in amorphous materials remains one of the most challenging problems in condensed matter physics (Anderson 1995; Angell 1995b, 2000; Debenedetti 2001; Merolle 2005). A central tenet of the physics of the glass transition is that of the cooperatively rearranging region (CRR) (Sillescu 1999; Ediger 2000; Donth 2001b; Stevenson 2006; Adam 1965) which, as defined by Adam and Gibbs (Adam 1965), is "the smallest region that can undergo a requisite transition to a new configuration without a requisite simultaneous configurational change on and outside its boundary." Experimental studies indicate that the size of a CRR is approximately 1-4 nm (Donth 1982, 1984, 1996, 1999, 2000, 2001a; Hempel 2000; Vyazovkin 2004; Tran 2004, Robertson 2004; Ellison 2005a; Korus 1997; Mitteilungen 1982; Khale 1999; Barut 1998; Tracht 1998; Reinsberg 2001; Qin 2003; Arndt 1996, 1997; Hong 2002; Erwin 2002; Richert 1996; Berthier 2005) and may be considered as the lower limit for the size of a dynamic heterogeneous region (Ediger 2000).

Since the discovery more than a decade ago that confinement of polymer films at the nanoscale can lead to large deviations in *Tg* compared to the bulk state (Keddie 1994a, 1994b), many experimental studies (Kawana 2001, 2003; Fukao 1999, 2000; Forrest 1996, 1997; Sharp 2003a, 2003b, 2003c; Mukherjee 2002; Tanaka 2004; Li 2004; Blum 2006; Bernazzani 2002; Svanberg 2007) and simulations (Varnik 2002; Torres 2000; Baljon 2004; Riggleman 2006; Peter 2006) have been carried out in a quest to characterize and explain the observed phenomena. Two prominent explanations accounting for the impact of nanoconfinement on *Tg* are finite size effects and interfacial

effects. Finite size effects are hypothesized to occur when the length scale of the system, i.e., film thickness, and the length scale governing *Tg*, i.e., a CRR, coincide (Fukao 2000, 2001). Interfacial effects are expected to increase in significance with an increase in the ratio of interfacial area to volume (Keddie 1994a, 1994b; Ellison 2003).

The definition of a CRR has been used to justify two- and three-layer models that offer explanations of the deviation from *Tg*(bulk) in nanoscopically confined polymer films (Keddie 1994b; Forrest 2000). These models assume that perturbations to *Tg* at the free surface (air-polymer interface) or the polymer-substrate interface are limited to length scales roughly the size of a CRR. (By some interpretations, CRRs are always independent of one another and should not impact the dynamics of adjacent CRRs; with these interpretations, perturbations to *Tg* at the free surface or substrate interface are believed to be limited to a layer thickness of one CRR and unable to propagate from the interface into the film interior.) However, reductions in *Tg* from *Tg*(bulk) have been reported for films as thick as 300-400 nm when the films lack attractive interactions with the substrate on which they are supported (Ellison 2005a). Because of the large difference in the length scale at which *Tg*-nanoconfinement effects have been observed in polymer films and the accepted length scale of a CRR, it can be concluded that deviations in *Tg* are not directly related to the size scale of a CRR (Forrest 1996). In addition, it is unclear how perturbations limited to the very small length scale of a CRR can lead to significant changes in the average *Tg* of polymer films with thicknesses that are one or even two orders of magnitude larger than a CRR.

The picture that *Tg* dynamics are perturbed by interfacial effects only over the length scale of a CRR has been experimentally refuted by a recent study employing a fluorescence/multilayer technique that found that perturbations to *Tg* at the free surface of a film are able to propagate into the film interior (Ellison 2003). In particular, this study showed that the perturbed *Tg* dynamics at the free surface of polystyrene (PS) led to *Tg*s

differing from *Tg*(bulk) at distances of several tens of nanometers from the PS free surface. This behavior was explained to result from the strongly perturbed CRRs in the free-surface layer affecting the average cooperative dynamics in adjoining layers of CRRs, and to a lesser extent the CRRs of the next layer, and so on.

This chapter reports the first study to characterize the distribution of *Tg*s for polymer films that possess strong attractive interactions with the substrate. The results demonstrate not only that strongly perturbed *Tg* behavior in an interfacial layer of a polymer film propagates over length scales equivalent to a number of layers of CRRs but that perturbations to *Tg* caused by attractive interactions with the substrate can be observed over length scales of several hundred nanometers. This was accomplished using a fluorescence/multilayer method (Ellison 2003, 2004a, 2005a; Priestley 2005a, 2005b) to measure *Tg* in layers at the free surface, substrate-polymer interface, and known distances away from the interfaces of PMMA films supported on silica. It is observed that the free surface and substrate act in opposition to one another in modifying *Tg* dynamics. For example, the *Tg* of a 12-nm-thick free-surface layer of a bulk PMMA film is reduced by 7-8 K compared with *Tg*(bulk) while the *Tg* of a 12-nm-thick substrate layer of a bulk PMMA film is increased by 10 K compared with *Tg*(bulk). Using a bilayer film geometry in which the *Tg* of a 12-nm-thick free-surface layer is measured as a function of confinement of the overall film, it is demonstrated that perturbed *Tg* dynamics at the substrate interface can percolate across a 200-nm-thick PMMA film to affect the *Tg* dynamics at the free surface. Furthermore, when the overall PMMA film thickness is less than 90 nm, the *Tg* in the free-surface layer actually exceeds *Tg*(bulk). This behavior can occur only if perturbations to *Tg* dynamics propagate over many layers of CRRs. These results disallow the simple layer models as explanations of *Tg*-nanoconfinement effects and, more importantly, require re-evaluation of the interpretation of the CRR, a central tenet of glass transition physics.

5.2 Experimental

Poly(methyl methacrylate) was synthesized by free radical polymerization, with *Mn* = 355,000 g/mol and PDI = 1.54 obtained by gel permeation chromatography (universal calibration relative to PS standards). The onset *Tg* = 394 K, as determined by DSC (Mettler Toledo DSC822e) on second heating with a heating rate of 10 K/min. The chromophore 4-tricyanovinyl-[N-(2-hydroxyethyl)-N-ethyl]aniline (TC1) was synthesized by reaction with tetracyanoethylene (TCI America) and 2-(N-ethylaniline)ethanol (TCI America) dissolved in dimethyl formamide (Fisher) at 55 ^{o}C for 15 min and then recrystallized from glacial acetic acid. The 1-pyrenyl butanol-labeled (Aldrich) and TC1-labeled methacrylate monomers were synthesized through an esterification reaction with methacryloyl chloride (Aldrich) in the presence of triethylamine (Aldrich) and dichloromethane (Aldrich) at 0 ^{o}C for 2 hr. Labeled PMMA was synthesized by reaction of MMA monomer (Aldrich) in the presence of a trace amount of either pyrene-labeled or TC1-labeled methacrylate monomer. The pyrene-labeled PMMA contained 1.22 mol % (1 in 82 repeat units) of pyrene-labeled monomer and the TC1-labeled PMMA contained 1.37 mol% (1 in 73 repeat units) of the TC1-labeled monomer determined by UV-Vis absorbance spectroscopy (Perkin Elmer Lambda 35). For pyrene-labeled PMMA, *Mn* = 456,000 g/mol, PDI = 2.0, and the onset *Tg* = 395 K. For TC1-labeled PMMA, *Mn* = 509,000 g/mol, PDI = 1.67, and the onset *Tg* = 394 K. All polymer was washed by dissolving in toluene (Fisher) and precipitating in methanol (Fisher) at least five times to remove residual solvent and then dried in a vacuum oven at *Tg* + 15 K for 24 hr.

Single-layer films were prepared by spin casting polymer/toluene solutions onto quartz slides (Hall 1998a). The films were allowed to dry in vacuum at *Tg* + 5 K for 8 hr. Multilayer films were prepared by spin casting polymer/toluene solutions onto either a quartz slide or a NaCl salt disk. Films spun cast onto NaCl salt disks were floated on top

of films spun cast onto quartz slides by submersing the salt disk in a water bath. After preparation of the multilayer film, it was dried in vacuum at room temperature for 12 hr and then annealed at Tg + 25 K for 10 min to ensure a completely consolidated film. Film thicknesses were measured with a Tencor P10 profilmeter.

All polymers were of sufficiently high molecular weight to ensure that interlayer diffusion was at most a several nanometers during the experimental time, which includes the time to create a consolidated film. The estimated interlayer diffusion could be determined from nuclear reaction analysis data (Shearmur 1998). For the conditions employed in this study, the total diffusion time of 40 min was much less than the polymer disentanglement time. The disentanglement time can be calculated by the following equation: $\tau_D = (2Rg^2)/(\pi^2 Ds)$, where Rg is the radius of gyration of the polymer and Ds is the bulk self-diffusion coefficient. For PMMA (lowest molecular weight and fastest diffusing component used in these studies) at Tg + 25 K, the disentanglement time was 3850 min using $Ds = \sim 3\text{x}10^{-18}$ cm^2/s from nuclear reaction analysis diffusion data (Shearmur 1998). Since the total experimental time above Tg was substantially smaller than the disentanglement time (experimental time above Tg was only 1% of disentanglement time), the maximum interlayer penetration distance was substantially less than the PMMA Rg (~18.5 nm), with a reasonable estimate of a few nanometers. It is important to note that the above estimate is an upper limit as the polymer used in the study (355,000 g/mol, 456,000 g/mol and 509,000 g/mol) is of higher molecular weight than that used in (100,000 g/mol and 127,000 g/mol) the interlayer diffusion study (Shearmur 1998).

Steady-state fluorescence emission spectra were taken as a function of temperature (on cooling) using a Photon Technology International fluorimeter in a front-face geometry (with emission at 90^o relative to excitation and the film at an angle of 28^o relative to excitation) with 3.0 mm excitation (6 nm bandpass) and 3.0 mm emission slits

(12 nm bandpass) used for TC1-labeled PMMA experiments and 1.25 mm excitation (2.5 nm bandpass) and 1.25 mm emission slits (5 nm bandpass) used for pyrene-labeled PMMA experiments. The wavelengths used to excite TC1 and pyrene were 480 nm and 254 nm, respectively. The emission spectra of TC1 and pyrene were measured at 540-690 and 360-460 nm, respectively. The *Tg* values of the labeled films were determined by fitting the temperature dependence of the integrated fluorescence intensity to linear correlations in both the rubbery and glassy states. In fitting the data to linear correlations, only data well outside *Tg* were used in the fitting procedure. (Additional information on the fluorescence technique used to monitor *Tg* is provided in Chapters 3,4 and 6.)

5.3 Distribution of Tgs in Polymer Films with Attractive Substrate Interactions

The fluorescence of chromophores covalently attached (labeled) to the polymer at trace levels was used to measure *Tg* in single-layer and multilayer PMMA films supported on silica substrates. Multilayer films consist of a single, labeled PMMA layer and one or two unlabeled PMMA layers of known thickness. Heating the multilayer films for a short time above *Tg* produces a consolidated film. The polymer is of sufficiently high molecular weight to ensure that labeled PMMA diffuses, at most, a few nanometers during the measurements. (See Section 5.2 for further detail.)

Figure 5-1 shows the normalized integrated fluorescence intensity as a function of temperature for pyrene-labeled and 4-tricyanovinyl-[N-(2-hydroxyethyl)-N-ethyl]aniline (TC1)-labeled PMMA films. Data points were obtained by taking the integrated intensity of the fluorescence emission spectrum of the labeled polymer as a function of temperature. (See insets in Figure 5-1.) Linear correlations were fit to data points in both the rubbery and glassy states, with the intersection providing a measure of *Tg*. The *Tg* values of the 250-nm-thick pyrene-labeled PMMA and 200-nm-thick TC1-labeled PMMA films are 394 K and 395 K, respectively, and are within 1 K of *Tg*(bulk)

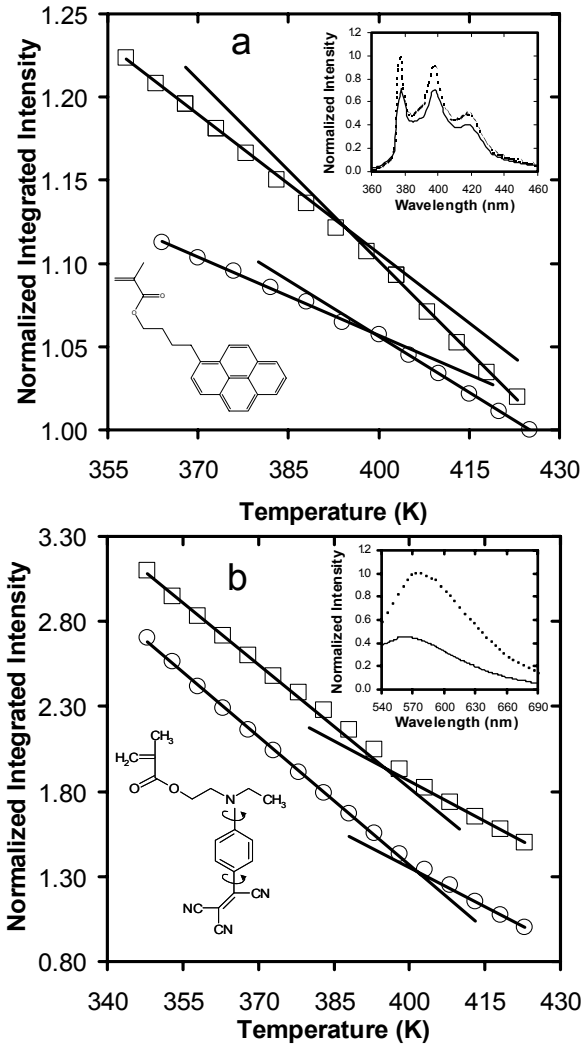

Figure 5-1: **(a)** Temperature dependence of the normalized integrated fluorescence intensity of 250-nm-thick (□) and 50-nm-thick (○) pyrene-labeled PMMA films. The solid lines are fits of the data in both the rubbery and glassy states, with the intersection of the lines defining *Tg*. (Insets) Emission spectra of pyrene at 423 K (solid line) and 358 K (dotted line) of the 250-nm-thick film and monomer used in labeling procedure. **(b)** Temperature dependence of the normalized integrated fluorescence intensity of 200-nm-thick (□) and 35-nm-thick (○) TC1-labeled PMMA films. The solid lines are fits of the data in both the rubbery and glassy states, with the intersection of the lines defining *Tg*. (Insets) Emission spectra of TC1 at 423 K (solid line) and 358 K (dotted line) of the 200-nm-thick film and monomer used in labeling procedure.

determined by differential scanning calorimetry (DSC) of the labeled PMMA.

The difference in the temperature dependence of the fluorescence intensity exhibited by the pyrene-labeled PMMA and TC1-labeled PMMA is related to the mechanism by which each chromophore undergoes non-radiative decay from its excited state and is explained briefly below.

While the values of *Tg* obtained using pyrene- and TC1-labeled PMMA are consistent, the slope changes in the temperature dependences of the normalized integrated fluorescence emission intensity are opposite each other. The difference in the change in slope of the temperature dependence of fluorescence intensity for the two chromophores is related to the different mechanism by which each chromophore undergoes non-radiative decay from its excited state. Pyrene, a band definition chromophore, undergoes non-radiative decay by vibrational motions (Valeur 2002; Lakowicz 1999); thus, the emission intensity follows the density of the polymer and the temperature dependence of the emission intensity is smaller below *Tg* than above *Tg*. Numerous band definition chromophores have been used to determine *Tg* in bulk polymeric glass formers (Ellison 2002b, 2003, 2004a, 2005a; Priestley 2005a, 2005b; Turrion 2005; de Deus 2004; Meyer 1990). The TC1 dye, a "rotor" chromophore, undergoes non-radiative decay by rotational motion as depicted by the inset in Figure 5-1b (Valeur 2002). To facilitate the rotational motion of the chromophore, a certain amount of free volume is required (Loutfy 1982); thus, it is believed that changes in polymer density impede the rotational motion to a greater extent in the glassy state than in the liquid state. As a result, the temperature dependence of the emission intensity is greater in the glassy state than the rubbery state. Because of the enhanced sensitivity of "rotor" chromophores to density changes that occur in the glassy state, they have been widely used to monitor physical aging of polymeric glass formers (Priestley 2005a, 2005b; de Deus 2004; Ellison 2002a, 2002b; Royal 1992b, 1993; Rittigstein 2007).

According to Figure 5-1, the *Tg*s of a 50-nm-thick pyrene-labeled PMMA film and a 35-nm-thick TC1-labeled-PMMA film are 399 K and 402 K, respectively. This indicates that there is an increase in *Tg* with decreasing film thickness for PMMA films supported on silica. The increase in *Tg* with decreasing thickness is related to hydrogen bond formation that can occur between the ester groups on PMMA and the hydroxyl groups on the silica substrate (Keddie 1994a; Grohens 2002; Priestley 2005a, 2005b). The formation of hydrogen bonds is believed to reduce the cooperative segmental mobility of the polymer at and near the silica interface, thus resulting in an increase in *Tg* with decreasing film thickness as the ratio of interfacial area to volume becomes increasingly large.

Figure 5-2 shows the effect of film thickness (*d*) on *Tg*(film) – *Tg*(bulk) obtained by fluorescence of pyrene- and TC1-labeled PMMA films. The increase in *Tg* with decreasing film thickness is identical for pyrene- and TC1-labeled PMMA films and is qualitatively consistent with other studies of single-layer PMMA films supported on silica substrates (Keddie 1994a; Fryer 2001; Park 2004). For $d > \sim 90$ nm, *Tg* is independent of thickness. For $d < \sim 90$ nm, *Tg* increases roughly linearly on a logarithmic scale with decreasing thickness. For a 20-nm-thick film, *Tg*(film) – *Tg*(bulk) = 9 K.

The direct impact of the substrate on the local *Tg* near the polymer-substrate interface of a bulk PMMA film is determined using a bilayer film geometry (see Figure 5-3a inset) in which a labeled PMMA layer of known thickness (*h*) is sandwiched between the substrate and an unlabeled PMMA layer which is 240-nm-thick. The overall bilayer film thickness is sufficiently large that *Tg*(film) = *Tg*(bulk). Figure 5-3a shows that *Tg*(substrate layer) – *Tg*(bulk) = 10 K for a 12-nm-thick substrate layer. When the thickness of the substrate layer is increased, the value of *Tg*(substrate layer) – *Tg*(bulk) gradually approaches zero at *h* = 70-80 nm. In a similar experiment conducted by Ellison

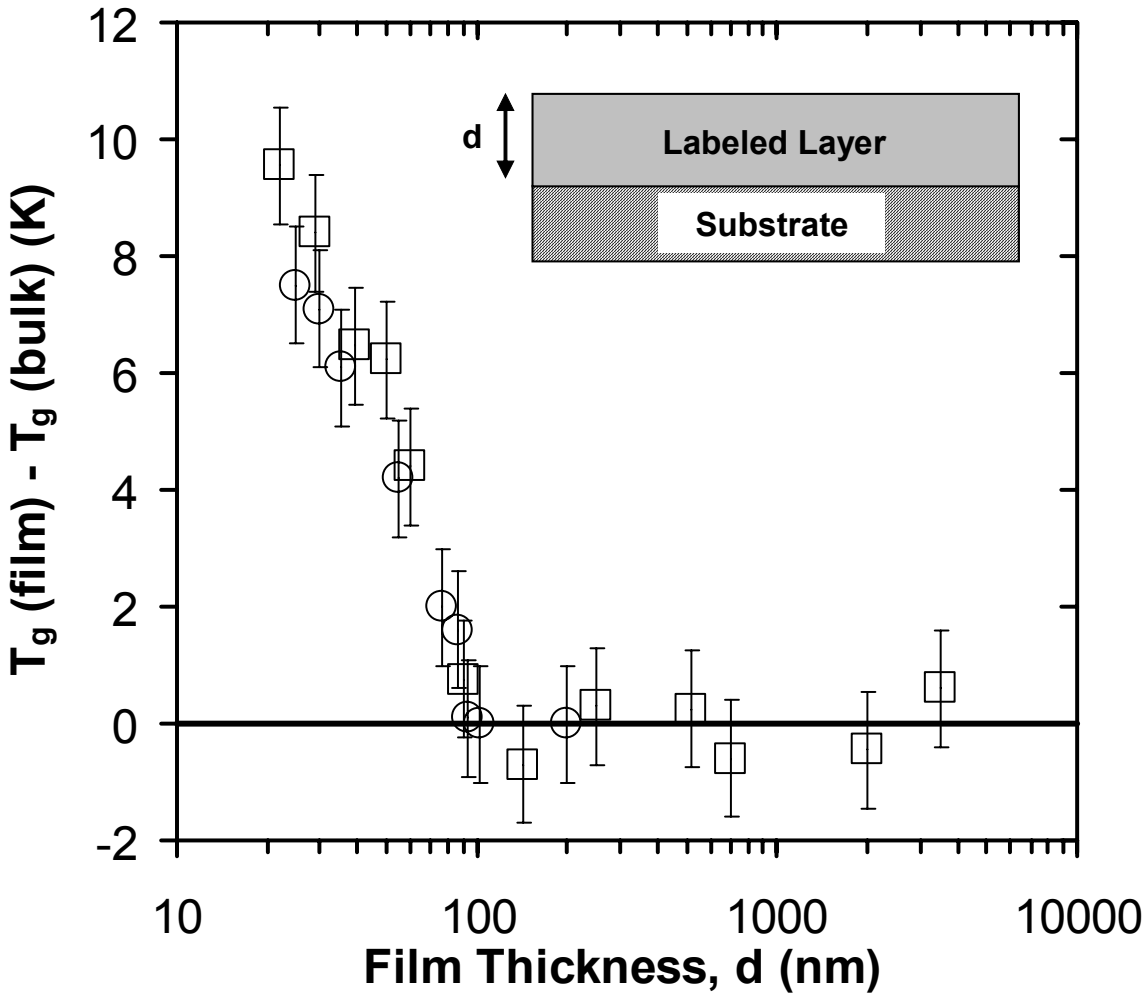

Figure 5-2. *Tg*(film) - *Tg*(bulk) of pyrene-labeled PMMA (□) and TC1-labeled PMMA (○) single layer films as a function of film thickness (*d*). Within experimental error, both chromophores detect identical increases in *Tg* of PMMA as a function of film thickness. (Inset) Film geometry used in experiments.

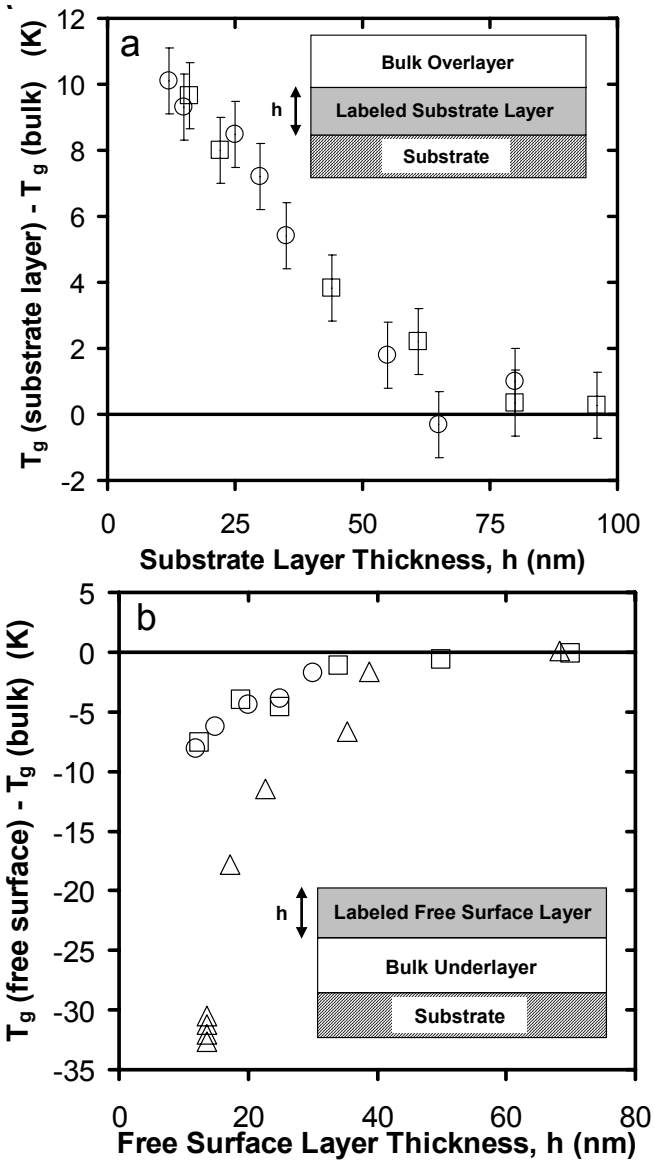

Figure 5-3. Measurement of substrate- and free-surface layer *Tg* values using bilayer films in which one layer is labeled with either pyrene (□) or TC1 (○). **(a)** *Tg*(substrate layer) - *Tg*(bulk) of labeled substrate layer film as a function of the labeled substrate layer film thickness (*h*). Film thickness of bulk overlayer film is 240 nm. (Inset) Film geometry used in experiments. **(b)** *Tg*(free surface) - *Tg*(bulk) of free-surface layer film as a function of free-surface layer film thickness (*h*). Thickness of bulk underlayer is 240 nm. Pyrene-labeled PS (triangles) data are from Ellison *et al.* (Ellison 2003). (Inset) Film geometry used in experiments.

et al. (Ellison 2003) with a 14-nm-thick substrate layer in a bulk PS bilayer film found that *Tg*(substrate layer) – *Tg*(bulk) = 0 K. The difference in the *Tg* behavior of the PS and PMMA substrate layers can be explained by hydrogen bonding effects that are present at the PMMA/silica substrate interface (Keddie 1994a; Grohens 2002; Priestley 2005a, 2005b; Park 2004; Mundra 2006, 2007a, 2007b) but absent at the PS/silica substrate interface (Keddie 1994a, 1994b; Ellison 2003, 2005a).

Placement of a labeled PMMA layer atop a bulk film allows for local *Tg* measurements at the free surface of PMMA. Labeled PMMA layers of known *h* are floated onto the surface of a 240-nm-thick PMMA film supported on silica. The overall bilayer film thickness is sufficiently large that *Tg*(film) = *Tg*(bulk). The impact of the free surface on modifying *Tg* dynamics is opposite that of the silica substrate. Figure 5-3b shows that *Tg*(free surface) – *Tg*(bulk) = - 7-8 K for a 12-nm-thick free-surface layer. When the thickness of the labeled free-surface layer is increased, the value of *Tg*(free surface) – *Tg*(bulk) gradually approaches zero at *h* = 40 nm. For purposes of comparison, the free-surface layer *Tg* measurements of PS from Ellison *et al.* (Ellison 2003) are replotted in Figure 5-3b. As seen in Figure 5-3b, the free-surface layer thicknesses at which PMMA and PS begin to exhibit reductions in *Tg* are approximately the same. However, the magnitude of the reduction in *Tg* at the free surface is much weaker in PMMA than in PS. These results demonstrate that the ability of a free surface to perturb *Tg* dynamics is strongly dependent on the chemical structure of the polymer. This observation is in accord with *Tg* measurements done on 40-nm-thick freely standing (two free surfaces) PMMA (*Mn* = 718,000 g/mol) and PS (*Mn* = 690,000 g/mol) films, for which the values of *Tg* were reduced by ~15 K and ~52 K, respectively, compared to *Tg*(bulk) (Roth 2003).

Regarding the effects of surfaces and interfaces on *Tg* shown in Figure 5-3, the increase in *Tg* near the silica substrate is understood qualitatively to arise from hydrogen

bonding interactions between the ester side groups of PMMA and the hydroxyl groups on the silica substrate. In the absence of hydrogen bonding interactions, as in the case of PS films supported on silica substrates, no change in *Tg* is expected or observed. In contrast, the underlying cause of the large difference in the magnitude of the free surface effects in PMMA and PS films is not yet understood even at a qualitative level. There is no molecular-scale mechanism or theory by which to explain the observations. Further study of the effect of repeat unit structure on perturbations to *Tg* at free surfaces of films is warranted.

Employing a 12-nm-thick labeled middle layer, trilayer films are used to determine the length scale over which the free surface and substrate modify *Tg* dynamics within bulk PMMA films. As illustrated in Figure 5-4, when an 8-nm-thick unlabeled free-surface layer is placed on top of a 12-nm-thick labeled middle layer (meaning that the labeled-layer depth within the film is 8-20 nm), the *Tg* of the labeled layer is reduced by only 2 K compared to *Tg*(bulk). When the unlabeled free-surface layer thickness is 12 nm, the labeled middle layer reports *Tg*(bulk). In the opposite case, when a 12-nm-thick labeled middle layer is displaced 12 nm from the substrate interface, its *Tg* is increased by 5 K compared to *Tg*(bulk). As shown in Figure 5-4, it is not until the labeled middle layer is displaced ~ 50-70 nm from the substrate interface that it reports a *Tg* value that is within experimental error equal to *Tg*(bulk).

These experiments demonstrate several key points. First, there is a distribution of *Tg*s near the free surface and substrate interface of bulk PMMA films supported on silica substrates. Second, the results disallow the concept of simple two- and three-layer models to explain the *Tg*-nanoconfinement effect (Keddie 1994b; Forrest 2000) and instead imply that a distribution of *Tg*s should be incorporated into any model being used to explain *Tg*-nanoconfinement behavior (Ellison 2003). Third, the length scale over which the substrate interactions modify *Tg* dynamics within a bulk PMMA film is greater than

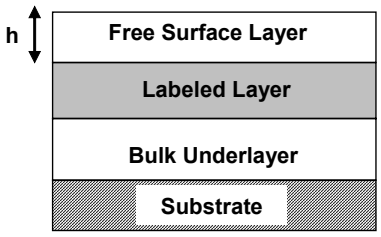

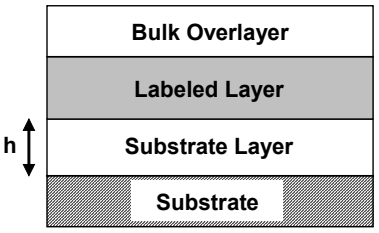

Surface Layer Thickness, h (nm)	Labeled Layer Depth (nm)	T_g (film) - T_g (bulk) (K)
8	8 - 20	-2
12	12 - 24	0

Substrate Layer Thickness, h (nm)	Labeled Layer Depth (nm)	T_g (film) - T_g (bulk) (K)
12	12 - 24	5
26	26 - 36	4
56	56 - 68	1

Figure 5-4. Determination of the distribution of *Tg*s as a function of depth displaced from either the free surface or substrate-polymer interface using trilayer films in which the middle layer is labeled with either pyrene (□) or TC1 (○). Labeled middle layer is 12-nm-thick, while bulk overlayer / underlayer film thickness is 240 nm. Free surface / substrate layer film thickness (*h*) is varied in trilayer film studies.

that associated with free-surface effects, consistent with the notion that perturbations to *Tg* caused by substrate effects are stronger than those caused by free-surface effects for PMMA supported on silica.

Figure 5-5 allows one to quantify the relative strengths of the competing free-surface and substrate effects and the length scales over which the stronger substrate effects modify *Tg* dynamics in confined PMMA films. Specifically, the impact of the substrate on the *Tg* of a 12-nm-thick labeled free-surface layer is measured as a function of overall film thickness (*h'*). The length scale separating the 12-nm-thick free-surface layer from the substrate is adjusted by controlling the underlayer thickness. As shown in Figure 5-5, when $h' > 250$ nm (**I**), the *Tg* within the free-surface layer is reduced by 7-8 K from *Tg*(bulk). At these thicknesses, the free-surface *Tg* dynamics are unaffected by the increased *Tg* at the polymer-substrate interface. When $90 \text{ nm} < h' < 250$ nm (**II**), the free-surface layer *Tg* increases with decreasing *h'* but remains below *Tg*(bulk). At these thicknesses, the effects of the strongly reduced cooperative segmental mobility at the polymer-substrate interface percolate across the film, increasing the free-surface layer *Tg*. When $h' < 90$ nm (**III**), the *Tg* within the free-surface layer actually exceeds *Tg*(bulk) and continues to increase with decreasing *h'*; this means that the perturbed *Tg* dynamics at the substrate that percolate across the film are sufficiently strong within the free-surface layer to dominate the perturbations to *Tg* caused by the free surface. Thus, under certain circumstances of nanoconfinement with attractive polymer-substrate interactions, the *Tg* of an ultrathin free-surface layer may exceed *Tg*(bulk). This is the first report of such an effect.

Figure 5-6 illustrates the effect of overall film thickness on *Tg*(substrate layer) – *Tg*(bulk) of a 12-nm-thick substrate layer within a PMMA bilayer film. When the overall film thickness is 250-260 nm, *Tg*(substrate layer) – *Tg*(bulk) = 9-10 K. As shown in Figure 5-6, decreasing the overall thickness results in a decrease in the substrate layer *Tg*.

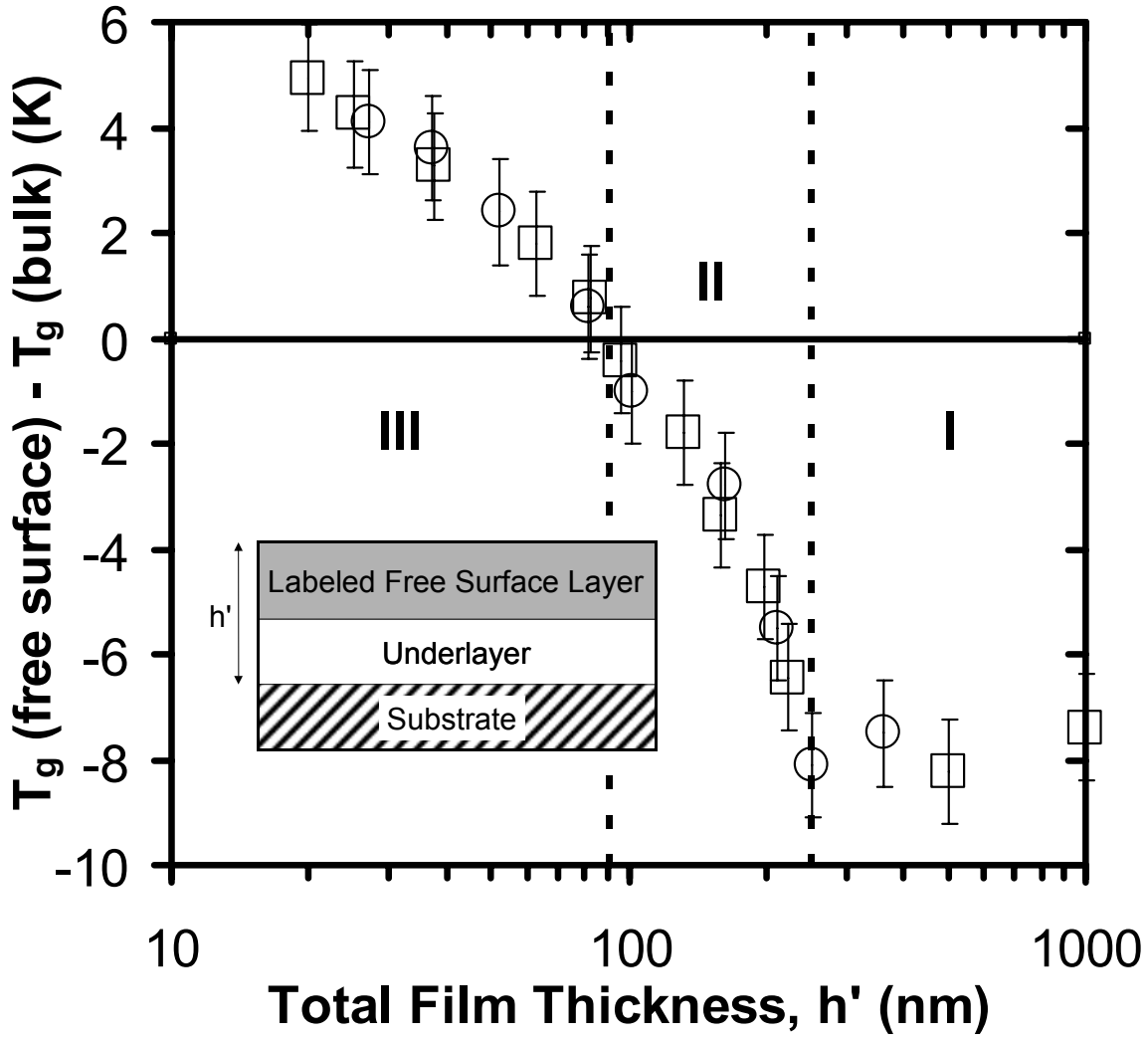

Figure 5-5. *Tg*(free surface) - *Tg*(bulk) of pyrene-labeled (□) or TC1-labeled (○) free-surface layer as a function of overall film thickness (*h'*). The labeled free-surface layer thickness is held constant at 12 nm while the underlayer thickness is varied.

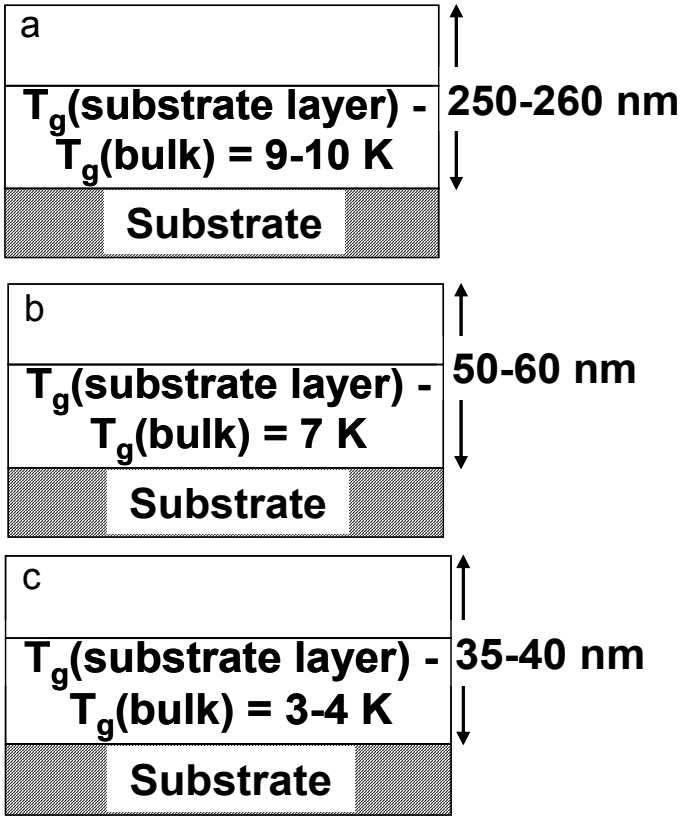

Figure 5-6. Influence of overall film thickness on *Tg*(substrate layer) - *Tg*(bulk) of a 12-nm-thick substrate layer within a bilayer film. The overall film thickness is **(a)** 250-260 nm, **(b)** 50-60 nm, and **(c)** 35-40 nm.

When the overall thickness of the bilayer film is reduced to 50-60 nm, *Tg*(substrate layer) – *Tg*(bulk) = 7 K. Further reduction of the overall thickness to 35-40 nm leads to *Tg*(substrate layer) – *Tg*(bulk) = 3-4 K.

According to Figure 5-5 and Figure 5-6, when the overall bilayer film thickness exceeds 250 nm, *Tg*(free surface) – *Tg*(bulk) = – 7-8 K for a 12-nm-thick free-surface layer and *Tg*(substrate layer) – *Tg*(bulk) = 9-10 K for a 12-nm-thick substrate layer. The difference between the *Tg*s at the free surface and substrate is 16-18 K. When the overall bilayer film thickness is reduced to 35-40 nm, *Tg*(free surface) – *Tg*(bulk) = 3-4 K for a 12-nm-thick free-surface layer as well as for a 12-nm-thick substrate layer. The difference between the *Tg*s at the free surface and substrate is 0 K. It is also noteworthy that in 35- to 40-nm-thick bilayer films, the *Tg*s of the free-surface and substrate layers are identical within experimental error to the *Tg* of a 35- to 40-nm-thick single-layer PMMA film (see Figure 5-2). Thus, with increasing nanoscale confinement, the gradient in *Tg* across a PMMA film is reduced and, within the experimental uncertainty of the multilayer method, can be eliminated under circumstances of extreme confinement. The observation that nanoconfinement leads to a reduction in the gradient in *Tg* across a PMMA film is consistent with similar measurements conducted on PS films by Ellison *et al.* (Ellison 2003). The results associated with both PS and PMMA films indicate that below a certain overall thickness the *Tg* dynamics adjust to satisfy the constraint that the gradient in *Tg* dynamics across an ultrathin polymer film cannot be too sharp and abrupt (Ellison 2003).

A comparison of Figure 5-2 and Figure 5-3a reveals that *Tg*(film) – *Tg*(bulk) = 6 K for a 50-nm-thick single-layer PMMA film and *Tg*(substrate layer) – *Tg*(bulk) = 2 K for a 50-nm-thick substrate-layer in a bulk bilayer PMMA film. This indicates that placing a layer with bulk *Tg* dynamics over a 50-nm-thick substrate layer can lead to faster cooperative dynamics and a lower *Tg* in the substrate layer. The observation that

the *Tg* dynamics of a layer is affected by the dynamics of an adjacent layer have been previously reported for PS films (Ellison 2003). For example, the *Tg* of a 14-nm-thick labeled PS free-surface layer in a bulk bilayer film is ~ 5 K higher than the *Tg* of a 14-nm-thick single-layer film. This indicates that placing a PS layer with average bulk *Tg* dynamics underneath a 14-nm-thick PS layer results in slower cooperative dynamics and a higher *Tg* in the free-surface layer.

This latter observation has recently been explained in the context of the coupling model (Ngai 2006), which recognizes the importance of many-molecule or many-segment relaxation dynamics associated with the glass transition. The placement of a bulk layer with slower dynamics underneath a 14-nm-thick surface layer imposes intersegmental constraints on the surface layer. These constraints result in slower dynamics and a higher *Tg* in the 14-nm-thick free-surface layer than in the 14-nm-thick film (Ngai 2006). A similar explanation can be given for some of the PMMA results. Placement of a layer with bulk *Tg* dynamics atop a 50-nm-thick substrate layer imposes intersegmental interactions on the substrate layer, resulting in faster dynamics and a lower *Tg*. However, it is worth mentioning that $Tg - Tg(\text{bulk}) = 9$ K for both a 20-nm-thick single-layer film and a 20-nm-thick substrate layer in a bulk bilayer film. Thus, for a 20-nm-thick film in which it is possible for most of the PMMA chains to be pinned at the substrate interface (Baschnagel 2003) via hydrogen bonds, placing a thick layer atop it has no measurable impact on its *Tg*. This means that the substrate effects are strong enough to dominate the effects of intersegmental constraints imposed by the bulk overlayer film.

The results reported in Figures 5-3 to 5-6 can occur only if perturbations caused by surfaces or interfaces to *Tg* dynamics propagate many layers of CRRs within the films. That is, if on average the cooperative dynamics in a layer are perturbed substantially relative to bulk, then, on average, many adjoining layers must also have

their dynamics perturbed, albeit to lesser extents. This idea is consistent with simulations (Donati 1998; Glotzer 2000) and experiments (Ellison 2003; Weeks 2000) indicating that glass-formers do not typically have abrupt transitions in neighboring regions of local dynamic heterogeneity from very fast dynamics to slow dynamics and is consistent with dielectric noise studies (Russell 2000) suggesting that a minimum length scale (> 40 nm) is required to obtain the full breadth of the distribution of cooperative relaxation dynamics in polymers near *Tg*.

From a scientific point of view, the results in Figs. 5-3 to 5-6, associated with *Tg* behavior that is strongly perturbed by interfacial effects, stand in opposition to the simple definition of a CRR offered more than forty years ago (Adam 1965) in which configurational changes within a CRR are assumed to occur independently of neighboring CRRs. Instead, the results highlight the long-range effects of substrate interactions on *Tg* dynamics and are qualitatively consistent with recent models (Merabia 2004; Long 2001) and simulations (Baljon 2004) suggesting that percolation of slow-relaxing regions associated with attractive polymer-substrate interactions can explain enhancements in average *Tg*s in confined films.

5.4 Conclusions

The study in this chapter employs an innovative fluorescence/multilayer method to investigate the impact of nanoconfinement and interfacial effects on the *Tg* of PMMA films supported on silica substrates. With single-layer PMMA films that are less than 90-nm-thick, *Tg* increases roughly linearly with decreasing logarithmic thickness. The use of bilayer films reveals that, compared to *Tg*(bulk), *Tg* is reduced at the free surface by 7-8 K for a 12-nm-thick free-surface layer and increased at the substrate interface by 10 K for a 12-nm-thick substrate layer of a bulk film, resulting in a *Tg*-gradient across the film. Measurements of confined bilayer films reveal that the stronger substrate effects percolate across the film to modify the *Tg* dynamics at the free surface. Thus, with

nanoconfinement, the stronger substrate effects dominate the free-surface effects, providing an explanation for the increase in average *Tg* with decreasing single-layer PMMA film thickness. With extreme confinement, the *Tg*-gradient across the film thickness is suppressed, with both substrate layer and free-surface layer *Tg*s exceeding *Tg*(bulk). These results demonstrate that strongly perturbed *Tg* dynamics at the interfaces propagate across many layers of CRRs within the films, meaning that configurational changes associated with cooperative segmental dynamics within a CRR do not occur independently of neighboring CRRs. Thus, insight into the fundamental nature of the glass transition may be gained by measuring the nanoscale distributions of *Tg*s in confined polymers.

CHAPTER 6

DEVELOPMENT OF A NOVEL INTRINSIC FLUORESCENCE TECHNIQUE FOR CHARACTERIZING THE Tg OF POLYSTYRENE AND STYRENE CONTAINING RANDOM COPOLYMERS IN THIN AND ULTRATHIN FILMS

6.1 Introduction

Nanoscale confinement of polymers can lead to significant deviations from bulk polymer behavior, including those related to crystallization (Frank 1996b; Reiter 2001; Loo 2000; Jones 2004), physical cross-linking in associative polymers (Kim 2002b), thermal expansion coefficients (Orts 1993; Oh 2004; Kanaya 2001, 2003; Soles 2004b; Beaucage 1993; Mukherjee 2002), the glass transition temperature (*Tg*) (Keddie 1994a, 1994b, 1995; Ellison 2002a, 2002b, 2003, 2004a, 2004b, 2005a, 2005b; Beaucage 1993; Mukherjee 2002; Tanaka 2004; Li 2004; Blum 2006; Bernazzani 2002; Pratt 2005; Baljon 2005; van den Berg 2004, 2006), and physical aging (Priestley 2005a, 2005b; Kawana 2003). Some of the earliest as well as very recent studies of thermal expansion coefficient and *Tg* behavior in nanoconfined polymer films have indicated that there can be significant effects associated with the process and thermal history of the films (Orts 1993; Kanaya 2003; Soles 2004b; Beaucage 1993; Ellison 2002a). Several studies have specifically suggested that some of the unusual or anomalous *Tg* behavior observed in ultrathin films may be associated with stresses that are built in during the spin coating or spin casting process and remain unrelaxed during the *Tg* measurement (Mukherjee 2002; Kawana 2003; Prest 1980a). While it has been appreciated for at least twenty-five years that polymer film formation by spin coating and even the much milder solvent casting process can lead to orientation and non-equilibrium conformations of polymer chains and thereby residual stress effects (Prest 1980a, 1980b; Cohen 1981; Ree 1997; Pottinger 1994; Lin 1993), there has been relatively little direct comparison (Kanaya 2003; Soles

2004b) of how the thermal history of spin-coated polymer films leads to relaxation of residual stresses in polymer films and whether the apparent *Tg* is affected by unrelaxed residual stresses.

A potentially powerful manner with which to obtain a qualitative measure of the residual stresses in spin-coated films of polystyrene (PS) in combination with *Tg* values in polymer films is intrinsic fluorescence. Intrinsic fluorescence of PS consists both of monomer and excimer fluorescence, the former due to emission from a single excited-state phenyl ring and the latter due to emission from an excited-state dimer consisting of two phenyl rings in a parallel, sandwich-like conformation with an inter-ring separation distance of 3-4 Angstroms (Vala 1965). Intrinsic fluorescence of PS and other polymers has been shown to be highly sensitive to issues ranging from local polymer conformational populations in solution and phase behavior in solvents and polymer blends to local microenvironments in bulk homopolymers (Basile 1962; Torkelson 1981, 1983, 1984; Gelles 1982a, 1982b; Major 1986; Tsai 1988a, 1988b; Itagaki 1990, 1996; Xie 1993; Clauss 1995; Ylitalo 1996; Sanz 2002; Corrales 2004; Alberty 2005). In particular, excimer formation in PS solutions and blends is almost exclusively associated with trans-trans conformations in meso dyads along the PS chain (Gelles 1982a; Bokobza 1977); i.e., an increase in trans conformations along the local isotactic regions of a PS chain will result in an increase in intramolecular excimer fluorescence.

In 1975, Frank (Frank 1975) reported that excimer fluorescence of a guest aromatic vinyl polymer, poly(2-vinylnaphthalene), dissolved in a polymer host can be used to monitor relaxation of the non-equilibrium chain conformation distribution of the guest polymer at temperatures near the *Tg* of the host polymer. Later, in 1989 Frank and co-workers (Kosbar 1989) demonstrated that the ratio of excimer fluorescence intensity to monomer fluorescence intensity, *Ie*/*Im*, in spin-cast PS films increased with increasing spin speed (leading to decreasing thickness) and thereby radial stress. The elevated *Ie*/*Im*

values obtained in spin-cast films were qualitatively consistent with the results of a study (Kosbar 1989) showing that uniaxial alignment of PS films leads to an increase in *Ie*/*Im* values. It was rationalized that chain orientation via spin-casting can lead to an increase in the concentration of trans conformations along the chains (associated with intramolecular excimer forming sites), the concentration of intermolecular excimer forming sites, and a higher rate of energy migration to excimer forming sites. (It should be noted that the use of intrinsic fluorescence to monitor relaxation of residual stress associated with processing of polymer films is fundamentally different from studies employing extrinsic probe or label fluorescence to monitor structural relaxation or physical aging in glassy polymer films (Ellison 2002a; Priestley 2005a, 2005b; Gupta 1983; Shmorhun 1990; Royal 1992, 1993; van den Berg 2006).)

Several years ago, Ellison and Torkelson demonstrated that the temperature dependence of the intrinsic fluorescence of a 12-μm-thick PS film may be used to determine *Tg* (Ellison 2002b). At that time, they were not able to obtain *Tg* values for ultrathin PS films (≤ 100 nm) using intrinsic fluorescence due to a low signal-to-noise ratio and instead used probe or label fluorescence (pyrenyl dyes or molecular "rotor" dyes) for *Tg* measurements (Ellison 2002a, 2002b, 2003, 2004a, 2004b, 2005a, 2005b). With improved instrumentation and experimental technique, it is now possible to obtain high signal-to-noise ratios for intrinsic fluorescence measurements of thin and ultrathin films of PS and styrene (S)/methyl methacrylate (MMA) random copolymers.

This chapter describes the first research showing that intrinsic fluorescence from thin and ultrathin films of PS and S/MMA random copolymers can be used to characterize *Tg*. Fluorescence is revealed to be a powerful technique not only to characterize *Tg* in thin and ultrathin films of styrene containing random copolymers and the competing effects of free-surfaces and substrate interactions in these systems but also to determine the effect of process conditions and the relative state of relaxation of the

residual stresses present in the system. (For further details on the use of intrinsic fluorescence to determine the effect of process conditions and the relative state of relaxation of the residual stresses associated with local chain conformations, see Chapter 11.)

6.2 Experimental

6.2.1 Copolymer Synthesis and Characterization

Polystyrene and S/MMA random copolymers were synthesized by bulk free radical polymerization at 343 K using benzoyl peroxide (Aldrich, 97%) as initiator. Styrene and methyl methacrylate (Aldrich) and were deinhibited with inhibitor remover (Aldrich) and dried over CaH_2. Copolymer composition was controlled by varying the comonomer content used in the copolymerizations; fractional conversions were limited to less than 10% to avoid composition drift. Resulting copolymers were purified by dissolution in toluene (Fisher, 99.9%) and precipitation in methanol (Fisher, 99.9%) at least five times to remove residual monomer and initiator. Samples were dried in a vacuum oven at ~ 393 K for several days prior to use.

The styrene mole fraction (F_S) of each copolymer was measured via ^{1}H NMR (Varian Inova 500 Mhz spectrometer) spectroscopy with $CDCl_3$ as solvent and was in good agreement with expectations based on reactivity ratios for the S/MMA system (Brandrup 1999). Number average molecular weights of PS and all copolymers exceeded 100,000 g/mol (gel permeation chromatography relative to PS standards in tetrahydrofuran (THF)). The bulk *Tg*s of PS and the copolymers were measured by differential scanning calorimetry (DSC) using a Mettler-Toledo DSC822e at a 10 K/min heating rate on the second heating cycle after quenching from elevated temperature at 40 K/min. Table 6-1 provides details on PS and copolymer characterization.

Table 6-1: Characterization of S/MMA copolymers used in this study: F_S is the cumulative S mol fraction in the copolymers; M_S and M_{MMA} are the mol fractions of S and MMA in the monomer mix used to make the copolymers; f_{SS} and N_S are the S-S dyad fraction and number average sequence length of S units in the copolymers, respectively. Also provided are the bulk *Tg* values determined by DSC and fluorescence.

F_S	M_S	M_{MMA}	f_{SS}	N_S	$f_{SS}N_S$	*Tg*(onset) DSC	*Tg* Fluor.
1.000	1.000	0.000	1.000	---	---	378 K	378 K
0.782	0.865	0.135	0.597	4.34	2.591	376 K	379 K
0.652	0.730	0.270	0.372	2.41	0.895	377 K	377 K
0.581	0.637	0.363	0.266	1.91	0.508	378 K	377 K
0.390	0.343	0.657	0.073	1.27	0.093	376 K	377 K
0.215	0.124	0.876	0.027	1.07	0.029	379 K	377 K
0.088	0.025	0.975	0.013[a]	1.01	0.013	378 K	378 K

[a] Denotes fraction calculated from reactivity ratios.

6.2.2 Film Studies

Relatively thick films (~ 5 μm) were prepared by solution casting concentrated solutions of PS or copolymers dissolved in THF onto high-purity fused quartz slides. The slides were initially washed with a 10% sodium hydroxide/70% ethanol/20% water solution and then solvent washed. These thick films were dried for 24 hr in a petri dish followed by vacuum drying at room temperature for 24 hr and then at 383 K for 36 hr. The slow drying process was used to prevent bubble or crack formation. Films that developed bubbles or cracks were discarded. Thin and ultrathin films were prepared by spin coating dilute PS or copolymer solutions in THF of various concentrations at speeds of 500 to 4000 rpm for 60 sec, yielding film thicknesses ranging from 20 nm to 1000 nm (Hall 1998a; Spangler 1990, 1992). Films used for *Tg* measurements were annealed in a vacuum oven for 24 hr at 383 K. Film thickness was measured with a Tencor P10 profilometer (calibration was verified by using a 14-nm step height standard from VLSI standards) by taking an average of at least ten measurements close to the center of the film where fluorescence was measured.

6.2.3 Instrumentation

A Spex Fluorolog-2DMIB fluorimeter was used to measure fluorescence of films with thickness exceeding 2000 nm. Measurements employed a front-faced geometry with 2.5 mm excitation and emission slits (band pass = 4.5 nm). For thin and ultrathin films, fluorescence was measured using a PTI QM-2001 SE fluorimeter using a front-face geometry with 1 mm excitation (bandpass = 4.0 nm) and 1 mm emission slits (band pass = 2.0 nm). As the PTI fluorimeter has greater excitation intensity than the Spex fluorimeter, the smaller slit size was used with the PTI instrument to prevent films from photobleaching at high temperature. Film temperature was controlled using a microprocessor controller (Minco Products) with a Kapton ribbon heater attached to a flat aluminum plate with a hole in the center to prevent scattering or fluorescence from the

heater itself. For intrinsic fluorescence, excitation was done at 260 nm, and the emission spectrum was measured from 270 nm to 410 nm. Unless otherwise specified, fluorescence spectra used to measure *Tg* were recorded upon cooling after having annealed samples at ~ *Tg* + 40 K for 15-60 min. (For further information on measurement of *Tg*s by fluorescence, see Chapters 3 and 4.)

6.3 Intrinsic Fluorescence for Characterizing Tg in Thin and Ultrathin Films

6.3.1 Solution Studies

Figure 6-1 illustrates how fluorescence intensity and spectral shape are functions of S composition in dilute solutions of S/MMA copolymers and PS. Figure 6-1a compares the spectrum of PS with those of 58/42 mol% and 22/78 mol% S/MMA random copolymers. For PS, a maximum intensity is observed at ~ 328 nm, indicative of excimer fluorescence, with a second, lesser peak at ~ 285 nm. With decreasing S content in the copolymers, there is a reduction in excimer fluorescence and a major increase in monomer fluorescence. In addition, an isobestic or isoemissive point (point of common intensity) is observed at ~ 320 nm. This point is characteristic of the fact that the fluorescence in these systems, which contain equivalent concentrations of S repeat units, is associated with only two potentially interconvertible species (Hirayama 1969), excited-state monomer and excimer.

Figure 6-1b compares the spectral shapes of PS with 78/22 mol% S/MMA copolymer and of 22/78 mol% S/MMA copolymer with 9/91 mol% S/MMA copolymer. In the case of PS and the high S content copolymer, the spectral shapes are identical at wavelengths of 335 nm and greater, indicating that, within error, all fluorescence in this range is due to excimer fluorescence. However, PS and the high S content copolymer differ greatly in spectral shapes at lower wavelengths due to the increasing amount of monomer fluorescence with decreasing S content. In the case of the two lowest S content copolymers, the spectral shapes are nearly identical and, within error, indicate a nearly

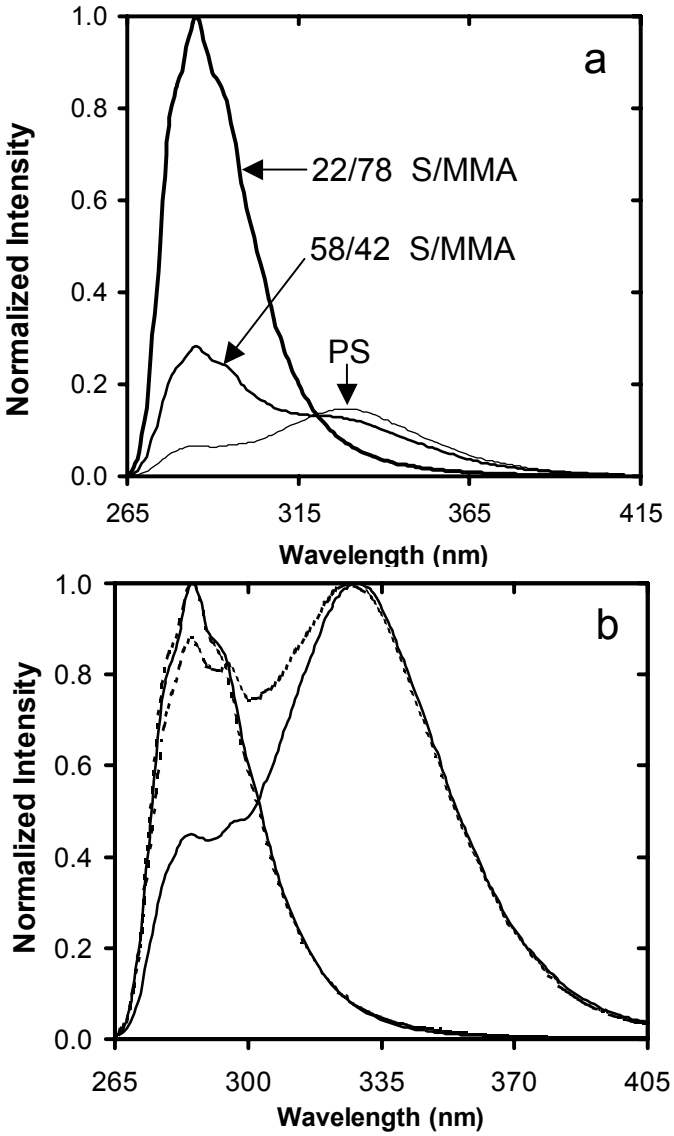

Figure 6-1: **(a)** Fluorescence emission spectra of dilute solutions of PS and S/MMA copolymers in THF as a function of S mol fraction. Solutions contain an equal S repeat unit concentration of 0.50 g/L. Spectra are normalized to one at the peak intensity of the 22/78 mol% S/MMA copolymer. **(b)** Fluorescence emission spectra of dilute solutions of PS and S/MMA copolymers in THF. Spectra with peak intensities at ~328 nm are for PS (bold line) and 78/22 mol% S/MMA copolymer (dotted line). Spectra with peaks at ~285 nm are for 9/91 mol% S/MMA (bold line) and 22/78 mol% S/MMA (dotted line). Solutions contain an equal S repeat unit concentration of 0.50 g/L. Spectra are normalized to one by their individual peak intensity.

complete absence of excimer fluorescence. The details of the fluorescence spectra presented in Figure 1 are in accord with previous studies of the fluorescence of dilute solutions of PS and random S/MMA copolymers (Torkelson 1981, 1984; Gelles 1982a; Tsai 1988a, 1988b; Itagaki 1990; Xie 1993; David 1973; Reid 1978; Hoyle 2001).

6.3.2 Film Studies

Figure 6-2 compares the intrinsic, room-temperature fluorescence emission spectra of neat, bulk films of PS and two S/MMA copolymers; each spectrum has been normalized to unity at the peak intensity. The neat, bulk PS film exhibits mostly excimer fluorescence and little monomer fluorescence, much less than that observed in dilute solution relative to excimer fluorescence (Figure 6-1). A significant shift from excimer to monomer fluorescence is observed with decreasing styrene content in the copolymers. However, as with the neat PS, *Ie*/*Im* is significantly greater in a copolymer film of given composition than in a dilute copolymer solution of the same composition. This effect may be due to several factors (Torkelson 1983): different conformational states in the bulk film as compared to dilute solution favoring intramolecular excimer formation; interpolymer excimer formation in the bulk film; and an enhancement, relative to dilute solution, in the migration of the excited-state energy to an excimer-forming site in the bulk film.

Previous research (Ellison 2002b) has shown that the *Tg* value of bulk, neat PS can be measured by plotting intrinsic fluorescence intensity at a given wavelength as a function of temperature over a range of at least 60-70 K roughly centered at *Tg*. The *Tg* is determined via the intersection of the linear temperature dependences of intensity deep in the rubbery and glassy states. In the results described below, we employ plots of integrated intensity (integrated across the fluorescence spectrum) as a function of temperature. As reported recently in an extrinsic fluorescence study (Ellison 2005a) and in Chapter 4, this approach minimizes errors, leading to more precise *Tg* determinations.

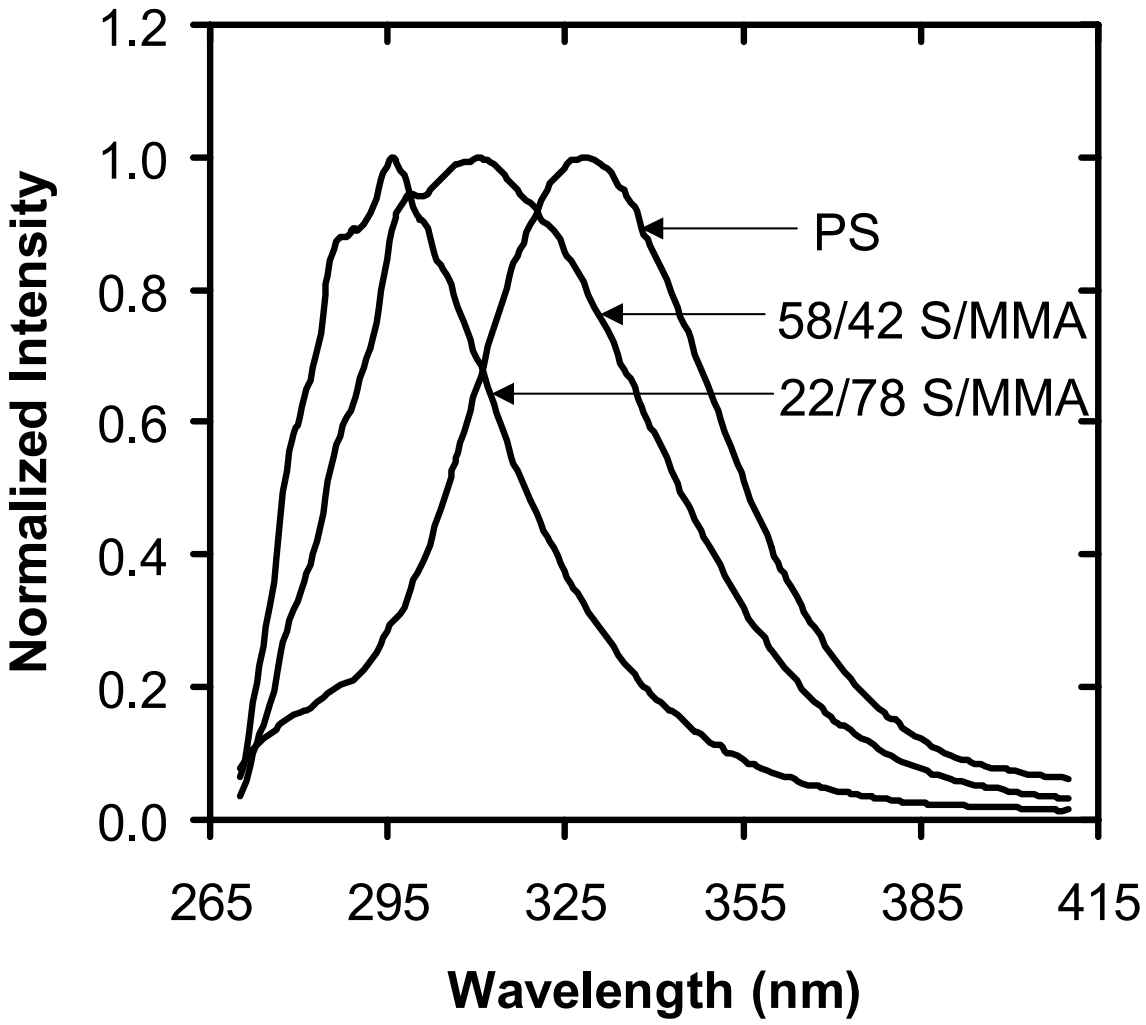

Figure 6-2: Intrinsic fluorescence emission spectra for bulk films (4-5 μm thick) of PS and 58/42 mol% S/MMA and 22/78 S/MMA random copolymers at room temperature. Intensity is normalized to one at the peak intensity each film.

(Within experimental error, identical *Tg* determinations are made when fluorescence is monitored as a function of temperature over a range of 100 - 110 K or a range of 60 - 70 K around *Tg*.)

Figure 6-3 shows *Tg* determinations for films of PS and selected S/MMA copolymers. Several points are noteworthy from this figure. In each case, there is a reduction in the strength of the glass transition (defined by the change between the rubbery-state and glassy-state temperature dependences of intensity) in the ultrathin films relative to the thin films, a result that is consistent with previous determinations of *Tg* in PS films using extrinsic pyrene probe fluorescence (Ellison 2003) and ellipsometry (Kawana 2001). (Figures 6-3c and 6-3e provide rescaled plots of data shown in Figures 6-3b and 6-3d for systems in which the *Tg* strength is particularly weak; these rescaled plots show that precise *Tg* values can nevertheless be obtained in such cases with fluorescence data of sufficient quality.) Second, the overall change in integrated intensity with temperature is much smaller in ultrathin films, a result also found using extrinsic pyrene fluorescence to determine *Tg* in PS and several other styrenic-based homopolymers (Ellison 2005a). Finally, in the case of low S mol% copolymers, e.g. 22/78 mol% and 9/91 mol% S/MMA, the temperature dependence of intensity in the glassy state is greater than that in the rubbery state, the opposite of what is observed in PS films or copolymers with 39 mol% or greater S content. In previous studies in which *Tg*s of PS and poly(methyl methacrylate) were measured via pyrene probe or label fluorescence (Ellison 2002a, 2002b, 2003, 2004a, 2005a; Priestley 2005a, 2005b), a greater temperature dependence of intensity was always observed in the rubbery state, in accord with the notion that a significant portion of the temperature dependence of fluorescence of pyrenyl dyes in glass-forming polymers reflects local density effects, i.e., a slightly denser local environment near a pyrene dye accommodates less nonradiative decay of the excited state leading to higher intensity. As the thermal expansion

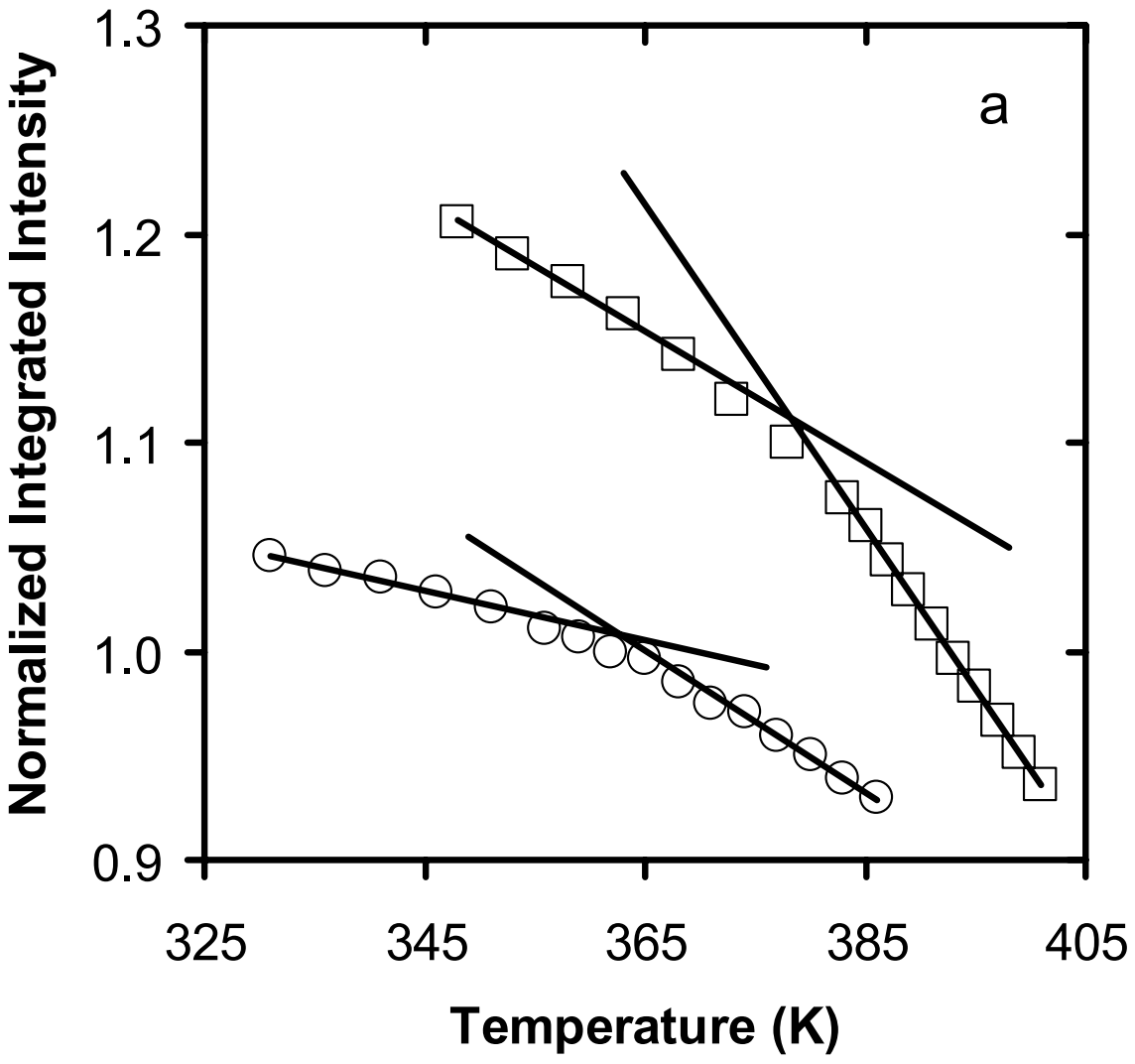

Figure 6-3: (a) Temperature dependence of the integrated intrinsic fluorescence intensity for 4570-nm-thick (□) and 22-nm-thick (○) PS films. (The integrated intensity is normalized to one at the respective *Tg* of each film and arbitrarily shifted.)

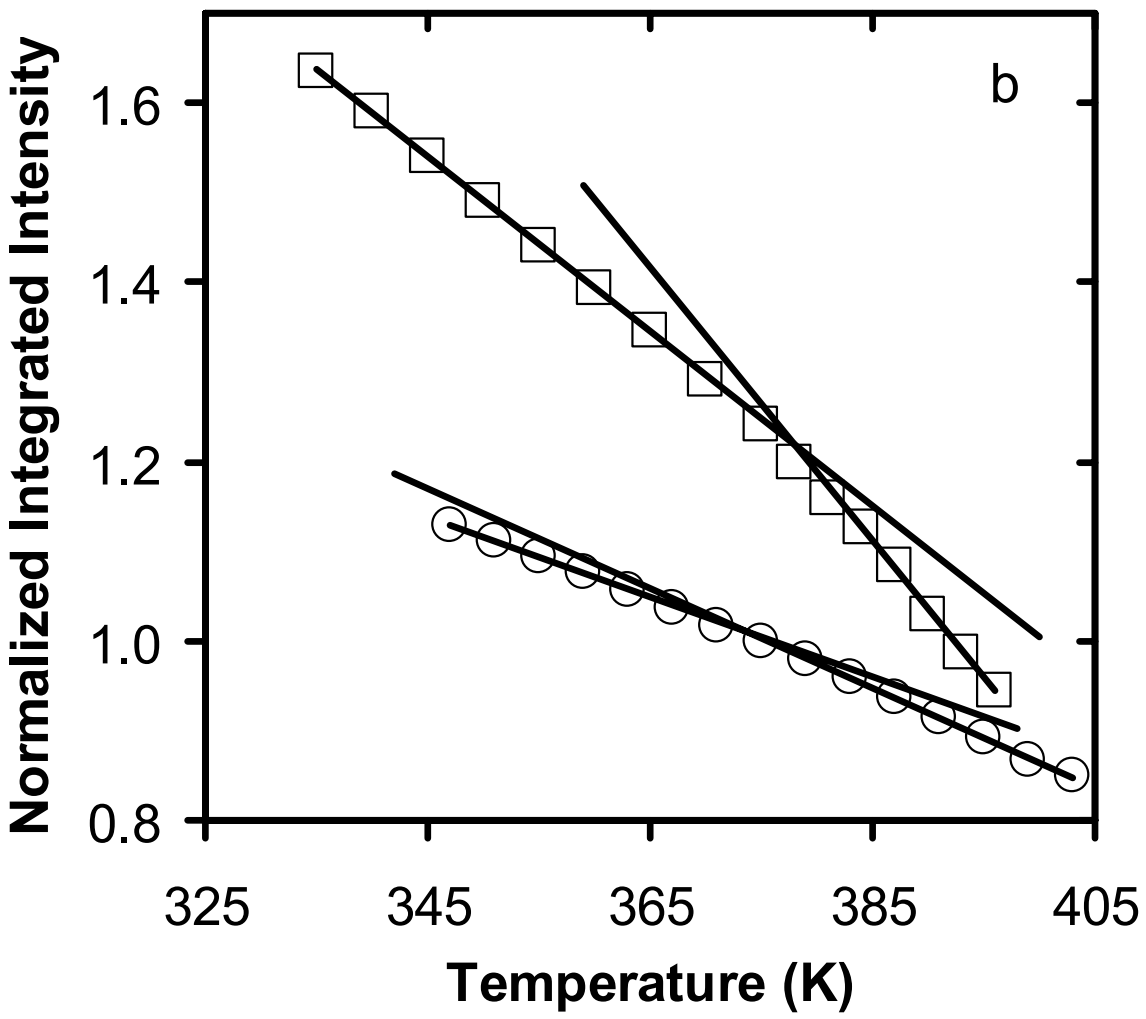

Figure 6-3: (b) Temperature dependence of the integrated intrinsic fluorescence intensity of the 39/61 mol% S/MMA random copolymer in 4690-nm-thick (□) and 21-nm-thick (○) films. (The integrated intensity is normalized to one at the respective *Tg* of each film and arbitrarily shifted.)

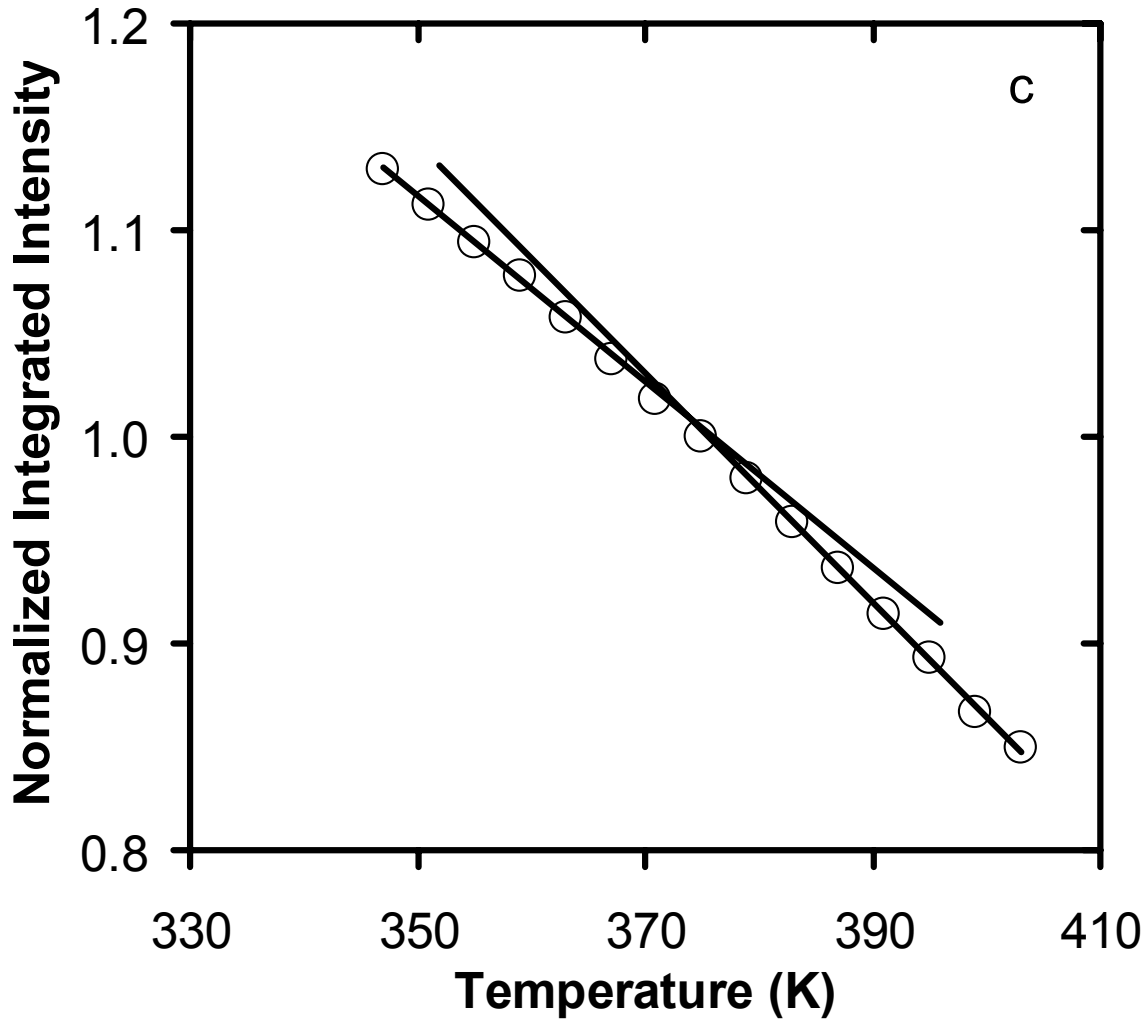

Figure 6-3: (c) Expanded plot of the data shown in Figure 6-3b for the 21-nm-thick film (○). (The integrated intensity is normalized to one at *Tg*.)

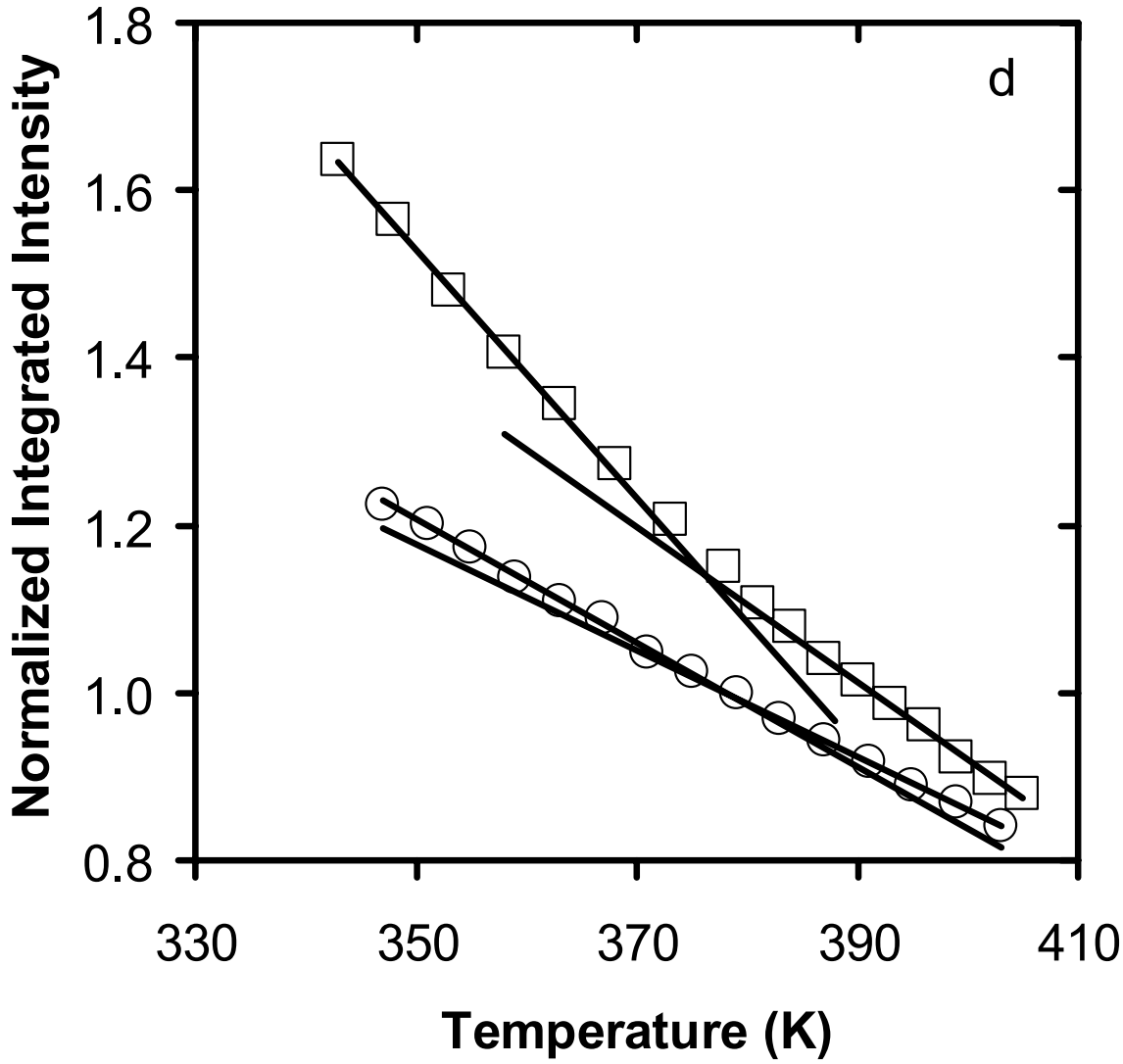

Figure 6-3: (d) Temperature dependence of the integrated intrinsic fluorescence intensity of the 22/78 mol% S/MMA random copolymer in 230-nm-thick (□) and 90-nm-thick (○) films. (The integrated intensity is normalized to one at the respective *Tg* of each film and arbitrarily shifted.)

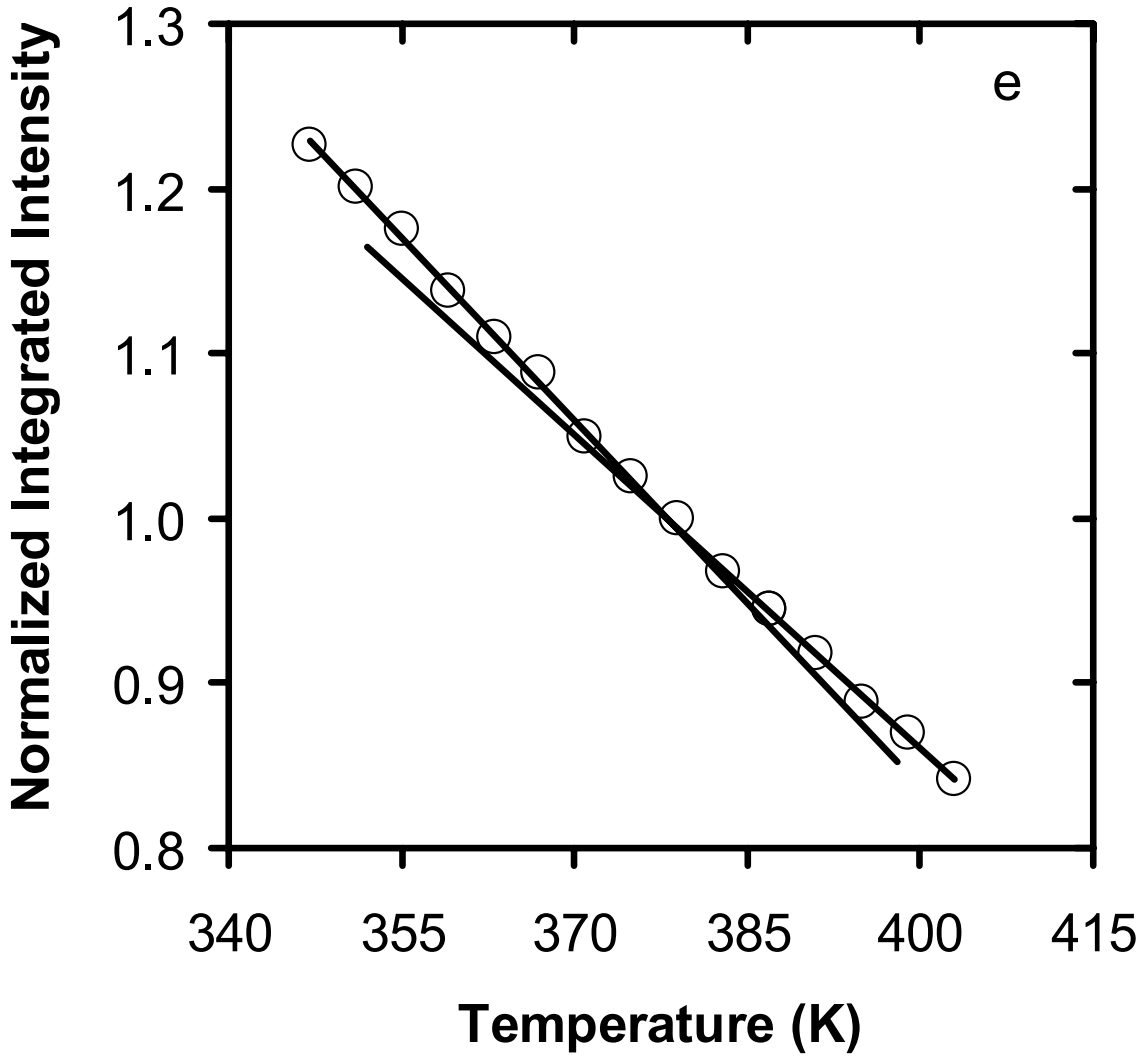

Figure 6-3: (e) Expanded plot of the data shown in Figure 6-3d for the 90-nm-thick film (○). (The integrated intensity is normalized to one at *Tg*).

coefficient is greater in the rubbery state than in the glassy state, this impact of density should yield a stronger temperature dependence of intensity in the rubbery state, consistent with the results observed in the higher S-content copolymers (where much of the fluorescence is due to excimers). Obviously, this explanation does not hold for the low S content copolymers (where nearly all fluorescence is due to emission from single excited-state phenyl rings rather than excimers).

It is interesting to note that previous research has shown that in certain cases the temperature dependence of the fluorescence of molecular "rotor" or twisted intramolecular charge transfer (TICT) probes or labels can be used to obtain *Tg* values in bulk (Loutfy 1986) and ultrathin (Baljon 2005; Priestley 2005a, 2007a; Mundra 2007b) polymer films and that there is a stronger temperature dependence of intensity in the glassy state than in the rubbery state. Obviously, the phenyl rings in the low S content copolymers under study here are not of the classic "rotor" or TICT type, and further study will be needed to explain the exact origin of the temperature dependence of fluorescence intensity observed in films of such copolymers. Nevertheless, intrinsic fluorescence measurements of bulk films yield *Tg*s in excellent agreement with those obtained by DSC. (See Table 6-1.)

Figure 6-4 shows the thickness dependence of $Tg - Tg_{,bulk}$ as a function of S content for various S-MMA copolymer compositions; in all cases, *Tg* data were obtained using the method shown in Figure 6-3. The data in Figure 6-4 indicate that the *Tg*-nanoconfinement effect may be "tuned" via copolymer composition. (For further details see Chapter 7, section 7.2.2 and discussion below.) The intrinsic fluorescence of PS shows a thickness dependence of $Tg - Tg_{,bulk}$ similar to that obtained with extrinsic fluorescence of pyrene doped into or covalently attached to neat PS. (The *Tg* data obtained from pyrene dopant or label fluorescence (Ellison 2003) were previously shown to be in good agreement with *Tg* data obtained by Keddie, Jones and Cory (Keddie

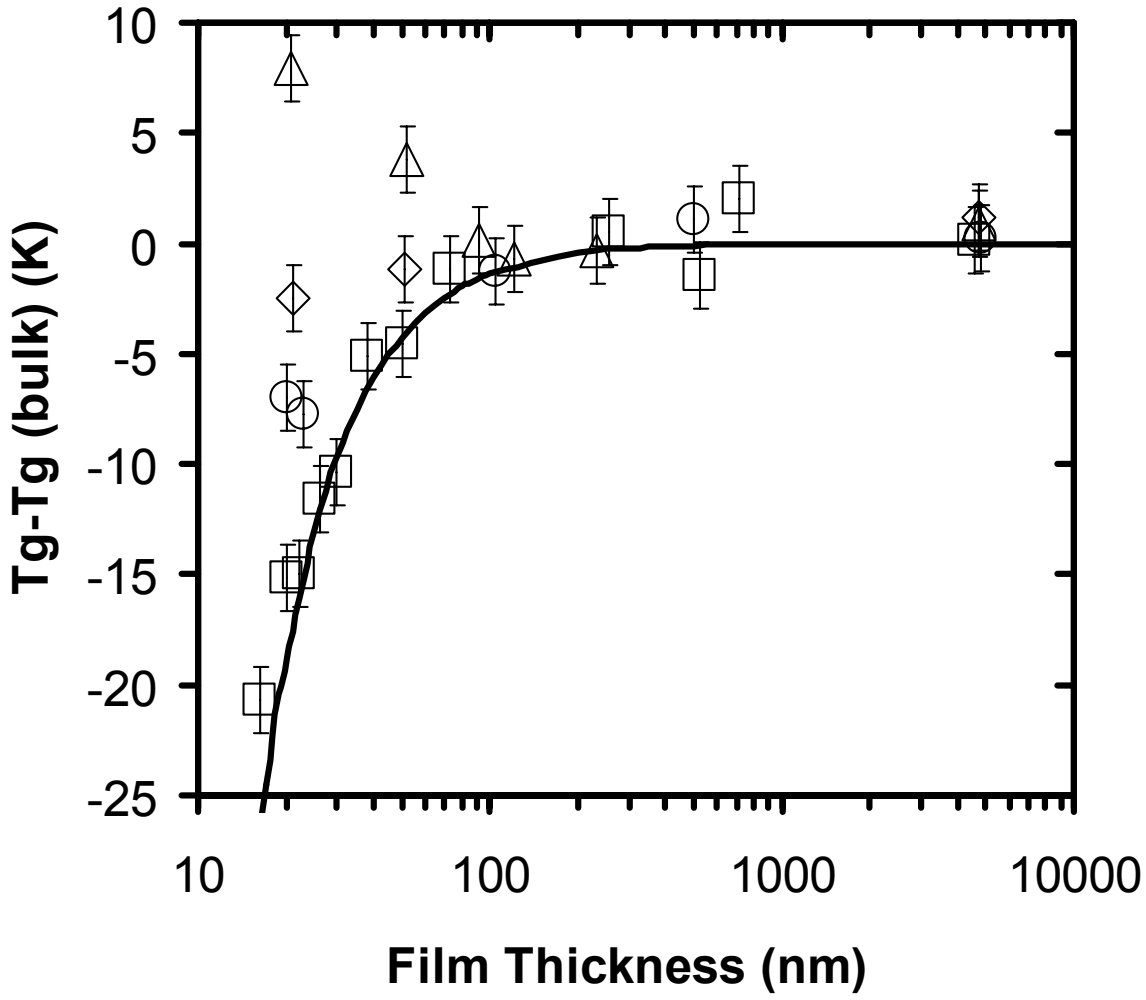

Figure 6-4: Film thickness dependence of *Tg* – *Tg*(bulk) as measured by intrinsic fluorescence: PS (□), 58/42 mol% S/MMA random copolymer (○), 39/61 mol% S/MMA random copolymer (◊), and 22/78 mol % S/MMA random copolymer (Δ). The curve represents a fit to PS film data from Chapter 4 measured using extrinsic probe fluorescence; the fit employs the empirical relation originally proposed by Keddie *et al.* (Keddie 1994b), yielding the parameter values A = 3.2 nm and δ = 1.63 (reported previously in Chapter 4).

1994a, 1994b) using ellipsometry.) As the styrene content is reduced from 100 mol% to 22 mol%, the effect of nanoconfinement on *Tg* changes from a reduction to an enhancement of *Tg* relative to *Tg*,bulk. This "tunability" of the *Tg*-nanoconfinement effect with copolymer composition as observed by intrinsic fluorescence is in good agreement with results of a recent ellipsometry study by Park *et al.* (Park 2004). In addition to PS and PMMA films, Park *et al.* (Park 2004) employed two MMA-rich copolymers, which yielded smaller reductions in *Tg* with decreasing thickness than those observed for neat PS films. The effect of copolymer composition can be explained by the difference in the polymer-substrate interaction. Styrene repeat units exhibit no attractive interaction with the substrate; thus, supported PS films undergo a *Tg* reduction with nanoconfinement due to the *Tg* reduction originating at the free surface (polymer-air interface) of the film (Ellison 2003). In contrast, MMA repeat units can undergo hydrogen bonding with the silanol units naturally present on the substrate (quartz) surface, which reduces the level of cooperative segmental mobility and thereby leads to an enhancement in *Tg* of PMMA films with nanoconfinement (Priestley 2007a; Mundra 2007a, 2007b).

It is noteworthy that the tunabililty of the *Tg*-nanoconfinement effect in supported S/MMA copolymer films yields an apparent near invariance of *Tg* with film thickness in the case of the 39/61 mol% S/MMA copolymer. This may be understood to arise from a balancing of the effects associated of the free surface leading to a reduction in *Tg* with nanoconfinement and attractive polymer-substrate interactions leading to an enhancement of *Tg*. Thus, the perturbations to *Tg* caused by free surfaces and polymer-substrate interfacial interactions remain present in this system even though the cumulative effect across a nanoconfined film yields an average measured *Tg* value very close to that of a bulk film.

6.4 Conclusions

Intrinsic fluorescence is measured in dilute solutions and thin and ultrathin films of PS and S/MMA random copolymers. Dilute solution fluorescence is characterized by a ratio of excimer to monomer fluorescence intensity. This ratio increases dramatically with increasing S-content in the copolymer and varies linearly with the S-S dyad fraction in the copolymer. This result is consistent with the notion that excimer fluorescence in dilute solution results from nearest neighbor S units with negligible impact of energy migration.

Thin and ultrathin film fluorescence is characterized via integrated fluorescence intensity. The *Tg* is determined from the intersection of the rubbery- and glassy-state temperature dependences of integrated intensity measured upon cooling from an equilibrated state. The *Tg*-nanoconfinement effect measured by intrinsic fluorescence in supported PS films agrees well with results from studies using extrinsic probe fluorescence (Ellison 2003, 2005a) and ellipsometry (Keddie 1994b). The nanoconfinement effect may be tuned using copolymer composition. As S-content decreases in S/MMA copolymers, the nanoconfinement effect changes from a decrease to an increase in *Tg* relative to bulk *Tg*, with an intermediate S-content copolymer exhibiting a nearly thickness-invariant *Tg*. The latter effect occurs because of a balance of the effects associated of the free surface leading to a reduction in *Tg* with nanoconfinement and attractive polymer-substrate interactions, involving hydrogen-bonds between the hydroxyl groups on the surface of the substrate and the ester groups in the MMA repeat units, leading to an enhancement of *Tg*.

CHAPTER 7

IMPACT OF VARIOUS PARAMETERS DIRECTLY RELATED TO POLYMER ON THE TUNABILITY OF THE Tg-NANOCONFINEMENT EFFECT

7.1 Introduction

The first systematic study of the effect of nanoconfinement on *Tg* of thin polymer films was offered by Keddie *et al.* (Keddie 1994a, 1994b). It involved the ellipsometric study of nanoconfined films of polystyrene (PS) spin coated onto silicon (111) wafers. They observed a reduction in *Tg* with a decrease in film thickness. Relative to bulk PS, a 25 K reduction in *Tg* was seen for a 10-nm-thick film. The onset of the deviation of the bulk *Tg* was seen at a thickness of ~ 40 nm. This effect was explained by hypothesizing the presence of a liquid-like layer at the free surface of high mobility and reduced *Tg*. Many later studies have confirmed this trend in PS films using a variety of techniques (Ellison 2002a, 2002b, 2003,2004a, 2005a; Fukao 1999, 2000; Kawana 2001; Forrest 1997, 2001; DeMaggio 1997). Similar although not identical trends were also reported for systems other than PS, for example, supported films of bisphenol-A polysulfone (BPAPS) (Kim 2000), poly(alpha-methyl styrene) (PαMS) (Kim 2000, 2001) and bisphenol-A polycarbonate (BPAPC) (Soles 2004a). However, the total number of studies for PS alone outnumbers the collective studies for other systems. Consequently, there is a great need for studies of systems other than PS.

Thus, it is clear that the impact of nanoconfinement on *Tg* is not restricted to a particular system. The systems listed immediately above, which exhibit a *Tg* reduction with nanoconfinement, have no particular interaction with the substrate. As a result, in these systems the modification of *Tg* with nanoconfinement was believed to originate at the free surface of the films. The direct proof came from the study by Sharp *et al.* (Sharp 2003a) where a supported PS thin film was capped with a 5-nm-thick metal layer,

changing the free surface to a solid-polymer interface (similar to that of the polymer-substrate interface). Upon replacing the free surface with the solid-polymer interface, Sharp *et al.* (Sharp 2003a) observed a *Tg* value invariant with film thickness down to a film thickness of 8 nm, indicating that PS has no attractive interaction with silicon oxide and also that the *Tg* reduction in ultrathin supported PS films is due to the presence of the free surface.

In contrast to systems with no interaction with the substrate, for instance PS, systems such as poly(methyl methacrylate) (PMMA) and poly(2-vinyl pyridine) (P2VP) may have attractive polymer-substrate interactions (due to presence of hydrogen bonding) with a native oxide substrate. Keddie *et al.* (Keddie 1994a) showed that PMMA on a gold substrate, with no potential for hydrogen bonding, yielded a decrease in *Tg* with decreasing film thickness, qualitatively similar to that seen with PS films. In contrast, PMMA on silicon (containing native oxide and hydroxyl groups at the surface) exhibited an increase in *Tg* with decreasing thickness; the onset of the increase in *Tg* with nanoconfinement was observed at a thickness of ~ 80 nm. Prucker *et al.* (Prucker 1998) carried out similar studies on PMMA and measured *Tg* reductions in thin films supported on a hydrophobic glass substrate. Grohens *et al.* (Grohens 1998) studied the impact of tacticity of PMMA in thin films and observed a major impact on the *Tg* deviation with film thickness. These studies showed that the response of *Tg* to thickness could be "tuned" to various degrees by changing the polymer-substrate interaction. In another study where the polymer-substrate interactions are highly attractive, van Zanten *et al.* (van Zanten 1996) reported an increase in *Tg* relative to bulk of ~ 50 K for a 7.7-nm-thick film of P2VP on a silicon substrate.

Separately, there have been studies of the thickness dependence of *Tg* in thin polymer blend films. It was found that the *Tg*-nanoconfinement effects are tunable by simply varying the blend composition (Kim 2002a; Pham 2002). Tsui *et al.* (Tsui 2001b)

also showed with a random copolymer of poly(styrene-co-methyl methacrylate) (PS-co-PMMA) that a small change in the interfacial energy noticeably influenced *Tg* in thin films. The interfacial energy was tuned by varying the styrene mole fraction in a random copolymer. Park *et al.* (Park 2004) studied the impact of nanoconfinement on *Tg* of random copolymer thin films of PS-co-PMMA and poly(2-vinyl pyridine-co-styrene) (P2VP-co-PS). They showed the impact of composition in tuning the *Tg*-nanoconfinement effect in thin random copolymer films. The choice of the two systems was supported by the fact that one system was moderately attractive to the substrate while the other was strongly attractive. Ellison *et al.* (Ellison 2004a) discovered that the *Tg*-nanoconfinement effect could be tuned by addition of low molecular weight diluent to the polymer. In the case of PS films, they found that the *Tg*-nanoconfinement effect was eliminated down to a thickness of 13 nm upon the addition of either 9 wt% pyrene or 4 wt% dioctyl phthalate (DOP) to the polymer. They also found that a 14-nm-thick film with 4 wt% DOP can have a *Tg* that is ~ 27 K higher than that of a neat PS film of identical thickness.

As mentioned above, most of the studies have focused on neat polymer or one particular type of a class of polymers. These systems do not encompass the full realm of important nanoconfined polymer systems nor do they allow critical determination of whether chemically similar classes of materials may be expected to behave similarly when confined. It is also surprising that a comprehensive study of the impact of manipulating the repeat unit structure, chain stiffness or backbone rigidity, and sample geometry or spatial confinement on the *Tg*-nanoconfinement effect, without modifying the interaction of the repeat unit with the substrate, has largely been unstudied.

In this chapter, the impacts of various parameters that can potentially modify or "tune" the *Tg*-nanoconfinement effect are explored in detail. In particular, the focus is to characterize the extent to which various parameters, such as molecular weight, variation

in composition of a random copolymer, slight modification to the repeat unit structure, changes in polymer chain stiffness or backbone rigidity, and addition of low molecular weight diluents, can alter or "tune" the *Tg*-nanoconfinement effect.

7.2 Impact of Various Parameters on the Tg-Nanoconfinement Effect

Sections 7.2.1 and 7.2.2 below summarize in single paragraphs the main effects of polymer molecular weight and random copolymer composition in tuning the *Tg*-nanoconfinement effect. These effects of the parameters and the experimental methods associated with *Tg*-nanoconfinement effect studies are provided in detail in Chapters 4 and 6 in this thesis. Sections 7.2.3, 7.2.4, and 7.2.5 below describe in details studies of involving the impact of other parameters in tuning the *Tg*-nanoconfinement effect.

7.2.1 Impact of Molecular Weight

The effect of nanoconfinement on the *Tg* of supported PS films is investigated in for the largest range of *MW*s examined to date in a single study (5,000-3,000,000 g/mol) (refer to Figure 4-4, Chapter 4). In contrast to two recent reports (Singh 2004; Miyazaki 2004), here it is observed that PS *MW* has no significant impact on the film thickness dependence of *Tg* - *Tg*,bulk. This result is consistent with the substantial evidence in the literature, indicating that *Tg*-nanoconfinement effects originate from interfaces and surfaces which impact the cooperative segmental mobility associated with *Tg* and are not due to other factors which may depend on *MW* such as degree of chain end segregation, entanglement density, etc. (For further details on the experimental procedure, refer to Chapter 4.) It is noteworthy that in contrast to substrate supported PS films, *Tg*-nanoconfinement effect in freely standing films is tuned by varying *MW*s of PS samples (Forrest 1997). Similar results are also seen for the freely standing PMMA films (Roth 2003).

7.2.2 Change in the Composition of Random Copolymers

The glass transition temperatures (*Tg*s) of polystyrene (PS) and styrene/methyl

methacrylate (S/MMA) random copolymer films are characterized by intrinsic fluorescence, i.e., monomer fluorescence from an excited-state phenyl ring and excimer fluorescence from an excited-state dimer of two phenyl rings. (For further details on intrinsic fluorescence to measure *Tg*, refer to Chapters 6 and 11.) The *Tg* is determined from the intersection of the rubbery- and glassy-state temperature dependences of integrated fluorescence intensity measured upon cooling from an equilibrated state. (Experimental procedure is provided in Chapter 6.) The *Tg*-nanoconfinement effect measured by intrinsic fluorescence in supported PS films agrees well with results from studies using extrinsic probe fluorescence (Ellison 2003, 2005a) and ellipsometry (Keddie 1994b) (Figure 6-4, Chapter 6). As S-content decreases in S/MMA copolymers, the nanoconfinement effect changes from a decrease to an increase in *Tg* relative to bulk *Tg*, with an intermediate S-content copolymer exhibiting a nearly thickness-invariant *Tg*. The latter effect occurs because of a balance of the effects associated with the free surface leading to a reduction in *Tg* with nanoconfinement and attractive polymer-substrate interactions, and those involving hydrogen bonds between the hydroxyl groups on the surface of the substrate and the ester groups in the MMA repeat units, leading to an enhancement of *Tg*. Therefore, it is evident that the *Tg*-nanoconfinement effect may be tuned by varying the copolymer composition.

7.2.3 Small Modification to the Repeat Unit Structure

7.2.3.1 Introduction

Due to the lack of understanding as to whether and how chemical structure plays an important role in "tuning" the effect of nanoconfinement on *Tg*, in this section it is demonstrated that modifications to the repeat unit structure can significantly impact the *Tg*-nanoconfinement effect in styrene-based polymers. In particular, poly(4-methylstyrene) (P4MS) and poly(4-tert-butylstyrene) (PTBS) systems are compared with PS. Here it is also revealed that small modification to the side group can change the

effect of nanoscale confinement on *Tg* in a series of poly(n-methacrylate) films supported on silica. The poly(n-methacrylate)s included in this study are poly(methyl methacrylate) (PMMA), poly(ethyl methacrylate) (PEMA), poly(propyl methacrylate) (PPMA), and poly(*iso*-butyl methacrylate) (PIBMA).

7.2.3.2 Experimental

Poly(4-methylstyrene) was from Scientific Polymer Products and used as received. Poly(4-tert-butylstyrene) was from Aldrich. Due to the presence of 4-tert-butylstyrene monomer in the as-received polymer, the PTBS sample was dissolved in toluene (99.9% purity) and precipitated seven times in methanol (99.9% purity) to ensure monomer removal prior to use. Pyrene (Aldrich Chemical, 99+% purity) and 1,10-bis-(1-pyrene)decane (BPD) (Aldrich, 99%) were used as received.

Poly(methyl methacrylate), PEMA, PPMA, and PIBMA were synthesized by free radical polymerization. The dye 4-tricyanovinyl-[N-(2-hydroxyethyl)-N-ethyl]aniline (TC1) was synthesized by reaction with tetracyanoethylene (TC1 America) and 2-(N-ethylaniline)ethanol (TC1 America) dissolved in dimethyl formamide (Fisher) at 55 ^{o}C for 15 min and then recrystallized from glacial acetic acid. The 1-pyrenyl butanol-labeled (Aldrich) and TC1-labeled methacrylate monomers were synthesized through an esterification reaction with methacryloyl chloride (Aldrich) in the presence of triethylamine (Aldrich) and dichloromethane (Aldrich) at 0 ^{o}C for 2 hr. The dye labeled poly(n-methacrylate)s were synthesized by reacting MMA monomer (Aldrich) in the presence of trace amounts of either pyrene-labeled or TC1-labeled methacrylate monomer. All labeled polymer was washed by dissolving in toluene (Fisher) and precipitating in methanol (Fisher) at least five times to remove residual solvent and then dried in a vacuum oven at *Tg* + 15 K for 24 hr. Table 7-1 lists the number average molecular weight *Mn*, polydispersity index *Mn*/*Mw*, bulk *Tg*, and label content of the samples studied.

Table 7-1: Molecular Weight and Bulk *Tg* for Materials Employed in this Study.

Material	*Mn* (g/mol)	*Mw*/*Mn*	*Tg*,bulk (K) (onset, DSC)	*Tg*,bulk (K) (fluor.)	Label Content (mol %)
P4MS	279,000	1.57	376	376	-
PTBS	32,000	3.31	404	404	-
PMMA	355,000	1.54	394	-	-
PEMA	460,000	1.70	348	-	-
PIBMA	300,000	2.00	337	-	-
TC1-labeled PMMA	509,000	1.67	394	395	1.4
Pyrene-labeled PEMA	202,000	1.80	348	347	0.6
Pyrene-labeled PPMA	188,000	1.78	320	320	0.3
TC1-labled PIBMA	181,000	1.96	337	339	0.6

The bulk *Tg* of each polymer was determined using a Mettler Toledo 822 differential scanning calorimeter (DSC). Sample masses of 5-10 mg were placed in sealed aluminum pans with a pinhole in the top to allow all measurements to be conducted in a nitrogen environment. The *Tg* measurements were determined on heating at 10 K/min after annealing the samples at temperature at least 70 K above the bulk *Tg* to erase the prior thermal history. The *Tg* values reported are the onset values.

The number average *Mn* and polydispersity index *Mw*/*Mn* were determined using a Waters Breeze GPC equipped with a refractometer and fluorescence detector. Molecular weight values were determined relative to polystyrene standards or universal calibration using the appropriate Mark-Houwink constants. Tetrahydrofuran was used as the eluent.

The label content of each dye-labeled polymer was determined using a Perkin Elmer Lambda 35 UV-Vis absorbance spectrophotometer. A trace amount of labeled polymer was dissolved in chloroform at a known concentration, and the absorbance spectrum of the solution was measured. Assuming that only the dye contributes to the absorbance spectrum, the concentration of the dye in the solution can be determined using the Beer-Lambert law. Relating the concentration of polymer in the solution to the concentration of dye in the solution gives an estimation of the label content.

Thin films were prepared by spin coating (Hall 1998a) dilute solutions of polymer in toluene onto glass slides. The glass slides were initially washed with a 10% sodium hydroxide/70% ethanol/20% water solution upon receipt and then solvent washed between experiments. Film thickness was measured with a Tencor P10 profilometer. Calibration of the profilometer was verified using a 14-nm-step-height standard (VLSI standards). At least ten measurements were taken in total at different locations close to the center of the film (where fluorescence was measured) and averaged with the typical standard deviation in these measurements being less than 1.5 nm for films thicker than ~

20 nm and ~ 1.0 nm for films thinner than ~ 20 nm.

A Spex Fluorolog-2DM1B fluorimeter was used for steady-state fluorescence measurements in P4MS and PTBS. Measurements employed a front-faced geometry with 2.5 mm excitation and emission slits (bandpass = 4.5 nm) for films with thickness less than 100 nm and 1.25 mm excitation and emission slits (bandpass = 2.25 nm) for films with thickness greater than 100 nm. In the worst case, the signal-to-noise ratio exceeded 30. The probe (pyrene or BPD) content in each film was less than 0.2 wt% of dry polymer content. (At probe concentrations less than 0.2 wt%, the *Tg* of pyrene or BPD-doped polymer is the same within error as that of neat polymer.) A clean quartz cover slide was placed on top of each film to reduce the potential for probe sublimation during the *Tg* measurement by fluorescence. (The film was adhered only to the glass substrate on which it was spin coated.) Film temperature was controlled by a microprocessor controller (Minco Products) with a Kapton ribbon heater attached to a flat aluminum plate that was also used as a clamping device to hold the sample. The excitation wavelength was 322 nm, and the emission spectrum was measured at 350 - 450 nm. Fluorescence spectra were recorded upon cooling after having annealed samples at ~ *Tg* + 40 K for 15 min.

Steady-state fluorescence emission spectra was taken as a function of temperature (on cooling) using a Photon Technology International fluorimeter or a SPEX Fluorog-2 DM1B fluorimeter with 3.0 mm excitation and emission slits (12 nm bandpass) used for TC1-labeled poly(n-methacrylate)s experiments and 1.25 mm excitation and emission slits (5 nm bandpass) used for pyrene-labeled poly(n-methacrylate)s experiments. The wavelength used to excite the TC1-labeled poly(n-methacrylate)s and pyrene-labeled poly(n-methacrylate)s was 480 nm and 254 nm, respectively. The emission spectra of TC1-labeled poly(n-methacrylate)s and pyrene-labeled poly(n-methacrylate)s were measured at 540-690 nm and 360-460 nm, respectively. The *Tg* values of the films were

determined by fitting the temperature dependence of the integrated fluorescence intensity to linear correlations in both the rubbery and glassy states. In fitting the data to linear correlations, only data well outside *Tg* were used in the fitting procedure. (Additional information on the fluorescence technique used to monitor *Tg* can be found in Chapters 3, 4, and 5.)

7.2.3.3 Impact of Small Modification to the Repeat Unit Structure on Tg-Nanoconfinement Effect

Figure 7-1 shows the temperature dependence of the integrated intensity for pyrene-doped P4MS at two thicknesses. Similar to the PS case (Figure 4-3, Chapter 4), P4MS shows a reduced strength in *Tg* in highly confined films. (As with PS, a weakening in the strength of *Tg* for P4MS is observed with decreasing thickness for films less than ~ 30-nm-thick.) The 24-nm-thick and 810-nm-thick P4MS films display *Tg*s of ~ 355 and 376 K, respectively. In the case of films of thickness less than 25 nm, the estimated error in *Tg* is ~ ± 2 K while for thicker films it is ~ ± 1 K.

Figure 7-2 shows the thickness dependence of *Tg* for P4MS compared to the PS data fit to the empirical function from Keddie *et al.* (Keddie 1994b) as shown in Figure 4-4, Chapter 4. For 24-nm-thick films, P4MS exhibits a *Tg* value that is reduced by 21 K relative to *Tg*,bulk while PS exhibits a *Tg* value that is reduced by ~ 14 K relative to *Tg*,bulk (Figure 4-4, Chapter 4). This indicates that the addition of one methyl unit on the 4-position of the phenyl ring in the PS repeat unit can have a significant effect on the thickness dependence of *Tg*. However, it is interesting to note that the onset thickness at which *Tg* begins to show a significant deviation from *Tg*,bulk, which is defined here to be a 3 K reduction relative to *Tg*,bulk, is virtually the same (~ 45-50 nm) for P4MS and PS.

Kim *et al.* (2001) have reported on the *Tg*-nanoconfinement effect observed in poly(α-methylstyrene) (PαMS), in which a methyl unit is located on the α-carbon along the chain backbone. Their data indicate that the onset thickness of the *Tg* reduction is

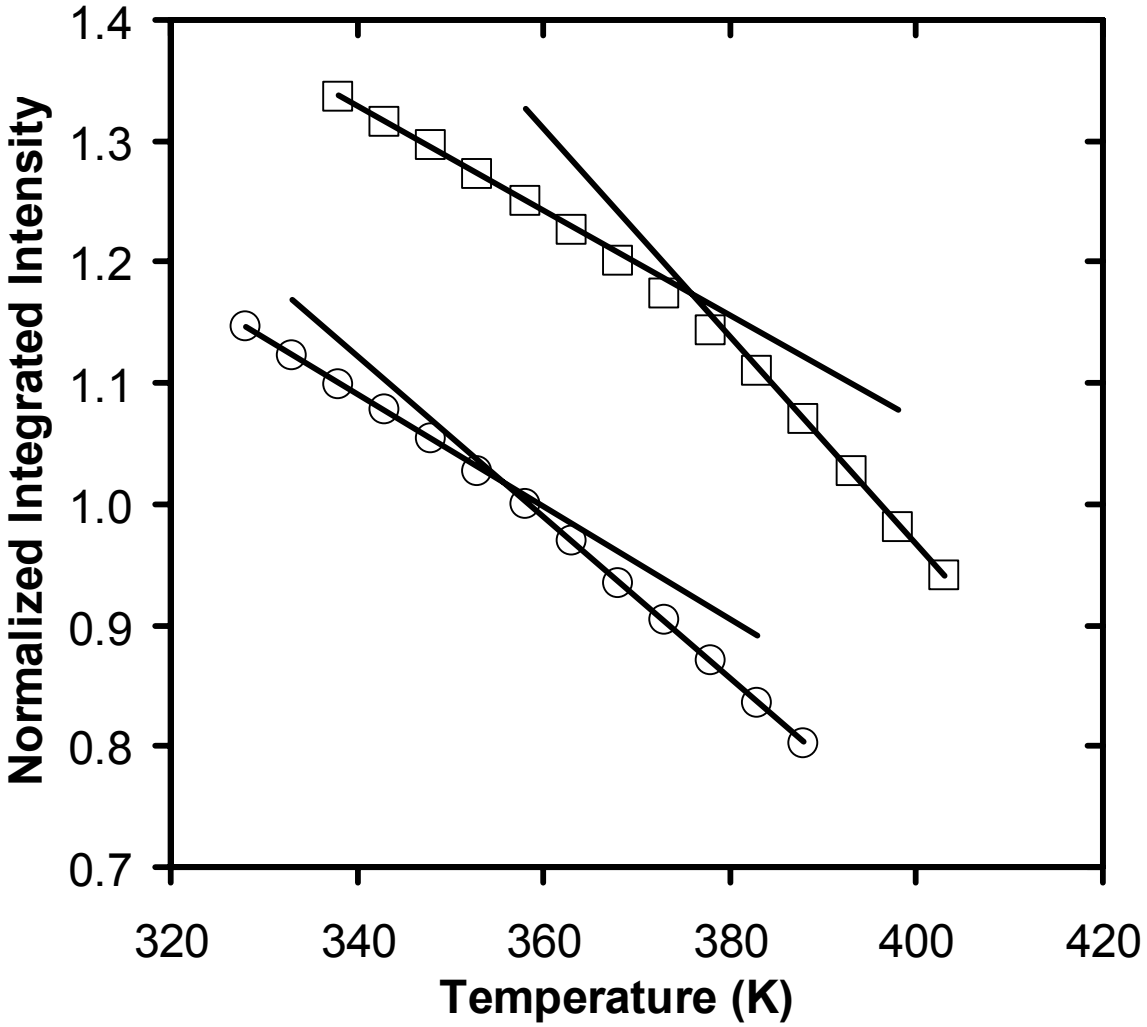

Figure 7-1: The temperature dependence of the integrated intensity of pyrene dopant in 810-nm-thick (□) and 24-nm-thick (○) P4MS films (*Tg*,bulk = 376 K) films. (The integrated intensity has been normalized to one at 368 K and 358 K, respectively, and arbitrarily shifted.)

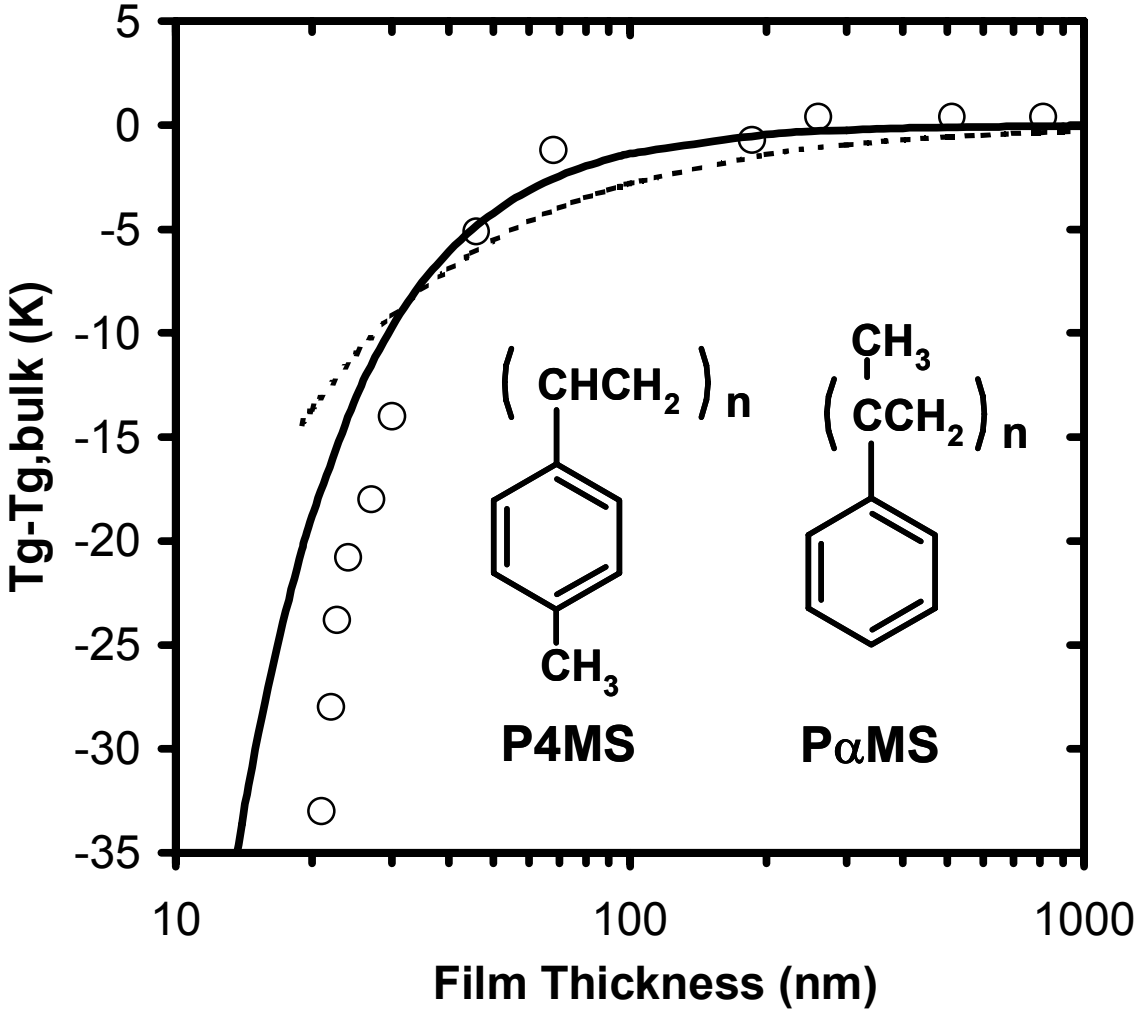

Figure 7-2: *Tg* – *Tg*,bulk as a function of film thickness for P4MS (○) films as measured by pyrene dopant fluorescence. The bold curve represents a least squares fit of the PS data (refer to Figure 4-4, Chapter 4) to the empirical relation of Keddie *et al.* (Keddie 1994b) with parameter values A = 3.2 nm and δ = 1.63; the dotted curve is a reproduction of the curve reported in a study of PαMS *Tg*-nanoconfinement effects (Kim 2001). The inset shows the P4MS and PαMS repeat unit structures.

greater (~ 90-95 nm) for PαMS than for PS or P4MS. In addition, as shown in Figure 7-2, the shape of the thickness dependence of *Tg* for PαMS differs from that of PS or P4MS, decreasing much less steeply at thicknesses less than 40 nm. In agreement with our PS results, Kim *et al.* (2001) reported no effect of *MW* on the reduction of *Tg* as a function of thickness for PαMS with *MW*s of 23,000 and 450,000 g/mol.

Fluorescence has also been used to measure the *Tg*-nanoconfinement effect in PTBS, which differs from the repeat unit structure of PS by the addition of a tert-butyl group to the 4-carbon on the phenyl ring. The addition of the tert-butyl group reduces the bulk density of the polymer by 10% compared to PS (from 1.04 to 0.94 g/cm^3) (Ellison 2005a) and increases bulk *Tg* from ~ 373 to 404 K. In contrast, the densities and *Tg* values of P4MS and PS are nearly identical. This decreased density in PTBS may be attributed to significantly hindered packing of the repeat units of PTBS relative to PS which results in an increased free volume. Likely associated with these differences, it has been observed that pyrene dopant is particularly susceptible to sublimation from PTBS films during annealing of the film above *Tg*. To avoid sublimation issues, BPD, shown as the inset in Figure 7-3a, was chosen as a fluorescence dopant as it has a diffusion coefficient in polymers near *Tg* that is several orders of magnitude lower than that of pyrene (Deppe 1996b). Various tests in PTBS indicated that BPD exhibits relatively little sublimation in the temperature range of interest.

Figure 7-3a shows the temperature dependence of the fluorescence emission spectra for BPD doped at trace levels (less than 0.2 wt %) into a 1190-nm-thick PTBS film. The BPD dopant spectral shape is roughly similar to that of pyrene dopant in PS, with emission peaks at ~ 378, 398, and 418 nm. Figure 7-3b shows the temperature dependence of the integrated intensities for two BPD-doped PTBS films; the 1190-nm-thick film exhibits a *Tg* value of 404 K, equal to *Tg*,bulk, while the 30-nm-thick film exhibits a *Tg* of 368 K. The 30-nm-thick PTBS film also shows a reduction in the

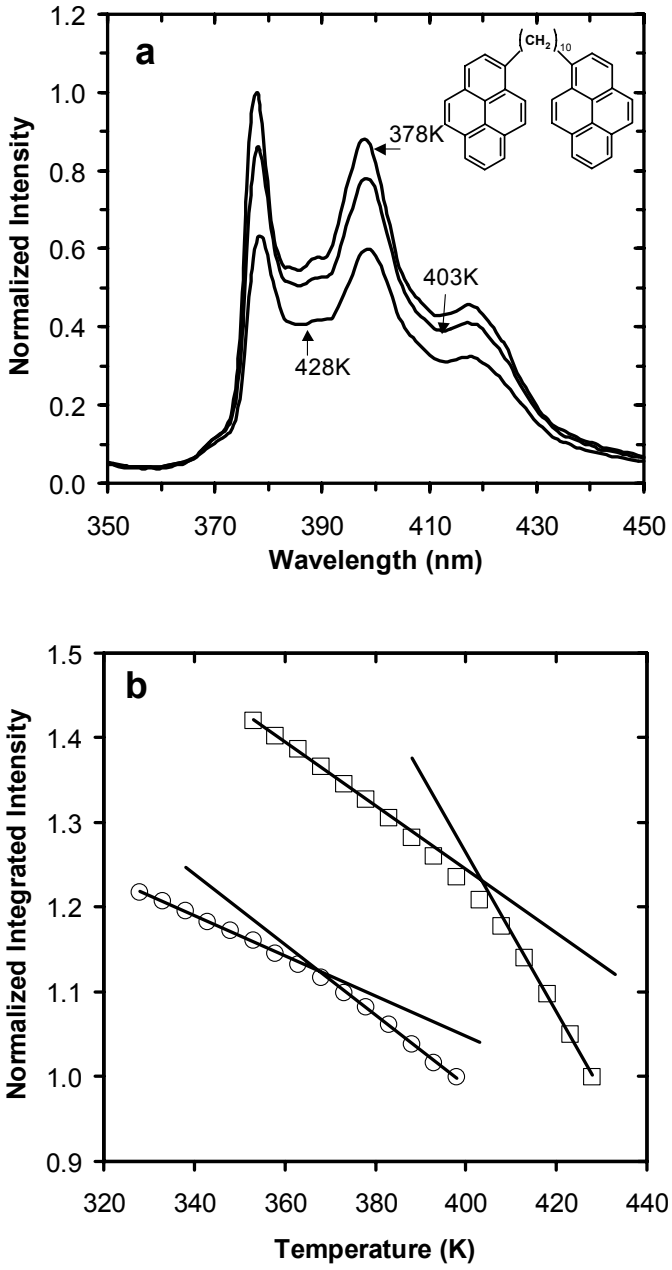

Figure 7-3: (a) Fluorescence emission spectra of BPD dopant in a 1190-nm-thick PTBS film taken at 378 K, 403 K and 428 K. The inset shows the structure of BPD. **(b)** The temperature dependence of the integrated intensity of BPD dopant in 1190-nm-thick (□) and 30-nm-thick (○) PTBS (*Tg*,bulk = 404 K) films. (The integrated intensity has been normalized to one at 428 K and 398 K, respectively, and arbitrarily shifted).

strength of *Tg* compared to the 1190-nm-thick film, qualitatively consistent with that shown for PS in Figures 4-3a,b (Chapter 4) and P4MS shown in Figure 7-2. (A weakening in the strength of *Tg* for PTBS is observed with decreasing thickness for films less than ~ 30 - 35-nm-thick. The estimated error in the determination of *Tg* is ± 1 K for films with thickness exceeding 30 nm and ± 2 K for thinner films.)

Figure 7-4 compares the thickness dependence of *Tg* for PTBS and the dependences for P4MS and PS. Also shown are the *Tg* values of two 200,000 g/mol PS films doped with BPD, showing that BPD and pyrene dopant measure a consistent thickness dependence of *Tg* in PS. Figure 7-4 makes clear that there are dramatic differences in the *Tg*-nanoconfinement effect of PTBS as compared to that of either PS or P4MS. First, the onset thickness for *Tg* reduction in PTBS, estimated from Figure 7-4 to be 300-400 nm, is much larger than in PS or P4MS. (Strikingly, this value of onset thickness indicates that the effect is not necessarily limited to the "nano" length scale, often taken as 100 nm or less.) To the best of my knowledge, this is the largest thickness at which the *Tg*-nanoconfinement effect has ever been observed in supported or unsupported polymer films with or two free surfaces. In addition, the 47 K reduction in *Tg* relative to *Tg*,bulk observed in the 25-nm-thick PTBS film is, the largest nanoconfinement related *Tg* reduction observed experimentally in supported polymer films.

This strongly enhanced thickness dependence of *Tg* in PTBS relative to PS and even P4MS demonstrates that there is substantial tunability of the *Tg*-nanoconfinement effect. Given the invariance demonstrated in the *Tg*-nanoconfinement effect as a function of PS *MW* (from 5,000 to 3,000,000 g/mol) (Figure 4-4, Chapter 4), such dramatic differences in the impact of nanoconfinement on PTBS relative to PS may be considered surprising. However, as the addition of the tert-butyl group to PS reduces the bulk density substantially (nearly to that of styrene monomer, which has a density of 0.90

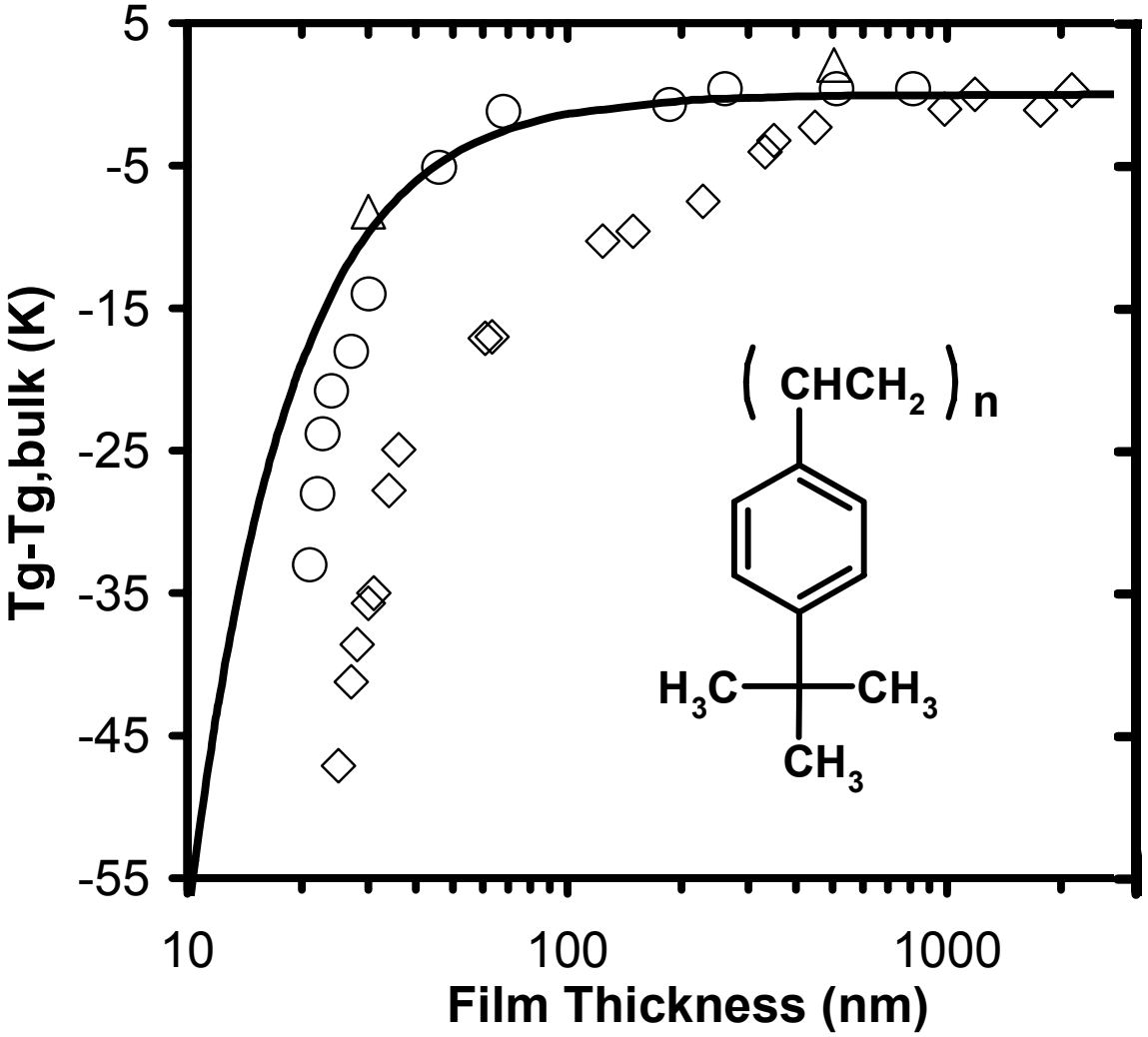

Figure 7-4: *Tg* – *Tg*,bulk as a function of film thickness for P4MS (○) films as measured by pyrene dopant fluorescence, PTBS (◊) films as measured by BPD dopant fluorescence, and PS (Δ) (*Mn* = 200,000 g/mol) films as measured by BPD dopant fluorescence. The bold curve represents a fit of the PS data in Figure 4-4 (Chapter 4) to the empirical relation of Keddie *et al.* (Keddie 1994b). The inset shows the structure of the PTBS repeat unit.

g/cm^3) while resulting in a more rigid chain due to steric effects, it may be unreasonable to expect that there should be much similarity in the *Tg*-nanoconfinement of PS and PTBS, except for the fact that the *Tg* values are expected to decrease with decreasing thickness below some onset thickness as there is no attractive interaction between polymer and substrate in both PS and PTBS films.

Up to the present time, these factors of overall density and chain stiffness have not been described in the literature as being associated with *Tg*-nanoconfinement effects. Here we hypothesize that it is chain stiffness rather than polymer density that may be responsible for or at least is associated with the much more dramatic *Tg*-nanoconfinement effect in PTBS as compared to PS and P4MS. This hypothesis is supported by the fact that a recent study (Soles 2004a) reported that polycarbonate, which has significantly greater chain stiffness than PS, exhibits a substantial *Tg* reduction relative to its *Tg*,bulk.

Figure 7-5 further illustrates that slight modifications to the repeat unit structure of a series of poly(n-methacrylate)s can have a profound impact on how confinement affects *Tg*. Figure 7-5 plots *Tg*(film)-*Tg*(bulk) versus film thickness for TC1-labeled PMMA, pyrene-labeled PEMA, pyrene-labeled PPMA, and TC1-labeled PIBMA. For TC1-labeled PMMA, the increase in *Tg* with confinement is consistent with previous studies of single-layer PMMA films supported on silica (Keddie 1994a; Prucker 1998). The increase in *Tg* with confinement has been related to attractive polymer-substrate interactions, i.e., hydrogen bonding between the ester side groups of PMMA and the hydroxyl groups on silica that reduce segmental mobility at the substrate interface (Priestley 2007a). Changing the side group of PMMA from a methyl group to either an ethyl (PEMA) or propyl (PPMA) group leads to an opposite effect of confinement on *Tg*. Changing the methyl group of PMMA to an *iso*-butyl group (PIBMA) leads to an average *Tg* across the film that is apparently invariant with confinement. Related research involving bilayer / fluorescence studies of PiBMA films indicate that the apparent

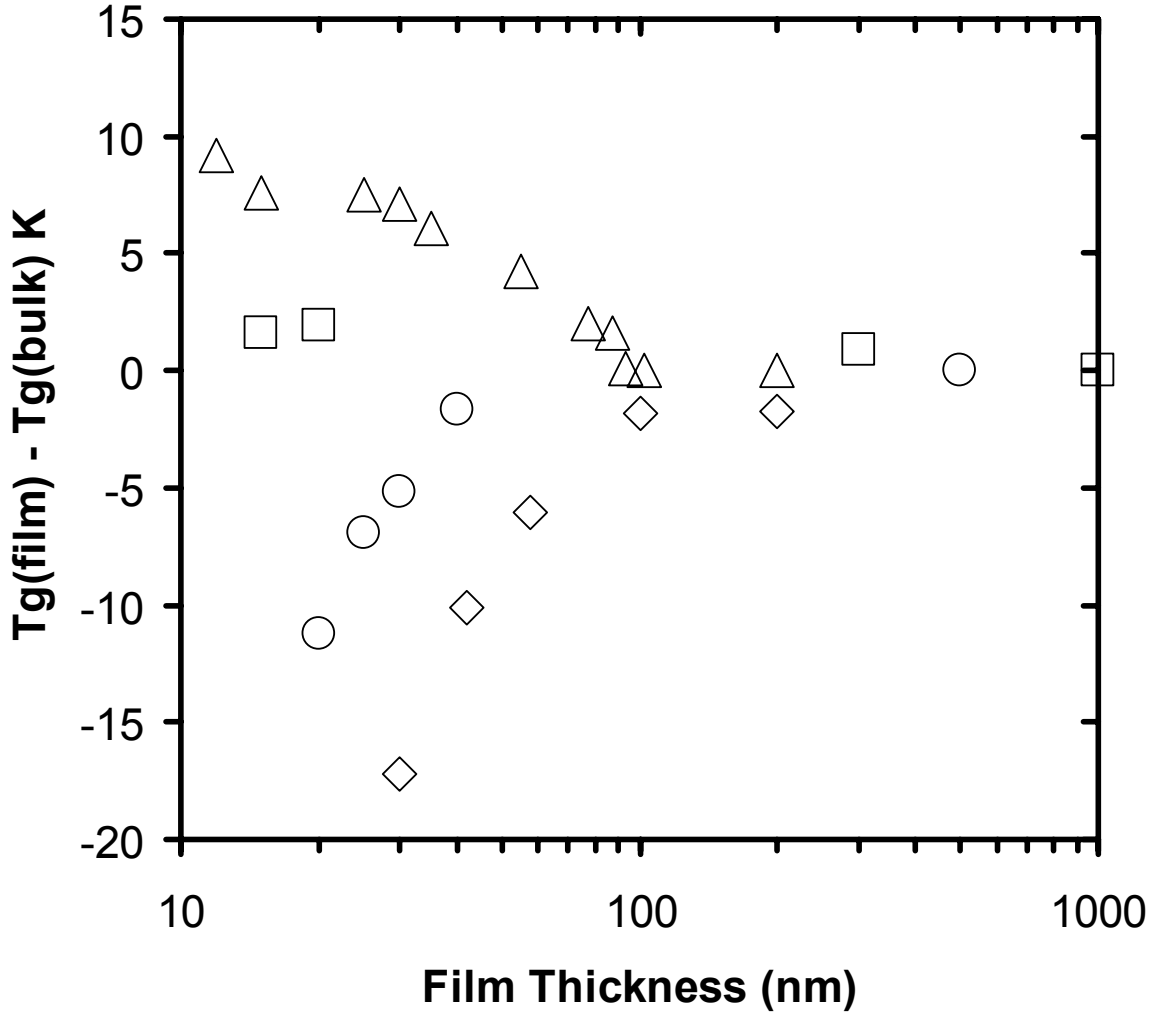

Figure 7-5: Deviation from bulk *Tg* as a function of film thickness for TC1-labeled PMMA (Δ), TC1-labeled PIBMA (□), pyrene-labeled PEMA (○), and pyrene-labeled PPMA (◊) films.

invariance of average film *Tg* with confinement is due to canceling effect of free surfaces (which reduce *Tg*) and PiBMA–substrate interfaces (which enhance *Tg*).

Clearly, it is evident that these small modifications to the repeat unit structure of methacrylate-based polymers have an enormous impact on *Tg*-nanoconfinement effects. From previous work conducted on PS and PMMA, it is known that the free surface and substrate-interface impact *Tg* dynamics differently for different polymers (Ellison 2003; Svanberg 2007; Roth 2006; Priestley 2007a). It is possible that the modifications to the repeat unit structure of the methacrylate-based polymers affect how the free surface and substrate interface impact the local *Tg*s and thereby the average *Tg*s across the films. (Note that the choice of dye molecule does not influence the direction in which *Tg* deviates from bulk *Tg* with confinement, as both TC1-labeled PMMA (data shown in Figure 7-5) and pyrene-labeled PMMA (data shown in Figure 5-2, Chapter 5) exhibit nearly identical increases in *Tg* with confinement (Priestley 2007a; Figure 5-2, Chapter 5).)

7.2.4 Modification of Polymer Chain Stiffness or Backbone Rigidity

7.2.4.1 Introduction

Confinement-induced changes in *Tg* have been widely reported for polymeric glass-formers because of the ability to spin cast stable ultrathin films with known thicknesses. Most of the work has been restricted to the systems with simple carbon-carbon backbone structure such as PS and PMMA with relatively little effort on other systems with complicated backbone structure, such as bisphenol-A-polycarbonate (BPAPC), poly(alpha-methyl styrene) (PαMS), poly(4-methyl styrene) (P4MS), poly(tert-butyl styrene) (PTBS), and bisphenol-A polysulfone (BPAPS) (Soles 2004a; Ellison 2005a; Kim 2000), among others. Apart from the small number of studies devoted to these systems, in some cases (Soles 2004a), the reported error bars are very large, making it difficult to reach meaningful conclusions. The total number of studies

for PS alone outnumbers the collective studies for other systems; consequently, there is a great need for studies of systems other than PS if a better understanding of the fundamental nature of *Tg* and the effect of confinement is to be realized.

The use of fluorescence to measure *Tg* in bulk polymers was first suggested more than twenty-five years ago by Loutfy (Loutfy 1981, 1982) and later employed by others (Bradley 1993; Lenhart 2001). The *Tg* value may be characterized as the temperature at which there is an intersection in the rubbery- and glassy-state in the temperature dependences of peak intensity. Using chromophores doped into or covalently attached to the polymer (extrinsic fluorescence), Ellison and Torkelson (Ellison 2002a, 2002b) were able to characterize *Tg* in various systems and demonstrated that this technique was sensitive enough to measure the *Tg* values in extremely thin films with high precision.

A potentially powerful manner with which to obtain *Tg* values in polymer films is intrinsic fluorescence, i.e., fluorescence resulting from the polymer itself, without addition of fluorescence dye as dopant or label. (For further details on intrinsic fluorescence, see Chapters 6 and 11.) Several years ago, Ellison and Torkelson demonstrated that the temperature dependence of the intrinsic fluorescence of a 12-μm-thick PS film may be used to determine *Tg* (Ellison 2002b). At that time, they. (2002b) did not obtain *Tg* values for ultrathin films (≤ 100 nm) using intrinsic fluorescence due to a low signal-to-noise ratio and instead used extrinsic fluorescence for *Tg* measurements (Ellison 2002a, 2002b, 2003, 2005a). With improved instrumentation and experimental technique, it is now possible to obtain high signal-to-noise ratios for intrinsic fluorescence measurements of thin and ultrathin PS films. (See Chapter 6 of this thesis.)

Here, intrinsic fluorescence is used to obtain *Tg* values in thin and ultrathin BPAPS films, which have a bulk *Tg* value of ~ 190 °C. Extrinsic probe fluorescence, involving use of a wavelength-shifting high-temperature stability dye, is used to characterize *Tg* in thin and ultrathin BPAPC films. By comparing the *Tg* data obtained in

the BPAPC and BPAPS systems to those in PS system, this is the first study to compare quantitatively the impact of backbone rigidity or polymer chain stiffness on the *Tg*-nanoconfinement effect in systems. Also, it is the first study to use intrinsic fluorescence as a characterization tool of the *Tg*–nanoconfinement effect in polymer systems where the phenyl ring is not present as a side group but as part of the backbone structure. The wavelength-shifting high-temperature stability probe is used to measure *Tg* by monitoring the change in the intensity of the emission spectrum via a ratio of emission intensities below and above the wavelength of maximum emission.

7.2.4.2 Experimental

Bisphenol-A-polycarbonate (nominal *Mn* = 17,300 g/mol, *Mw*/*Mn* = 1.65, *Tg*,bulk = 415 K) and BPAPS (nominal *Mn* = 20,400 g/mol, *Mw*/*Mn* = 3.30, *Tg*,bulk = 463 K) were secondary standards purchased from Scientific Polymer Products, Inc. and used as received. 7-(dimethylamino)-1-methylquinolinium tetrafluoroborate (supplied by Dr. Wolter F. Jager of the Delft University of Technology) was synthesized by adding methyl iodine (0.21 mL, 3.39mmol) to a solution of 7-(dimethylamino)quinoline (0.53 g, 3.08 mmol) in 5 mL of methanol. The mixture was refluxed overnight. It was diluted with ether once it cooled to room temperature. The precipitate was filtered and washed with ether (twice, 50 mL), re-dissolved in methanol (15 mL), and added to a saturated sodium tetrafluoroborate solution (100 mL). This aqueous solution was then extracted with dichloromethane (4 times, 50 mL). The layers were then concentrated to a yellow solid, which was purified by recrystallization from methanol/ether to give pure 7-(dimethylamino)-1-methylquinolinium tetrafluoroborate (0.58 g, 69%) as yellow crystals. (Further detail on the synthesis of 7-(dimethylamino)-1-methylquinolinium tetrafluoroborate dye is reported by van den Berg *et al.* (van den Berg 2006a, 2006b).) All *Tg*,bulk values were measured as *Tg*,onset values by differential scanning calorimetry (Mettler Toledo DSC822) at a heating rate of 10 K/min on the second heating cycle after

quenching from elevated temperature at a rate of 40 K/min and were found to be on average within ± 1K of *Tg*,bulk values measured by fluorescence methods. 1,10-bis-(1-pyrene)decane (BPD) (Molecular Probes) was used as received.

Thin films were prepared by spin coating (Hall 1998a) dilute solutions of polymer in 1,2-dichloroethane (Sigma-Aldrich, 99 + % pure, used as received) onto glass slides. The slides were initially washed with a 10% sodium hydroxide/70% ethanol/20% water solution (Ellison 2002a) and then solvent washed between experiments. Film thickness was measured with a Tencor P10 profilometer (calibrated using a 14-nm-step-height standard from VLSI standards). At least ten measurements were taken in total at different locations close to the center of the film where fluorescence was measured.

A Spex Fluorolog-2DM1B fluorimeter was used for steady-state fluorescence measurements in BPAPS. Measurements employed front-faced geometry with 5 mm excitation and emission slits (bandpass = 9 mm) for films with thickness (h) < 30 nm, 2.5 mm excitation and emission slits (bandpass = 4.5 nm) for films with thickness 30 nm < h < 100 nm and 1.25 mm excitation and emission slits (bandpass = 2.25 nm) for films with thickness > 100 nm. In the worst case, the signal-to-noise ratio exceeded 25. For steady state fluorescence measurements in BPAPC films, a PTI QM-2001 SE fluorimeter using front-face geometry with 1 mm excitation (bandpass = 2 nm) and 1 mm emission (bandpass = 4 nm) for films > 100 nm and 1.5 mm excitation (bandpass = 3 nm) and 1.5 mm emission (bandpass = 6 nm) for films < 100 nm was used. As the PTI fluorimeter has greater excitation intensity due to its superior beam focus compared to the Spex fluorimeter, the smaller slit size was used with the PTI instrument to prevent films from photobleaching at high temperature. In the worst case, the signal-to-noise ratio exceeded 50. The probe (BPD or 7-(dimethylamino)-1-methylquinolinium tetrafluoroborate) content in each film was < 0.2 wt% of dry polymer content. (At this probe concentration the *Tg* value of the doped polymer is the same within error as that of neat polymer). A

clean quartz cover slide was placed on top of each film to reduce the potential for probe sublimation during the *Tg* measurement by fluorescence. (The film was adhered only to the glass substrate on which it was spin coated.) An integrated programmable heating source (Instec) was used for controlling temperature in films with no fluorescence probe (i.e., for the intrinsic measurements). For films doped with a fluorescence probe, temperature was controlled by a microprocessor controller (Minco Products) with a Kapton ribbon heater attached to a flat aluminum plate that was used as a clamping device to hold the sample. For extrinsic measurements, the excitation wavelength was 322 nm for BPD and 400 nm for 7-(dimethylamino)-1-methylquinolinium tetrafluoroborate, and emission spectra was measured at 360 - 460 nm and 460 to 700 nm, respectively. For intrinsic fluorescence, excitation was done at 260 nm, and an emission spectrum was measured from 275 to 415 nm for BPAPC and 270 to 450 nm for BPAPS. Fluorescence spectra were recorded upon cooling after having annealed samples at ~ *Tg* + 30-40 K for 15 min. (Further details on measurement of *Tg* by fluorescence are given in Chapters 3, 4, 5, and 6.)

7.2.4.3 Tunability of the Tg-Nanoconfinement Effect with Modification of Polymer Chain Stiffness/Backbone Rigidity

Figure 7-6a shows the fluorescence emission spectrum of BPD dopant in a 1000-nm-thick BPAPC film, normalized by the peak of highest intensity. There is a reduction in the overall intensity with increasing temperature. Previous studies have shown (Ellison 2002a, 2002b, 2003, 2004a, 2004b, 2005c; Mundra 2006, 2007a, 2007b) that *Tg* values can be obtained by plotting the intensity near one or several of the peak wavelengths as a function of temperature. Over a 60-70 K or 100-110 K (Mundra 2006) temperature-range roughly centered at *Tg*, two linear temperature dependences of intensity are observed, with the intersection being identified as *Tg*. Careful inspection of Figure 7-6a reveals that the exact values of the two slopes in such a plot may depend on

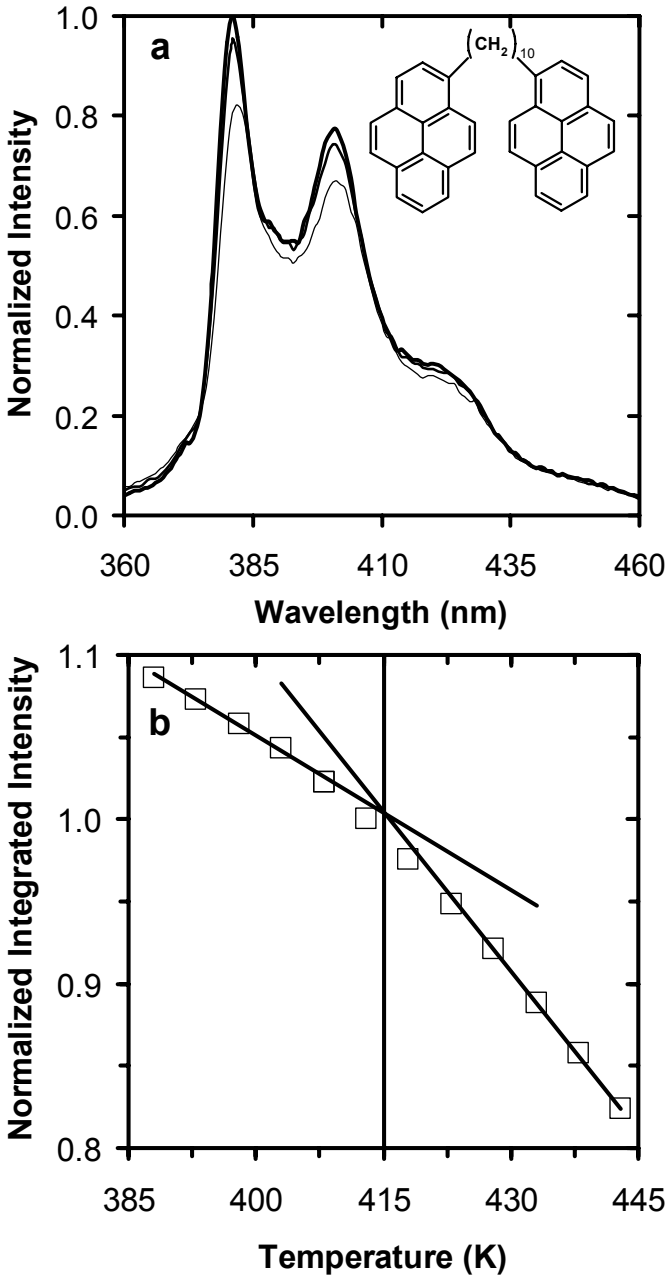

Figure 7-6: (a) Fluorescence emission spectra of 1,10-bis(1-pyrene)decane (BPD) dopant in a 1000-nm-thick bisphenol-A-polycarbonate (BPAPC) film taken at 388 (bold curve), 413 (middle curve) and 443 (curve with lowest intensity) K. The inset shows the structure of BPD. **(b)** Temperature dependence of the integrated intensity of BPD dopant in 1000-nm-thick BPAPC film. (The integrated intensity has been normalized to one at 413 K.) The vertical line represents the bulk *Tg*.

the emission wavelength selected, because the temperature dependence of intensity is stronger at the peaks than at the minima (valleys) of the emission spectrum. Such effects have been observed by others (Vigil 1997; Brown 2004) studying the temperature dependence of fluorescence in various polymers and can be attributed to the temperature dependence of the different vibronic bands of the dopants used. In order to minimize these effects, integrated intensity is plotted as a function of temperature. As reported recently (Ellison 2005a; Mundra 2006, 2007a, 2007b; Priestley 2007a), this approach minimizes errors, leading to more precise *Tg* measurements.

Figure 7-6b shows the temperature dependence of the integrated intensity of BPD doped BPAPC in 1000-nm-thick film. The BPD dye was used as a dopant instead of pyrene to avoid issues related to sublimation. The vertical bold line in Figure 7-6b represents the bulk *Tg* value. In previous studies in which *Tg*s of polymer systems were measured via fluorescence (Ellison 2002a, 2002b, 2003, 2005a), a greater temperature dependence of intensity was observed in the rubbery state, in accord with the notion that a significant portion of the temperature dependence of fluorescence of pyrenyl dyes in glass-forming polymers reflects local density effects, i.e., a slightly denser local environment near a pyrene dye accommodates less nonradiative decay of the excited state leading to higher intensity. As the thermal expansion coefficient is greater in the rubbery state than in the glassy state, this impact of density yield a stronger temperature dependence of intensity in the rubbery state, which is consistent with the results observed in case of BPAPC. The overall change in the temperature dependence of the integrated intensity was small in the bulk BPAPC films. In accord with earlier fluorescence studies (Ellison 2002a, 2002b, 2003) of *Tg* nanoconfinement, a further weakening in the strength of *Tg* was also observed in highly nanoconfined BPAPC ultrathin films. This made it extremely challenging at best and impossible at worst to characterize ultrathin films for *Tg* measurement using BPD probe. Therefore, intrinsic fluorescence was used in place of

extrinsic fluorescence by BPD to characterize this system.

Figure 7-7a shows the intrinsic fluorescence emission spectra of a 750-nm-thick film of BPAPC at 373, 413 and 448 K, respectively. There is a reduction in the overall intensity with increasing temperature. Spectra are normalized to one at the peak intensity at 373 K. Figure 7-7b shows the temperature dependence of the integrated intrinsic intensity of BPAPC in a 750-nm-thick film. The vertical bold line in Figure 7-7b represents the bulk *Tg* value. Previous research has shown that in certain cases the temperature dependence of the fluorescence of molecular "rotor" or twisted intramolecular charge transfer (TICT) probes or labels used to obtain *Tg* values in polymer films resulted in a stronger temperature dependence of intensity in the glassy state than in the rubbery state (Mundra 2007b; Priestley 2005a, 2007a; Baljon 2005; Loutfy 1986). A similar observation was made recently (Mundra 2006) from the intrinsic fluorescence of a low styrene content copolymer with methyl methacrylate. The rigid nature of the phenyl rings in BPAPC, being part of the backbone structure, could be very sensitive to the small changes restricting the mobility of the chains especially in the glassy region, resulting in a stronger temperature dependence of the integrated intensity in the glassy region. Further study will be needed to explain the exact origin of the temperature dependence of fluorescence intensity observed in films of such a polymer. Nevertheless, intrinsic fluorescence measurements of bulk films yield *Tg*s that are in excellent agreement with those obtained by differential scanning calorimetry.

For the relatively thick films, the overall intensity was very low. The uneven emission spectrum (Figure 7-7a) is due to the noise impacting the overall quality of the signal. This was worse for thinner films, as the intensity was even lower. Clearly, the intrinsic fluorescence of BPAPC is inadequate to measure *Tg* in ultrathin films. Instead, an extrinsic fluorescence dye is required that is stable at high temperatures, has high quantum yield and is effective in characterizing *Tg* in thin and ultrathin BPAPC films.

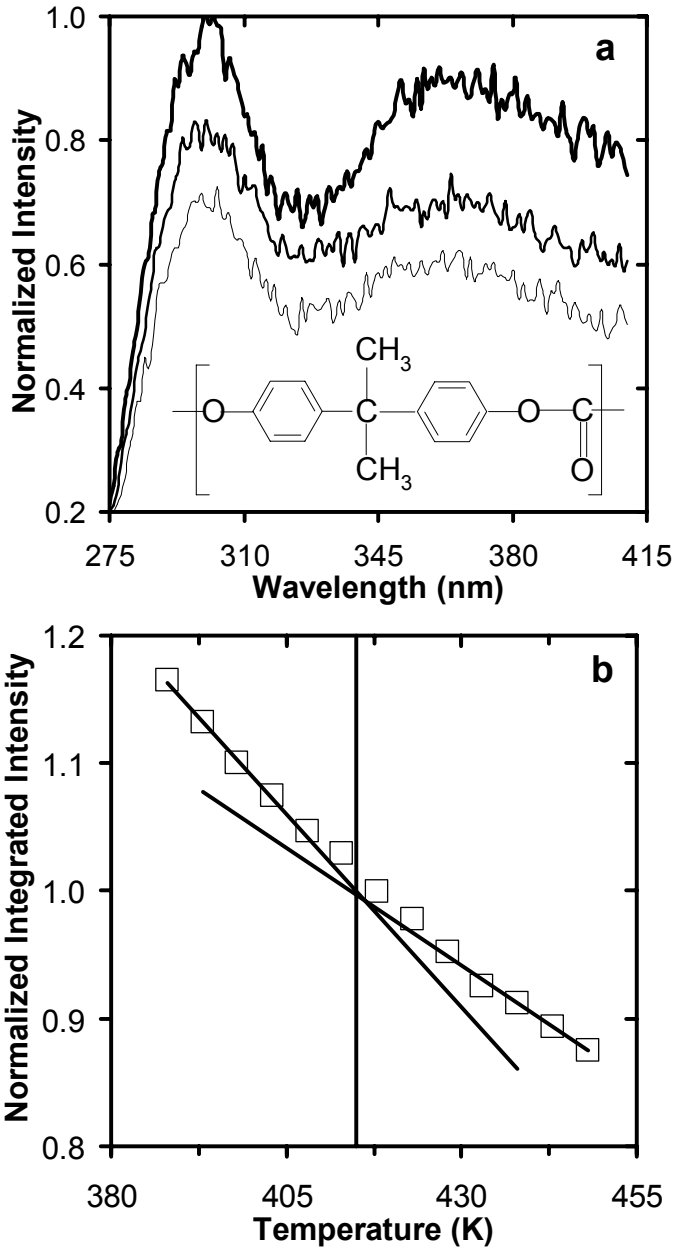

Figure 7-7: (a) Intrinsic fluorescence emission spectra of a 750-nm-thick film of BPAPC at 373 (bold curve), 413 (middle curve) and 448 (lowest intensity curve) K. Spectra are normalized to one at the peak intensity at 373 K. The inset shows the structure of BPAPC. **(b)** Temperature dependence of the integrated intrinsic fluorescence intensity for a 750-nm-thick BPAPC film. (The integrated intensity is normalized to one at 418 K.) The vertical line represents the bulk *Tg*.

In recent studies by Jager and coworkers (van den Berg 2006a, 2006b), 7-(dimethylamino)-1-methylquinolinium tetrafluoroborate was synthesized and used as a high temperature stability fluorescent probe for measuring *Tg* and physical aging in bulk BPAPC and PMMA films. The same dye, 7-(dimethylamino)-1-methylquinolinium tetrafluoroborate, was provided by Dr. Jager and used to characterize *Tg* in thin and ultrathin BPAPC films. However, the procedure by which *Tg* was determined was modified to allow for measuring *Tg* in thin as well as in ultrathin films. The resulting procedure was much more robust than those used in the studies by van den Berg (van den Berg 2006a, 2006b) using the same dye.

Figure 7-8a shows the fluorescence emission spectrum of 7-(dimethylamino)-1-methylquinolinium tetrafluoroborate dopant in a 900-nm-thick BPAPC film at 368, 413, and 448 K, respectively; each spectrum is normalized by the peak of highest intensity. There is a reduction in the overall intensity with increasing temperature. The overall change in the emission intensity as a function of temperature is substantial even for ultrathin films. In recent studies, Jager and coworkers (van den Berg 2006a, 2006b) have shown that *Tg* values can be obtained in BPAPC and PMMA by plotting the wavelength at the peak intensity as a function of temperature. Over a broad temperature-range near *Tg*, linear temperature dependences of the peak intensity wavelength are observed in the glassy and the rubbery state, with the intersection being identified as *Tg*. Since the wavelength-shifting probes are self-referencing (Ellison 2004b), the concerns pertaining to sample composition and geometry are automatically eliminated. In spite of this added advantage, the procedure is still very tedious as the overall change in the wavelength is limited to about 10 nm for a temperature range of 120-130 K (van den Berg 2006a, 2006b). This requires a large number of repetitive measurements to reduce the impact of background noise and to obtain reasonable quality data. In order to minimize these effects, intensity ratios at two different emission wavelengths were used as a function of

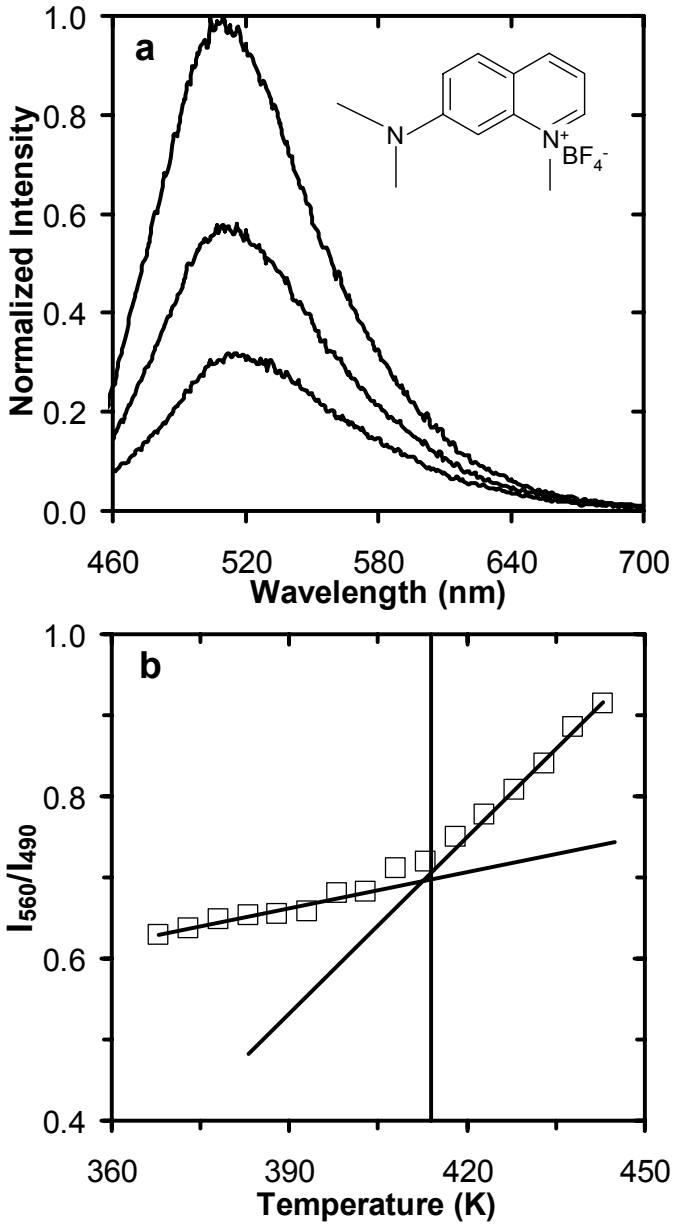

Figure 7-8: **(a)** Fluorescence emission spectra of 7-(dimethylamino)-1-methylquinolinium tetrafluoroborate dopant in a 900-nm-thick bisphenol-A-polycarbonate (BPAPC) film taken at 368 (highest intensity curve), 413 (middle curve) and 448 (lowest intensity curve) K. Spectra are normalized to one at the peak intensity at 368 K. The inset shows the structure of 7-(dimethylamino)-1-methylquinolinium tetrafluoroborate. **(b)** I_{560}/I_{490} of 7-(dimethylamino)-1-methylquinolinium tetrafluoroborate dopant in a 900-nm-thick BPAPC film.

temperature. This is also a self-referencing approach, but allows a much bigger window as the overall change in intensity as a function of temperature is large. With the overall optimization of the whole process, emission spectra over a much broader wavelength range (460 to 700 nm) were acquired, as compared to the small wavelength range reported previously by Jager and coworkers (van den Berg 2006a, 2006b). This approach minimizes errors, which leads to precise *Tg* measurements.

Figure 7-8b shows the ratio of intensities measured at 560 and 490 nm as a function of temperature for a 900-nm-thick BPAPC film doped with 0.2 wt % 7-(dimethylamino)-1-methylquinolinium tetrafluoroborate. The intensity at 560 nm was taken as the best-fit value to a linear fit between 550 and 570 nm, and the intensity at 490 was taken as the best-fit value to a straight line between 480 and 500 nm. This step was introduced to further reduce the impact of the noise level in the emission signal. The same procedure was employed for all *Tg* measurements. The maximum uncertainty in estimating *Tg* values by the intersection of linear temperature dependences of intensity ratios in the rubbery and glassy state was about ~ 2 – 3 K for all film thicknesses employed in this study.

Figure 7-9 shows the thickness dependence of *Tg* for BPAPC films. The data were obtained using the same procedure mentioned above and shown in Figure 7-8. The bold solid curve represents the best fit to the empirical relation proposed by Keddie *et al.* (Keddie 1994b) to previously published *Tg* data obtained from pyrene dopant or label fluorescence (Ellison 2005a) and intrinsic fluorescence of PS (Mundra 2006). The fit was shown to be in good agreement (Ellison 2005a; Mundra 2006) with the *Tg* data obtained by Keddie, Jones and Cory (Keddie 1994b) using ellipsometry. The dotted curve represents a fit of all the BPAPC data to the relation $Tg(h) = Tg,\text{bulk}(1-(A/h)^{\delta})$ originally proposed by Keddie *et al.* (Keddie 1994b) with A = 5.0 nm and δ = 1.85. In PS and BPAPC, the repeat units exhibit no attractive interaction with the substrate; thus,

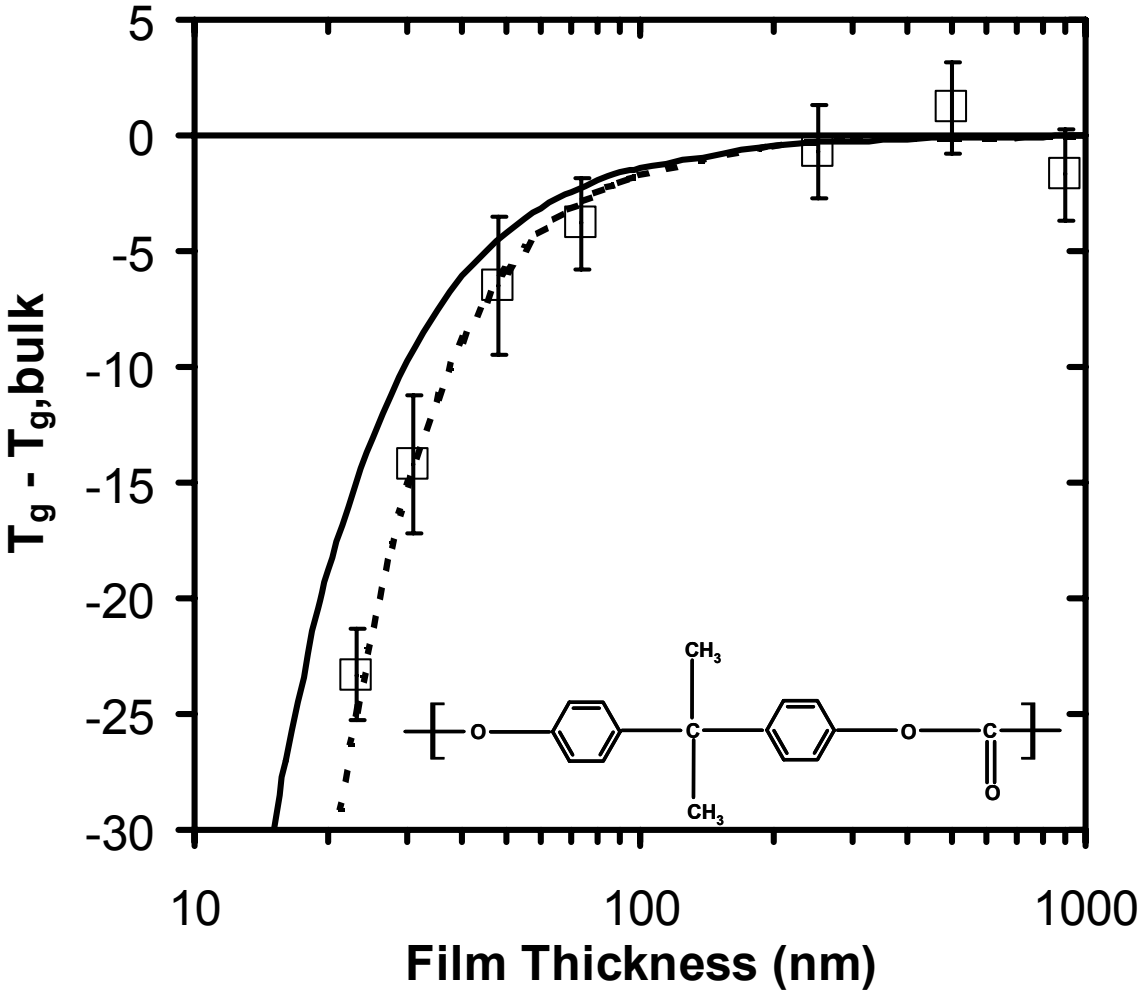

Figure 7-9: *Tg*-*Tg*,bulk as a function of film thickness for BPAPC (□) films as measured by 7-(dimethylamino)-1-methylquinolinium tetrafluoroborate dopant fluorescence. The bold curve represents a fit to PS film data from Figure 4-4 (Chapter 4) measured using extrinsic probe fluorescence; the fit employs the empirical relation originally proposed by Keddie *et al.* (Keddie 1994b), yielding the parameter values A = 3.2 nm and δ = 1.63. The dotted curve represents a fit to BPAPC film data using same empirical relation (Keddie 1994b), yielding the parameter values A = 5.0 nm and δ = 1.84. The inset shows the structure of BPAPC.

supported films undergo a *Tg* reduction with nanoconfinement due to the *Tg* reduction originating at the free surface (polymer-air interface) of the film (Ellison 2003). Figure 7-9 also draws a comparison between the *Tg* data as a function of film thickness for BPAPC and PS. For 23-nm-thick films, BPAPC exhibits a *Tg* value that is reduced by 23 K relative to *Tg*,bulk while PS exhibits a *Tg* value that is reduced by 15 K relative to *Tg*,bulk (Figure 4-4, Chapter 4). This indicates that by changing the rigidity of the polymer backbone structure, the thickness dependence of *Tg* is significantly affected. It is also interesting to note that the onset thickness at which *Tg* begins to show a significant deviation from *Tg*,bulk, which is defined as a 3K reduction relative to *Tg*,bulk, is increased slightly from ~ 40-50 nm for PS to ~ 75 nm for BPAPC.

Previous studies of the *Tg*-nanoconfinement effect observed in PαMS, P4MS, PTBS, and BPAPS (Ellison 2005a; Kim 2000) indicated that the onset thickness of the *Tg* reduction is greater for all of these systems than for PS. In some cases the onset thickness of the *Tg* reduction was seen to be as high as ~ 300 nm (Ellison 2005a). In addition, the shape of the thickness dependence of *Tg* was also observed to be different from that of PS in a few of these systems. The data in Figure 7-9 indicate that the *Tg*-nanoconfinement effect may be "tuned" by a slight change in the backbone structure or polymer backbone rigidity. The only other investigation of BPAPC by Soles *et al.* (Soles 2004a) has also shown reduction in *Tg* as a function of film thickness, and the shape of the thickness dependence of *Tg* is roughly similar to the results reported here. However, direct quantitative comparison is difficult as the error bars for some of the data points reported in the study by Soles were as large as ± 12-15 K.

To further understand the impact of the rigidity of the backbone structure, fluorescence was used to measure the thickness dependence of *Tg* in BPAPS, which has even higher backbone rigidity as compared to BPAPC. The bulk *Tg* value of BPAPS is extremely high (463K), therefore, most of the conventional pyrenyl based fluorescent

probes were ineffective in characterizing *Tg* as a function of film thickness due to issues related to dye sublimation or enhanced photobleaching at higher temperatures. Fortunately, intrinsic fluorescence was sensitive to *Tg* in thin as well as ultrathin films. Unlike BPAPC, the repeat unit structure of BPAPS includes four separate aromatic rings as part of the backbone structure, resulting in a very strong intrinsic emission signal, even in ultrathin films of BPAPS at high temperature.

Figure 7-10a shows the intrinsic emission spectrum for a 750-nm-thick BPAPS film at 428, 463, and 503 K, respectively. The spectral shape is different from the intrinsic emission spectrum in BPAPC with a peak at ~ 360 nm and shoulders at 315 and 420 nm. A decrease in temperature yields an increase in intensity and a spectral red shift. The increase in intensity is due to a densification of the medium, with a slightly denser environment yielding a higher intensity due to a reduced rate of nonradiative decay. Shifts in the emission spectra are also seen for charge resonance probe (van den Berg 2006a) and intramolecular charge transfer (ICT) probes (Ellison 2004b; Jager 2005) in a number of polymer systems. If the excited state of the probe is not in equilibrium with its surrounding medium, a slight reorientation of the medium can transform the excited state to its ICT state, which is of reduced energy and thus results in a spectral shift. The highly rigid structure of BPAPS repeat unit associated with the shape of the emission spectrum being highly sensitive to the surrounding medium. A similar spectral shift is also seen in BPAPC system, although the shift in the wavelength of peak intensity is relatively small (~ 1–2 nm).

Figure 7-10b shows the temperature dependence of the integrated intrinsic intensity of BPAPS in a 750-nm-thick film. The vertical bold line in Figure 7-10b represents the bulk *Tg* value. Intrinsic fluorescence measurements of bulk BPAPS films yield a *Tg* value in excellent agreement with those obtained by differential scanning calorimetry. Due to a high quantum yield, a substantial change in the intensity as a

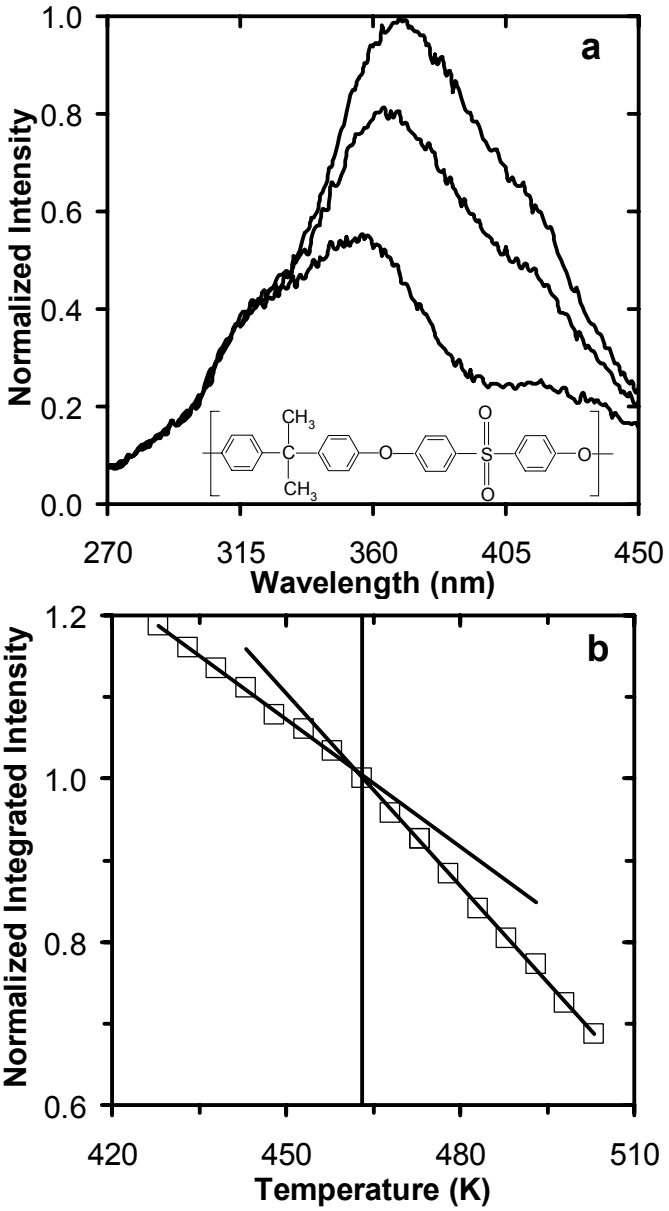

Figure 7-10: **(a)** Intrinsic fluorescence emission spectra of a 750-nm-thick film of bisphenol-A-polysulfone (BPAPS) at 428 (highest intensity curve), 463 (middle curve) and 503 (lowest intensity curve) K. Spectra are normalized to one at the peak intensity at 428 K. The inset shows the structure of BPAPS. **(b)** Temperature dependence of the integrated intrinsic fluorescence intensity for a 750-nm-thick BPAPS film. (The integrated intensity is normalized to one at 463 K.) The vertical line represents the bulk *Tg*.

function of temperature, and a stronger transition as compared to BPAPC, the maximum error in estimating the *Tg* values by the intersection of linear temperature dependences of integrated intensity in the rubbery and glassy state was smaller (± 1.5 K) in BPAPS than in BPAPC (± 2-3 K) for all film thicknesses employed.

Figure 7-11 compares the thickness dependence of *Tg* for BPAPS, BPAPC, and PS films. The curves are fits to the empirical function from Keddie *et al.* (Keddie 1994b). Similar to PS and BPAPC, the repeat units in BPAPS exhibits no attractive interaction with the substrate; thus, supported films undergo a *Tg* reduction with nanoconfinement due to the *Tg* reduction originating at the free surface (polymer-air interface) of the film (Ellison 2003). Figure 7-11 makes it clear that there are notable differences in the *Tg*-nanoconfinement effect of BPAPS as compared to that of either PS or BPAPC. The onset thickness for *Tg* reduction in BPAPS is larger than PS or BPAPC, estimated from Figure 7-11 at ~ 130 nm. For a 34-nm-thick films, BPAPS exhibits a *Tg* value that is reduced by 24 K relative to *Tg*,bulk while PS exhibits a *Tg* value that is reduced by 8 K relative to *Tg*,bulk for a film of similar thickness (Figure 4-4, Chapter 4). This further demonstrates that the rigidity of the polymer backbone structure is an important factor in tuning the *Tg*-nanoconfinement effect in polymers. In a solitary study, Kim *et al.* (Kim 2000) have also reported a *Tg*-nanoconfinement effect in BPAPS. Their data indicate that the onset thickness of the *Tg* reduction in BPAPS is similar (~ 140 nm) to that observed in this study. The shape of the thickness dependence of *Tg* for BPAPS is also similar in the study by Kim *et al.* (Kim 2000), except the reduction is less steep for ultrathin films.

Currently, factors such as the overall density and chain stiffness have not been studied in depth in association with the *Tg*-nanoconfinement effects. Obviously, while interesting issues remain to be discovered regarding *Tg*-nanoconfinement effects in polymer systems with simple carbon-carbon backbone structure, it may be possible that

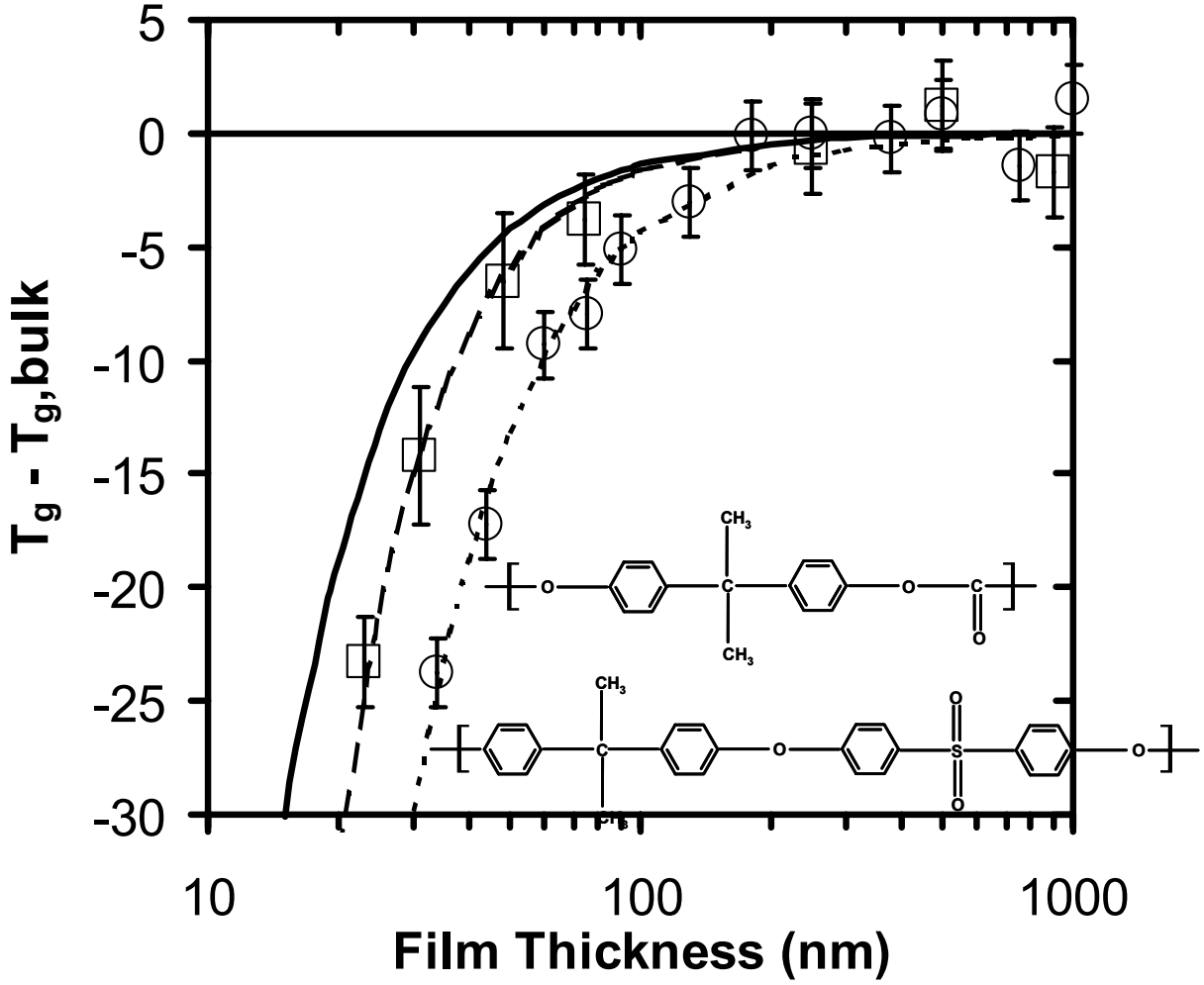

Figure 7-11: *Tg*-*Tg*,bulk as a function of film thickness for BPAPC (□) and BPAPS (○) films as measured by 7-(dimethylamino)-1-methylquinolinium tetrafluoroborate dopant fluorescence and intrinsic fluorescence, respectively. The bold curve represents a fit to PS film data from Figure 4-4 (Chapter 4) measured using extrinsic probe fluorescence; the fit employs the empirical relation originally proposed by Keddie *et al.* (Keddie 1994b), yielding the parameter values A = 3.2 nm and δ = 1.63. The dashed curve represents a fit to BPAPC film data using same empirical relation (Keddie 1994b), yielding the parameter values A = 5.0 nm, δ = 1.84 and A = 5.4 nm, δ = 1.60 in BPAPC and BPAPS, respectively. The inset shows the structure of BPAPC and BPAPS.

much greater insight may be gained by undertaking the challenges to study the impacts of film thickness on *Tg* in polymer systems that bear little resemblance to PS like those employed in this study.

7.2.5 Addition of Low Molecular Weight Diluents

7.2.5.1 Introduction

At a fundamental level, the presence of small-molecule diluents in polymers is known to reduce the extent of cooperativity by relaxing constraints on cooperative segmental mobility defining *Tg* (Casalini 2000; Hamilton 1996; Santangelo 1994a, 1994b; Roland 1993). As there has been interest (Forrest 2001) in connecting length scales associated with cooperative segmental mobility to those at which *Tg*-nanoconfinement effects are observed, the addition of small molecule diluents to polymer allows the length scales of cooperativity to be altered without otherwise changing the polymer-substrate interactions. This then allows for a critical, qualitative test of whether these two length scales are connected. Secondly, it is not clear that a material with added small amounts of diluents would be expected to behave similarly to the neat material when confined. An example of differing *Tg*-nanoconfinement behavior for chemically similar polymers is the effect of adding diluent on the *Tg*-nanoconfinement effect discovered by Ellison *et al.* (Ellison 2004a). They noticed a tunable aspect of adding diluents (either pyrene or dioctyl phthalate) on the *Tg*-nanoconfinement effect in PS films. They found that the *Tg*-nanoconfinement effect was eliminated down to a thickness of 13 nm upon the addition of either 9 wt% pyrene or 4 wt% DOP to the polymer.

In this study, the impact of the addition of low molecular weight diluents on the *Tg*-nanoconfinement effect of supported PMMA and poly(vinyl acetate) (PVAc) films is explored. This study includes addition of a common small molecule diluent known as dioctylphthalate (DOP) in PMMA and inadvertent addition of water vapor from the

ambient atmosphere in the case of PVAc. In both cases, it will be shown that the *Tg*-nanoconfinement effect is significantly affected by the presence of diluents. The results for PMMA and PVAc systems will be compared to those obtained by Ellison *et al.* (Ellison 2004a)

7.2.5.2 Experimental

The chromophore 4-tricyanovinyl-[N-(2-hydroxyethyl)-N-ethyl]aniline (TC1) was synthesized by reaction with tetracyanoethylene (TC1 America) and 2-(N-ethylaniline)ethanol (TC1 America) dissolved in dimethyl formamide (Fisher) at 55 ^{o}C for 15 min and then recrystallized from glacial acetic acid. TC1-labeled methacrylate monomer was synthesized through an esterification reaction with methacryloyl chloride (Aldrich) in the presence of triethylamine (Aldrich) and dichloromethane (Aldrich) at 0 ^{o}C for 2 hr. Labeled PMMA was synthesized by reaction of MMA monomer (Aldrich) in the presence of a trace amount of TC1-labeled methacrylate monomer. The TC1-labeled PMMA contained 1.37 mol% (1 in 73 repeat units) of the TC1-labeled monomer determined by UV-Vis absorbance spectroscopy (Perkin Elmer Lambda 35). For TC1-labeled PMMA, Mn = 509,000 g/mol, Mw/Mn = 1.67 measured by gel permeation chromatography using universal calibration with PS standards. All polymer was washed by dissolving in toluene (Fisher) and precipitating in methanol (Fisher) at least five times to remove residual solvent and then dried in a vacuum oven at Tg + 15 K for 24 hr. Poly(vinyl acetate) was graciously provided by Prof. Gregory B. McKenna (O'Connell 2005) of Texas Tech University with Mw = 157,000 and PDI = 2.73 and was used as received. Dioctylphthalate (DOP) (Aldrich, 99%) was used as received.

Bulk Tg (Tg,bulk) values were measured by differential scanning calorimetry (DSC) (Mettler-Toledo DSC822, second heat, onset method, 10 K/min) and also via fluorescence methods and ellipsometry, and were found to agree within experimental error. Thin films of polymers were prepared by spin coating (Hall 1998a) dilute solutions

of polymer onto quartz slides. Film thicknesses were determined using a Tencor P10 profilometer.

For thin and ultrathin PMMA films, fluorescence was measured using a PTI QM-2001 SE fluorimeter using front-face geometry. As the PTI fluorimeter has greater excitation intensity than the Spex fluorimeter, a smaller slit size was used with the PTI instrument to prevent films from photobleaching at high temperature. A clean quartz cover slide was placed on top of each film to reduce the potential for probe sublimation during the *Tg* measurement by fluorescence. (The film was adhered only to the glass substrate on which it was spin coated.) Film temperature was controlled by a microprocessor controller (Minco Products) with a Kapton ribbon heater attached to a flat aluminum plate that was also used as a clamping device to hold the sample.) For further details, refer to Chapters 4 and 6.)

An M-2000D^{TM} spectroscopic ellipsometer (J. A. Woollam Co., Inc.) with an integrated programmable heating source (Instec) was used for measurements characterizing film thickness as a function of temperature above and below *Tg* with several heating and cooling cycles for PVAc systems.

In fitting the temperature dependence of fluorescence in the rubbery and glassy states, only data points well outside *Tg* were used for the linear fits, and typical correlation coefficients (R^2) were better than 0.990. To initiate the fitting procedure, data points were added to the rubbery- and glassy-state linear regressions one-by-one at the extrema in the temperature range of the data. The correlation coefficient was monitored as more data points were added (approaching *Tg* from the extrema in the temperature range of the data) to each of the linear regressions. If the R^2 value began to steadily decrease below a threshold value (i.e., < 0.990) as more data points were added, then these data points were removed to produce a value of R^2 higher than the threshold value and the linear regressions were considered acceptable. The linear fits in both the rubbery

and glassy states included a minimum of four fluorescence data points (usually more), spanning a minimum of 15 K in temperature. This procedure was followed regardless of whether fitting linear functions to the fluorescence intensity data at particular emission wavelength(s) or the integrated intensity as a function of temperature. When using integrated intensities to identify *Tg*, spectra were taken over a sufficient range of wavelengths that integration could be done from instrument baseline at the lowest wavelengths to the same instrument baseline at the highest wavelengths. In all cases, regardless of using intensities or integrated intensities, the sample was reheated to the starting temperature following the measurements taken upon cooling to verify that the sample did not lose a substantial amount of fluorescence probe molecules due to photobleaching, sublimation, etc. Typically, the intensity after reheating the sample is within 10% of the original intensity before the measurements were taken upon cooling. In fitting the temperature dependence of film thickness in the rubbery and glassy states in PVAc system using ellipsometer, only data points well outside *Tg* were used for the linear fits, and typical correlation coefficients (R^2) were better than 0.9990.

7.2.5.3 Addition of Dioctylphthalate in Thin and Ultrathin PMMA Films

Figure 7-12 shows the *Tg* values of the TC1-labeled PMMA as a function of film thickness. Three cases are illustrated, one the neat polymer (see Figure 7-12) and the other two cases in which a low molecular weight diluent, dioctyl phthalate (DOP), is present at low levels in the film. The neat polymer shows a substantial increase in *Tg* with decreasing thickness below 90 nm, in reasonable agreement with reports by others (Keddie 1994a; Hartmann 2002) who investigated *Tg* values in thin and ultrathin PMMA films. It is noteworthy that this significant nanoconfinement effect can be suppressed by adding as little as 4 wt% DOP to the polymer. At that level of DOP, the films show no effect of nanoconfinement on *Tg*, within experimental error, down to film thicknesses of 20 nm. At 2 wt% DOP, the observed *Tg*-nanoconfinement effect is intermediate to those

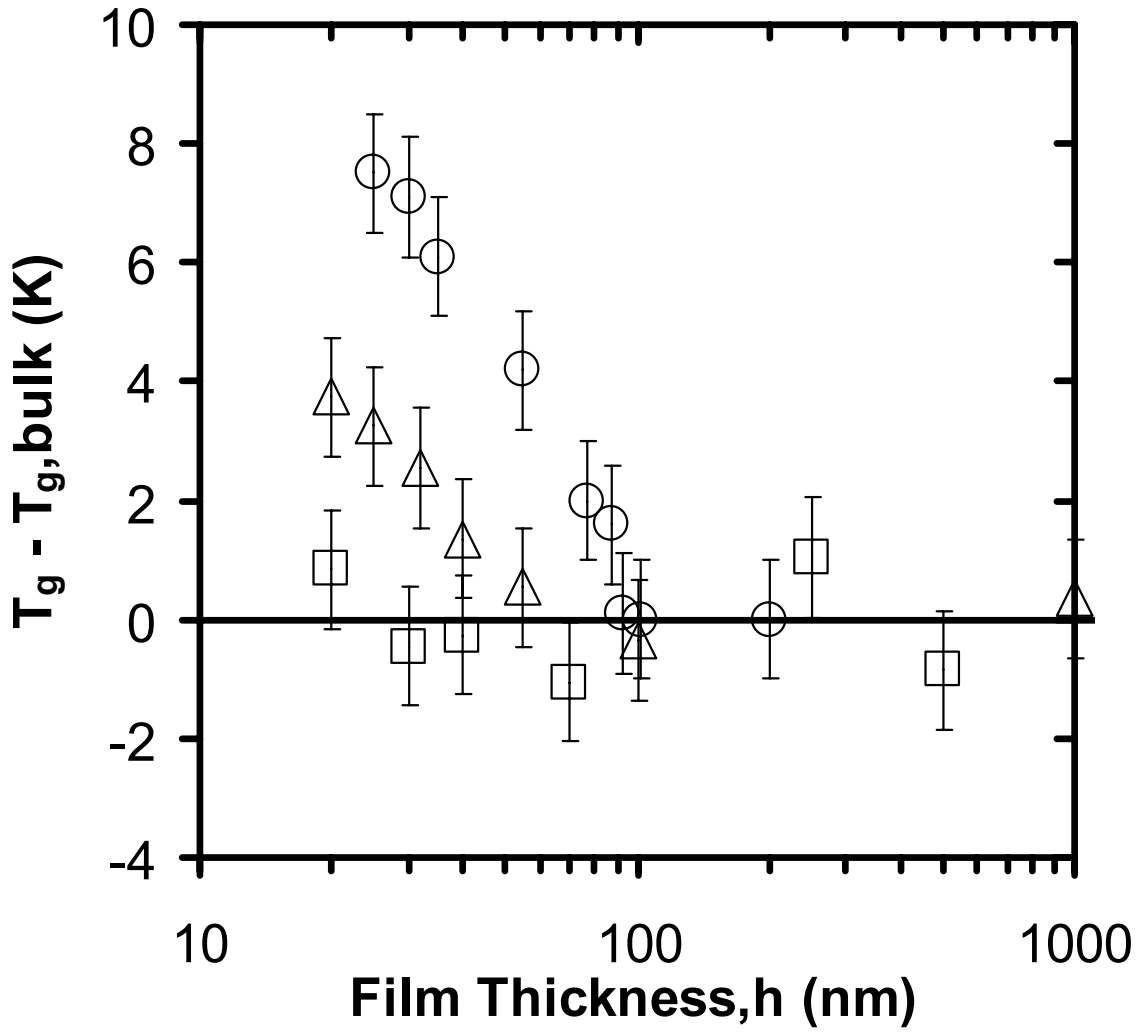

Figure 7-12: Deviation from bulk *Tg* as a function of film thickness for neat TC1-labeled PMMA (○) film and TC1-labeled PMMA film with 2 wt% (Δ) and 4 wt % (□) DOP.

observed in neat polymer and the polymer with 4 wt% DOP. Related effects of DOP addition to PS thin and ultrathin films were reported earlier (Ellison 2004a). The results in Figure 7-12 and by Ellison *et al.* (Ellison 2004a) show that the effect of low molecular weight diluent addition in suppressing and potentially eliminating the *Tg*-nanoconfinement effect is applicable to a number of polymer systems and is operative in cases in which *Tg* increases or decreases with nanoconfinement. The underlying cause for this effect is worthy of further study for it may hold the key to controlling and tuning the *Tg*-nanoconfinement effect in many polymeric media.

7.2.5.4 Addition of Water Vapor in Poly(vinyl acetate) Thin and Ultrathin Films due to Absorption from Surrounding

O'Connell and McKenna (O'Connell 2005) recently reported no change in *Tg* with decreasing thickness of poly(vinyl acetate) (PVAc) freely standing films down to a film thickness of 27.5 nm. They argued that the phenomenon of *Tg*-nanoconfinement effect is not universal, implying that not all polymer systems exhibit a change in *Tg* with confinement. However, the observed effect may be explained by the presence of small molecule diluents, i.e., water sorbed by PVAc from the atmosphere. As shown recently by Ellison *et al.* (Ellison 2004a) and Mundra *et al.* (Mundra 2007b) via experiments and by Riggleman *et al.* (Riggleman 2006) via simulation, the effect of low molecular weight diluent addition suppresses and potentially eliminates the *Tg*-nanoconfinement effect.

It is also well known that PVAc is hygroscopic in nature and absorbs 1 to 3 % of water vapor readily. As no special precaution was taken to avoid uptake of water vapor by PVAc system by O'Connell and McKenna (O'Connell 2005), it is hypothesized that their samples had sorbed water, leading to an apparent absence of a *Tg*-nanoconfinement effect. It is also interesting to note that Fukao *et al.* (Fukao 2001) have reported a reduction in *Tg* with decreasing film thickness in supported PVAc films.

To test the hypothesis, the *Tg*-nanoconfinement effect was studied in PVAc films.

Before measuring *Tg* in thin and ultrathin films, it was necessary first to confirm whether the bulk *Tg* was impacted by plasticization from water vapor. Figure 7-13 shows the bulk *Tg* values measured by differential scanning calorimetry (DSC) as a function of annealing time for PVAc samples annealed at 120 ºC. Clearly Figure 7-13 shows that the bulk *Tg* value is reduced by 10 K for the unannealed sample due to presence of water vapor. It is worth mentioning that this reduced *Tg* value for the unannealed sample is in agreement with bulk *Tg* value reported by O'Connell *et al.* (O'Connell 2005), consistent with the presence of water vapor in their samples.

Figure 7-14a shows ellipsometry measurements of the normalized film thickness as function of temperature for 6-nm-thick and 630-nm-thick films in the unannealed state (with equilibrium water sorption from the atmosphere). The *Tg* for 630-nm-thick film was 306 K and for 6-nm-thick film was 305 K. Evidently, due to the presence of water in the PVAc films, no *Tg*-nanoconfinement effect is seen down to a film thickness of 6 nm. Figure 7-14b shows the normalized film thickness as a function of temperature for annealed or "dry" films of thickness 620 and 6 nm. (The "dry" films were obtained by annealing for 180 min at 120 ºC). The *Tg* for 620-nm-thick film was 310 K; The *Tg* for 6-nm-thick film was 300 K. Once water vapor is removed from the films, the *Tg*-nanoconfinement effect is observed with *Tg* reductions of about 10 K for 6-nm-thick film.

Figure 7-15 plots $Tg - Tg$,bulk as a function of film thickness for both wet and dry films. Clearly, the impact of water, which acts as a low molecular weight diluent in PVAc system, is evident. These results are in good agreement with those of Fukao (Fukao 2001). Furthermore, they also explain the results in the freely standing films of PVAc reported by O'Connell and McKenna (O'Connell 2005). The underlying cause for this tunability in *Tg*-nanoconfinement effect with the addition of low molecular weight diluent is not fully understood. Therefore, this type of study in other systems is worthy of

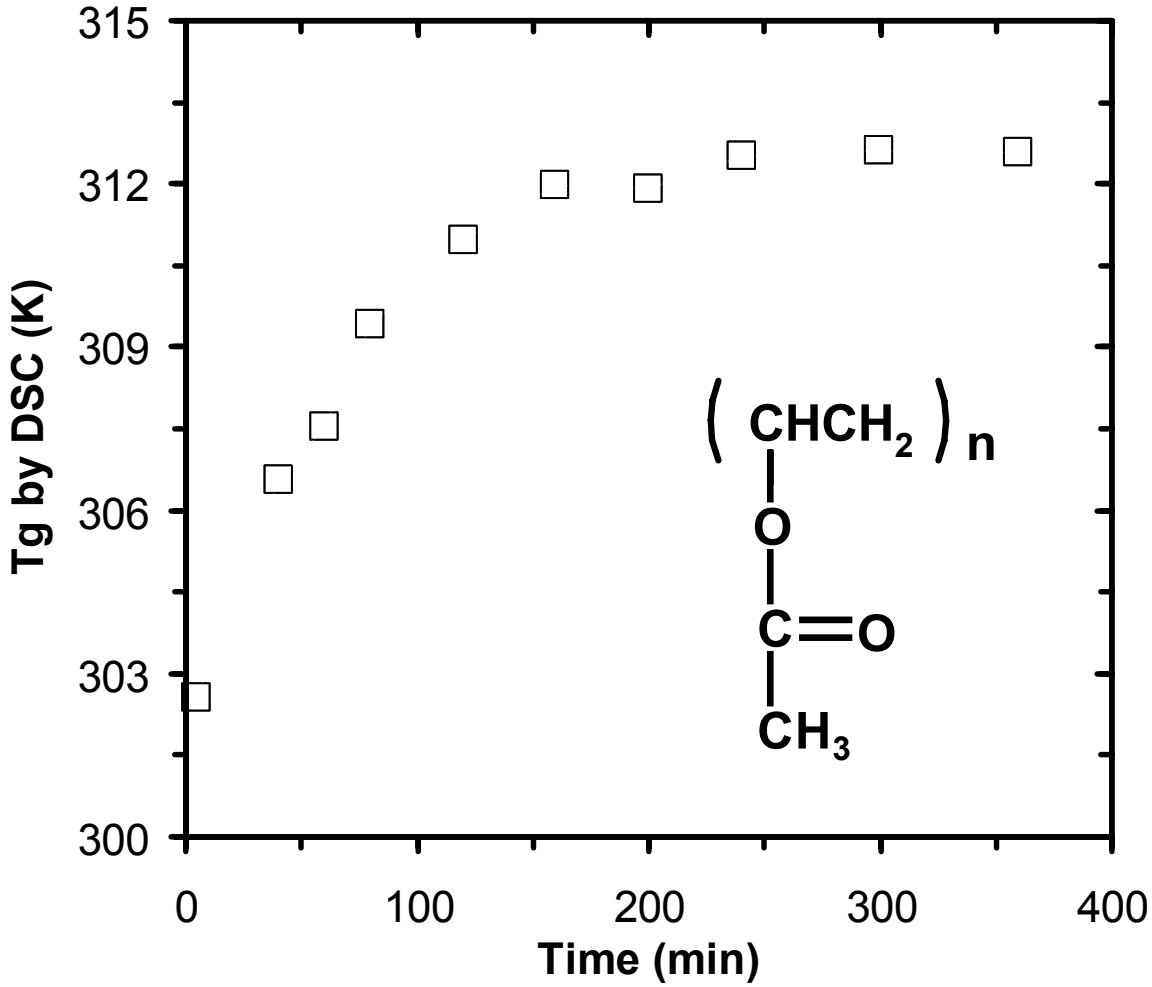

Figure 7-13: *Tg* of poly(vinyl acetate) (PVAc) measured by differential scanning calorimetry (DSC) as a function of annealing time at 120 °C. The inset shows the repeat unit structure of PVAc.

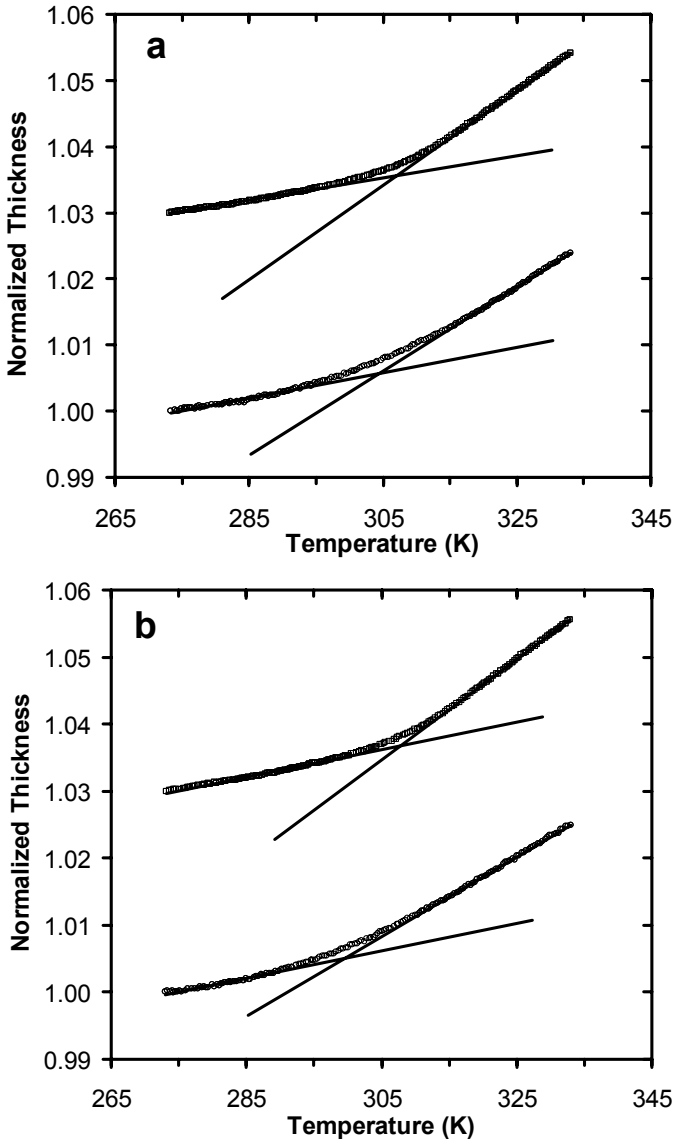

Figure 7-14: **(a)** The temperature dependence of the normalized thickness of "wet" PVAc films of thickness 630 nm (top) and 6 nm (bottom) (Tg,bulk = 306 K). (The thickness have been normalized to one at 273 K, and vertically shifted for clarity.) **(b)** The temperature dependence of the normalized thickness of "dry" PVAc films of thickness 620 nm (top) and 6 nm (bottom) (Tg,bulk = 310 K). (The thickness have been normalized to one at 273 K, and vertically shifted for clarity.)

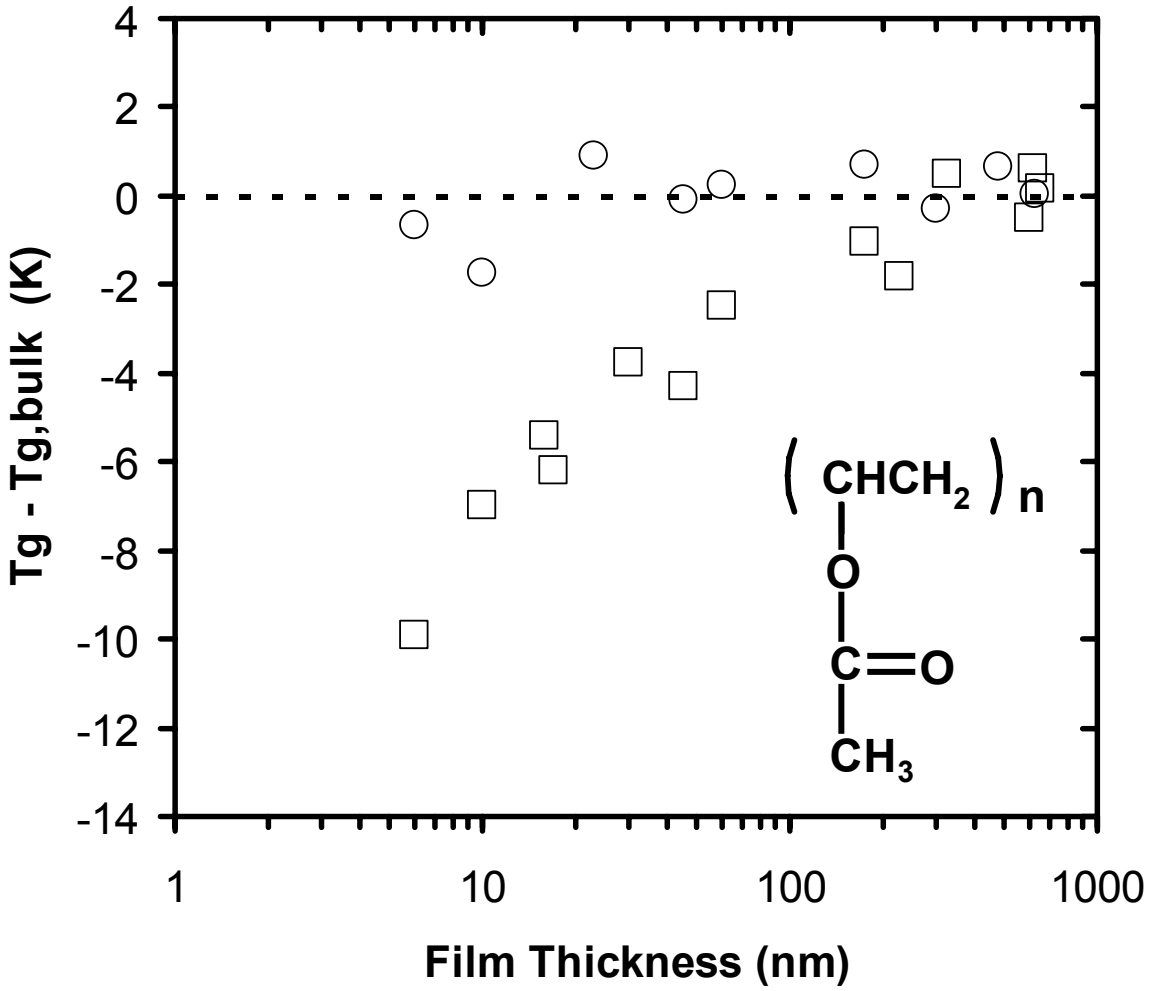

Figure 7-15: *Tg* – *Tg*,bulk as a function of film thickness for PVAc wet (○) and dry (□) films as measured by ellipsometer. The inset shows the repeat unit structure of PVAc.

further consideration for it may hold the key to controlling and tuning the *Tg*-nanoconfinement effect in many polymeric media.

7.3 Conclusions

In this chapter the impact of various parameters that can potentially modify or "tune" the *Tg*-nanoconfinement effect are explored in detail. Among the parameters investigated are molecular weight, composition of a random copolymer, slight modification to the repeat unit structure, changes in polymer chain stiffness or backbone rigidity, and addition of low molecular weight diluents.

The effect of nanoconfinement on the *Tg* of PS films is investigated over the largest *MW* range ever reported in a single study (5,000 g/mol to 3,000,000 g/mol). In contrast to two recent reports (Singh 2004; Miyazaki 2004), in this study, it is observed that PS *MW* has no impact on the film thickness dependence of *Tg* - *Tg*,bulk. This result is consistent with the substantial evidence in the literature indicating that *Tg*-nanoconfinement effects originate from interfaces and surfaces which impact the cooperative segmental mobility associated with *Tg* and are not due to other factors which may depend on *MW* such as degree of chain end segregation, entanglement density, etc.

In the case of S/MMA random copolymers, the *Tg*-nanoconfinement effect is tuned by variation in copolymer composition. As S-content decreases in S/MMA copolymers, the *Tg*-nanoconfinement effect changes from a decrease to an increase in *Tg* relative to bulk *Tg*, with an intermediate S-content copolymer exhibiting a nearly thickness-invariant *Tg*.

In contrast to the absence of an effect of *MW* on the *Tg*-nanoconfinement effect in PS, small modifications to the repeat unit structure of PS have a dramatic impact on the *Tg*-nanoconfinement effect. A stronger film thickness dependence of *Tg* is observed for P4MS compared to PS, while PTBS exhibits a stronger dependence than both PS and P4MS. The *Tg* reduction for a 21-nm-thick PTBS film is 47 K relative to *Tg*,bulk, which

is the largest deviation from *Tg*,bulk ever observed for supported polymer films. Furthermore, the onset thickness for the *Tg*-nanoconfinement effect is 300-400 nm in PTBS, the largest thickness for which such a *Tg*-nanoconfinement effect has been reported.

Small modifications to the side group of PMMA are also observed to have dramatic impact on the *Tg*-nanoconfinement effect of PMMA films. The average *Tg* across a film of PiBMA is invariant with nanoconfinement. In contrast, the *Tg* of PMMA increases with nanoconfinement while those of PEMA and PPMA decrease with nanoconfinement.

The *Tg*-nanoconfinement effect is also "tuned" by the change in the backbone rigidity of the repeat unit structure. The strength of the thickness dependence of *Tg* is greater for BPAPC than for PS, while BPAPS exhibits even stronger dependence than both PS and BPAPC. Thus, the strength of the thickness dependence of *Tg* follows the order of the rigidity of the polymer backbone structure. In particular, for a 34-nm-thick film of BPAPS, *Tg* is reduced by 24 K relative to *Tg*,bulk, while BPAPC and PS films of the same thickness exhibit *Tg* values which are reduced by 12 K and 8 K, respectively. The onset thickness for *Tg* reduction in BPAPS (~ 130 nm) is almost three times the onset thickness for PS (~ 40-50 nm).

Finally, the addition of small molecule diluents has a significant impact on the tunability of *Tg*-nanoconfinement effects in polymer films. The *Tg*-nanoconfinement effect is eliminated down to a film thickness of 20 nm in PMMA films by addition of small molecule diluents such as DOP. In PVAc, the *Tg*-nanoconfinement effect is eliminated down to a film thickness of 6 nm when water is sorbed from the atmosphere, resulting in a small percent of water dispersed naturally in the polymer matrix.

CHAPTER 8

EFFECT OF SPATIAL CONFINEMENT ON Tg OF PATTERNED POLYMER NANOSTRUCTURES: TUNABILITY OF THE Tg-NANOCONFINEMENT EFFECT

8.1 Introduction

Miniaturization of devices has led to an array of emerging applications that require polymer nanostructures for diverse disciplines ranging from tissue engineering (Griffith 2002), molecular electronics (Huang 2001a), and microfluidic devices (Therriault 2003) to sacrificial templates (Xia 1999) and photonic materials (Lin 1998). The crucial role played by polymer resists for generating sub-100 nm features during the lithographic process in the microelectronics industry is another strong motivating factor for evaluating the properties of polymer nanostructures (Resnick 2003; Bratton 2006; Marceau 2006). While the potential benefit of miniaturization is one of the drivers for fabrication of nanostructures, the size-dependent properties observed in several material systems (Zhu 2001; Alivisatos 1996; Li 2001) necessitates a thorough evaluation of the physical properties of these nanostructures.

As in many dimensionally constrained material systems, the physical properties of polymer nanostructures can deviate significantly from those measured in the bulk state. For example, properties of thin polymer films such as the glass transition temperature (*Tg*) (Keddie 1994a, 1994b; Serghei 2005; Baschnagel 2005; Jain 2004; Campoy-Quiles 2006), physical aging (Kawana 2003; Huang 2006; Fukao 2005), modulus (Yoshimoto 2005; Van Workum 2003; Stafford 2004, 2006; Hartschuh 2004, 2005), compliance (O'Connell 2006), and diffusion coefficients (Frank 1996a, Hall 1998b) are seen to deviate from bulk values. In the case of *Tg* behavior, studies of ultrathin polymer films have included substrate-supported and freely standing films. With some exceptions

(O'Connell 2005), when film thickness decreases below a critical value for substrate-supported films, an increase in *Tg* is generally observed for polymers exhibiting strong attractive interactions with the substrate (Keddie 1994a; van Zanten 1996; Forrest 2001; Grohens 2002; Pham 2002; Ellison 2002a; Fryer 2001; Mundra 2006), and a decrease in *Tg* is observed for polymers lacking such attractive interactions with the substrate (Keddie 1994a, 1994b, 1995; Kawana 2001; DeMaggio 1997; Fukao 1999, 2000; Forrest 1997, 2001; Singh 2004; Miyazaki 2004; Ellison 2002a, 2002b, 2003, 2005a, 2005b; D'Amour 2004; Mundra 2006; Rittigstein 2007). For freely standing films, *Tg* generally decreases when thickness decreases below some critical value (Forrest 1996, 1997, 1998, 2000, 2001, 2002; Dalnoki-Veress 1999, 2000, 2001; Roth 2003, 2005).

In contrast to the many studies devoted to the effect of confinement on the properties of thin polymer films, there is a notable paucity of research (Stafford 2006; Hartschuh 2004, 2005) focused on the effect of confinement in one-dimensional (1-D) polymer nanostructures, and none directly reports *Tg* values. This lack of reports on the *Tg* of nanostructures is likely due to the fact that many of the experimental methods used to measure *Tg* in thin and ultrathin films, such as ellipsometry and X-ray reflectivity, are inapplicable to polymer nanostructures. However, such a study is important because the knowledge of how thermophysical properties are altered upon confinement in these nanostructures is vital to the advancement of various nanotechnology applications. The current study is made possible by the first use of an ensemble fluorescence technique, recently developed to characterize distributions of and average *Tg* values in ultrathin films and nanocomposites (Ellison 2002a, 2002b, 2003, 2004a, 2004b, 2005a; Priestley 2005a, 2005b; Rittigstein 2006, 2007), to determine *Tg* values in 1-D nanopatterned systems.

One-dimensional polymer nanostructures can be obtained by various patterning techniques, including imprint lithography (Chou 1996; Resnick 2003), dip pen

nanolithography (Piner 1999; Noy 2002), photolithography (Xu 2005), electrostatic lithography (Lyuksyutov 2003), capillary techniques (Donthu 2005a), and electron beam lithography (EBL) (Donthu 2005b). Among these, EBL is attractive because it is a mask-less technique that enables one to readily fabricate nanostructures simply by designing the pattern via computer rather than having to prepare different masks as with other projection lithography techniques. In addition, the poly(methyl methacrylate) (PMMA) system studied here is one of the most common electron beam resists with extensive literature (Chen 1993; Donthu 2005b; Dobisz 2000) on the EBL patterning process that can be readily adopted for our study. The technological relevance of PMMA to the microelectronics industry and the fact that comparisons can be made to studies of the effect of nanoconfinement on *Tg* in PMMA films supported on silica (Mundra 2006, 2007a; Keddie 1994a; Park 2004) are other motivating factors for studying this system. EBL was employed to fabricate PMMA nanopatterns on silica of various line width (*LW*) and thickness (*h*). This chapter details the first study of the effect of 1-D nanopatterned geometry, including nanoline thickness and line width, on *Tg* in a confined polymer system as well as compares the results to those of thin films (2-D geometry) of the same thickness. Such an investigation is important because the mechanical robustness of nanopatterned polymers may be affected by reductions in *Tg* that are associated with the high free-surface (polymer-air interface) area present in nanopatterns.

8.2 Experimental

Poly(methyl methacrylate) labeled with the fluorescent dye 4-tricyanovinyl-[N-(2-hydroxyethyl)-N-ethyl]aniline (TC1) was synthesized by free radical polymerization of methyl methacrylate (Aldrich) with a trace amount of TC1-labeled methacrylate (Priestley 2005b). The TC1-labeled methacrylate was synthesized by an esterification reaction of TC1 with methacryloyl chloride (Aldrich) in the presence of triethylamine (Aldrich) and dichloromethane (Aldrich) at 0 ^{o}C for 2 h. The TC1 probe was synthesized

by a route discussed in detail in Chapter 5. The resulting TC1-labeled PMMA was washed by multiple dissolution and precipitation steps in toluene and methanol to remove traces of residual unreacted TC1-labeled monomer. The purified TC1-labeled PMMA contained 1.37 mol% (1 in 73 repeat units) TC1-labeled monomer, as determined by UV-vis absorbance spectroscopy (Perkin Elmer Lambda 35), and a number-average molecular weight (*Mn*) of 509,000 g/mol and a polydispersity index (*Mw*/*Mn*) of 1.67, as obtained by gel permeation chromatography using universal calibration and polystyrene standards. The bulk *Tg* of this material was 394 K as determined by differential scanning calorimetry (Mettler Toledo DSC822e; onset method, second heating cycle at a 10 K/ min heating rate) and 395 K as determined by fluorescence method.

Phosphorous-doped Si (100) substrates with 140 Å thermal oxide layers were cleaned in a piranha solution (3:1 volume ratio of H_2SO_4 and 30 % H_2O_2), thoroughly washed with deionized (DI) water and rinsed in isopropanol. Solutions of TC1-labeled PMMA in toluene of various concentrations were spin coated onto the substrates as a function of spin speed to obtain films of desired thickness (Hall 1998a). Substrates coated with TC1-labeled PMMA were patterned using a Quanta 600F (FEI Co.) environmental scanning electron microscope integrated with a nanopattern generator lithography system. Samples were exposed to a primary electron beam operating at 10 kV with a spot size adjusted to give a beam current of 340 pA (± 4 pA) and overall doses of 200 - 400 $\mu C/cm^2$. The patterns were developed using a methyl isobutyl ketone:isopropanol (MIBK:IPA) (1:3 volume ratio) solution for 1 min at room temperature. (Separate experiments confirmed that a fine powder of PMMA with *Mn* = 65,000 g/mol or less dissolved in the developer solution within 1 min. This ensured that the line edges of the final, patterned samples did not contain any low molecular weight PMMA with a molecular-weight-dependent *Tg*.) The patterned samples were imaged using atomic force microscopy (Digital Instruments Nanoscope IIIa) operating in tapping

mode with a high-aspect-ratio Si cantilever with a nominal tip radius of 2 nm. After *Tg* measurement, samples were coated with Au/Pd alloy films of about 10 nm thickness and imaged using the same SEM instrument used for patterning.

The samples for thin film measurements were prepared by spin coating toluene solutions of TC1-labeled PMMA onto quartz slides; the resulting films were dried in a vacuum oven at ~5 K above the film *Tg* for 8 h. Film thicknesses were an average of ten measurements (standard deviation less than 2%) taken at different locations on the films using a profilmeter (Tencor P10).

Steady-state fluorescence emission spectra were taken as a function of temperature (on cooling) using a Photon Technology International fluorimeter in a front-faced geometry (with emission at 90^{o} relative to excitation with the sample fixed at a 28^{o} angle relative to excitation) with 3 mm excitation slits (12 nm bandpass) and 3 mm emission slits (6 nm bandpass). The excitation wavelength was 480 nm, and the emission spectra were measured at 540-700 nm. The *Tg* values were determined from the intersection of linear fits to the temperature dependence of the integrated fluorescence intensity in both the rubbery and glassy states; only data well away from *Tg* were used for the linear fits, with typical correlation coefficients (R^2) being better than 0.990. The sample temperature was controlled within +/- 0.1 K using a temperature controller and a flat ribbon heater (Minco Products) mounted on a thin aluminum plate. (Additional information on the use of this fluorescence technique to monitor *Tg* is given in Chapter 3, 4, and 5.)

8.3 Impact of Sample Geometry or Spatial Confinement on the Tunability of the Tg-Nanoconfinement Effect

Optical microscopy images of TC1-labeled PMMA patterns on oxidized Si substrate are shown in Figure 8-1a. The magnified image in the inset shows the periodicity of the pattern whereas the low magnification image shows a relatively large field of view of the patterned area. For each sample, these patterns are generated over a

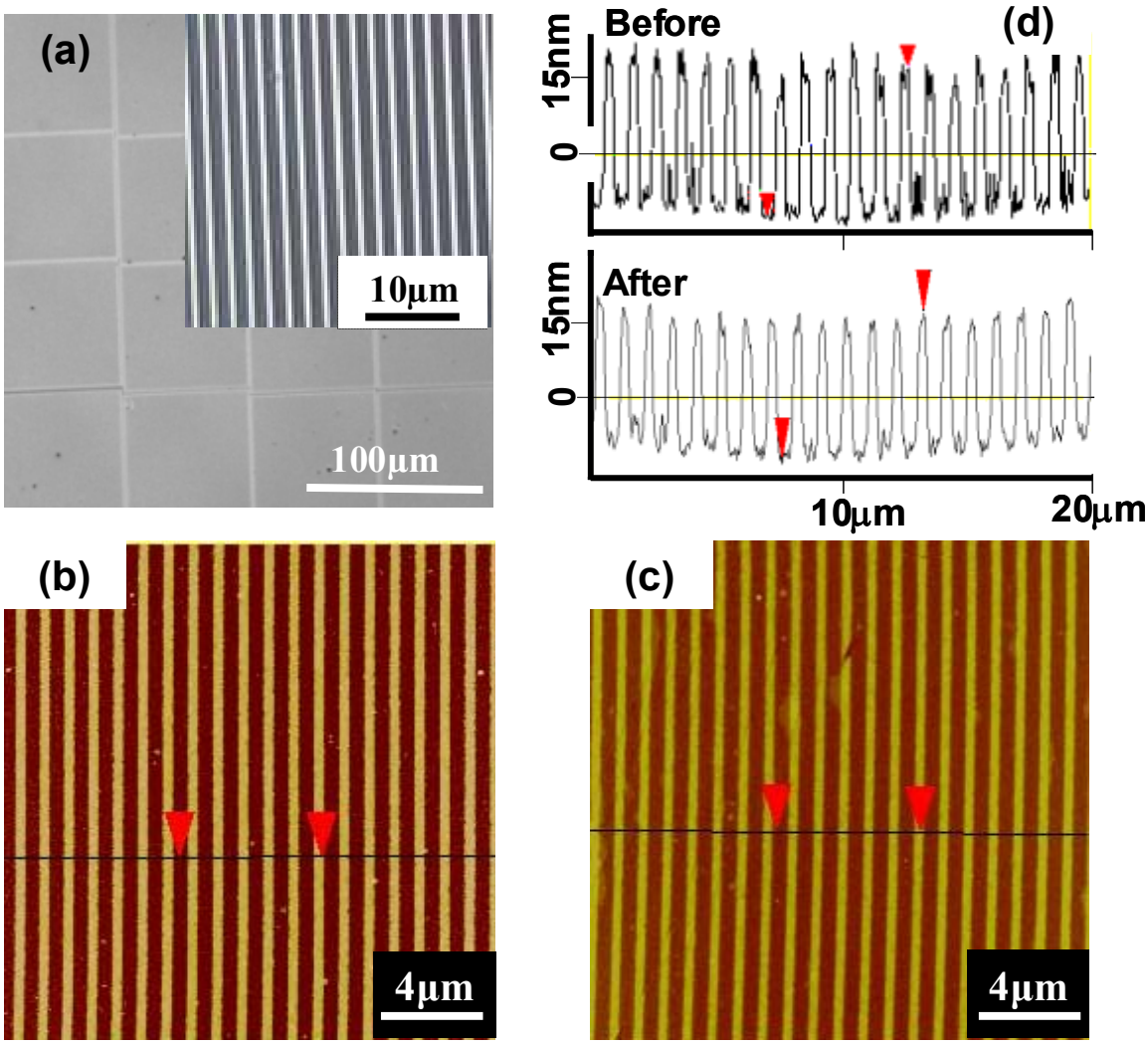

Figure 8-1: **(a)** Optical images of TC1-labeled PMMA lines on oxidized Si (100) substrate showing regular order of patterns over large areas and geometry of nanopattern employed in the current study. **(b)** AFM image of 30-nm-thick pattern with a line width of 260 nm before *Tg* measurement, and **(c)** AFM image of the same sample after *Tg* measurement, demonstrating that lines remain continuous even after thermal cycling through *Tg*. **(d)** AFM thickness profile of the same pattern before and after *Tg* measurement showing no significant change in line dimensions.

2 mm x 2 mm area by "stitching-together" 100 μm x 100 μm areas exposed in a single electron beam exposure run. Using this general scheme, patterned lines with *LW* ranging from 50 nm to 1300 nm on films ranging from 15 nm to 175 nm in thickness are generated. The structural height (thickness) of these patterns is controlled via the initial film thickness achieved by spin coating (Hall 1998a).

One of the initial concerns is to evaluate any possible dimensional distortion and discontinuity of patterned lines upon thermal cycling during *Tg* measurement. The temperature schedule used to measure *Tg* involved heating the sample rapidly to a temperature well above *Tg* (~*Tg* + 25 to 30 K), holding at temperature for 12 min, and then cooling at a rate of 1.0 K/min to a temperature well below *Tg*. Figure 8-1b shows a typical AFM topographic image of a 30-nm-thick nanopattern with *LW* = 260 nm before heating and cooling the sample for *Tg* measurement while Figure 8-1c shows the AFM image of the same sample after *Tg* measurement. It is clear from these images that the lines remain continuous without any noticeable agglomeration or compaction. Figure 8-1d shows the AFM profiles of this sample before and after *Tg* measurement and indicates that, within experimental error, the average pattern height, *h*, remains unchanged due to thermal cycling associated with the *Tg* measurement. This implies that the PMMA nanolines are reasonably mechanically robust with negligible flow of PMMA over the tens of minutes and temperature range employed to measure *Tg*, including the achievement of temperatures several tens of degrees above *Tg*. The height profiles in Figure 8-1d show that the surface roughness within a single line is less than 3 nm before *Tg* measurement and is reduced further after the *Tg* measurement, with the surface of the lines becoming smoother on average. This effect may be driven by the surface line tension. Nevertheless, the height and line width of the patterned lines are unchanged by the thermal schedule used in this study. Similar results are obtained with nanolines of various *h* and *LW*.

The stability of PMMA patterns in this study is in stark contrast to the shape evolution or "melting" of PMMA patterns recently reported by Jones *et al.* (Jones 2006). This is likely due to several factors. First, the PMMA used by Jones *et al.* (Jones 2006) had *Mn* = 15,000 g/mol. Thus, their sample was below the critical molecular weight for entanglement for PMMA (Fuchs 1996), meaning that a viscous flow response would be expected at temperatures slightly above *Tg*. (Jones *et al.* (Jones 2006) annealed their patterns at 11-20 K above their bulk PMMA *Tg*.) However, the PMMA sample used in this study had *Mn* = 509,000 g/mol and *Mw* = 850,000 g/mol. Thus, it is highly entangled and would be expected to exhibit a rubbery plateau response rather than a viscous flow response at temperatures in excess of *Tg* in the temperature schedule. Second, the height of the patterns employed in this study is typically much smaller than the 320 nm initial height associated with the patterns studied by Jones *et al.* (Jones 2006). They noted that the rate of pattern relaxation is accelerated at the shortest annealing times where the pattern height is at its maximum. Third, Jones *et al.* (Jones 2006) used nanoimprint lithography to make their patterns. The stresses involved in molding their high aspect ratio ($h/LW = 2.5$) patterns are very large, and the shape evolution is driven in part to relieve these stresses. Finally, the presence of a residual layer of PMMA under the patterns made by Jones *et al.* (Jones 2006) is also expected to play an important role in the rate of pattern relaxation because with "large residual layers, the layer acts as an infinite reservoir for the receding patterns."

Ensemble fluorescence is a powerful technique that has been used recently to measure *Tg* in confined polymer systems (Ellison 2002a, 2002b, 2003, 2004a, 2004b, 2005a; Priestley 2005a, 2005b; Rittigstein 2006, 2007). With this approach, *Tg* is identified by the intersection of the liquid-state and glassy-state temperature dependences of the fluorescence of a probe that is doped into or covalently attached to the polymer at trace levels. The measurements are made upon cooling from temperatures above *Tg*,

which means that the *Tg* measurement is made after erasing thermal history and relaxing some of the stresses induced during sample preparation (Mundra 2006). (With many of the nanopatterns, a second measurement of *Tg* is made immediately after the first measurement is done. If there is any residual organic-based developer left in the nanopatterns which could affect *Tg*, some or all of it would be removed during the first *Tg* measurement and reheating to perform the second *Tg* measurement. However, the measured *Tg*s are identical in the first and second measurements indicating that, within experimental uncertainty, there is no influence of exposure of the PMMA to the developer on the thermal response of the final, nanostructured films.) Figure 8-2a shows the fluorescence spectra of 18-nm-thick TC1-labeled PMMA nanolines with *LW* of 50 nm at two different temperatures. The probability of excited-state chromophores returning to the ground state via nonradiative decay increases with temperature and nanoscale mobility in the system, which results in a significant reduction in fluorescence intensity with increasing temperature. The TC1 chromophore is a "rotor" probe (Hooker 1995) that de-excites nonradiatively by rotational motion as depicted in the inset in Figure 8-2a; the inset shows the structure of the TC1-labeled monomer used to make TC1-labeled-PMMA.

Figure 8-2b shows the normalized integrated emission intensity as a function of temperature of the TC1-labeled PMMA in an 18-nm-thick film and an 18-nm-thick nanopattern with $LW = 50$ nm. Lines are fit to data points deep in the rubbery and glassy states. The *Tg* is identified by the intersection of the linear fits to the glassy-state and rubbery-state data (Ellison 2002a, 2002b, 2003, 2004a, 2004b, 2005a; Priestley 2005a, 2005b; Rittigstein 2006, 2007). The 18-nm-thick TC1-labeled PMMA film exhibits a *Tg* of 405 K, which is 10 K higher than the *Tg* of bulk TC1-labeled PMMA. (The bulk PMMA *Tg* of 395 K is depicted by the vertical dotted line in Figure 8-2b.) In contrast, a nanostructured, patterned geometry with the same 18 nm thickness and $LW = 50$ nm

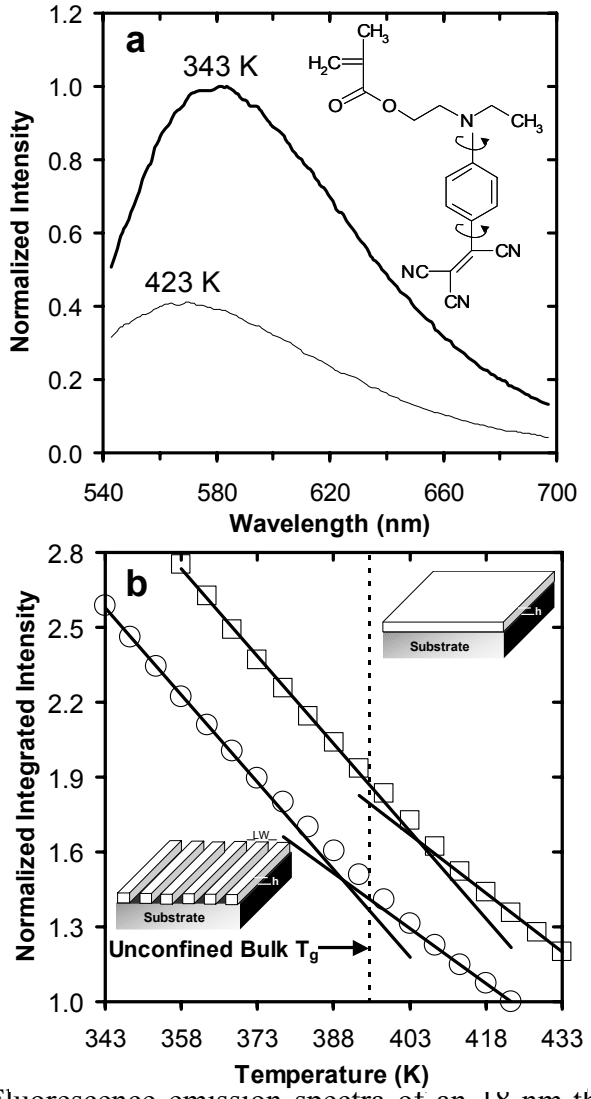

Figure 8-2: **(a)** Fluorescence emission spectra of an 18-nm-thick nanopattern of TC1-labeled PMMA with a line width of 50 nm measured at 423 K and 343 K. The intensities have been normalized by the peak intensity at 343 K. The inset shows the structure of TC1-labeled monomer used in making TC1-labeled PMMA. **(b)** Temperature dependence of integrated fluorescence intensity of TC1-labeled PMMA: 18-nm-thick film (□) and 18-nm-thick nanolines with LW = 50 nm (○). (The integrated intensity has been normalized to the peak intensity at 433 K and 423 K, respectively, and shifted vertically for clarity.) The intersection of vertical dotted line with x-axis represents the *Tg* of PMMA in bulk form. Inset shows sample geometries.

exhibits a *Tg* of 390 K, which is 5 K lower than the *Tg* of bulk TC1-labeled PMMA.

The 10 K increase in *Tg* relative to bulk of the 18-nm-thick TC1-labeled PMMA film is in excellent agreement with other results obtained regarding the effect of decreasing thickness on *Tg* in PMMA films supported on silica substrates (Keddie 1994a; Park 2004). This effect is understood to arise from attractive interfacial interactions resulting from hydrogen bond formation between hydroxyl groups naturally present on the silica surface and the ester side groups in PMMA (Priestley 2007a). The hydrogen bonds reduce cooperative segmental mobility and thereby lead to an increase in *Tg* in ultrathin films.

In contrast, the result showing the 5 K reduction in *Tg* relative to bulk in the 18-nm-thick PMMA nanolines with *LW* of 50 nm is the first of its kind. This effect may be understood to arise from the fact that the 18-nm-thick nanopatterned system has a much higher free-surface (polymer-air interface) area than the 18-nm-thick ultrathin film. In the case of the nanopatterned PMMA system, the ability of the free surface to yield a reduction in *Tg* (Ellison 2003) is in competition with the ability of the attractive interactions at the polymer-substrate interface to yield an increase in *Tg* (Priestley 2007a). Because of the much greater free-surface area relative to the polymer-substrate interfacial area, on balance the free-surface effects are dominant and lead to a reduced *Tg* in the nanopatterned geometry. This result illustrates the importance of confining geometry in defining the nature of *Tg* in confined systems.

To further validate the competing effects of free-surface area and PMMA-silica interfacial area on *Tg*, the *Tg* values of PMMA nanopatterns with various geometries are measured. Figure 8-3 summarizes the effects of film thickness and pattern geometry (*LW*) on the *Tg* of TC1-labeled PMMA films and nanopatterns. Consistent with previously published data on PMMA ultrathin films (Keddie 1994a; Park 2004; Mundra 2007a, 2007b; Fryer 2001), at thicknesses less than 80 - 90 nm, the *Tg*s of the PMMA

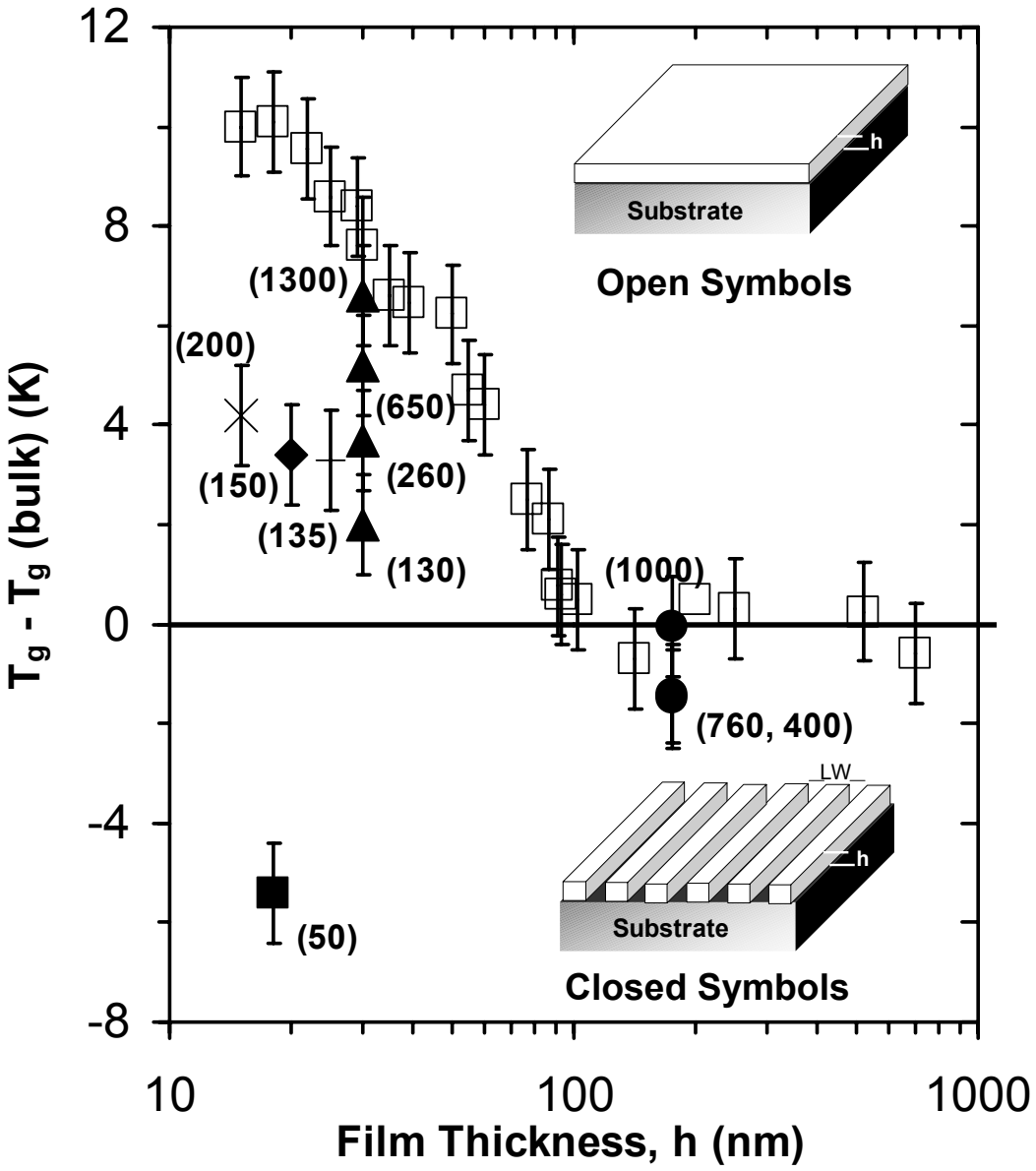

Figure 8-3: *Tg* – *Tg*(bulk) as a function of film thickness for TC1-labeled PMMA films (□) and nanolines with thickness of 175 nm (●), 30 nm (▲), 25 nm (+), 20 nm (♦), 18 nm (■), and 15 nm (×), respectively. The numbers in parentheses specify the line widths (*LW*). The error bars correspond to the error (± 1 K) in estimating *Tg* values by the intersection of linear temperature dependences of integrated intensity in the rubbery and glassy states. The insets show schematics of sample geometries employed for *Tg* characterization.

films increase with decreasing thickness, with an 18-nm-thick film exhibiting a 10 K increase relative to the bulk *Tg*. In the case of our patterned lines made by EBL, when *h* is 175 nm and *LW* values are 400 nm, 760 nm or 1000 nm, the *Tg*s are nearly identical to bulk *Tg*. (Values of *LW* are shown in parentheses in Figure 8-3.) In these cases, the added free-surface area in the patterned lines is insufficient to perturb the value of *Tg* from that of the 175-nm-thick film from which they are made. In contrast, significant perturbations to *Tg* are observed in 30-nm-thick nanolines with *LW* = 130 nm, with a 5 K difference in *Tg* being apparent in systems with *LW* values of 130 nm and 1300 nm. The reduction in *Tg* with decreasing *LW* is because of the increasing effects of the free surface that compete with the effects of attractive polymer-substrate interactions.

Striking effects are observed in the 15-nm-thick and 18-nm-thick patterned lines. In a 15-nm-thick pattern with *LW* = 200 nm, *Tg* is increased by ~4 K relative to bulk *Tg* and is reduced by ~6 K relative to the *Tg* of a 15-nm-thick PMMA film. These results are indicative of the competition between free-surface and polymer-substrate effects, with the polymer-substrate effect dominating the free-surface effects in the patterned system. On the other hand, in an 18-nm-thick nanopattern with *LW* = 50 nm, *Tg* is reduced by ~5 K relative to bulk *Tg* (*Tg*(bulk)) and by ~15 K relative to the *Tg* of an 18-nm-thick PMMA film. In this case, the effects of the free surface present on three sides of the nanolines dominate over the effect of attractive polymer-substrate interactions present on the fourth side of the nanolines.

We note that these results can be rationalized based on measurements by Roth and Dutcher (Roth 2003) of the thickness dependence of *Tg* of freely standing PMMA films, with two free surfaces and no substrate. Using a nearly monodisperse PMMA sample with *Mw* = 790,000 g/mol, close to the *Mw* value of 850,000 g/mol for our TC1-labeled PMMA, they observed a reduction in *Tg* of ~15 K relative that of bulk PMMA in a 50-nm-thick freely standing PMMA film. The 18-nm-thick nanopattern with *LW* = 50 nm

exhibits $Tg = Tg(\text{bulk}) - 5$ K, i.e., 10 K above that of the 50-nm-thick freely standing PMMA film. The increase in the nanopattern *Tg* relative to that of the freely standing films arises from the attractive substrate interactions that are present in the nanopattern and absent in the freely standing film.

To represent more simply the effect of the ratio of free-surface area to PMMA-silica interfacial area in modifying the *Tg* of the nanopatterns relative to the thin or ultrathin films from which they were made, the data in Figure 8-3 are re-plotted in Figure 8-4. The latter figure emphasizes the variations in *Tg* of the 1D-patterned nanostructures with various *LW*s compared to the thin films having the same thickness.

These results demonstrate that the knowledge of how confinement modifies *Tg* in supported polymer films (2-D case) cannot be simply extended without modification to predict the *Tg* behavior of polymer 1-D nanopatterns supported on a substrate. This is because the properties of the patterned polymer 1-D nanostructures are influenced by the combined effects of the free surfaces and the attractive substrate interactions. This means that the detailed geometry must be considered in any experimental studies or simulations of the thermal properties of such nanostructures. Furthermore, given that the strength of the attractive polymer-substrate interactions can be tuned by modification of the substrate surface (Fryer 2001) and polymer or copolymer composition (Mundra 2006; Park 2004), the magnitude of the interaction must be carefully accounted for in any simulation of nanostructure physical or mechanical properties. The experimental *Tg* results from this study are also in qualitative agreement with a recent simulation study (Van Workum 2003) of apparent modulus of polymer nanostructures, which reported that the elastic constants show a significant reduction from bulk behavior with decreasing line width and that the surface-to-volume ratio is a key parameter in defining the nanostructure properties.

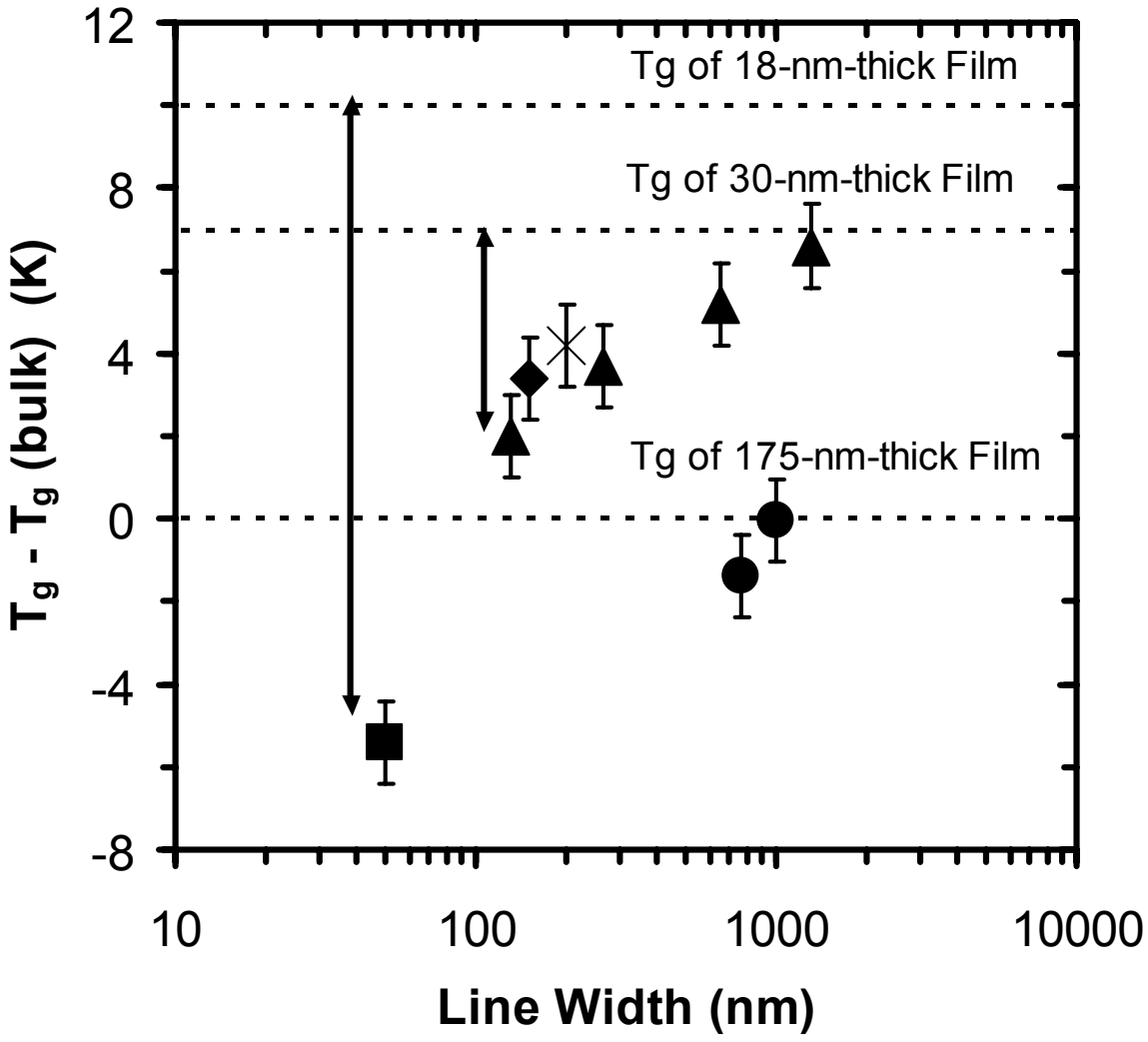

Figure 8-4: *Tg*(nanopattern) – *Tg*(bulk) as a function of line width for nanolines of various thickness: 175 nm (●), 30 nm (▲), 25 nm (+), 20 nm (♦), 18 nm (■), and 15 nm (×). The horizontal dotted lines show the values of *Tg* for the corresponding thin films of particular thicknesses relative to that of bulk PMMA. The error bars correspond to the error (± 1 K) in estimating *Tg*.

8.4 Conclusions

This is the first study of the determination of *Tg* as a function of confinement in 1-D polymer nanostructures. With PMMA nanolines supported on silica, the important roles of the ratio of free-surface area to polymer-substrate interface area and the attractive polymer-substrate interactions in defining the nanostructure *Tg* are demonstrated. Attractive polymer-substrate interactions results in a substantial increase of *Tg* with decreasing thickness in ultrathin PMMA films. However, when such attractive polymer-substrate interactions are present in nanopatterned polymers, an increase in the ratio of free-surface area to the polymer-substrate interfacial area can substantially reduce the *Tg* of 1-D nanostructures supported on a substrate, even to temperatures below the *Tg* of the bulk polymer, thereby "tuning" the *Tg*-nanoconfinement effect.

CHAPTER 9

STRENGTH OF GLASS TRANSITION TEMPERATURE (Tg) IN POLYMER THIN AND ULTRATHIN FILMS: IMPACT OF MOLECULAR WEIGHT (MW) AND SLIGHT MODIFICAITION TO THE REPEAT UNIT STRUCTURE

9.1 Introduction

In addition to the attention focused on *Tg*-nanoconfinement effects, the accompanying changes in thermal expansivity upon nanoconfinement are of particular interest due to the potential to advance the understanding of nanoconfinement effects in general and the possibility to further shed light on the origin of the *Tg*-nanoconfinement effects. In previous fluorescence studies of *Tg*-nanoconfinement effects (Ellison 2002a, 2002b), it was proposed that the temperature dependence of fluorescence emission spectra was due to changes in sample density surrounding the chromophore which reduce the non-radiative decay rate of the excited state (Ellison 2005c) resulting in a higher fluorescence intensity at lower temperatures. It is under this explanation that the temperature dependence of integrated intensity and the thermal expansivity measured by ellipsometry, X-ray reflectivity, etc. are directly related and would follow similar trends.

This chapter details the first study of the impact of polystyrene (PS) molecular weight (*MW*) and slight modification to the PS repeat unit structure on the strength of *Tg* in thin and ultrathin films. (The strength of *Tg* is defined as the rubbery state temperature dependence of integrated intensity (*Sr*) minus the glassy state temperature dependence of the integrated intensity (*Sg*) divided again by that of the rubbery state, *Sr*.) Such an investigation is important, as it may reveal why there is a reduced strength of *Tg* in thinner films and aid in understanding the origin of the tunability of the *Tg*-nanoconfinement effect.

9.2 Experimental

Polystyrene standard (*Mn* = 200,000 g/mol, *Mw*/*Mn* = 1.08, *Tg*,bulk by DSC = 373 K, and *Tg*,bulk by fluorescence = 373 K) was purchased from Pressure Chemical Co. and used as received. Samples of PS films with *Mn* = 5,000 g/mol (*Tg*,bulk by DSC = 358 K, and *Tg*,bulk by fluorescence = 358 K) were prepared by co-dissolving a high *MW* PS standard (*Mn* = 200,000 g/mol, *Mw*/*Mn* = 1.08) with a low *MW* PS standard (*Mn* = 1,850 g/mol, *Mw*/*Mn* = 1.14) in toluene (99.9% purity) prior to film preparation. Poly(4-methylstyrene) (P4MS) (*Mn* = 279,000 g/mol, *Mw*/*Mn* = 1.57, *Tg*,bulk by DSC = 376 K, and *Tg*,bulk by fluorescence = 376 K) was from Scientific Polymer Products and used as received. Poly(4-tert-butylstyrene) (PTBS) (*Mn* = 32,000 g/mol, *Mw*/*Mn* = 3.31, *Tg*,bulk by DSC = 404 K, and *Tg*,bulk by fluorescence = 404 K) was from Aldrich. Due to the presence of 4-tert-butylstyrene monomer in the as-received polymer, the PTBS sample was dissolved in toluene (99.9% purity) and precipitated seven times in methanol (99.9% purity) to ensure monomer removal prior to use. The *Tg*,bulk values were measured as *Tg*,onset values by differential scanning calorimetry (DSC) (Mettler Toledo DSC822) on second heat at 10 K/min. Polymer *MW* was determined by gel permeation chromatography (GPC) (Waters) relative to a PS calibration. Pyrene (Aldrich Chemical, 99+% purity) and 1,10-bis(1-pyrene)decane (BPD) (Aldrich, 99%) were used as received.

Thin films were prepared by spin coating (Hall 1998a) dilute solutions of polymer in toluene onto glass slides. The glass slides (VG9 ionically doped float glass filters (Schott Glass© 2007), 2”x2” 2mm thick) were initially washed with a 10% sodium hydroxide/70% ethanol/20% water solution upon receipt and then solvent washed between experiments. Film thickness was measured with a Tencor P10 profilometer. Calibration of the profilometer is verified using a 14-nm-step-height standard (VLSI standards). At least ten measurements were taken in total at different locations close to the center of the film (where fluorescence was measured) and averaged with the typical

standard deviation in these measurements being less than 1.5 nm for films thicker than ~ 20 nm and ~ 1.0 nm for films thinner than ~ 20 nm.

A Spex Fluorolog-2DM1B fluorimeter was used for steady-state fluorescence measurements. Measurements employed a front-faced geometry with 2.5 mm excitation and emission slits (bandpass = 4.5 nm) for films with thickness less than 100 nm and 1.25 mm excitation and emission slits (bandpass = 2.25 nm) for films with thickness greater than 100 nm. In the worst case, the signal-to-noise ratio exceeded 30. The probe (pyrene or BPD) content in each film was less than 0.2 wt% of dry polymer content. (At probe concentrations less than 0.2 wt%, the *Tg* of pyrene-doped polymer was the same within error as that of neat polymer, a circumstance that also holds for BPD.) A clean quartz cover slide was placed on top of each film to reduce the potential for probe sublimation during the *Tg* measurement by fluorescence. (The film was adhered only to the glass substrate on which it was spin coated.) Film temperature was controlled by a microprocessor controller (Minco Products) with a Kapton ribbon heater attached to a flat aluminum plate that was also used as a clamping device to hold the sample. The excitation wavelength was 322 nm for all samples, and the emission spectrum was measured at 350 - 450 nm. Fluorescence spectra were recorded upon cooling after having annealed samples at ~ *Tg* + 40 K for 15 min. In the case of PS with *Mn* = 5,000 g/mol dewetting problems were reduced or eliminated by annealing for 15 min at ~ *Tg* + 35 K.

In fitting the temperature dependence of fluorescence in the rubbery and glassy states, only data points well outside *Tg* were used for the linear fits, and typical correlation coefficients (R^2) were better than 0.990. To initiate the fitting procedure, data points were added to the rubbery- and glassy-state linear regressions one-by-one at the extrema in the temperature range of the data. The correlation coefficient was monitored as more data points were added (approaching *Tg* from the extrema in the temperature

range of the data) to each of the linear regressions. If the R^2 value began to steadily decrease below a threshold value (i.e., < 0.990) as more data points were added, then these data points were removed to produce a value of R^2 higher than the threshold value and the linear regressions were considered acceptable. The linear fits in both the rubbery and glassy states included a minimum of four fluorescence data points (usually more), spanning a minimum of 15 K in temperature. Spectra were taken over a sufficient range of wavelengths that integration could be done from instrument baseline at the lowest wavelengths to the same instrument baseline at the highest wavelengths. In all cases, the sample was reheated to the starting temperature following the measurements taken upon cooling to verify that the sample did not lose a substantial amount of fluorescence probe molecules due to photobleaching, sublimation, etc. Typically, the intensity after reheating the sample was within 10% of the original intensity before the measurements were taken upon cooling.

9.3 Impact of Molecular Weight and Repeat Unit Structure on the Strength of Tg in Thin and Ultrathin Films

Figure 9-1a shows the temperature dependence of integrated intensity for PS with *Mn* = 5,000 g/mol at two thicknesses (500 nm and 29 nm, *Tg* = 356 K and 344 K, respectively). Similarly, Figure 9-1b shows a higher *MW* PS with *Mn* = 200,000 g/mol at two thicknesses (24 nm and 810 nm, *Tg* = 358 K and 373 K, respectively). In accord with earlier fluorescence studies (Ellison 2002a, 2002b, 2003, 2004a, 2005a) of the *Tg*-nanoconfinement effect as well as other studies (Kawana 2001), these figures demonstrate a weakening in the strength of *Tg* in highly nanoconfined PS films.

Figure 9-2 shows the temperature dependence of the integrated intensity for pyrene-doped P4MS at two thicknesses. Similar to the PS case (Figure 9-1), P4MS shows a reduced strength in *Tg* in highly confined films. The 24-nm-thick and 810-nm-thick P4MS films display *Tg*s of ~ 355 and 376 K, respectively.

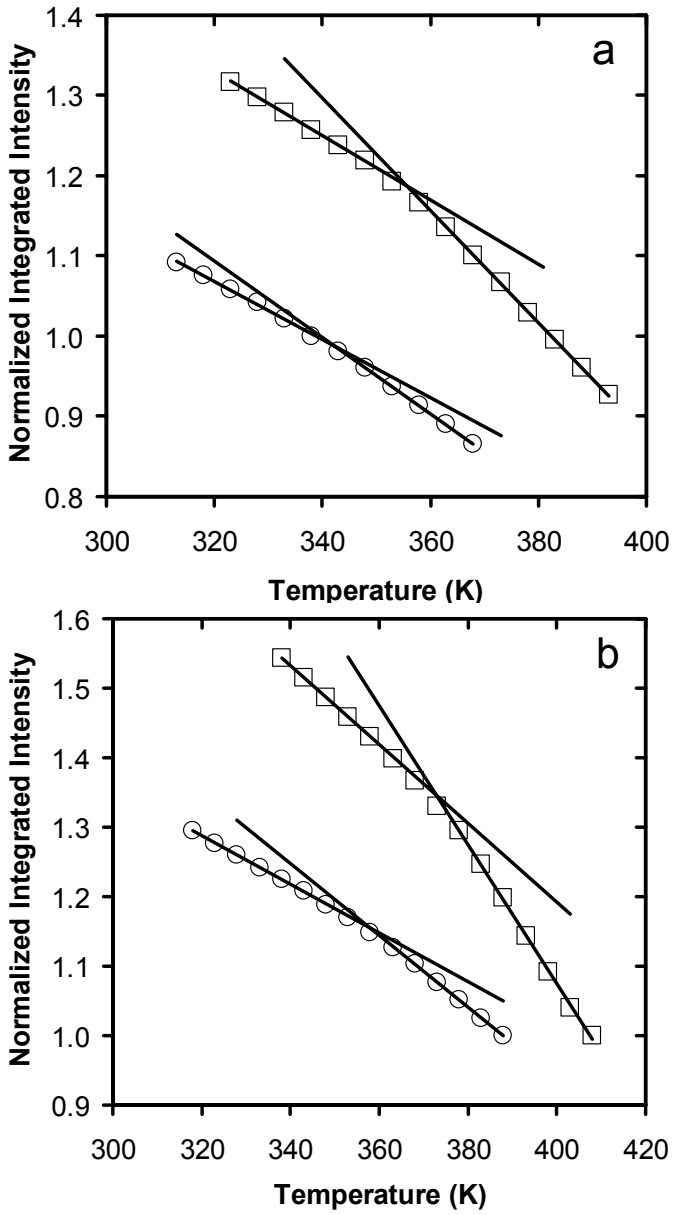

Figure 9-1: **(a)** Temperature dependence of the integrated intensity of pyrene dopant in 500-nm (□) and 29-nm (○) thick PS (*Mn* = 5,000 g/mol, *Tg*,bulk = 358 K) films (the integrated intensity has been normalized to one at 378 K and 338 K, respectively, and arbitrarily shifted). **(b)** Temperature dependence of the integrated intensity of pyrene dopant in 810-nm (□) and 24-nm (○) thick PS (*Mn* = 200,000 g/mol, *Tg*,bulk = 373 K) films (the integrated intensity has been normalized to one at 408 K and 388 K, respectively, and arbitrarily shifted).

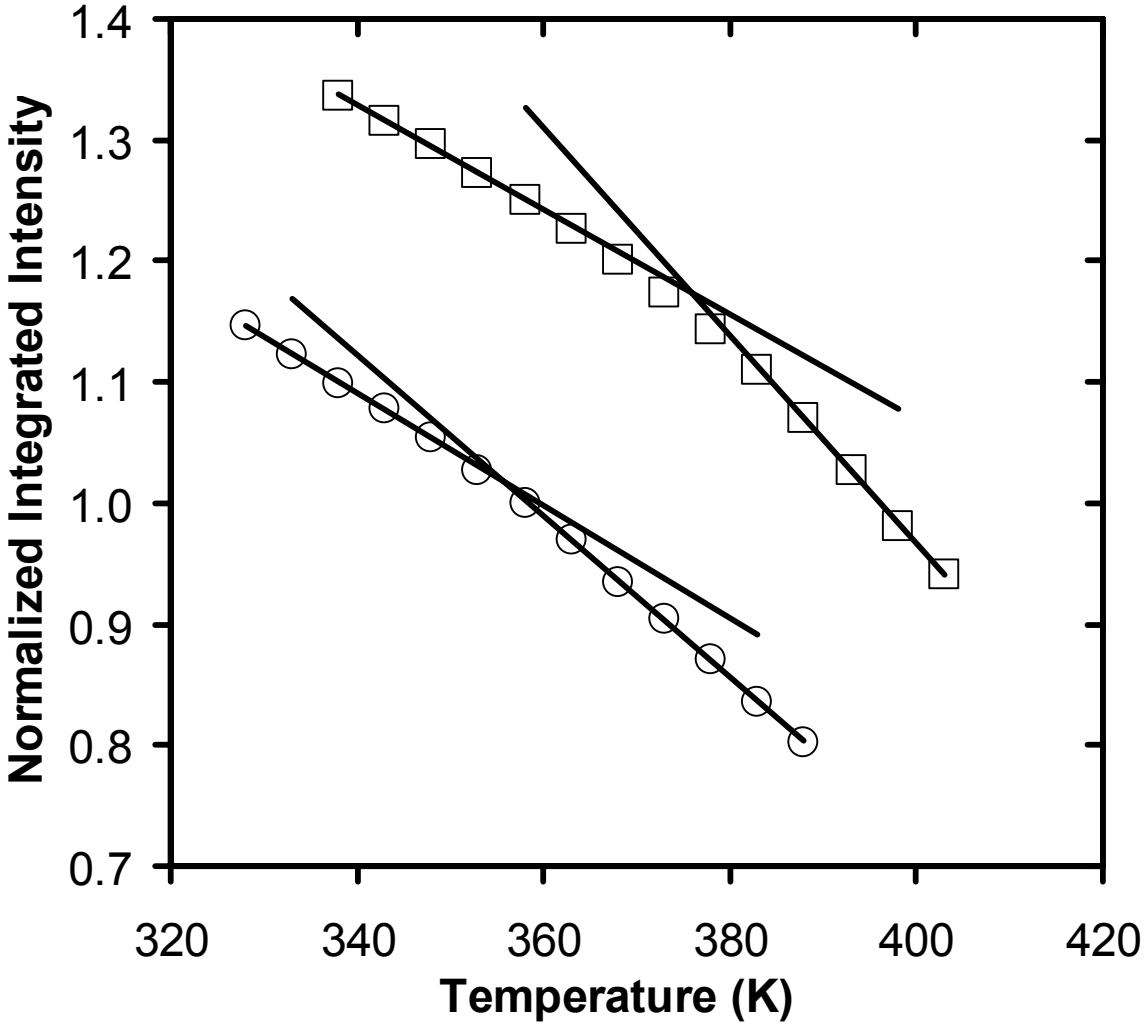

Figure 9-2: Temperature dependence of the integrated intensity of pyrene dopant in 810-nm-thick (□) and 24-nm-thick (○) P4MS films (*Tg*,bulk = 376 K) films. (The integrated intensity has been normalized to one at 368 K and 358 K, respectively, and arbitrarily shifted.)

Fluorescence is also used to measure the strength of *Tg* in PTBS, which differs from the repeat unit structure of PS by the addition of a tert-butyl group to the 4-carbon on the phenyl ring. The addition of the tert-butyl group reduces the bulk density of the polymer by 10% compared to PS (from 1.04 to 0.94 g/cm^3) (Ellison 2005a) and increases bulk *Tg* from ~ 373 to 404 K. In contrast, the densities and *Tg* values of P4MS and PS are nearly identical. This decreased density in PTBS may be attributed to significantly hindered packing of the repeat units of PTBS relative to PS which results in an increased free volume. Likely associated with these differences, it is observed that pyrene dopant is particularly susceptible to sublimation from PTBS films during annealing of the film above *Tg*. To avoid sublimation issues, BPD, shown as the inset in Figure 9-3a, is chosen as a fluorescence dopant as it has a diffusion coefficient in polymers near *Tg* that is several orders of magnitude lower than that of pyrene (Deppe 1996b). Various tests in PTBS indicated that BPD exhibits relatively little sublimation in the temperature range of interest.

Figure 9-3a shows the temperature dependence of the fluorescence emission spectra for BPD doped at trace levels (< 0.2 wt %) into an 1190-nm-thick PTBS film. The BPD dopant spectral shape is roughly similar to that of pyrene dopant in PS, with emission peaks at ~ 378, 398, and 418 nm. Figure 9-3b shows the temperature dependence of the integrated intensities for two BPD-doped PTBS films; the 1190-nm-thick film exhibits a *Tg* value of 404 K, equal to *Tg*,bulk, while the 30-nm-thick film exhibits a *Tg* of 368 K. The 30-nm-thick PTBS film also shows a reduction in the strength of *Tg* compared to the 1190-nm-thick film, qualitatively consistent with that shown for PS in Figures 9-1 and P4MS shown in Figure 9-2.

Figure 9-4 shows the strength of *Tg* for PS *MW*s of 5000 g/mol and 200,000 g/mol as a function of film thickness. The strength of *Tg* is defined as follows:

$$\text{Strength of } Tg = (Sr - Sg)/Sr \times 100 \qquad 9.1$$

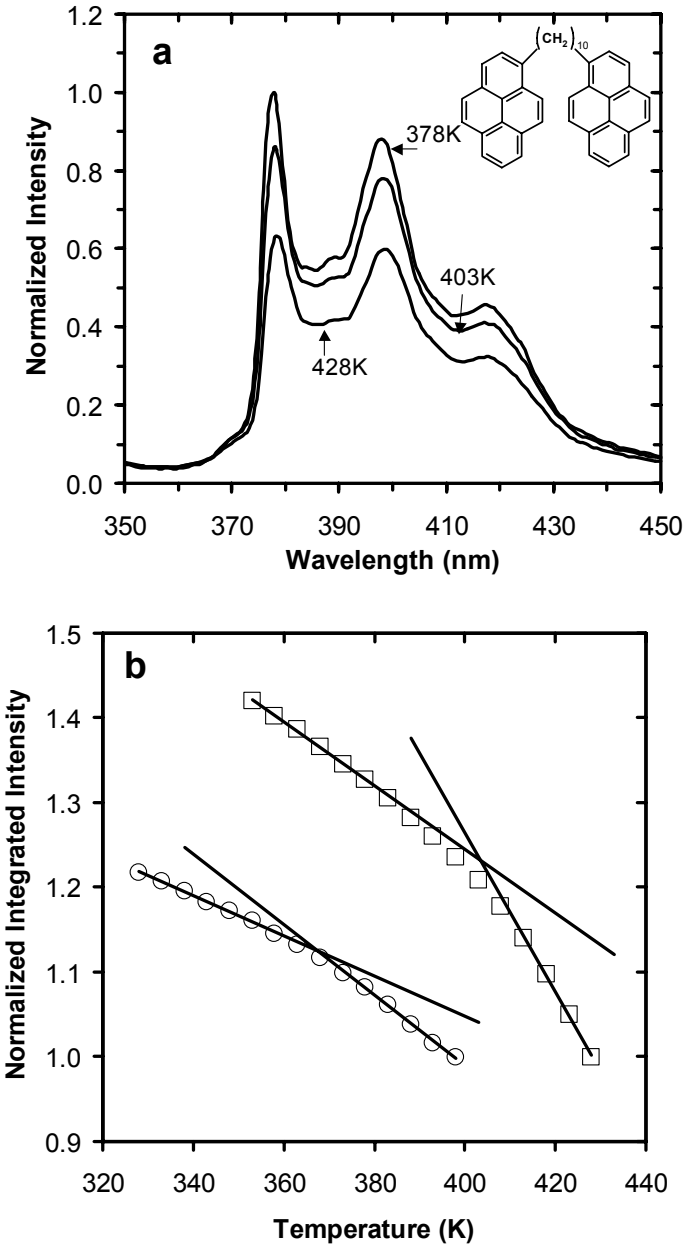

Figure 9-3: (a) Fluorescence emission spectra of BPD dopant in a 1190-nm-thick PTBS film taken at 378 K, 403 K and 428 K. The inset shows the structure of BPD. **(b)** Temperature dependence of the integrated intensity of BPD dopant in 1190-nm-thick (□) and 30-nm-thick (○) PTBS (*Tg*,bulk = 404 K) films. (The integrated intensity has been normalized to one at 428 K and 398 K, respectively, and arbitrarily shifted).

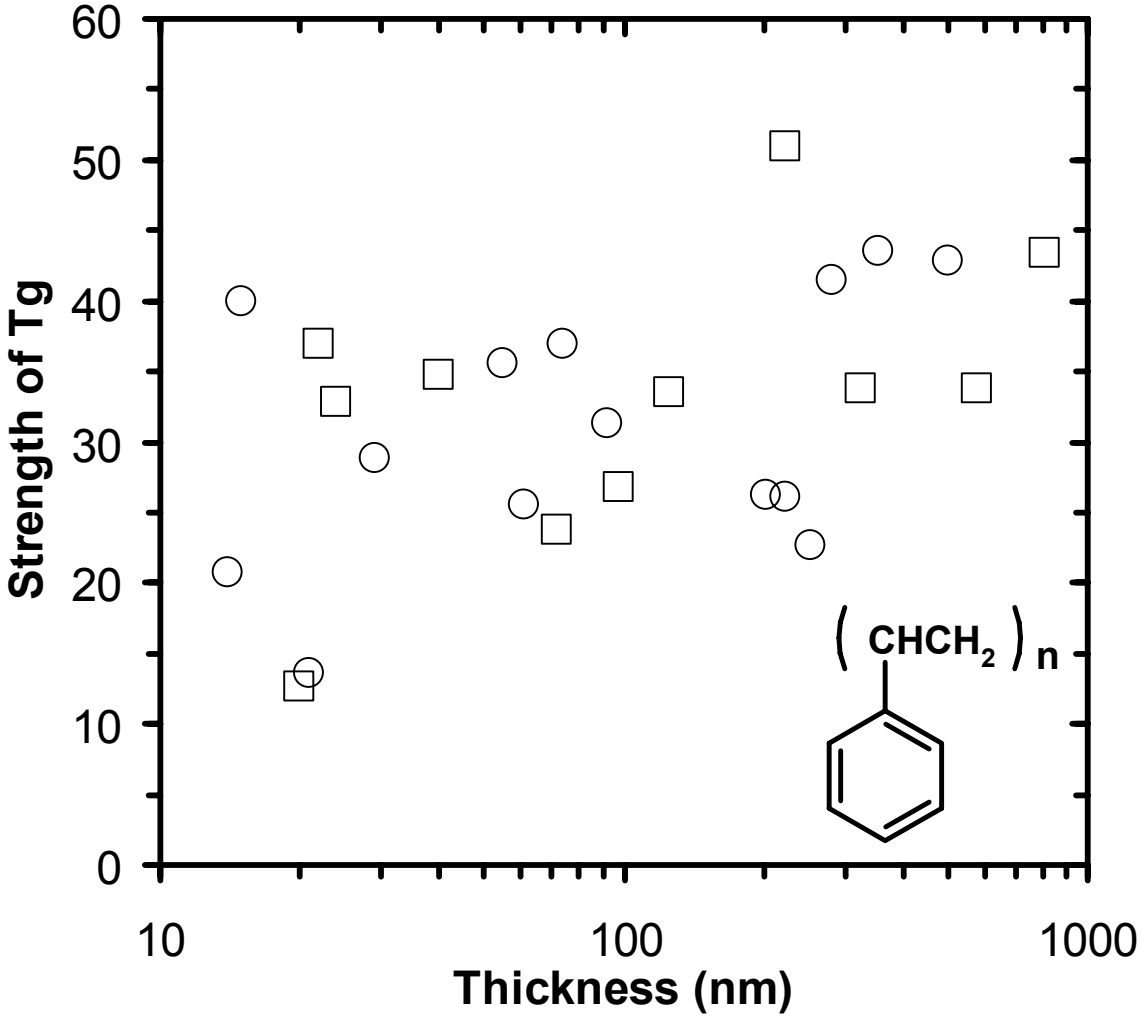

Figure 9-4: Plot showing the strength of *Tg* as a function of film thickness for PS films of molecular weights, *Mn* = 5000 g/mol (○) and *Mn* = 200,000 g/mol (□), respectively. The inset shows the structure of the PS repeat unit. (The strength of *Tg* is defined as the rubbery state temperature dependence of integrated intensity (*Sr*) minus the glassy state temperature dependence of the integrated intensity (*Sg*) divided again by that of the rubbery state, *Sr*.)

where *Sr* is the rubbery state temperature dependence of integrated intensity and *Sg* is the glassy state temperature dependence of the integrated intensity.

Prior to extracting the *Sg* and *Sr* values, the integrated intensities were normalized to unity at *Tg* for all film thicknesses. (According to this definition of the strength of *Tg*, as the strength approaches zero the *Tg* becomes progressively more difficult to identify as the value of *Sg* and *Sr* approaches each other.). In figure 9-4, the strength of *Tg* decreases with decreasing logarithmic film thickness in a nearly identical manner for both PS *MW*s. Interestingly there appears to be no correlation between the film thickness dependence of *Tg* (refer to Figure 4-4, Chapter 4) and the film thickness dependence of the strength of *Tg*. In addition, the strength of *Tg* is approximately 15 % higher for *Tg*s identified with BPD as compared to pyrene. Previously, Ellison *et al.* (Ellison 2004a) have observed in other cases that the overall flexibility and number or type of excited state decay mechanisms may contribute to a differing strength of *Tg* in the same polymer.

In a similar manner as that for PS, Figure 9-5 shows that the strength of *Tg* for P4MS and PTBS decreases with decreasing film thickness. However, in contrast to PS, P4MS and PTBS exhibit a greater strength of *Tg* for films thicker than 40 nm and undergo larger overall decreases with decreasing film thickness. Figure 9-5 suggests that for film thicknesses exceeding 30 nm, the strength of *Tg* is greater for PTBS than for P4MS, but this can be attributed to the use of the BPD probe for PTBS. Similar to the PS case, there appears to be no correlation between the thickness dependence of *Tg* and the thickness dependence of the strength of *Tg* for P4MS or PTBS (refer to Chapter 7, Section 7.2.3). In a separate study using fluorescence, Ellison *et al.* (Ellison 2004a), investigating the tunability of the *Tg*-nanoconfinement effect by the addition of low *MW* diluents, have shown that the addition of sufficient levels of diluents results in a thickness-independent *Tg* and a strength of *Tg* that is invariant in films as thin as 10 nm.

However, examination of *Sg* and *Sr* individually is more revealing of the

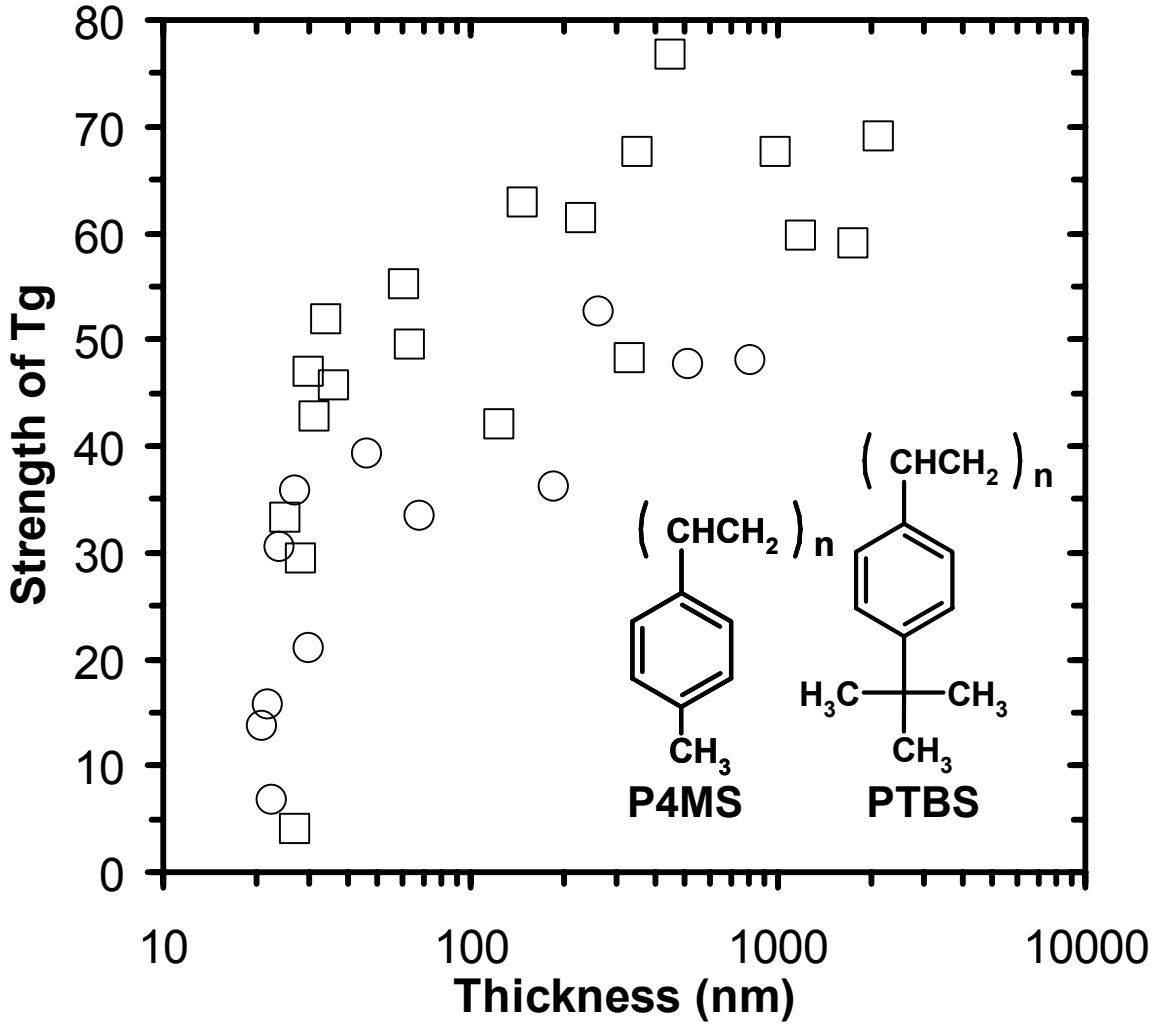

Figure 9-5: Plot showing the strength of *Tg* as a function of film thickness for P4MS (○) and PTBS (□) films, respectively. The inset shows the structure of the P4MS and PTBS repeat units. (The strength of *Tg* is defined as the rubbery state temperature dependence of integrated intensity (*Sr*) minus the glassy state temperature dependence of the integrated intensity (*Sg*) divided again by that of the rubbery state, *Sr*.)

underlying nature of the strength of *Tg*. Figures 9-6a and 9-6b show the thickness dependence of *Sg* and *Sr* for 5000 g/mol and 200,000 g/mol PS, respectively. It is observed that both *Sg* and *Sr* increase approximately with decreasing film thickness. However, *Sr* undergoes much larger increase (to smaller negative values) than *Sg* as film thickness decreases indicating that the reduced strength of *Tg* in thinner PS films appears to be a result of *Sr*, which approaches *Sg*. Figures 9-7a and 9-7b show similar effects for P4MS and PTBS, respectively. While these results have revealed why there is a reduced strength of *Tg* in thinner films, they have provided no information regarding the origin of the tunability of *Tg*-nanoconfinement effect.

The observation of a reduced strength in *Tg* (sometimes called a reduced contrast in *Tg*) as film thickness decreases has been reported for both supported (Keddie 1994b; Kawana 2001; DeMaggio 1997; Forrest 2001; Singh 2004; Miyazaki 2004; Ellison 2002a, 2002b, 2005a) and unsupported or freely standing (Forrest 1998; Vigil 1997) films. This study has shown that *Sg* may increase slightly or change relatively little while *Sr* increases much more substantially and approaches *Sg* as film thickness is decreased. These results are in qualitative agreement with many studies (Kawana 2001; DeMaggio 1997; Forrest 2001; Miyazaki 2004; Forrest 1998; Vigil 1997) of thermal expansion coefficients in the rubbery and glassy states. However, these results are in disagreement with those of Keddie *et al.* (Keddie 1994b), who observed an increasing glassy state thermal expansivity with decreasing film thickness and a constant rubbery state thermal expansion coefficient, and those of Singh *et al.* (Singh 2004), who observed an increasing glassy and rubbery state thermal expansion coefficient with decreasing film thickness. At this point it is unclear as to what factors might contribute to these differences. However, it is noteworthy that Singh *et al.* (Singh 2004) have measured *Tg* upon heating from the glassy state which may have lead to unrelaxed internal stresses caused by film preparation methods such as spin coating (McKenna 2000; Bernazzani 2002). These

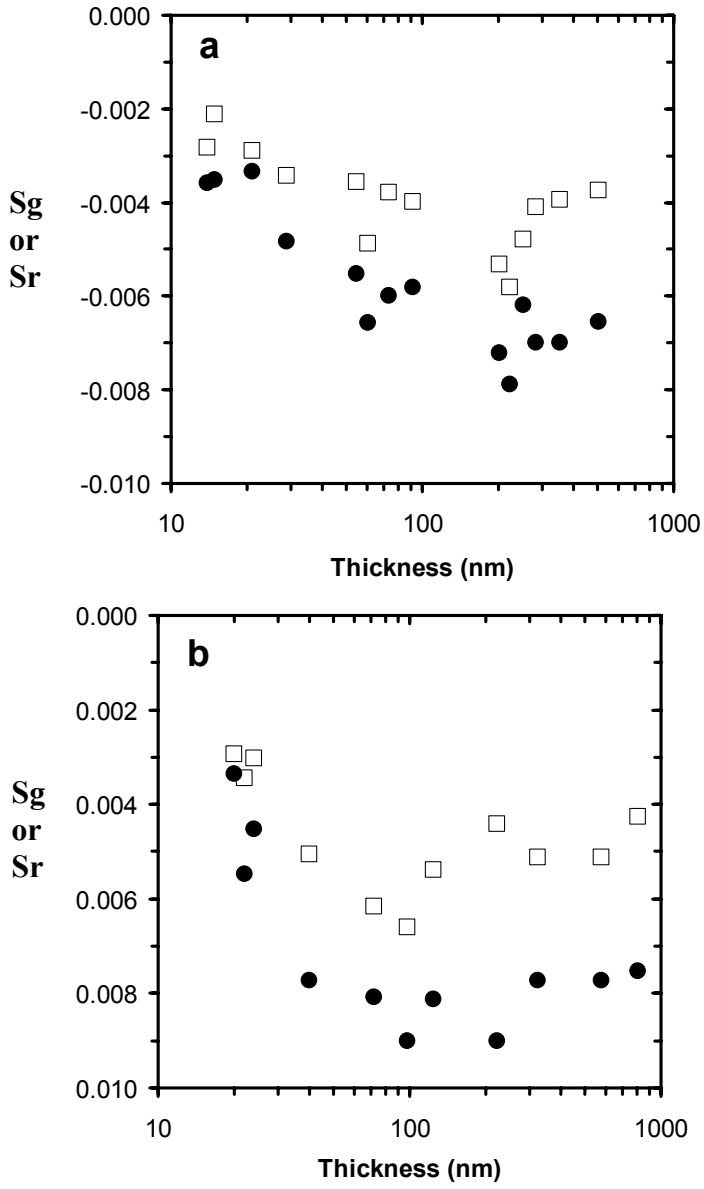

Figure 9-6: **(a)** Temperature dependence of integrated intensity for the glassy state (*Sg*) (□) and the rubbery state (*Sr*) (●) as a function of film thickness in PS sample (*Mn* = 5000 g/mol). **(b)** Temperature dependence of integrated intensity for the glassy state (*Sg*) (□) and the rubbery state (*Sr*) (●) as a function of film thickness in PS sample (*Mn* = 200,000 g/mol).

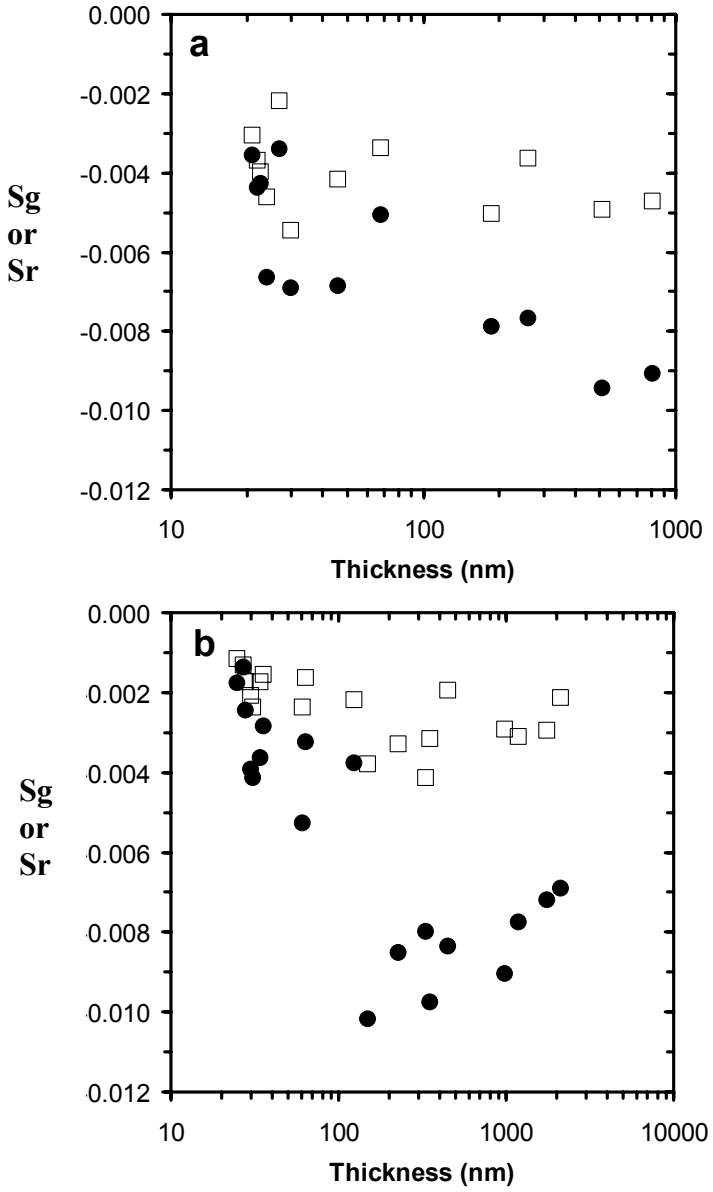

Figure 9-7: (a) Temperature dependence of integrated intensity for the glassy state (*Sg*) (□) and the rubbery state (*Sr*) (●) as a function of film thickness in P4MS sample. **(b)** Temperature dependence of integrated intensity for the glassy state (*Sg*) (□) and the rubbery state (*Sr*) (●) as a function of film thickness in PTBS sample.

internal stresses may impact polymer dynamics (Mundra 2006), which in turn may potentially impact the thermal expansion coefficient values as the internal stresses relax during the measurement.

9.4 Conclusions

This study explored in detail the strength of *Tg* (related to the difference in the rubbery and glassy state measurables defining *Tg*) as a function of PS *MW* and with slight modification to the PS repeat unit structure in thin and ultrathin films. For both PS *MW*s, the strength of *Tg* is decreased with decreasing logarithmic film thickness in a nearly identical manner. No correlation between the film thickness dependence of *Tg* (refer to Figure 4-4, Chapter 4) and the film thickness dependence of the strength of *Tg* is observed. Similar to the PS case, no correlation between the thickness dependence of *Tg* and the thickness dependence of the strength of *Tg* for P4MS or PTBS (refer to Chapter 7, Section 7.2.3) is observed. However, examination of *Sg* and *Sr* individually revealed that both *Sg* and *Sr* generally (becomes less negative in value) increase with decreasing film thickness for PS films. However, *Sr* undergoes much larger increase (to smaller negative values) than *Sg* as film thickness decreases indicating that the reduced strength of *Tg* in thinner PS films appears to be a result of *Sr*, which approaches *Sg*. Similar effects for P4MS and PTBS are also seen.

CHAPTER 10

DRAMATIC REDUCTION OF DYE DIFFUSION IN THIN POLYMER FILMS: EFFECTS OF CONFINEMENT NEAR THE NANOSCALE STUDIED BY A NOVEL FLUORESCENCE METHOD

10.1 Introduction

Besides *Tg*, other key polymer properties are affected by confinement. These include polymer chain diffusion (Frank 1996a; Pu 2001a, 2001b; Zheng 1997; Kuhlmann 1998; Kawaguchi 2003), probe diffusion (Hall 1998b), dewetting behavior (Reiter 1992, 1993, 2001a, 2001b, 2005), viscosity (Masson 2002), and hole growth (Dalnoki-Veress 1999; Masson 2002).

In spite of the efforts by various groups, the understanding of mobility associated with diffusion in confined geometry is very limited. The techniques used for diffusion studies in confined systems are often experimentally demanding. Also, results from the relatively few quantitative studies to date indicate an increase in, decrease in, or invariance of mobility related to diffusion with nanoconfinement, making it difficult to draw meaningful conclusions. A concise review of the work associated with diffusion in confined polymeric systems is provided below.

Reiter (Reiter 1993) provided the first direct evidence of enhanced mobility in thin polymer films by optical microscopy studies of dewetting at temperatures below the bulk *Tg*. Films with thicknesses less than 100 nm were seen to dewet at temperatures even below bulk *Tg*. Using a fluorescence recovery after patterned photobleaching (FRAPP) technique, Frank *et al.* (Frank 1996a) found that the in-plane diffusion of PS labeled with a fluorescent dye decreased with decreasing film thickness below 150 nm. For example, the PS diffusion coefficient for a 60-nm-thick film was reduced by a factor of 2 as compared to the bulk value. They correlated the film thickness at which the onset

of this behavior was first seen with the extended end-to-end length of the polymer chain; however, they did no study as a function of PS *MW*. In another study (Tseng 2000b) of in-plane diffusion of rubrene dye molecules in PS thin films, an enhancement in diffusion was seen with reduction in film thickness. The onset of this increase was seen at thickness close to 100 nm, and an increase of the diffusion coefficient by two orders of magnitude was reported. Fluorescence nonradiative energy transfer (NRET) or fluorescence resonance energy transfer (FRET) studies by Hall *et al.* (Hall 1997b, 1998b) showed a small decrease in the out-of-plane dye diffusion in PS for films less than 150 nm. In contrast, no change in probe diffusion was found in poly(isobutyl methacrylate) (PiBMA) and poly(2-vinyl pyridine) (P2VP) films down to thicknesses of 50 nm and 88 nm, respectively. A detailed analysis of the fluorescence NRET technique and impact of probe size, shapes, and interactions on diffusion coefficient can be found in references from the Torkelson research group (Hall 1997b, 1997c, 1998c, 1999; Dhinojwala 1994a; Deppe 1996a).

Rafailovich and coworkers (Zheng 1997; Pu 2001a) used dynamic secondary ion mass spectroscopy (SIMS) to measure the out-of-plane diffusion of deuterated PS (dPS) in a matrix of PS showed a decrease in the diffusion coefficient with reduction in thickness. The thickness at which the onset of the confinement effect was seen was correlated to the radius of gyration of the polymers. In another study from the same group (Pu 2001b), no change was seen in the out-of-plane diffusion coefficient of a small-molecule probe in a freely standing PS film. They used the WLF equation to describe the temperature dependence of diffusion and "back calculated" the *Tg* values, concluding that there was no change in *Tg* down to a thickness of 33 nm. This is in disagreement with direct study of *Tg* for freely standing films from many other studies (Forrest 1996, 1997, 1998; Dalnoki-Veress 2001; Mattsson 2000; Miyazaki 2007). In bilayer experiments on PS/dPS using neutron reflectivity experiments, Kuhlmann *et al.*

(Kuhlmann 1998) showed that out-of-plane diffusion coefficient in thin PS films was unchanged, except for a slight decrease when the bilayer interface was placed near the substrate. In a different study using neutron reflectivity and dynamic SIMS on a similar system (Kawaguchi 2003), enhanced mobility at the interface of a bilayer of PS/dPS was seen. Lin *et al.* (Lin 1997) studied out-of-plane polymer interdiffusion using neutron reflectometry in bilayers of hydrogenated and deuterated PMMA. The diffusion near the attractive solid substrate was impacted by more than two orders of magnitude as thickness was reduced. Two other studies have also reported the impact of nanoconfinement on diffusion (Boiko 1998; Tseng 2000a). Apart from the experimental studies, a few simulation studies have also investigated the impact of confinement on mobility associated with diffusion. These studies have indicated that the effect of confinement on polymer diffusion should be asymmetric, with enhanced diffusion in the plane of the film and suppressed diffusion out of the plane of the film for supported films (Baschnagel 1996; Mansfield 1989; Bitsanis 1990) and for freely standing films (Doruker 1999).

The lack of consensus among the studies cited above indicates that more work is required in order to make a just assessment of the impact of nanoconfinement on mobility associated with diffusion. In conjunction with this, it would be useful to develop a simplified, high-resolution technique in order to access changes in diffusion coefficients of small molecules and polymers as a function of confinement.

This chapter introduces a simple, yet extremely powerful technique, based on fluorescence trilayer measurements, to quantify changes in diffusion coefficients of small dye molecules a function of confinement, in polymer films near *Tg*. This technique involves a trilayer study, with the bottom layer consisting of a polymer doped with a fluorescent non-radiative energy transfer (NRET) type small molecule, which acts as an acceptor probe. A neat layer of a polymer is placed on top of this layer. Another layer

consisting of a polymer with a NRET-type small molecule donor dye covalently attached to the polymer chain is then placed on top of the neat polymer layer. Figure 10-1 shows the schematic of the sample geometry. The steady-state fluorescence intensity of the donor molecule attached to the polymer is then measured as a function of time. As the donor probe is attached to a polymer of substantial *MW*, the diffusion of donor is negligible in comparison to that of a small-molecule acceptor dye doped in a polymer of substantial *MW* (Ellison 2003; Whitlow 1991; Priestley 2007a; Shearmur 1998). (For further details see Section 5.2, Chapter 5.) As the acceptor comes within several nanometers of the donor label, NRET will take place from the donor to the acceptor (Hall 1997c, 1998c). Consequently, a drop in donor fluorescence intensity is observed. The time required by the first acceptor molecule to travel the distance equal to the thickness of the middle layer or the neat polymer layer (called the "break-through" time) can be directly related to the diffusion coefficient. Using this technique, the translational diffusion coefficient of decacyclene and Disperse Red 1 (DR1) in PS thin and ultrathin films is characterized.

This technique not only allows the characterization of mobility related to diffusion, but also allows the measurement of the temperature dependence of diffusion coefficients in thin and ultrathin films. By varying the thickness of the donor and the acceptor layer, one can further characterize the impact of the polymer-air and polymer substrate interfaces in modifying the mobility related to diffusion. Thus, this technique stands out as an extremely versatile and powerful characterization tool, yet extremely easy and simple to handle, for studying diffusion in thin and ultrathin films.

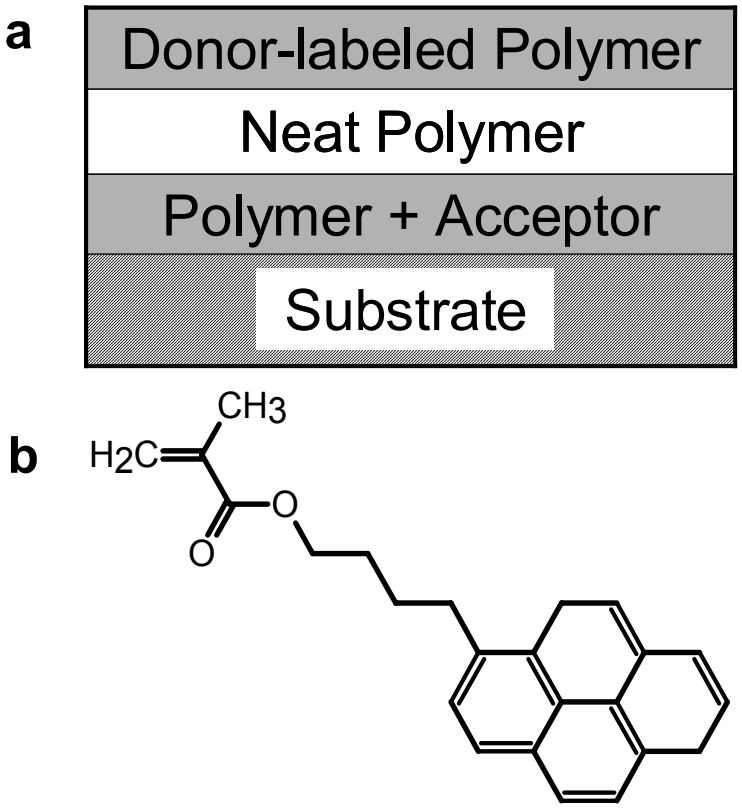

Figure 10-1: **(a)** Schematic of the sample geometry used in this study. **(b)** Pyrene-labeled MMA monomer used as NRET type donor in this study.

10.2 Diffusion Model

Consider the problem involving diffusion into, through or out of a slab bounded by the planes x = 0 and x = *l*. The general solution for diffusion within parallel boundaries, which obeys the following conditions (Barrer 1951)

$$\partial C/\partial t = D(\partial^2 C/\partial t^2), \tag{10.1}$$

$$\text{at } t = 0,\ C = f(x) \text{ for } 0 \le x \le l, \tag{10.2}$$

$$C = 0 \text{ at } x = 0 \text{ and } x = l \text{ for all } t, \tag{10.3}$$

may be written as follows:

$$C = \frac{2}{l}\sum_{n=1}^{n=\infty} e^{-(n\pi/l)^2 Dt} \sin\frac{n\pi x}{l}\int_0^l f(x')\sin\frac{n\pi x'}{l}dx' \tag{10.4}$$

Diffusion from one layer to another may be treated by regarding the system as being a single layer with impermeable boundaries in which the distribution at time t = 0 s is as follows:

$$f(x) = C_0 \text{ for } 0 < x < h, \tag{10.5}$$

$$f(x) = 0 \text{ for } h < x < l,\ (l > h) \tag{10.6}$$

The solution for this particular case is

$$C = C_0\left(\frac{h}{l} + \frac{2}{\pi}\sum_1^\infty \frac{1}{n} e^{-(n\pi/l)^2 Dt} \cos\frac{n\pi x}{l}\sin\frac{n\pi h}{l}\right) \tag{10.7}$$

For any numerical ratio of h/l, this equation may be readily expanded as a series, each term of which may be given a numerical value.

Now one can evaluate diffusion coefficient (D) from measurements as a function of time of the total solute, which has diffused across the boundary. If Q is the total solute concentration, it is given by the equation,

$$Q = -\int_0^t D\left(\frac{\partial C}{\partial x}\right)_{x=h} dt \tag{10.8}$$

From equation 10.7 one has, at $x = h$,

$$\frac{\partial C}{\partial x} = -C_0 \frac{2}{l} \sum_1^{\infty} e^{-(n\pi/l)^2 Dt} \sin^2 \frac{n\pi h}{l} \qquad 10.9$$

Upon substituting equation 10.9 in 10.8 and integrating,

$$Q = C_0 \frac{1}{2\pi^2} \sum_1^{\infty} \frac{1}{n^2} \sin^2 \frac{n\pi h}{l} \left[1 - \exp\left\{ -\frac{Dn^2\pi^2 t}{l^2} \right\} \right] \qquad 10.10$$

Now, in our case, consider a film with diffusant entering from one side at $t = 0$ s. Both distribution and the concentration at any point of the film vary with time. The amount of diffusant (or solute) Q_t, which passes through the film in time t, is given equation 10.10 which can be represented in a more simplified form by the following equation (Crank 1967):

$$\frac{Q_t}{l * C_1} = \frac{D * t}{l^2} - \left(\frac{1}{6}\right) - \left(\frac{2}{\pi^2}\right) \left[\Sigma \left\{ \left(\frac{(-1)^n}{n^2} \right) * \exp\left(\frac{-D * n^2 * \pi^2 * t}{l^2} \right) \right\} \right] \qquad 10.11$$

where, l is the middle film thickness, and D is the acceptor diffusion coefficient. At sufficiently long time,

$$Q_t = \left(\frac{D * C_1}{l} \right) * \left(t - \frac{l^2}{6D} \right) \qquad 10.12$$

Then, the diffusion coefficient (D) is given by:

$$D = \frac{l^2}{6 * t_{break-through}} \qquad 10.13$$

where $t_{break\text{-}through}$ is the time taken by the diffusant to travel the distance equal to the thickness of the middle layer or the neat polymer layer as shown in Figure 10-1a.

10.3 Experimental

Pyrene-labeled methacrylate monomer (see Figure 10-1b) was synthesized by esterification of methacryloyl chloride and 1-pyrenyl butanol (Deppe 1996a, 1996c). 0.67 mol% of pyrene-labeled methacrylate was reacted at 348 K with bulk styrene and benzoyl peroxide as initiator, resulting in pyrene-labeled PS with 1 in 170 repeat units (0.59 mol%) containing a pyrenyl label (by UV-vis absorbance, Perkin-Elmer Lambda 35). To remove residual monomer, the pyrene-labeled PS was washed by seven dissolution/precipitation steps in toluene/methanol and placed in vacuo at 378 K for 3 days. The pyrene-labeled PS had Mn = 440 kg/mol and Mw = 780 kg/mol (gel permeation chromatography (Waters Breeze) calibrated with PS standards) and a bulk Tg = 372 K (differential scanning calorimetry (DSC; Mettler Toledo DSC822e); onset method on second heat using a 10 K/min heating rate after quenching from above Tg at a rate of 40 K/min). The unlabeled PS, which was used as a neat polymer layer (middle of three layers) or as a layer next to the substrate doped with Disperse Red 1 (DR1) or decacyclene as acceptor dye (0.2 wt% doping level), had Mn = 400 kg/mol and Mw/Mn = 1.06 (reported by the supplier, Pressure Chemical) and a neat, bulk Tg = 374 K (by DSC). Non-polymeric reagents and dyes were from Aldrich and used as received.

Thin and ultrathin films (25 – 800 nm thickness) were spin-coated (Hall 1998a) from solutions of PS in toluene onto NaCl infrared crystal windows (Aldrich) or glass substrates. Film or layer thickness was verified by spin coating a second identical film at the same time onto a glass substrate and measuring its thickness by profilometry (Tencor P10) using at least ten measurements near the center of the film and averaging. The profilometer calibration was verified using a 14-nm step-height standard (VLSI Standards). After floating films from the NaCl substrate in a water reservoir, these films were picked up using a substrate on which one or two polymer layers were already present, resulting in multilayer films (Ellison 2003; Priestley 2007a; Roth 2007a, 2007b)

of the geometry shown in Figure 10-1a. In all trilayer films, the donor-labeled layer and the acceptor doped layer were each 33 – 35-nm-thick. Before placement of the second or third layer, excess water was allowed to evaporate under ambient conditions. On completion, trilayer films were dried at room temperature for at least 12 h prior to measurement.

Steady-state fluorescence was measured using a PTI QM-2001 SE fluorimeter with a front-face geometry. 1.0 or 1.5 mm slits were used for excitation (band-pass = 4 nm or 6 nm) and emission (band-pass = 2 nm or 3 nm). Film temperature (376 K) was controlled using a microprocessor controller (Minco Products) with a Kapton ribbon heater attached to a flat aluminum plate. Samples were excited at 322 nm with the emission measured from 396 nm to 399 nm, near a peak in the pyrene emission spectrum. To maximize the signal to noise ratio, the intensity integrated over 396-399 nm is used in data analysis.

10.4 Dye Diffusion in Thin and Ultrathin Films

Figures 10-2 and 10-3 show typical data resulting from the diffusion experiments using decacyclene and DR1, respectively, as the diffusing acceptor dyes. The insets in the figures show the molecular structures of the dyes. In both cases, at short times the fluorescence from the donor-labeled PS layer is nearly independent of experimental time. This behavior is associated with the fact that until the acceptor dye initially diffuses across the width of the middle polymer layer in the trilayer film (see Figure 10-1a), no change in the donor-labeled intensity will occur due to NRET or FRET effects. At longer times, after the acceptor dye breaks through the interface between the initially neat PS layer and the donor-labeled PS layer, there is a much sharper reduction in donor fluorescence intensity with experimental time associated with NRET or FRET between the excited-state donor and the acceptor, resulting in a loss of donor fluorescence.

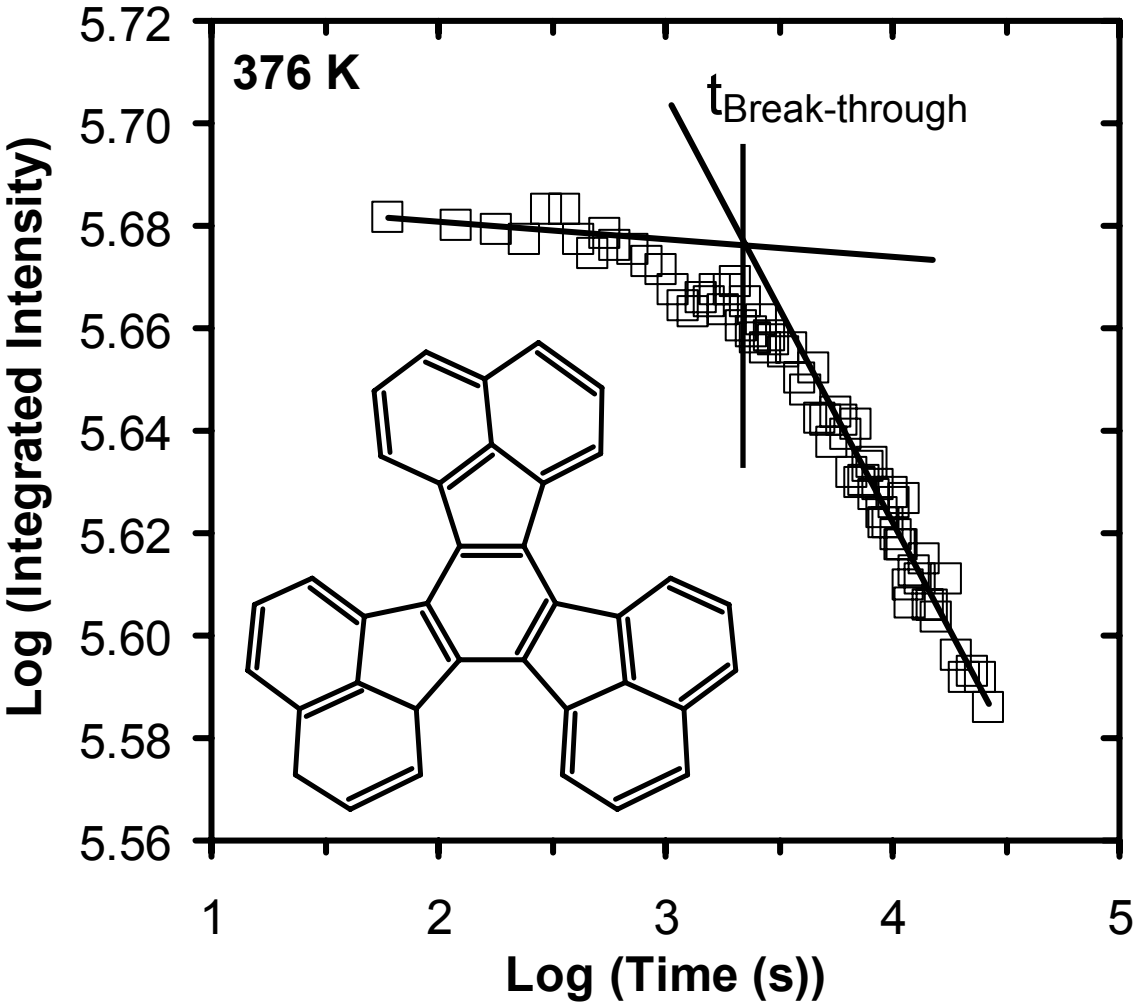

Figure 10-2: Plot of logarithmic integrated fluorescence intensity as a function of logarithmic time (s) for a 45-nm-thick layer of PS (middle layer thickness) under investigation. For all of the samples, the thickness of the top and the bottom layers was kept at ~ 33-35 nm. Inset shows the structure of decacyclene used as NRET type acceptor.

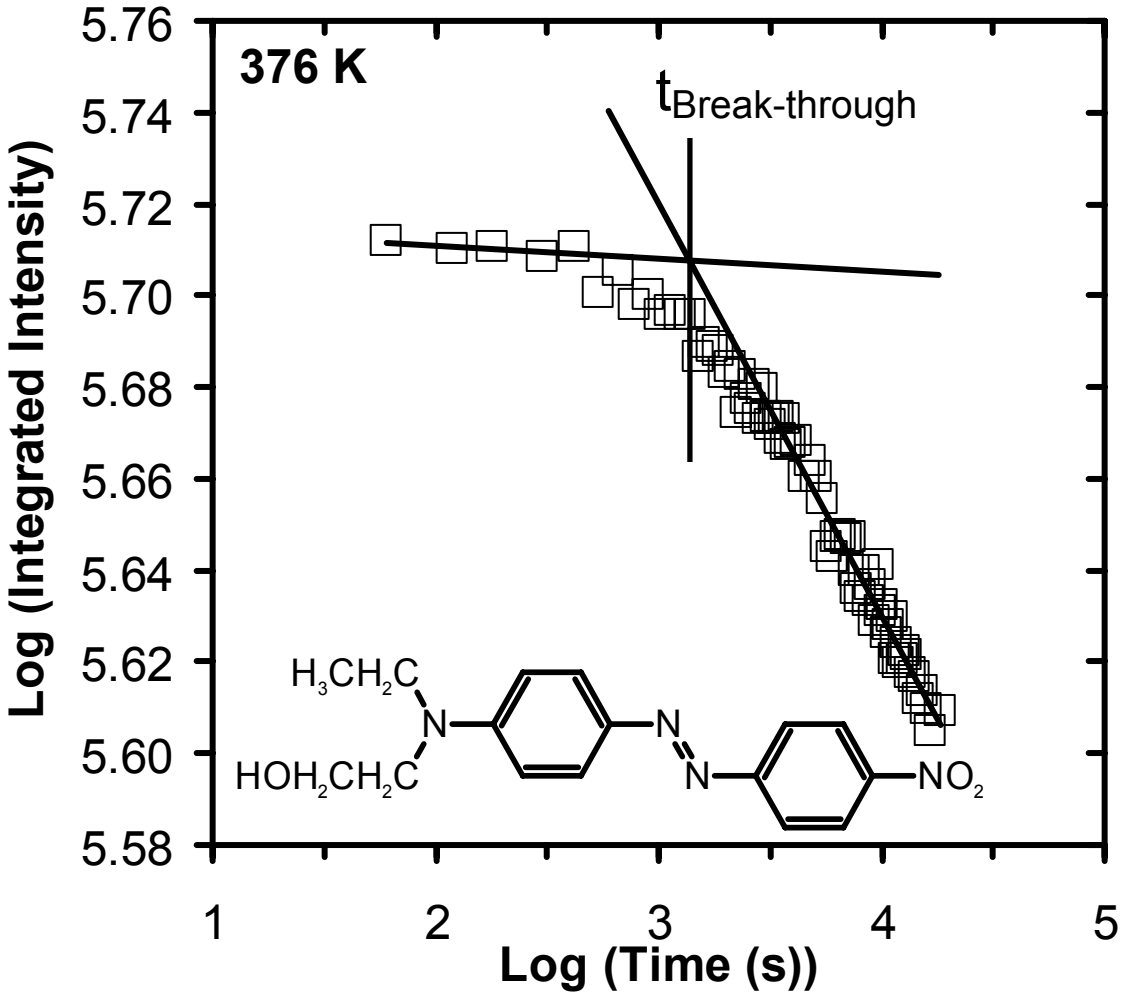

Figure 10-3: Plot of logarithmic integrated fluorescence intensity as a function of logarithmic time (s) for a 430-nm-thick layer of PS (middle layer thickness) under investigation. For all of the samples, the thickness of the top and the bottom layers was kept at ~ 33-35 nm. Inset shows the structure of DR1 used as NRET type acceptor.

Assuming that the acceptor undergoes translational diffusion by a simple Fickian process, the translational diffusion coefficient, D, for an acceptor dye may be determined using the classic equation (Equation 10.13) by Crank *et al.* (Crank 1967). The breakthrough time is estimated by the intersection of the lines fit to the short-time and long-time data in Figures 10-2 and 10-3. For the experiments associated with Figures 10-2 and 10-3, the neat polymer layers (middle layer in Figure 10-1a) are 45 nm and 430-nm-thick, respectively, and the breakthrough times are 2260 s and 1375 s, respectively. Thus, at the conditions of these experiments, including a temperature of 376 K, application of equation 10.13 leads to $D = 1.5 \times 10^{-15}$ cm^2/s for decacyclene and $D = 2.2 \times 10^{-13}$ cm^2/s. The greater than factor of 100 difference in the values of D is consistent with previous studies in bulk polymer near Tg showing very large effects of dye size and shape on dye translational diffusion coefficient, with the smaller DR1 having a much greater D value in polymer near Tg (Deppe 1996a, 1996b; Hall 1998c).

In 1998, Hall and Torkelson (Hall 1998b) employed a bilayer film method requiring a much more complex NRET analysis (Dhinojwala 1994a; Deppe 1996a, 1996b) to determine the effect of confinement on the translational diffusion coefficient of decacyclene in several polymers near Tg, including PS. The bilayer nature of the experiment and the data analysis disallowed the study of dyes with diffusion coefficients substantially greater than that of decacyclene. However, the experiments by Hall and Torkelson (Hall 1998b) were done at the same temperature as the current study, allowing for direct comparison of the decacyclene diffusion coefficients in PS obtained in the 1998 study and the present study. As shown in Figure 10-4a, there is excellent agreement between the D values from the two studies when the overall film thickness exceeds ~ 125 nm, with D being independent of thickness. For thinner trilayer films, the agreement is good, showing a small decrease in D with decreasing overall film thickness. It is likely that some of the small difference between the D values in the films with overall thickness

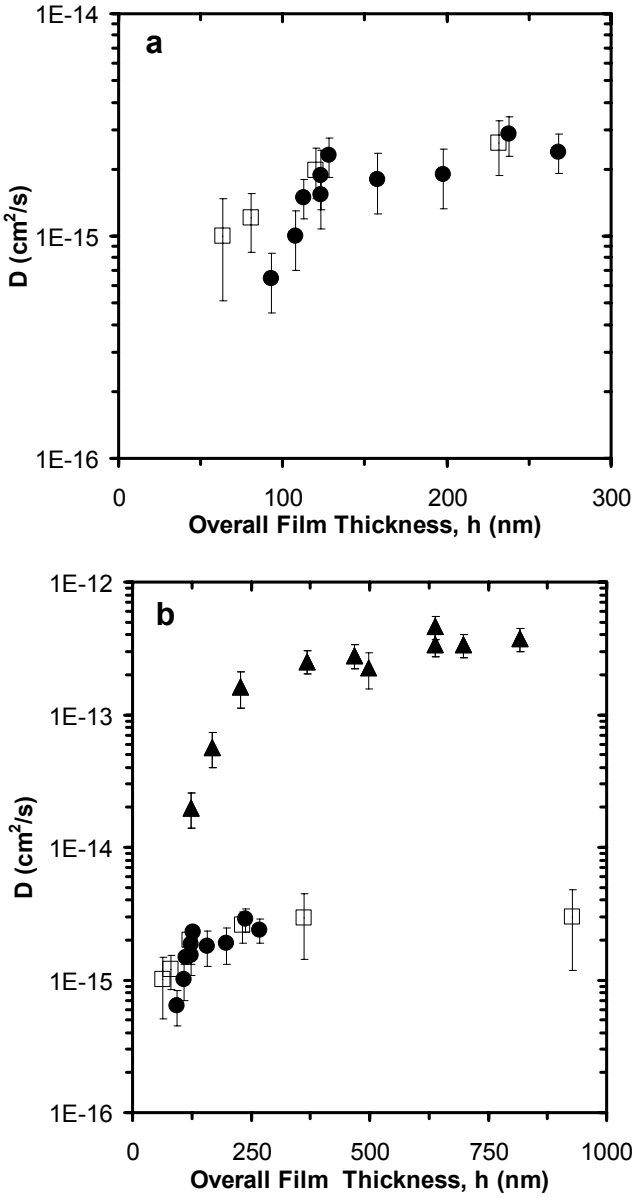

Figure 10-4: **(a)** D as a function of overall film thickness for decacyclene in PS (•) at 376 K. (Donor and acceptor layers are of equal thickness of ~ 33-35 nm each). D as a function of overall film thickness for decacyclene in PS (□), reported previously in reference by Hall *et al.* (Hall 1998b) **(b)** D as a function of overall film thickness for DR1 in PS at 376 K. (Donor and acceptor layers are of equal thickness of ~ 33-35 nm each).

below ~125 nm may be associated with the different diffusion geometries in the two experiments. (The current experiment is sensitive to diffusion in a middle layer at least 33-35 nm away from the polymer-air interface or free surface of the trilayer film while the 1998 experiment is sensitive to diffusion in the upper half of a bilayer film.) In any case, the comparison in Figure 10-4a indicates that the simple experimental method used in the current study yields effective measurements of dye diffusion coefficient in polymer films, whether confined near the nanoscale or yielding bulk behavior.

Figure 10-4b compares the effect of confinement on the translational diffusion of decacyclene and DR1 in PS at several degrees above *Tg*. (Note that for all thicknesses of trilayer films used in this study, there is no *Tg*-nanoconfinement effect according to Ellison *et al.* (Ellison 2003, 2005a). Thus, all effects of confinement on *D* are observed under conditions of constant *Tg*.) Two striking differences are observed between the effect of confinement on *D* for the two dyes. First, the *D* value for DR1 in PS is reduced by more than an order of magnitude from its bulk behavior when the trilayer film is 125-nm-thick; in contrast, the maximum observed reduction of the *D* value for decacyclene in PS is ~ 40% when the trilayer film is 95-nm-thick. Second, the *D* value for DR1 exhibits a reduction from bulk behavior when overall film thickness is less than ~ 300 nm, more than twice the thickness at which confinement effects are evident in the *D* value for decacyclene.

The much larger effect of confinement on the translational diffusion of the smaller dye is hypothesized to result from issues related to the effect of confinement on dynamic heterogeneity in polymers near *Tg* (Ediger 2000; Hall 1998c, 1997c). Ten years ago, studies of rotational reorientation dynamics and translational diffusion coefficients of DR1 and 4-(dimethylamino)-4'-nitrostilbene (DANS) in poly(isobutyl methacrylate) (Hall 1997c) near *Tg* established that the average reorientational relaxation times, $<\tau_{rot}>$, of DR1 and DANS were nearly identical in the rubbery state and followed the

expectations for the temperature dependence of the average alpha-relaxation dynamics, which can be fit by the Williams-Landel-Ferry (WLF) equation. However, there were differences in the *D* values associated with the two dyes, and the temperature dependences of the *D* values in the rubbery state were much weaker than that of $<\tau_{rot}>$. The difference in the temperature dependence is associated with a breakdown in Stokes-Einstein behavior (Hall 1998c), which is a characteristic of dynamic heterogeneity near *Tg* (Cicerone 1995, 1997). Discrete relaxation time distributions were determined from the second-order nonlinear optical data that yielded the distribution of rotational relaxation times of the dyes in the polymers (Hall 1997c). Figure 10-5 shows that at *Tg* – 2 K, the breadth of the relaxation distribution extended over 10 orders of magnitude in time. With increasing temperature above *Tg*, the relaxation distribution shifted to shorter times and the relaxation breadths narrowed, extending over 7 orders of magnitude in time at *Tg* + 10 K and over 6 orders of magnitude in time at *Tg* + 27 K. Most noteworthy was the fact that with increasing temperature above *Tg*, the long-time side of the relaxation distribution shifted significantly to shorter times while the short-time side of the relaxation distribution shifted only slightly to yet shorter times.

The long-time side of the rotational relaxation distribution for a dye whose mobility is coupled to the cooperative segmental mobility or alpha-relaxation of the polymer is in turn a reflection of the long-time side of the alpha-relaxation distribution of the polymer itself. With very broad relaxation distributions covering many orders of magnitude in time, the average relaxation time itself is also a reflection of the long-time side of the distribution. The value of the glass transition temperature is sometimes associated with an average alpha-relaxation time of ~100 s (Ediger 1996; Angell 1995b). Thus, parameters that affect the long-time side of the alpha-relaxation distribution at temperatures near *Tg* will in turn affect the value of *Tg*.

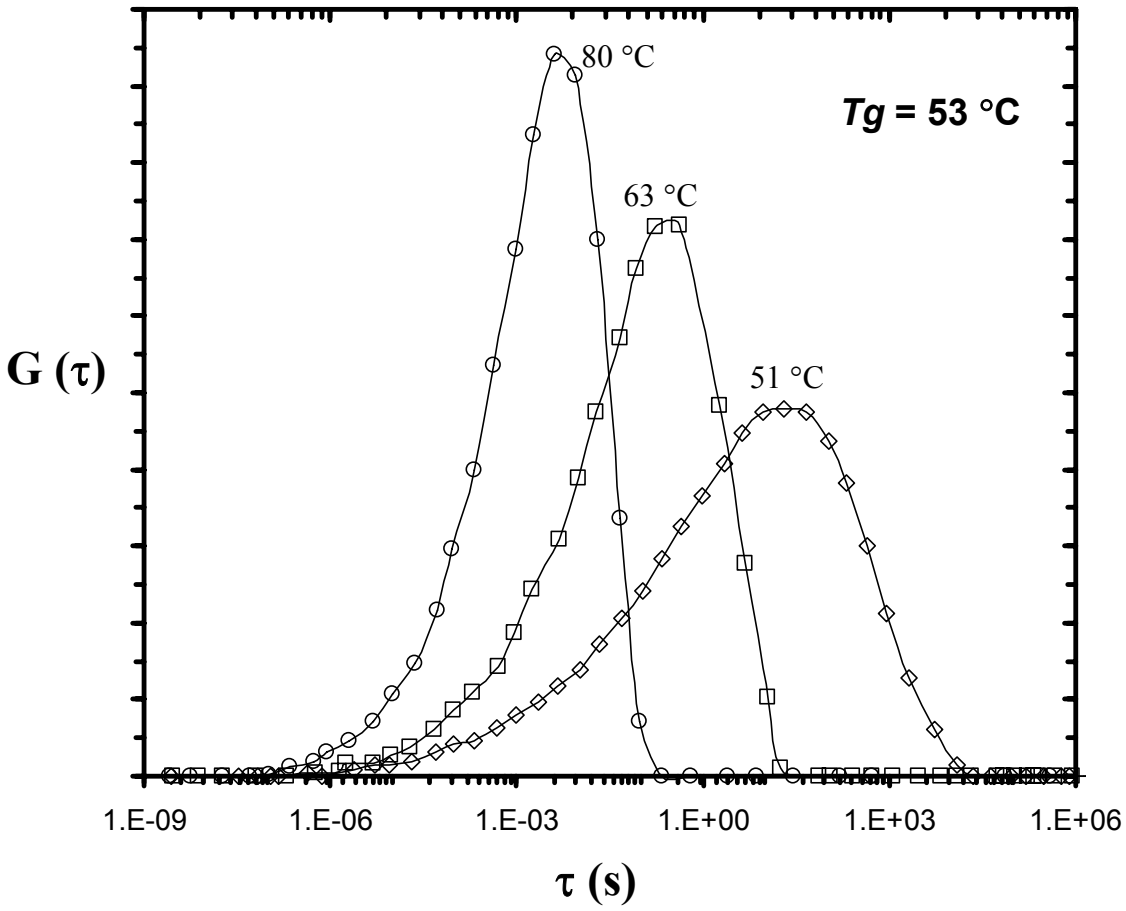

Figure 10-5: Discrete relaxation time distribution calculated using KWW parameters for DR1 in PiBMA. (Data extracted from a reference by Torkelson and coworkers (Hall 1997c).) Curves are drawn to guide eye.

Many studies, from 1994 to present (Keddie 1994a, 1994b; Ellison 2003; Mundra 2006), have shown that the *Tg* of PS is strongly affected by confinement in thin films with thickness less than ~60 nm. The discussion immediately above simply makes clear that confinement at such length scales must alter the long-time side of the alpha-relaxation distribution of PS from its bulk values. However, in contrast, no previous experimental study has yet demonstrated that confinement at or near the nanoscale affects the several percent of the very fastest, cooperatively relaxing regions in a dynamically heterogeneous polymer near *Tg*.

The effects reported in Figure 10-4b are consistent with confinement causing a shift in the short-time side of the relaxation distribution to longer times, thereby reducing the level of dynamic heterogeneity relative to the bulk state. This may be understood from the following reasoning that describes how the magnitude of the translational diffusion coefficient is defined by the fastest relaxing regions in a dynamically heterogeneous system. As described by Hall *et al.* (Hall 1997c), the value of *D* can be related to a summation over all dyes and all jumps of the ratio of the square of the diffusive jump length to the relaxation time during which each jump is made. Related but not identical descriptions have been given by Ediger and co-workers (Ediger 1996) and Glotzer and co-workers (Glotzer 2000). In the simplest possible (and artificial) picture of dynamic heterogeneity consisting of only very slow relaxing regions with a relaxation time of 10^{2} s and very fast relaxing regions with a relaxation time of 10^{-6} sec allowing for diffusive jumps of 1 nm, the ratio of the square of the jump length to relaxation time is 10^{-8} cm^2/s for a single fast relaxing region and $10^{-16}cm^2/s$ for a single slow relaxing region. If the overall system consisted of as little as 1% fast relaxing regions, the average translational diffusion coefficient associated with Fickian diffusion would be a strong reflection of the time scale of the fast relaxing region and not of the slow relaxing region. (This can be best understood by considering the effect on the average diffusion

coefficient of changing the relaxation time of the fast relaxing regions by a factor of 10 and the relaxation time of the slow relaxing regions by a factor of 0.1; such a change would yield slower average translational diffusion and a smaller value of *D*.)

The hypothesis that, at temperatures near *Tg*, confinement of PS leads to a shifting of the short-time side of the alpha-relaxation distribution to longer times is also consistent with the differences in the magnitude of the effects between the two dyes shown in Figure 10-4b. The smaller DR1 dye exhibits a much greater reduction in *D* with confinement and the effect of confinement begins at a larger overall thickness. Previous studies by Torkelson and co-workers (Hall 1998c) have shown that the translational diffusion coefficient for decacyclene in rubbery polymers near T_g has a temperature dependence nearly as strong as those of the average alpha-relaxation times; in contrast, the translational diffusion coefficient for DR1 in the same rubbery polymers near T_g has a much weaker temperature dependence. This difference has been explained by noting that the smaller DR1 dye would be expected to be able to execute diffusive jumps with faster relaxing regions (involving a smaller number of cooperatively rearranging units) than those allowing for diffusive jumps with the larger decacyclene dye. In other words, when two dyes have their mobility coupled to the cooperative segmental dynamics of the polymer, to undergo a diffusive motion the larger dye will require a larger minimum number of repeat units undergoing cooperative motion in the local neighborhood of the dye. Under these circumstances, the temperature dependence of the *D* value for DR1 would be more characteristic of the weaker temperature dependence of the fast-time side of the relaxation distribution while the temperature dependence of the *D* value for decacyclene would be more characteristic of the stronger temperature dependence of the long-time side of the relaxation distribution. With this background, the differences in the magnitude of the effects of confinement on DR1 and decacyclene diffusion can be easily rationalized. Since the DR1 diffusion coefficient is

sensitive to shorter relaxation times, the first effects of confinement in modifying the fast-time side of the relaxation distribution should be reflected by DR1 and not decacyclene; this is why the *D* value of DR1 begins to deviate from bulk behavior at a greater overall film thickness than that of decacyclene. Larger magnitude effects of confinement should also be observed at a common thickness for the dye whose mobility is sensitive to the greater fraction of the whole relaxation distribution, that being DR1.

10.5 Conclusions

This study has demonstrated that the translational diffusion coefficient of a small-molecule dye can be reduced by more than an order of magnitude upon nanoscale confinement in PS near *Tg*. This study has also shown that the length scale at which confinement affects dye translational diffusion can be a factor of 5 larger than that at which a deviation from bulk behavior is observed in *Tg*. The effects observed in this study have been hypothesized to result from confinement resulting in a narrowing of the alpha-relaxation distribution (a narrowing of the dynamic heterogeneity) in the middle layer of trilayer polymer films. This hypothesis is supported by the observation of a reduction of the effect of confinement with an increase in dye size, which is consistent with expectations based on previous research of how changes in the short-time side of the relaxation distribution would lead to changes in the translational diffusion behavior of dyes, with larger dyes being less affected. Further investigation of this hypothesis can be undertaken with additional fluorescence studies, especially those allowing for measurement of the effect of confinement on dye diffusion as a function of temperature. Additionally, dielectric spectroscopy studies may also be useful in directly measuring how the short-time side of the alpha-relaxation distribution is altered by confinement.

The simple, novel approach described here to characterize diffusion coefficients in bulk and confined trilayer films can be extended to study many other important systems and problems. For example, using this approach, the effect of attractive

polymer-substrate interactions in altering dye translational diffusion can be studied as a function of distance from the polymer-substrate interface. Poly(methyl methacrylate) on silica allows for such a study. Similarly, the approach described here can be modified by covalently attaching DR1 to low molecular weight polymer that can be added to a high molecular weight polymer matrix, thereby allowing for the determination of how confinement affect the out-of-plane diffusion of polymers. Such a study would complement the first study of the effect of confinement on translational diffusion in polymers done a little more than a decade ago by Frank *et al.* (Frank 1996a), who observed a small reduction in the in-plane translational diffusion of polymer with confinement.

CHAPTER 11

A NOVEL INTRINSIC FLUORESCENCE TECHNIQUE FOR CHARACTERIZING THE STRESS RELAXATION ASSOCIATED WITH LOCAL CHAIN CONFORMATION IN POLYSTYRENE AND STYRENE CONTAINING RANDOM COPOLYMERS IN THIN AND ULTRATHIN FILMS

11.1 Introduction

Nanoscale confinement of polymers can lead to significant deviations from bulk polymer behavior, including those related to thermal expansion coefficients (Orts 1993; Oh 2004; Kanaya 2001, 2003; Soles 2004b; Beaucage 1993; Mukherjee 2002) and the glass transition temperature (*Tg*) (Keddie 1995; D'Amour 2004; Pham 2002, 2003; Priestley 2005a, 2005b, 2007a, 2007b, 2007c; Rittigstein 2006, 2007; Roth 2003, 2005, 2007a, 2007b; Beaucage 1993; Mukherjee 2002; Tanaka 2004; Li 2004; Blum 2006; Bernazzani 2002; Pratt 2005; Baljon 2005; van den Berg 2004, 2006). Some of the earliest as well as very recent studies of thermal expansion coefficient and *Tg* behavior in nanoconfined polymer films have indicated that there can be significant effects associated with the process and thermal history of the films (Orts 1993; Kanaya 2003; Soles 2004b; Beaucage 1993; Ellison 2002a). Several studies have specifically suggested that some of the unusual or anomalous *Tg* behavior observed in ultrathin films may be associated with stresses that are built in during the spin coating or spin casting process and remain unrelaxed during the *Tg* measurement (Mukherjee 2002; Kawana 2003; Prest 1980a). While it has been appreciated for at least twenty-five years that polymer film formation by spin coating and even the much milder solvent casting process can lead to orientation and non-equilibrium conformations of polymer chains and thereby residual stress effects (Prest 1980a, 1980b; Cohen 1981; Ree 1997; Pottinger 1994; Lin 1993), there has been relatively little direct comparison (Kanaya 2003; Soles 2004b) of how the thermal history

of spin-coated polymer films leads to relaxation of residual stresses in polymer films and whether the apparent *Tg* is affected by unrelaxed residual stresses.

A potentially powerful manner with which to obtain a qualitative measure of the residual stresses in spin-coated films of polystyrene (PS) in combination with *Tg* values in polymer films is intrinsic fluorescence. (For further details on intrinsic fluorescence refer to Chapter 6.) Intrinsic fluorescence of PS consists of both monomer and excimer fluorescence, the former due to emission from a single excited-state phenyl ring and the latter due to emission from an excited-state dimer consisting of two phenyl rings in a parallel, sandwich-like conformation with an inter-ring separation distance of 3-4 Angstroms (Vala 1965).

Intrinsic fluorescence of PS and other polymers has been shown to be highly sensitive to issues ranging from local polymer conformational populations in solution and phase behavior in solvents and polymer blends to local microenvironments in bulk homopolymers (Torkelson 1981, 1983, 1984; Gelles 1982a, 1982b; Major 1986; Tsai 1988a, 1988b; Itagaki 1990, 1996; Xie 1993; Clauss 1995; Ylitalo 1996; Sanz 2002; Corrales 2004; Alberty 2005). In particular, excimer formation in PS solutions and blends is almost exclusively associated with trans-trans conformations in meso dyads along the PS chain (Gelles 1982a; Bokobza 1977), i.e., an increase in trans conformations along the local isotactic regions of a PS chain will result in an increase in intramolecular excimer fluorescence.

In 1975, Frank (Frank 1975) reported that excimer fluorescence of a guest aromatic vinyl polymer, poly(2-vinylnaphthalene), dissolved in a polymer host can be used to monitor relaxation of the non-equilibrium chain conformation distribution of the guest polymer at temperatures near the *Tg* of the host polymer. Later, in 1989 Frank and co-workers (Kosbar 1989) demonstrated that the ratio of excimer fluorescence intensity to monomer fluorescence intensity, *Ie*/*Im*, in spin-cast PS films increased with increasing

spin speed (leading to decreasing thickness) and thereby radial stress. The elevated *Ie*/*Im* values obtained in spin-cast films were qualitatively consistent with the results of a study (Kosbar 1989) showing that uniaxial alignment of PS films leads to an increase in *Ie*/*Im* values. It was rationalized that chain orientation resulting from spin-casting can lead to an increase in the concentration of trans conformations along the chains (associated with intramolecular excimer forming sites), the concentration of intermolecular excimer forming sites, and a higher rate of energy migration to excimer forming sites. (It should be noted that the use of intrinsic fluorescence to monitor relaxation of residual stress associated with processing of polymer films is fundamentally different from studies employing extrinsic probe or label fluorescence to monitor structural relaxation or physical aging in glassy polymer films (Ellison 2002a; Priestley 2005a, 2005b; Gupta 1983; Shmorhun 1990; Royal 1992, 1993; van den Berg 2006).)

In this chapter it is shown that intrinsic fluorescence can be used to characterize the relative state of stress relaxation associated with local chain conformations resulting from the processing conditions such as spin coating in thin and ultrathin films of PS and styrene-methyl methacrylate (S/MMA) random copolymers. It is also revealed that intrinsic fluorescence is a powerful technique not only to characterize the effect of processing conditions and the relative state of relaxation of the residual stresses present in the system but also to help us understand the conditions required to relax these stress associated with local chain conformations. (For details on the use of intrinsic fluorescence to characterize *Tg* as a function of copolymer composition, see Chapter 6.)

11.2 Experimental

11.2.1 Copolymer Synthesis and Characterization

Polystyrene and S/MMA random copolymers were synthesized by bulk free radical polymerization at 343 K using benzoyl peroxide (Aldrich, 97%) as initiator. Styrene and methyl methacrylate (Aldrich) were deinhibited with inhibitor remover

(Aldrich) and dried over CaH_2. Copolymer composition was controlled by varying the comonomer content used in the copolymerizations; fractional conversions were limited to less than 10% to avoid composition drift. Resulting copolymers were purified by dissolution in toluene (Fisher, 99.9%) and precipitation in methanol (Fisher, 99.9%) at least five times to remove residual monomer and initiator. Samples were dried in a vacuum oven at ~ 393 K for several days prior to use.

The styrene mole fraction (F_S) of each copolymer was measured via ^{1}H NMR (Varian Inova 500 Mhz spectrometer) spectroscopy with $CDCl_3$ as solvent and was in good agreement with expectations based on reactivity ratios for the S/MMA system (Brandrup 1999). Number average molecular weights of PS and all copolymers exceeded 100,000 g/mol (gel permeation chromatography relative to PS standards in tetrahydrofuran (THF)). The bulk *Tg*s of PS and the copolymers were measured by differential scanning calorimetry (DSC) using a Mettler-Toledo DSC822e at a 10 K/min heating rate on the second heating cycle after quenching from elevated temperature at a rate of 40 K/min. Table 11-1 provides details on PS and copolymer characterization.

11.2.2 Film Studies

High purity fused quartz slides were used as a substrate for both PS and S/MMA random copolymers films. Slides were initially washed with a 10% sodium hydroxide/70% ethanol/20% water solution and then solvent washed. Thin and ultrathin films were prepared by spin coating dilute PS or copolymer solutions in THF of various concentrations at speeds of 500 to 4000 rpm for 60 sec, yielding film thicknesses ranging from 20 nm to 1000 nm (Hall 1998a; Spangler 1990, 1992). Films used for stress relaxation measurements experienced no annealing prior to measurement. Film thickness was measured with a Tencor P10 profilometer (calibration was verified by using a 14-nm step height standard from VLSI standards) by taking an average of at least ten measurements close to the center of the film where fluorescence was measured.

Table 11-1: Characterization of S/MMA copolymers used in this study: F_S is the cumulative S mol fraction in the copolymers; M_S and M_{MMA} are the mol fractions of S and MMA in the monomer mix used to make the copolymers; f_{SS} and N_S are the S-S dyad fraction and number average sequence length of S units in the copolymers, respectively. Also provided are the bulk *Tg* values determined by DSC and fluorescence.

F_S	M_S	M_{MMA}	f_{SS}	N_S	$f_{SS}N_S$	*Tg*(onset) DSC	*Tg* Fluor.
1.000	1.000	0.000	1.000	---	---	378 K	378 K
0.782	0.865	0.135	0.597	4.34	2.591	376 K	379 K
0.652	0.730	0.270	0.372	2.41	0.895	377 K	377 K
0.581	0.637	0.363	0.266	1.91	0.508	378 K	377 K
0.390	0.343	0.657	0.073	1.27	0.093	376 K	377 K
0.215	0.124	0.876	0.027	1.07	0.029	379 K	377 K
0.088	0.025	0.975	0.013[a]	1.01	0.013	378 K	378 K

[a] Denotes fraction calculated from reactivity ratios.

11.2.3 Instrumentation

Intrinsic fluorescence was measured using a PTI QM-2001 SE fluorimeter using front-face geometry with 1 mm excitation (bandpass = 4.0 nm) and 1 mm emission slits (band pass = 2.0 nm). Film temperature was controlled using a microprocessor controller (Minco Products) with a Kapton ribbon heater attached to a flat aluminum plate with a hole in the center to prevent scattering or fluorescence from the heater itself. For intrinsic fluorescence, excitation was done at 260 nm, and the emission spectrum was measured from 270 nm to 410 nm. For pyrene-doped samples, excitation was done at 322 nm, and the emission spectrum was measured from 360 nm to 460 nm. Pyrene (Aldrich, 99+% purity) was used as received.

An M-2000D^{TM} spectroscopic ellipsometer (J. A. Woollam Co., Inc.) with an integrated programmable heating source (Instec) was used for measurements characterizing film thickness as a function of temperature above and below *Tg* with several heating and cooling cycles. Several heating and cooling cycles were employed with each measurement.

11.3 Intrinsic Fluorescence Measurements for Characterizing Stress Relaxation in Thin and Ultrathin Films

11.3.1 Non-Isothermal Measurement (Heating and Cooling Cycles)

Fluorescence spectroscopy of PS and styrene-containing copolymer films is employed to investigate stress relaxation in spin-coated thin and ultrathin films that are not annealed above *Tg* prior to measurement. The experimental protocol for this section of our study involves heating spin-coated, unannealed samples by 5 K increments, remaining at temperature for 5 min, measuring fluorescence, and then heating by 5 K, etc. When a temperature is reached that is well above *Tg*, the sample is then cooled by 5 K, temperature is maintained for 5 min, fluorescence is measured, and then the sample is cooled by 5 K, etc.

Figure 11-1a shows the T-dependence during heating and cooling of the integrated intrinsic fluorescence intensity for a 260-nm-thick PS film. There is a major difference in the intrinsic fluorescence intensity during heating and cooling cycles for temperatures less than ~ 390 K; at temperatures greater than ~ 390 K, the fluorescence responses during heating and cooling are the same within experimental error.

These results indicate that stresses induced during spin coating affect the distribution of local conformational populations in the PS film, which in turn affect the levels of excimer and monomer fluorescence. It must be noted that excimer is often formed from excited-state monomer and results in the loss of monomer fluorescence. This fact in combination with the fact that excimer fluorescence has a low quantum yield means that integrated fluorescence intensity is reduced when there is more excimer formation. In Figure 11-1a, there is a sharp increase in intensity with increasing temperature as the unannealed film is heated from 348 K to 368 K. (Similar although not identical results to those shown in Figure 11-1a are obtained during the first heating cycle with other unannealed PS films of identical thickness but made with different spin-coating rotational speeds, ranging from 400 rpm to 3600 rpm, and different solution concentrations. The small differences in the fluorescence exhibited among these films during the first heating cycle may be a manifestation of small differences in residual stresses caused by the use of different spin speeds and solution concentrations.) The temperature dependence of intensity is the opposite in well-annealed PS films (see Figure 6-3, Chapter 6). This means that the increase in intensity observed upon heating to 368 K in Figure 11-1a is due to a change in local conformational population that disfavors excimer fluorescence. In other words, the stresses associated with spin coating of this film result in local conformations favoring excimer formation (trans conformations) beyond that present in well-equilibrated films, and annealing at temperatures significantly below *Tg* then leads to some stress relaxation and local conformational populations less

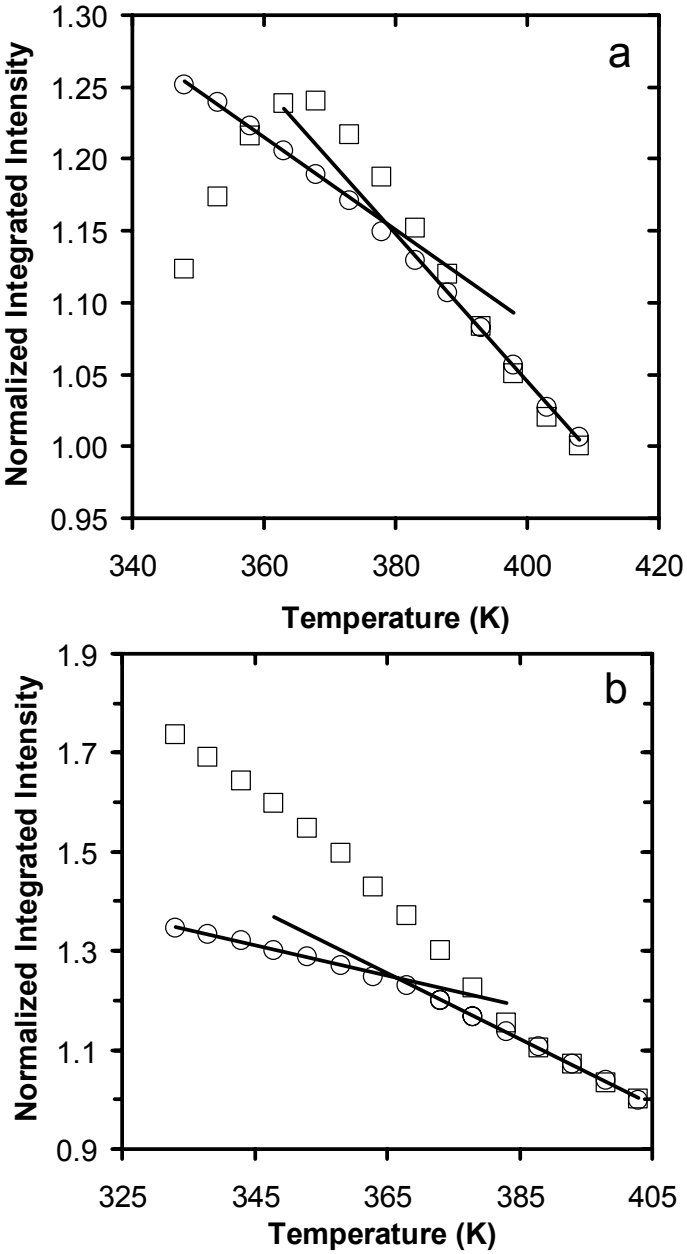

Figure 11-1: **(a)** Temperature dependence of the integrated intrinsic fluorescence intensity of a 260-nm-thick PS film during heating (□) and cooling (○) cycles. (The integrated intensities are normalized to one by the intensity at 408 K measured during heating.) **(b)** Temperature dependence of the integrated intrinsic fluorescence intensity of a 26-nm-thick PS film during heating (□) and cooling (○) cycles. (The integrated intensities are normalized to one by the intensity at 403 K measured during heating.)

favorable for excimers. (This behavior is consistent with that reported by Frank (Frank 1975) regarding the impact of spin coating on the fluorescence of PS films.) Upon further heating, there is a decrease in intensity. The fact that the intensities upon heating and cooling match at 393 K means that during the heating cycle there is sufficient stress relaxation when the temperature reaches 393 K for the local conformational population in the PS film to be identical within error to that in films experiencing yet further annealing.

This latter point is important because while some stress relaxation occurs during heating in the glassy state well below *Tg*, the non-equilibrated local conformational populations cannot be fully relaxed by heating a few degrees above *Tg* for several minutes. Instead, as measured via intrinsic PS fluorescence and using the heating protocol described above, the stresses induced by spin coating are relaxed only when a temperature of 393 K is reached, 15 K above the *Tg* of the film. Note that an accurate *Tg* value can be obtained only during the cooling cycle and not during the initial heating cycle; the *Tg* value obtained during from the cooling cycle measurement is 378 K, in good agreement with the *Tg* value measured by DSC for bulk PS and by intrinsic fluorescence in well-annealed PS films. See Table 11-1.

We note that the unusual fluorescence results exhibited during the first heating cycle in Figure 11-1a cannot be explained by the presence of residual solvent in the film after spin casting; instead, it must be associated with the relaxation of nonequilibrated local conformational populations resulting from the spin coating of the film. Spectroscopic ellipsometry was used to measure film thickness as a function of repeated heating and cooling cycles for a film that was spin coated using conditions identical to those used in making the film studied in Figure 11-1a. The as-spin-coated initial film had a thickness at 298 K that was 0.2% greater than the film exhibited at 298 K during all subsequent cooling cycles from temperatures well above *Tg*. This means that not more than ~ 0.2 wt% residual THF solvent was present in the film at the beginning of the

measurement shown in Figure 11-1a. This trace level of residual solvent could not lead to the unusual fluorescence behavior exhibited during the first heating cycle in Figure 11-1a.

Figure 11-1b shows the temperature dependence of the integrated fluorescence intensity during heating and cooling of a 26-nm-thick PS film. In contrast to the results in Figure 11-1a, there is a sharp drop in integrated intensity upon heating the unnannealed film. The integrated intensities upon heating and cooling are identical only for temperatures greater than or equal to 383 K.

These results indicate that stress relaxation of the unannealed, ultrathin PS film occurs during heating by an increase in local conformational population favoring excimer fluorescence; hence, there is a net reduction in integrated fluorescence intensity, the exact opposite of that observed in the thicker PS film. The reason for this difference between the thin and ultrathin films is unclear. Nevertheless, the results indicate that the effect of stresses on local conformational populations may differ significantly in thin and ultrathin PS films. Notably, the ultrathin PS film exhibits identical fluorescence intensities upon heating and cooling at ~ 17 K above the film *Tg* (*Tg* is ~ 366 K as measured during the cooling cycle). Thus, with the given heating protocol and accounting for the different *Tg*s in thin and ultrathin PS films, the temperatures above *Tg* required to achieve stress relaxation leading to apparently equilibrated local conformational populations in thin and ultrathin spin-coated PS films are nearly identical.

Figure 11-2 shows related results for heating and cooling of unannealed, thin and ultrathin PS films in which pyrene dopants are present at 0.2 wt%. The fluorescence data are the normalized integrated intensities of the pyrene dopant, which should not directly reflect local conformational populations in the PS films. In these cases, the differences observed between the fluorescence measurements obtained upon heating and cooling are much smaller than those in Figure 11-1 where measurements involved intrinsic

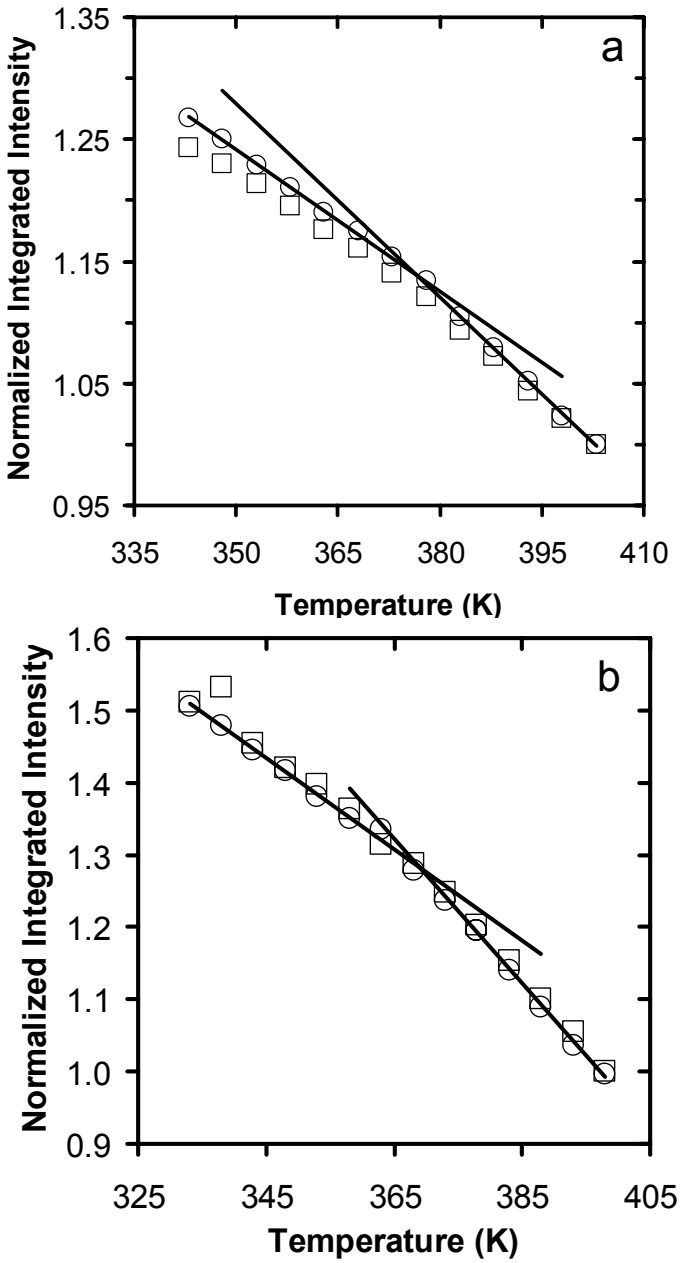

Figure 11-2: **(a)** Temperature dependence of the integrated extrinsic fluorescence intensity an 1180-nm-thick PS film doped with 0.2 wt % pyrene during heating (□) and cooling (○) cycles. (The integrated intensities are normalized to one by the intensity at 403 K measured during heating. **(b)** Temperature dependence of the integrated extrinsic fluorescence intensity of PS doped with 0.2wt % pyrene in 35-nm-thick film during heating (□) and cooling (○) cycles. (The integrated intensities are normalized to one by the intensity at 398 K measured during heating.

fluorescence from the PS chains themselves. While fluorescence can be a useful method to characterize relaxation of stresses in spin-coated films, Figure 11-2 indicates that this approach may yield little of value if the fluorescence is being obtained from probes that are not intrinsically a part of the chains themselves and do not reflect the conformational state of the polymer. However, the small difference observed between the pyrene probe fluorescence upon heating and cooling of PS films indicates that even probe fluorescence may be affected to a small yet measurable extent by unrelaxed stresses. Thus, when *Tg* values are obtained from probe fluorescence, whenever possible the data should be obtained upon cooling from a temperature well above *Tg*.

Figure 11-3 provides data similar to those in Figure 11-1 except that the system is a 58/42 mol % S/MMA copolymer, where significant levels of both monomer and excimer fluorescence are present, and the film thicknesses are 500 nm (Figure 11-3a) and 20 nm (Figure 11-3b). In contrast to the results given in Figure 11-1 for PS, with this copolymer system the temperature dependence is observed to be monotonic with temperature. However, as with Figure 11-1, the intensities in the heating and cooling cycles are only matched at temperatures significantly above the *Tg* of each film. In the case of the 500-nm-thick film, the match in intensity data occurs at ~ 22 K above the film *Tg* while in the case of the 20-nm-thick film the match in intensity occurs at ~ 17 K above the film *Tg*. Thus, these results indicate that the stress relaxation accompanying heating of unannealed S/MMA copolymer films is similar to that accompanying heating of unannealed PS films, meaning that the attractive hydrogen bonding interactions present at the substrate in the S/MMA copolymer film have little impact in suppressing stress relaxation associated with spin coating when the films are nearly 20 K above *Tg*. In both the PS and 58/42 mol % S/MMA copolymer films, a heating protocol of 5 K increments every 5 min requires that the temperature reach a value of 15-22 K above *Tg* for apparently full relaxation of stresses associated with non-equilibrated local

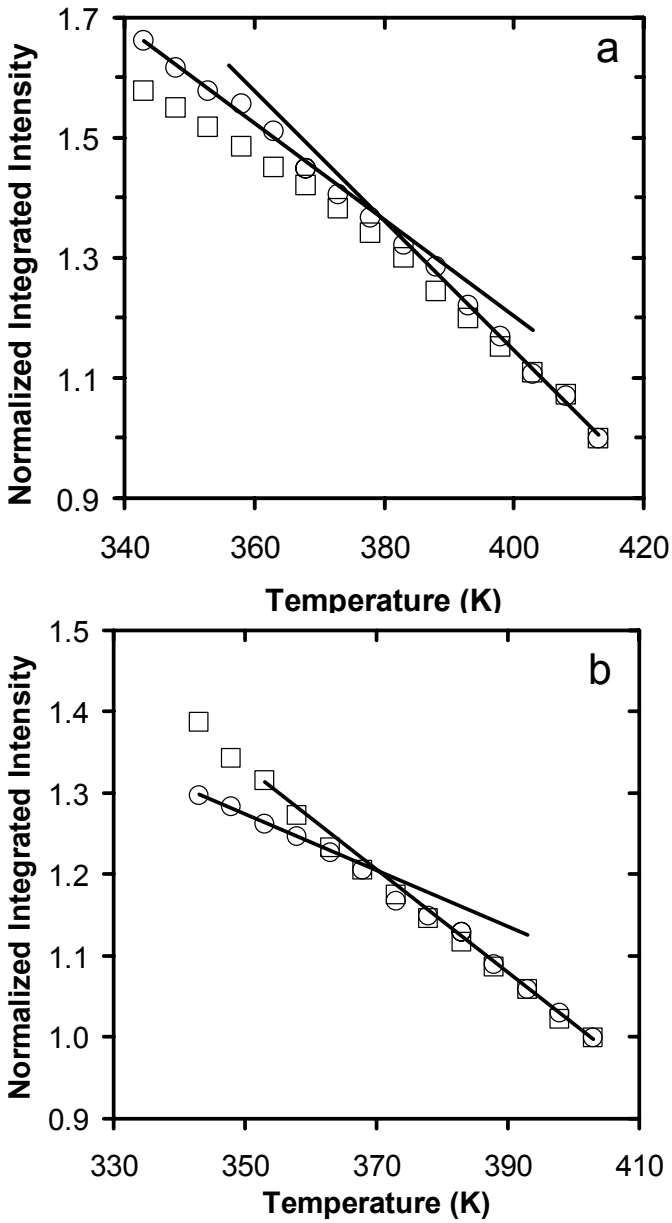

Figure 11-3: **(a)** Temperature dependence of the integrated intrinsic fluorescence intensity of a 500-nm-thick 58/42 mol% S/MMA film during heating (□) and cooling (○) cycles. (The integrated intensities are normalized to one by the intensity at 413 K measured during heating.) **(b)** Temperature dependence of the integrated intrinsic fluorescence intensity of a 20-nm-thick 58/42 mol% S/MMA film during heating (□) and cooling (○) cycles. (The integrated intensities are normalized to one by the intensity at 403 K measured during heating.)

conformational populations sensed by intrinsic fluorescence.

Figure 11-4 demonstrates that fluorescence can provide some characterization of stress relaxation of S/MMA random copolymers even when the S content is sufficiently low that excimer fluorescence is negligible. It may be possible that local conformational populations affect the rates of radiative and nonradiative decay of the excited monomer species in such copolymers, thereby accounting for the apparent sensitivity of their fluorescence intensities to stress relaxation. In particular, the data in Figure 11-4 are for the 22/78 mol % S/MMA copolymer system where the fluorescence spectrum is almost exclusively due to monomer fluorescence. Nevertheless, there are major differences in the fluorescence data obtained from unannealed films of this copolymer during heating and cooling cycles. As shown in Figure 11-4a, a 230-nm-thick film exhibits a significant increase in intensity upon heating from ~ 342 K to ~ 390 K; with further heating, the intensity decreases. The fluorescence intensities match in the heating and cooling cycles at a temperature of 396 K (and greater), which is ~ 19 K above the *Tg* obtained from the cooling cycle. In contrast, with a 50-nm-thick ultrathin film, there is a small increase in intensity upon heating from 348 K to 358 K; with further heating, the intensity decreases. The fluorescence intensities match in the heating and cooling cycles at 373 K (and greater), which is actually below the *Tg* of the ultrathin film. The cause of the latter outcome is uncertain. However, is possible that better sensitivity to local conformational populations is obtained in S-containing copolymers and homopolymers that exhibit significant levels of excimer fluorescence in addition to monomer fluorescence. Further study of this point is warranted.

While these results are interesting in their own right, they also are valuable in providing guidance for the characterization of rubbery and glassy state behavior and *Tg* values of thin and ultrathin films. The results presented above indicate that significant relaxation of local conformational populations obtained in unannealed, spin-coated thin

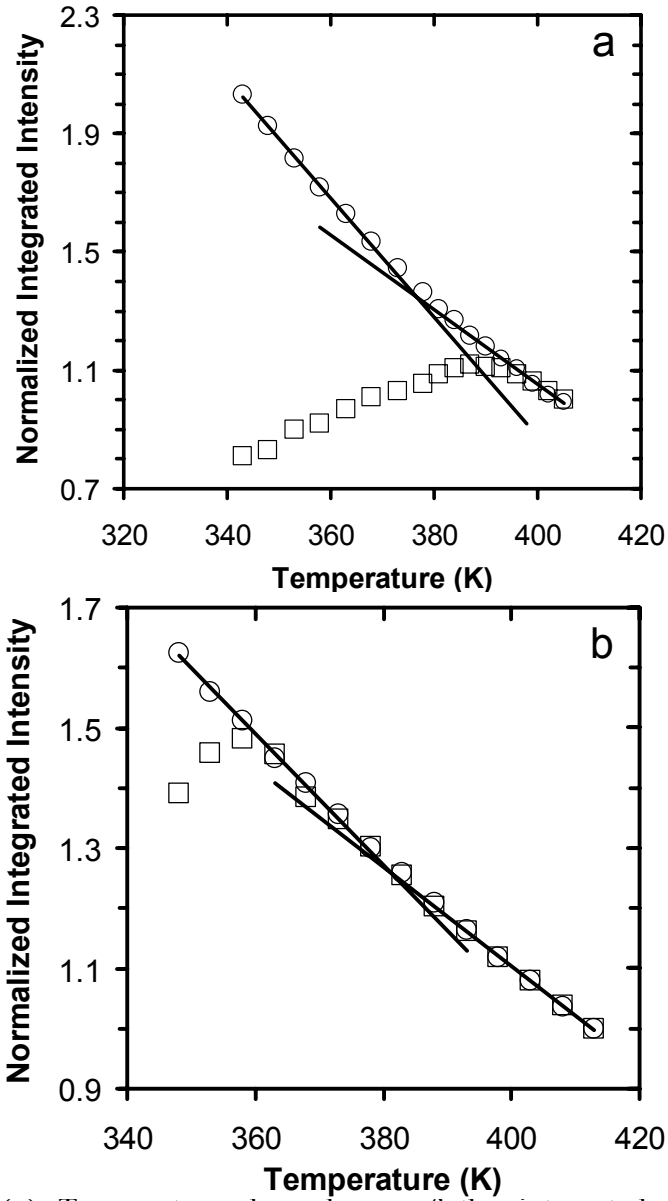

Figure 11-4: **(a)** Temperature dependence of the integrated intrinsic fluorescence intensity of a 230-nm-thick 22/78 mol% S/MMA film during heating (□) and cooling (○) cycles. (The integrated intensities are normalized to one by the intensity at 405 K measured during heating.) **(b)** Temperature dependence of the integrated intrinsic fluorescence intensity of a 50-nm-thick 22/78 mol% S/MMA film during heating (□) and cooling (○) cycles. (The integrated intensities are normalized to one by the intensity at 413 K measured during heating.)

and ultrathin films of PS and S-containing copolymers can occur in the glassy state. However, with the heating protocol employed in the present study, full relaxation of the local conformational populations, as observed via intrinsic fluorescence (which is sensitive to the presence of trans conformations in local isotactic runs along a chain of PS or a high-to-moderate S-content copolymer), does not typically occur until the films are heated ~ 15-22 K above the film *Tg*.

These results are in accord with the study of PS films by Frank and co-workers (Kosbar 1989) that found that the *Ie*/*Im* values of high molecular weight PS films made at high spin speed (but of unreported thicknesses) relaxed toward a steady-state value over 20 min during isothermal annealing at 383 K and over much longer times at temperatures below *Tg*. These results are also in qualitative agreement with a portion of a recent study by Reiter and co-workers (Reiter 2005) who found that when 40 - 65-nm-thick PS films (made via spin coating and never annealed above *Tg* prior to dewetting studies) were annealed for extended time frames in the glassy state, there were significant changes in the dewetting characteristics of these films at temperatures above *Tg*. A surprising feature of the study by Reiter and co-workers is that dewetting characteristics continue to be a function of annealing time below *Tg* even in films that experience dewetting at temperatures nearly 40 K above the bulk PS *Tg*. At such a high temperature, both our fluorescence data and those of Frank and co-workers (Kosbar 1989) indicate that local conformational populations should be equilibrated quickly relative to the time scales associated with dewetting. Further investigation is needed to determine whether intrinsic fluorescence is insufficiently sensitive to some frozen-in polymer conformations that affect the high-temperature dewetting characteristics studied by Reiter *et al.* (Reiter 2005) or another issue beyond that associated with non-equilibrated conformations may be contributing to the effects of glassy-state annealing on dewetting of spin-coated films.

The *Tg* characterization obtained by intrinsic fluorescence upon cooling relaxed

thin and ultrathin films of PS and S-containing copolymers agrees well with results obtained by other methods and in other studies. Hence, the film-thickness dependent *Tg*s that are often observed in ultrathin polymer films are not inherently a consequence of the spin-coating-induced stresses accompanying the film formation. That being said, it is important to note that if the spin-coating-induced stresses are not relaxed prior to measurement, as is the case of measuring film thickness upon heating of unannealed films, those stresses may affect the measurements being made because of the stress relaxation that occurs during heating. This is likely a significant contributing factor to the negative thermal expansion coefficients that have been obtained (Orts 1993) upon first heating of unannealed, spin-coated polymer films. (The extent to which effects of unrelaxed conformations contribute to cases in which negative, glassy-state thermal expansion coefficients have been reportedly observed (Soles 2004b, Mukherjee 2002) upon repeated heating and cooling above and below *Tg* in selected spin-coated ultrathin films is less clear; greater investigation is needed to determine the extent to which the heating protocols employed in such studies relax the unequilibrated conformations in those films.)

Finally, the results of this study indicate that simply heating a spin-coated polymer film to *Tg* and holding at temperature for a time scale equal to or several times that associated with the average cooperative segmental relaxation time, i.e., the α-relaxation time, is insufficient to relax fully the non-equilibrated conformations associated with spin-coating induced stresses (Reiter 2001b). Instead, as observed by intrinsic fluorescence, the full relaxation of spin-coating-induced stresses in thin and ultrathin films, in which attractive polymer-substrate interactions are either present or absent, can be achieved by heating well above *Tg* for time scales that are long relative to average relaxation times for cooperative segmental mobility. Further study of this behavior is warranted.

11.3.2 Isothermal Measurements above Tg

To further gain perspective as to how intrinsic fluorescence can be used to characterize stress relaxation associated with local chain conformation, measurements are carried out isothermally at temperatures above *Tg*. Figure 11-5 shows the relaxation of intrinsic PS fluorescence intensity as a function of annealing time at temperatures above *Tg*. In all cases, films are spin coated and maintained at room temperature in the glassy state prior to annealing above *Tg*. Figure 11-5 demonstrates that many tens of minutes are required to achieve or nearly achieve a steady-state local conformational population in both thin (500-nm-thick) and ultrathin (30-nm-thick) PS films when annealed at *Tg* + 10K. However, the ultrathin film exhibits a smaller overall change than the thin film when annealed at *Tg* + 10 K, reflecting a smaller change in conformational population during stress relaxation. Annealing at *Tg* + 30 K yields steady-state conformational populations, which can be associated with stress relaxation, within the first minute or so of annealing time. It should be noted that Kosbar *et al.* (Kosbar 1989) previously reported that changes could be observed in the ratio of excimer to monomer fluorescence intensities as a function of annealing time in spin cast PS films. However, no direct characterization of film thickness was given, and films were annealed for no longer than 20-30 min, never achieving steady-state values of fluorescence due to the low annealing temperatures employed. Kosbar *et al.* (Kosbar 1989) annealed at temperatures limited to a range from 348K to 388K and did not correlate the annealing temperatures to the *Tg* values of particular films.

The impact of molecular weight on the stresses associated with local chain conformations was also studied over two orders of molecular weight range varying from 30,000 g/mol to 3,000,000 g/mol. Figure 11-6 shows the relaxation of intrinsic PS fluorescence intensity as a function of annealing time at temperatures above *Tg* for molecular weight ranging from 30,000 g/mol to 3,000,000 g/mol. For all molecular

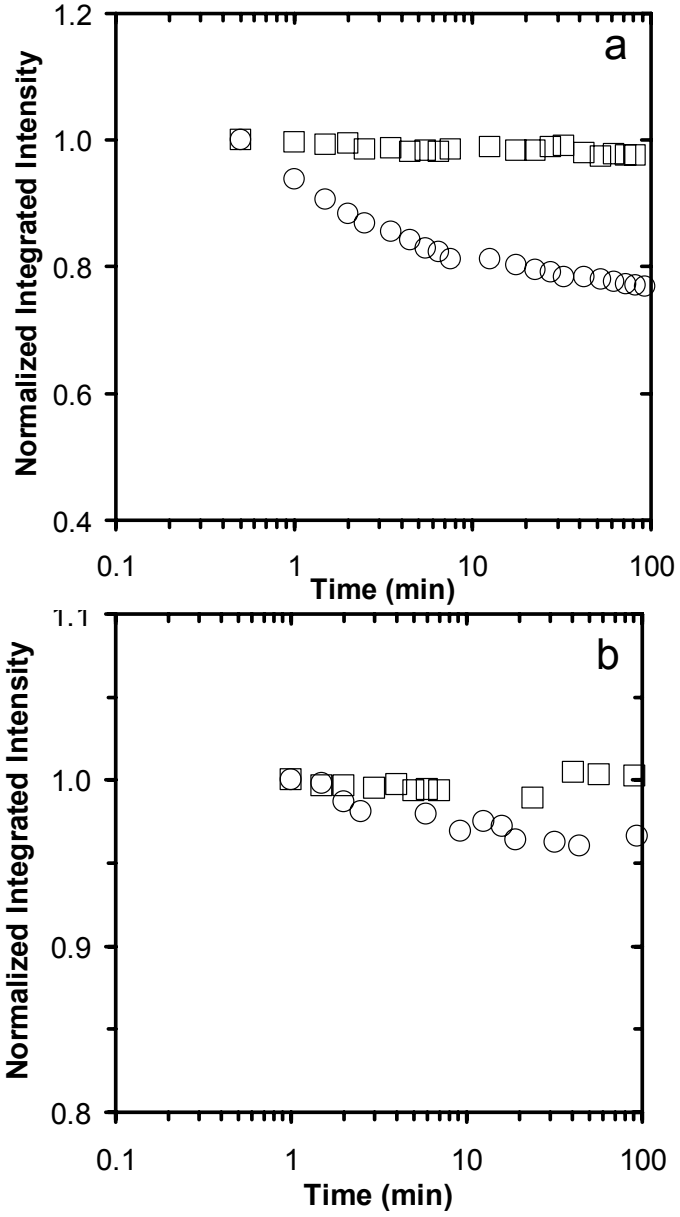

Figure 11-5: (a) Relaxation of integrated intrinsic PS fluorescence intensity as a function of annealing time for 500-nm-thick PS film (*Mn* = 290, 000 g/mol) at *Tg* + 10K (○) and *Tg* + 30K (□). **(b)** Relaxation of integrated intrinsic PS fluorescence intensity as a function of annealing time for 30-nm-thick PS film (*Mn* = 290, 000 g/mol) at *Tg* + 10K (○) and *Tg* + 30K (□).

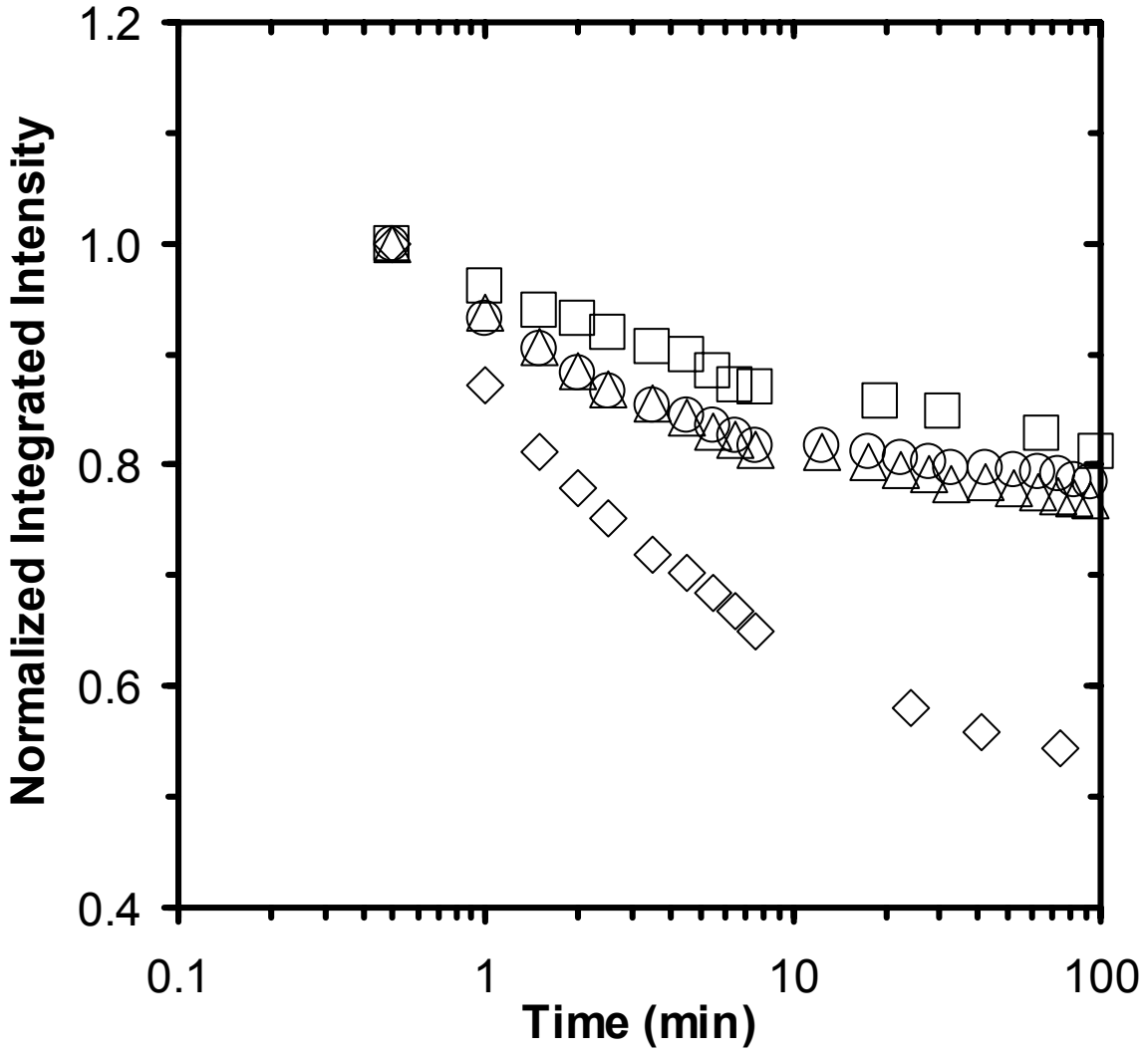

Figure 11-6: Relaxation of integrated intrinsic fluorescence intensity as a function of annealing time for 500-nm-thick film of PS (*Mn* = 30, 000 g/mol) (○), (*Mn* = 290, 000 g/mol) (Δ), (*Mn* = 3,000, 000 g/mol) (□), and 9/91 mol % S/MMA random copolymer (◊) at *Tg* + 10K.

weights, films were spin coated and maintained at room temperature in the glassy state prior to annealing above *Tg*. Figure 11-6 demonstrates that many tens of minutes are required to achieve or nearly achieve a steady-state local conformational population in 500-nm-thick PS films of 30,000, 290,000 and 3,000,000 g/mol molecular weights samples when annealed at *Tg* + 10 K. However, annealing at *Tg* + 30 K yields steady-state conformational populations for all the samples of different molecular weights, which can be associated with stress relaxation, within the first minute or so of annealing time (measurement at *Tg* + 30 K is not reported here, see Figure 11-5 for further detail). Thus, within the error associated with each measurement, no effect of molecular weight is evident in modifying the stresses associated with local chain conformations induced during sample preparation.

It is also interesting to note that for the 9/91 mol % S/MMA random copolymer, a slight difference is seen from the PS systems. At *Tg* + 30 K, a steady state conformational population is reached within the first minute or so of annealing time, similar to PS films. However, at *Tg* + 10 K, a much larger change in the intensity is seen for the random copolymer as compared to PS films of the same 500 nm thickness. Figure 11-6 also demonstrates that several tens of minutes are required to achieve or nearly achieve a steady-state local conformational population in 500-nm-thick 9/91 mol % S/MMA random copolymer film, slightly higher than what is seen for the case of PS films. Clearly, the presence of attractive interactions between MMA repeat units and the substrate have some minor impact on the relaxation of local chain conformations at temperature above *Tg*. Similar differences were seen by Reiter *et al.* (Reiter 2005) in poly(dimethyl siloxane) (PDMS) coatings on silicon wafers, which are characterized by a weak attractive interaction between the films and the substrates. Significantly longer relaxation times were seen for adsorbed polymers such as PDMS.

11.3.3 Evidence of Relaxation of Stresses Associated with Local Chain Conformations for Samples Aged Below Tg

Figure 11-7 shows the relaxation of stresses associated with local chain conformations measured at *Tg* + 10 K for PS films of 290,000 g/mol molecular weight. These 500-nm-thick films were aged below *Tg* at room temperature for different times. A film that was aged for 0 days shows similar response to an unaged 500-nm-thick film measured at *Tg* + 10 K, reported in Figure 11-5a. A film that was aged for 150 days shows the highest recovery in intensity when measured at *Tg* + 10 K indicating that stresses associated with local chain conformations are relaxed to significant extent for this sample. Intermediate responses were seen for films aged for 50 and 80 days, respectively. Similar results were seen by Reiter and co-workers (Reiter 2005) in their dewetting studies that focused on the influence on dewetting of storing (aging) PS films for increasing times below *Tg*. A huge reduction in the width of the rim for dewetting from the edge of the sample (*W*) was seen in contrast to the dewetting time for samples aged below *Tg*. The value of the maximum width (*Wmax*) of the rim differed considerably between samples that were nominally identical and differed only in age. Even though the dewetting time was constant for all the samples, *Wmax* differed by more than a factor of three. Reiter and coworkers argued that residual stresses represent an extra driving force for dewetting that adds up to the capillary forces acting at the contact line. In the course of aging these stresses tend to disappear, as the local chain conformations will adopt conformations closer to their equilibrium.

At this point, it is important to note that one should be cautious when comparing the observed thin film behavior of spin-coated films to equilibrated systems. The aging behavior of the stresses associated with local chain conformations is of different origin compared with physical aging in which systems starting from an equilibrated melt state and cooled below *Tg* relax slowly towards equilibrium. However, a detailed comparison

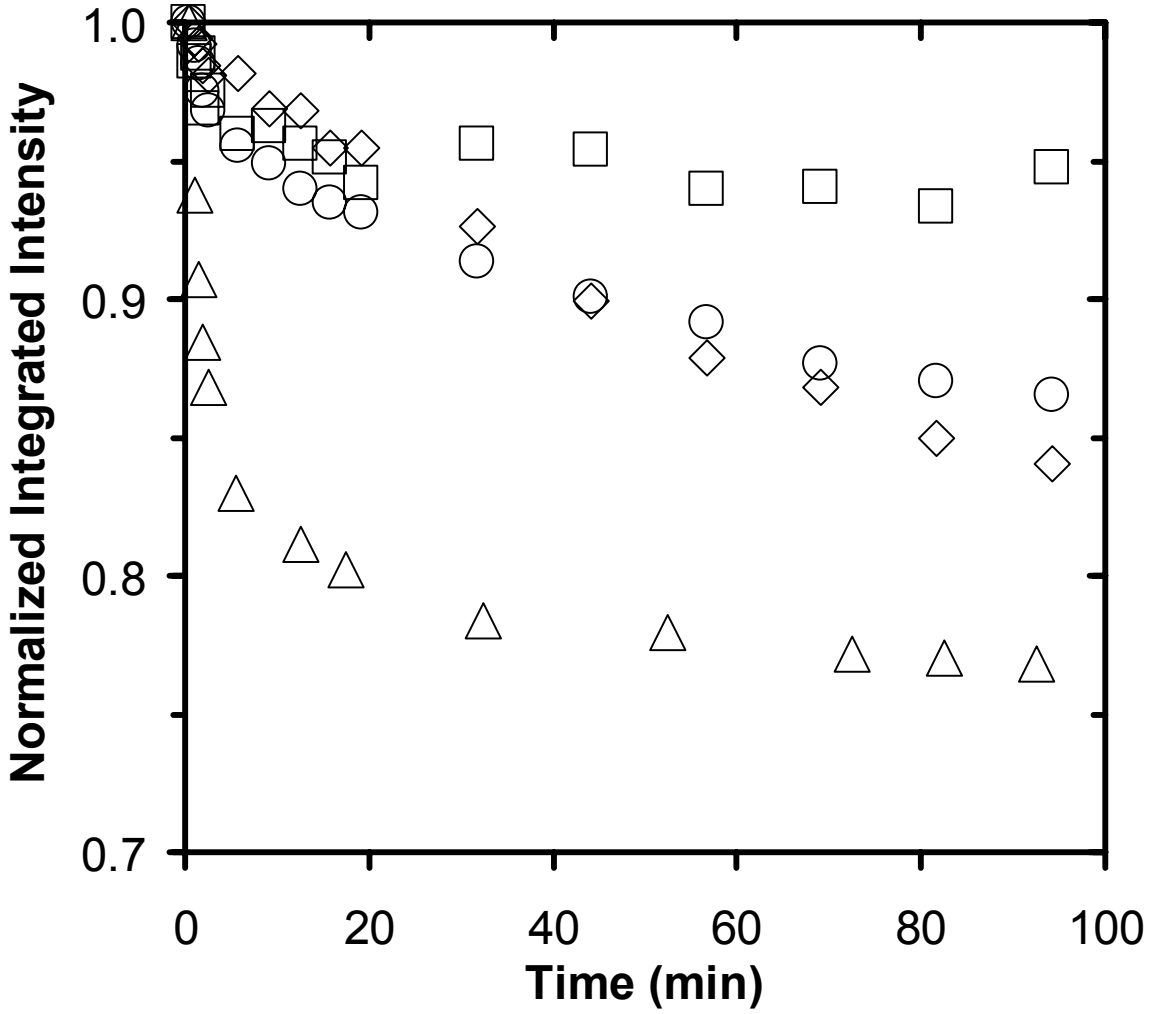

Figure 11-7: Relaxation of integrated intrinsic fluorescence intensity as a function of annealing time for 500-nm-thick film of PS (*Mn* = 290, 000 g/mol) aged at room temperature for 0 days (Δ), 50 days (◊), 80 days (○), and 150 days (□) at *Tg* + 10K.

of aging effects observed under different conditions may shed light on the fundamental relaxation processes in polymeric glasses and even on the nature of *Tg* itself.

11.4 Conclusions

In this chapter, it is shown that intrinsic fluorescence is a powerful tool for determining the annealing conditions needed to relax the unequilibrated local conformational populations that result in spin-coated PS and S/MMA copolymer films. The residual stresses induced by spin coating affect the conformational populations in the polymers; those populations affect excimer and monomer fluorescence, which in turn affect the integrated fluorescence intensity. Partial stress relaxation occurs during heating in the glassy state of thin and ultrathin films. However, with the heating protocol used here and as characterized by intrinsic fluorescence, full relaxation of the stresses induced by spin coating does not generally occur until the films, both thin and ultrathin, are heated to ~ 15-20 K above *Tg*. (In contrast, extrinsic probe fluorescence yields little sensitivity to residual stresses and their relaxation.) It is also demonstrated that many tens of minutes are required to achieve or nearly achieve a steady-state local conformational population in films when annealed at *Tg* + 10 K, with no impact of molecular weight. Finally, it is also shown that stresses associated with local chain conformations may be relaxed to a certain extent for samples stored or aged below *Tg*. These results, coupled with the characterization of the *Tg*-nanoconfinement effect, indicate that many observations of modified *Tg*-behavior in confined films are not caused by spin-coating induced stresses. Instead, the *Tg*-nanoconfinement effect is present in many polymers with well-equilibrated local conformational populations.

CHAPTER 12

EFFECT OF LOW MOLECULAR WEIGHT DILUENT ON Tg AND RELATED RELAXATION BEHAVIOR: DIRECT COMPARISON OF α-RELAXATION DYNAMICS, BREADTH OF RELAXATION TIMES DISTRIBUTION AND SIZE SCALE OF COOPERATIVELY REARRANGING REGIONS PROBED BY SECOND HARMONIC GENERATION AND DSC

12.1 Introduction

The alpha relaxation (α-relaxation) is a relaxation process that is associated with local segmental motion of repeat units along the chain backbone. It is the dominant relaxation process observed in polymers and is termed as the primary relaxation. The α-relaxation process is believed to be caused by the cooperative segmental motion of ~ 30-300 chain segments along the polymer backbone (Sperling 1992; Schmidt-Rohr 1991; Reinsberg 2001; Hempel 2000; Merabia 2004; Ellison 2005a). It is the relaxation process associated with glass transition temperature (*Tg*). Even low molecular weight glass formers exhibit the primary relaxation process (Gotze 1992). An understanding of the α-relaxation process is important as it constitutes the fundamental relaxation process underlying the molecular physics associated with *Tg*. Often, studies of the α-relaxation process involve adding low molecular weight diluents to modify the relaxation response systematically to understand the underlying physics. The same approach is followed here, but instead of simply measuring the α-relaxation as a function of the diluent content which is usually the case in the literature, an in-depth analysis of relaxation dynamics and closely related concepts such as cooperatively rearranging regions (CRRs) and the breadth of the relaxation times distribution is also provided.

This chapter provides the first direct quantitative analysis of the impact of diluent content in modifying the distribution of relaxation times, fragility and the length scale of

cooperative dynamics in various systems. This chapter also provides the correlation between the size scale of CRRs to the width or distribution of the α-relaxation spectrum and fragility index.

12.2 Background

The segmental mobility of the polymer chain is enhanced by addition of small molecule diluents. The increase in the mobility by diluent addition usually results in the reduction of the *Tg* of the polymer-diluent mixture. The chain segments near the diluent molecules may exhibit increased levels of translational and rotational motion due to a reduction in monomeric friction coefficient (Ferry 1980; Sears 1989). The ability to modify the polymer dynamics by varying the concentration of diluent molecules has led to a number of studies in various systems (Ferry 1980; Sears 1989; Bair 1981; Jensen 1998; Zhang 2003; Goodson 1993; Kohler 1990; Chen 1992; Stahelin 1993; Valley 1990). Numerous techniques have been employed to characterize the impact of diluent content on the segmental mobility of polymer matrix using electron spin resonance (Morris 1989; Bullock 1986), nuclear magnetic resonance (Liu 1990), dielectric relaxation spectroscopy (Zhang 2003; Saito 1963; Hains 1975; Dionisio 1993), nonlinear optics (Dhinojwala 1993, 1994a, 1994b), fluorescence anisotropy decay (Barkley 1981; Monnerie 1991), mechanical relaxation (Jensen 1998; Petrie 1972; Ljungberg 2005; Bazuin 1986), etc.

Most of the studies have characterized the impact of diluents on the segmental mobility by studying the impact on the *Tg* as a function of diluent concentration in the polymer matrix. As a result, the effect of addition of diluents on *Tg* reduction is fairly well understood. However, only a small numbers of studies have addressed the impact of diluent content on modifying the segmental relaxation time of the polymer matrix. In his dielectric relaxation study of poly(vinyl chloride) (PVC) with dioctyl phthalate (DOP) as diluent (up to 17.3 % by weight), Saito (Saito 1963) found that neat polymer has a

stronger temperature dependence of the α-relaxation than polymer samples with high diluent content. Morris *et al.* (Morris 1989) found that neat poly(vinyl acetate) (PVAc) has a stronger temperature dependence of the Williams-Landel-Ferry (WLF) function than mixtures of polymer and di-n-butyl phthalate. Likewise, Schausberger *et al.* (Schausberger 1995) found that a weaker temperature dependence of the WLF fit to their mechanical relaxation data was required as the diluent (DOP) content was increased from 0 % to 25 % by weight.

On the other hand, the impact of diluent content in modifying the width or distribution of segmental relaxation spectrum is still poorly understood. Both the free volume (Ferry 1980; Doolittle 1957) and the configurational entropy (DiMarzio 1963) approaches are effective in explaining the reduction in *Tg* upon addition of diluent in polymer matrix; however, they fail to explain the impact on the distribution of relaxation times. The intermolecular chain coupling theory by Roland and Ngai (Ngai 1993, 1998a, 1998b, 2000, 2006; Roland 1992, 1994, 1997), which is based on the idea proposed by Adam and Gibbs (Adam 1965), is effective in explaining the relaxation dynamics in a polymer-diluent system and qualitatively explains the impact on the distribution of relaxation times. Key questions about the local diluent-polymer environment remain unaddressed. Other unanswered questions include the effect of diluent addition on the width of the distribution of relaxation times which is related to the exponent (β_W) in the Kohlrausch-Williams-Watts (KWW) equation, fragility (a concept proposed by Angell (Angell 1991, 1995a, 1997)), and the length scale of cooperative dynamics and the correlation between them.

Fragility is a scaling formalism that was introduced by Angell in 1991 (Angell 1991) for comparison of temperature-dependent viscosity data of low molecular weight glass formers. This concept is important as it provides a fair comparison of the different systems with widely varying *Tg*s and temperature dependencies of relaxation dynamics.

A number of studies (Erwin 2002; Saiter 2004; Solunov 1999; Huang 2002; Hodge 1995, 1996, 1997; Duvvuri 2002, 2004; Roland 2003b; Fitz 1999; McKenna 2003; Huang 2001b; Angell 1995a, 1997, 2000; Bohmer 1993a; Plazek 1991; Pissis 1994; Bartos 1998) have used this concept to understand the critical length scales necessary for understanding the mechanisms of α-relaxations on a molecular scale, i.e., the critical size scale of the cooperative dynamics that is actually involved in the α-relaxation process.

12.3 Second Harmonic Generation - Nonlinear Optics Technique

Second harmonic generation (SHG), a subset of nonlinear optics (NLO), can be used to investigate polymer relaxations. This method requires the use of polar chromophores to generate the SHG signal, and these chromophores may rotate in the amorphous polymer matrix. The dynamics of these rotations are dependent on the specific experimental conditions as well as the nature and physical characteristics of probe and polymer. One can obtain information on polymer dynamics related to the α-relaxation provided the probe rotational dynamics is coupled to the α-relaxation dynamics. Coupling is necessary to insure that the probe motion reliably reflects the polymer relaxation behavior. A more complete treatment of some of the fundamental relationships involving NLO-SHG can be found in the following references: Dhinojwala 1993, 1994a, 1994b; Prasad 1990; Shen 1984; Boyd 1992.

There have been a number of studies to monitor polymer relaxation dynamics using SHG in a variety of polymer matrices using a range of probes. Due to its large bandwidth, this technique is ideally suited for a plasticization study involving the examination of the breadth of distribution of relaxation times near *Tg*. For further details about the NLO-SHG technique employed in this study, refer to Section 12.5.

12.4 Length Scale of Cooperative Dynamics by Differential Scanning Calorimetry

The length scale of CRRs near the glass transition has been investigated by differential scanning calorimetry (DSC) (Donth 1979, 1982, 1999, 1984, 1996, 2000,

2001a; Tran 2004; Korus 1997; Robertson 2004; Mitteilungen 1982; Khale 1999; Ellison 2005a; Hempel 2000; Vyazovkin 2004; Hong 2002), NMR (Barut 1998; Qin 2003; Reinsberg 2001; Tracht 1998), and other techniques (Erwin 2002; Arndt 1996, 1997; Richert 1996), and has been reported to lie in the range of ~ 1 - 5 nm for polymeric glass formers. Here we determine the size of a single CRR at *Tg*,bulk, ξ_{CRR}, using the thermal fluctuation theory and DSC method from Donth *et al.* (Donth 1979, 1982, 1999, 1984, 1996, 2000, 2001a). In this approach,

$$V_{CRR} = \xi^3_{CRR} = k_B Tg(\text{mid})^2 \Delta(1/Cv)/(\rho \delta T^2) \qquad 12.1$$

where V_{CRR} is volume of one CRR, ξ_{CRR} is the size (length scale) of one CRR, k_B is the Boltzmann constant, *Tg*(mid) is the Richardson midpoint *Tg*, $\Delta(1/Cv)$ is the step change in *1/Cv* at the dynamic *Tg*, ρ is the density of bulk polymer, δT is the mean temperature fluctuation of one average CRR, and *Cv* is the heat capacity at constant volume. The number of units present in one CRR (N_{CRR}) is given by the following:

$$N_{CRR} = (\rho V_{CRR} N_A)/Mo \qquad 12.2$$

where N_A is Avogadro's number and *Mo* is the *MW* of a single repeat unit. (For further specific details regarding the determinations of ξ_{CRR} and N_{CRR}, see section 12.5.)

Donth's approach has been described in the literature as being controversial (Erwin 2002) because the associated theoretical analysis has not been verified. While acknowledging this point, this issue was clarified in sufficient detail in Chapter 4 of this thesis, leading experiments that are straightforward and result in estimates of ξ_{CRR} that are consistent with the very few measurements of ξ_{CRR} obtained by NMR, dielectric spectroscopy and other methods.

12.5 Experimental

12.5.1 Materials and Method

Bisphenol-A-polycarbonate (BPAPC) (nominal *Mn* = 18,000 g/mol, *Mw*/*Mn* = 1.56, *Tg*,bulk = 418 K), bisphenol-A-polysulfone (BPAPS) (nominal *Mn* = 20,000 g/mol, *Mw*/*Mn* = 3.28, *Tg*,bulk = 463 K), poly(isobutyl-methacrylate) (PiBMA) (nominal *Mn* = 140,000 g/mol, *Mw*/*Mn* = 2.14, *Tg*,bulk = 327 K), polystyrene (PS) (nominal *Mn* = 120,000 g/mol, *Mw*/*Mn* = 3.58, *Tg*,bulk = 373 K), and poly(methyl acrylate) (PMA) (nominal *Mn* = 11,000 g/mol, *Mw*/*Mn* = 2.89, *Tg*,bulk = 277 K) were purchased from Scientific Polymer Products as secondary standards and were used as received. Disperse Red 1 (DR1) from Aldrich was recrystallized twice using toluene. N,N-diphenylamino-4-nitroazobenzene (also called Diphenyl Disperse Red 4, DPDR4) was donated by Dr. R. D. Miller and Dr. D. M. Burland (IBM Almaden Research Labs). All *Tg*,bulk values were measured as *Tg*,onset values by differential scanning calorimetry (Mettler Toledo DSC822) on second heat at a rate of 10 K/min.

Various combinations of diluents (0.5 – 10 wt% with respect to the weight of the polymer) and polymer (3 – 7 wt% polymer in solvent) were co-dissolved in chloroform. Each solution was spin coated (at 300 – 1000 rpm) onto either glass or a quartz substrate using a Headway Research spin coater. Typical film thicknesses were 2 – 4 μm. The final film thickness and film surface quality was controlled by spin speed, solvent choice, and polymer solution concentration (Hall 1998a). The films were dried under vacuum for 12 hr at room temperature and at a temperature slightly above *Tg* of the film (without excessive probe sublimation). Film thickness was measured with a Tencor P10 profilometer (calibrated using a 14-nm-step-height standard from VLSI standards).

As the spin coated samples are essentially isotropic, it is necessary to somehow align or introduce some directionality in the probe orientation so that significant changes in SHG signal can be observed. This is done by a “poling” procedure in which the

system is heated to *Tg* + 10 K and then a poling field or an electric field is applied. The dipolar chromophoric entities partially align with respect to the direction of the electric field. After this, the system temperature is reduced to measurement temperature of interest, the electric field is removed and changes in SHG signal intensity are observed. An in-plane/contact poling method was used. For further details see references (Dhinojwala 1993, 1994a, 1994b) or thesis by Hamilton (Hamilton 1996).

For the SHG measurements, the fundamental beam was generated using a Q-switched Nd:YAG laser with a wavelength of 1064 nm and a pulse frequency or 10 Hz . The beam was split by a partially silvered surface into two arms, a reference arm and a sample arm. Because a y-cut quartz yields a temporally stable SHG signal, it was used as a reference sample to measure simultaneously its signal as compared to the SHG signal from the polymer sample. The fundamental infrared beam was removed with a filter leaving only the SHG beam to be focused through a pair of cylindrical lenses and onto the monochromator tuned to 532 nm. The optical signal was then converted to an electrical signal by the photomultiplier tube. One hundred laser pulses from each laser arm were measured and averaged with a boxcar (Stanford Research SR250) and computer interface (Stanford Research SR245) in order to enhance the signal-to-noise ratio. The intensity of the incident, fundamental beam was controlled by the rotation of a pair of polarizers within the optical setup. This same type of experimental setup has been used by essentially every other group measuring SHG. With this approach and protocol, the shortest relaxation time possible is on the order of 10 seconds (100 pulse/10 Hz). To obtain measurement on time scale shorter than 10 seconds, a delay-trigger SHG method was used.

The method used by Levine (Levine 1976) was modified to encompass a broader time window so that accurate measurements of polymer dynamics can be made. The delay-trigger method has been adapted such that delay times ranging from 5 μs to 2 s is

available. This is accomplished by moving the electric field window with respect to fixed 10 Hz laser pulse. Slightly different protocols were used to collect SHG data at the various time scales depending on the delay time. The key feature is that the chromophore orientation is reset between laser pulses, which enables the investigation of probe orientation at very short times. The delay-trigger method can be used in conjunction with conventional methods to yield measurements of truly broad relaxation spectra (10^{-6} to 10^{6} seconds). It is possible to measure the dynamics as the field is removed (decay mode) and applied (onset mode). In a previous study (Hamilton 1996), the probe dynamics in the polymer have been shown to be identical during the decay and onset mode.

The value of $\chi^{(2)}_{ZZZ}$ (the second order nonlinear bulk susceptibility) is sensitive to the net chromophores orientation. A noncentrosymmetric structure is required to have a nonzero $\chi^{(2)}_{ZZZ}$ which may be obtained by partially aligning the chromophores doped into an amorphous matrix with a DC-electric field. When the field is removed, the chromophores relax to an isotropic state, and $\chi^{(2)}_{ZZZ}$ decays to zero. As $\chi^{(2)}_{ZZZ}$ cannot be measured directly, it is necessary to measure the SHG intensity, $I(2\omega)$. The two quantities are related by the following equation:

$$(I(2\omega))^{0.5} \propto \chi^{(2)}_{ZZZ} \propto NE_Z[(\mu\beta_Z)/(5k_BT) + \gamma] \qquad 12.3$$

where E_Z is the electric field applied in the z-direction, μ is the chromophores dipole, β_Z is the microscopic first hyperpolarizability, N is the number density of the chromophores within the medium, k_B is the Boltzmann constant, T is the temperature, and γ indicates the second harmonic signal that emerges after an interaction of the DC field with the incident ω laser beam, which is the SHG contribution due to the presence of a DC-electric field. The DC-electric field effect is taken into account by normalizing $\chi^{(2)}_{ZZZ}$ with respect to

its initial value (t = 0). The normalized orientational component of SHG signal, $\chi^{(2)}_{NO}$ obtained is the second harmonic signal attributed solely to the dipole orientation.

As the relaxations in polymers do not conform to a single exponential decay in either the rubbery or glassy regions, it is common to use a stretched exponential expression (also known as the Kohlrausch-Williams-Watts or KWW equation) to fit the data. In the case of SHG data,

$$\chi^{(2)}_{NO} = \exp\left(-(t/\tau)^{\beta_W}\right) \qquad 12.4$$

where τ is the characteristic time constant and β_W (with $0 < \beta_W < 1$) is related to the width of the relaxation spectrum. The value of β_W =1.0 corresponds to a single exponential decay, as β_W is lowered below 1.0, the distribution of relaxation times becomes increasingly broad and β_W = 0 corresponds to an infinitely broad relaxation distribution. An average relaxation time constant may be obtained with the following equation:

$$\langle \tau \rangle = {}_0\int^{\infty} \exp\left(-(t/\tau)^{\beta_W}\right) dt = (\tau/\beta_W)\Gamma((\tau/\beta_W)) \qquad 12.5$$

where Γ is gamma function. (Further details about the NLO-SHG technique employed here can be found in the following references by Torkelson research group (Dhinojwala 1993, 1994a, 1994b).)

Differential scanning calorimetry (Mettler Toledo DSC822) was used to measure the heat capacity for the determination of the size of the CRR. Initially, the furnace was heated to 973 K in the presence of oxygen to oxidize any impurity present from previous use. Specific heat capacities were measured against a sapphire standard. A blank pan was run followed by a sapphire standard immediately prior to characterization of each polymer sample. The calibration of the DSC instrument was regularly monitored via an indium standard. All DSC measurements were taken on the second heating (10 K/min) cycle after quenching (40 K/min) from elevated temperature. Samples were annealed for

at least 45 min at the elevated temperature (Tg + 70 K) before quenching to erase prior thermal history and, even more importantly, to optimize sample-pan contact. Unless otherwise specified, all thermograms used in heat capacity measurements and thereby the determination of the size of the CRR were taken from Tg,bulk – 70 K to Tg,bulk + 70 K in order to measure baselines accurately.

Differential scanning calorimetry thermograms were used to determine the unknown parameters for the fluctuation formula (Equation 12.1) (Donth 1982, 1996; Hempel 2000). Equation 12.2 was used for the calculation of the number of repeat units present in one CRR.

In Donth's construction, $\Delta(1/Cv)$ is estimated to be $\Delta(1/Cp)$ where Cp is the constant pressure heat capacity. The error in this estimation may be summarized by a parameter S where $S = \Delta(1/Cv)/\ \Delta(1/Cp)$ (Hempel 2000). From literature references (O'Reilly 1962, 1977a, 1977b), Donth estimated (Hempel 2000) that $S = 0.74 \pm 0.22$ for fourteen different polymers and four different small molecule glass formers with the S value extrema at 1.07 and 0.26. Donth used the average S parameter to make corrections to all of his V_{CRR} and ξ_{CRR} data. We have not made this correction to our V_{CRR} and ξ_{CRR} data to avoid overgeneralization of how Cp relates to Cv for all of our samples.

For small heat capacity steps across Tg, $\Delta(1/Cp) \approx \Delta Cp/Cp^{2}$ where ΔCp is the difference between the rubbery and glassy state heat capacities at Tg(mid) and Cp is the average of the rubbery and glassy state heat capacities at Tg(mid). Figure 4-1 (Chapter 4) shows Cp as a function of temperature for a PS sample. The values of Cp in the rubbery and glassy regions are obtained by extending tangents of $Cp(T)$ from deep in the rubbery and glassy states and are identified as the intersection points of the extrapolated lines with Tg(mid) as shown in Figure 4-1 (Chapter 4). ΔCp is determined by $\Delta Cp = Cp$(rubbery) - Cp(glassy), while Cp is obtained by $Cp = \{Cp(\text{rubbery}) + Cp(\text{glassy})\}/2$.

The experimental approach for determining the size of the CRR using a regular

DSC method involves some "rules of thumb" for determining the δT parameter prescribed by Donth (rather than the more rigorous method by Donth involving determination of δT from the KWW exponent in conjunction with measurements by thermally modulated DSC); he has argued that the accuracy of the characteristic size of a CRR is estimated to be within 85% and 125% of the calculated value. The "rule of thumb" for using DSC heating curves to obtain δT is that $\delta T = \Delta T / 2.5$, where ΔT is the temperature interval where the specific heat capacity thermogram varies between 16% and 84 % of the ΔCp step as shown in Figure 4-1, Chapter 4. As described above, exactly the same procedure was applied to all the measurements. In all cases, the bulk polymer *Mo* and ρ (Stahelin 1993; Morris 1989) values were used in the fluctuation formula. For all experiments in this study, the average standard deviations (expressed as a percentage of the average value) for ΔCp, Cp, ΔT, Tg(mid), ξ_{CRR}, N_{CRR} were 7.6, 7.4, 13.2, 0.27, 9.5 and 16.4 %, respectively.

40 μL aluminum DSC pans were used for all experiments. Sample pans were prepared in such a way that the mass of sample in each pan was close to 10 mg. All samples were annealed at temperatures of at least Tg + 100 K for 45 min in order to maximize sample-pan thermal contact. This was found to be critical in attaining quality, reproducible results. All measurements were taken on second heat with a constant heating rate of 10 K/min after quenching from above Tg at 40 K/min.

At least six measurements were made for each sample. The reported values are averages of all of these measurements. A blank pan and a sapphire standard were run immediately before every sample measurement in order to capture accurately the current state of instrument operation. (The blank sample curves were observed to vary slightly during the course of many measurements. This variation is normal and was within that expected by the equipment manufacturer, but if not appropriately accounted for, the variation can have large impact on heat capacity measurements.) The same blank sample

and sapphire standard were used for all measurements. The instrument calibration was checked with an indium standard after every six measurements.

12.6 Direct Comparison of α-Relaxation Dynamics, Breadth of Relaxation Times Distribution and Size Scale of Cooperatively Rearranging Regions Probed by Second Harmonic Generation and DSC

Figure 12-1 shows the repeat unit structure of polymers: (3) bisphenol-A-polycarbonate (BPAPC), (4) bisphenol-A-polysulfone (BPAPS), (5) poly(isobutyl-methacrylate) (PiBMA), (6) polystyrene (PS) and (7) poly(methyl acrylate) (PMA) and the repeat unit structures of (1) Disperse Red 1 (DR1) and (2) diphenyl Disperse Red 4 (DPDR4) which were used as diluents in this study.

Disperse Red 1 was chosen as a diluent because it also functions as a SHG chromophore. Disperse Red 1 exhibits different degrees of plasticization in PiBMA, PS and BPAPC systems, as evident by the data presented in Figure 12-2. Bulk *Tg* is depressed by 30 K by 10 wt% DR1 in BPAPC but by only 1.5 K in PiBMA for the same amount of diluent. These data are most conveniently compared in a diluent effectiveness plot (Figure 12-2) where the DSC measured glass transition temperature of plasticized systems (polymer and DR1) normalized by the *Tg* of the unplasticized polymer is plotted as a function of diluent content. Disperse Red 1 plasticization exhibits decreasing effectiveness in going from BPAPC to PS to PiBMA which can be explained by Gibbs-DiMarzio theory (DiMarzio 1959, 1963; Gibbs 1958); the plasticization data correlate well qualitatively with information on polymer chain stiffness. Because BPAPC has a more rigid backbone chain than PiBMA by virtue of an increased level of aromaticity, DR1 provides more configurational entropy to BPAPC than PiBMA resulting in the observed differences in *Tg* depression. Since the DR1/BPAPC plasticization effect is so large, this system appears to be an ideal case to answer the unresolved issues including the effect of plasticization on the width of the distribution of relaxation times, which is

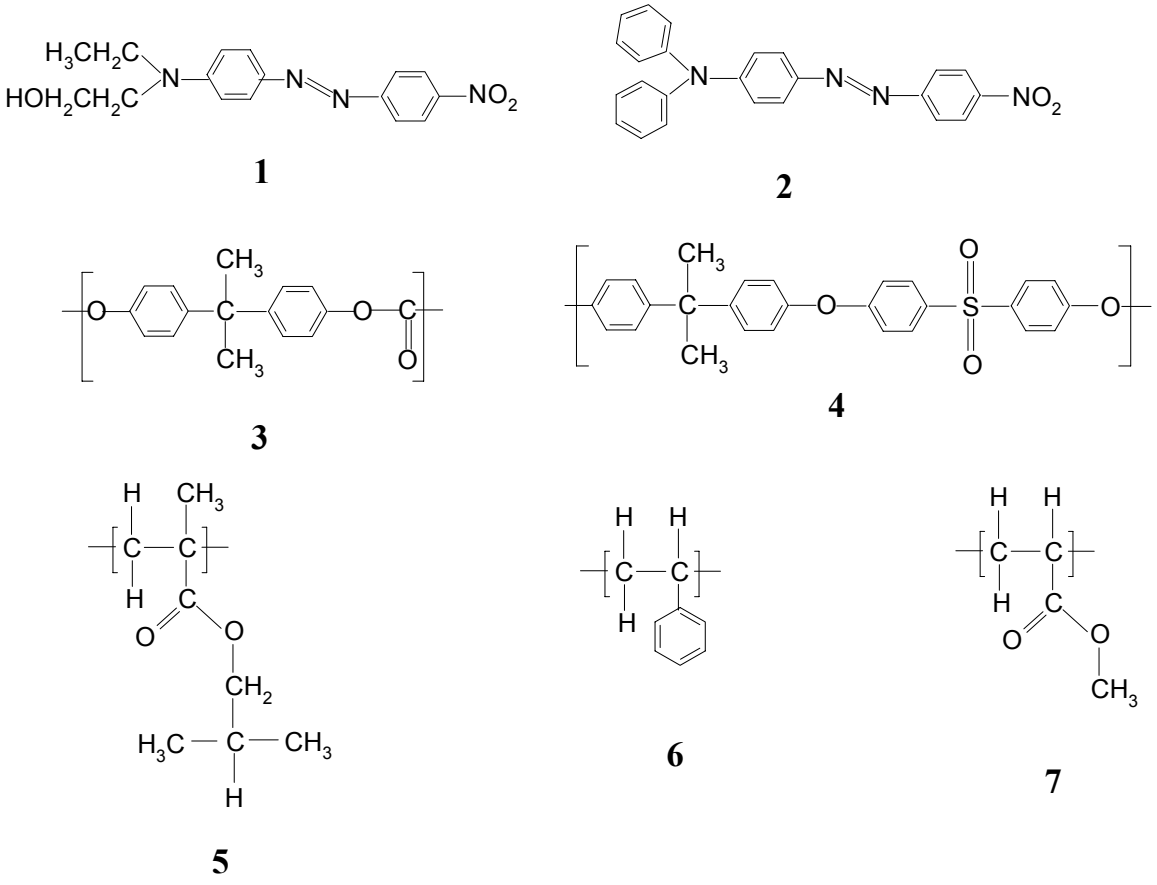

Figure 12-1: The repeat unit structures of plasticizer Disperse Red 1 (DR1) and diphenyl Disperse Red 4 (DPDR4) and polymers bisphenol-A-polycarbonate (BPAPC), bisphenol-A-polysulfone (BPAPS), poly(isobutyl-methacrylate) (PiBMA), polystyrene (PS) and poly(methyl acrylate).examined in this plasticization study (names in chronological order).

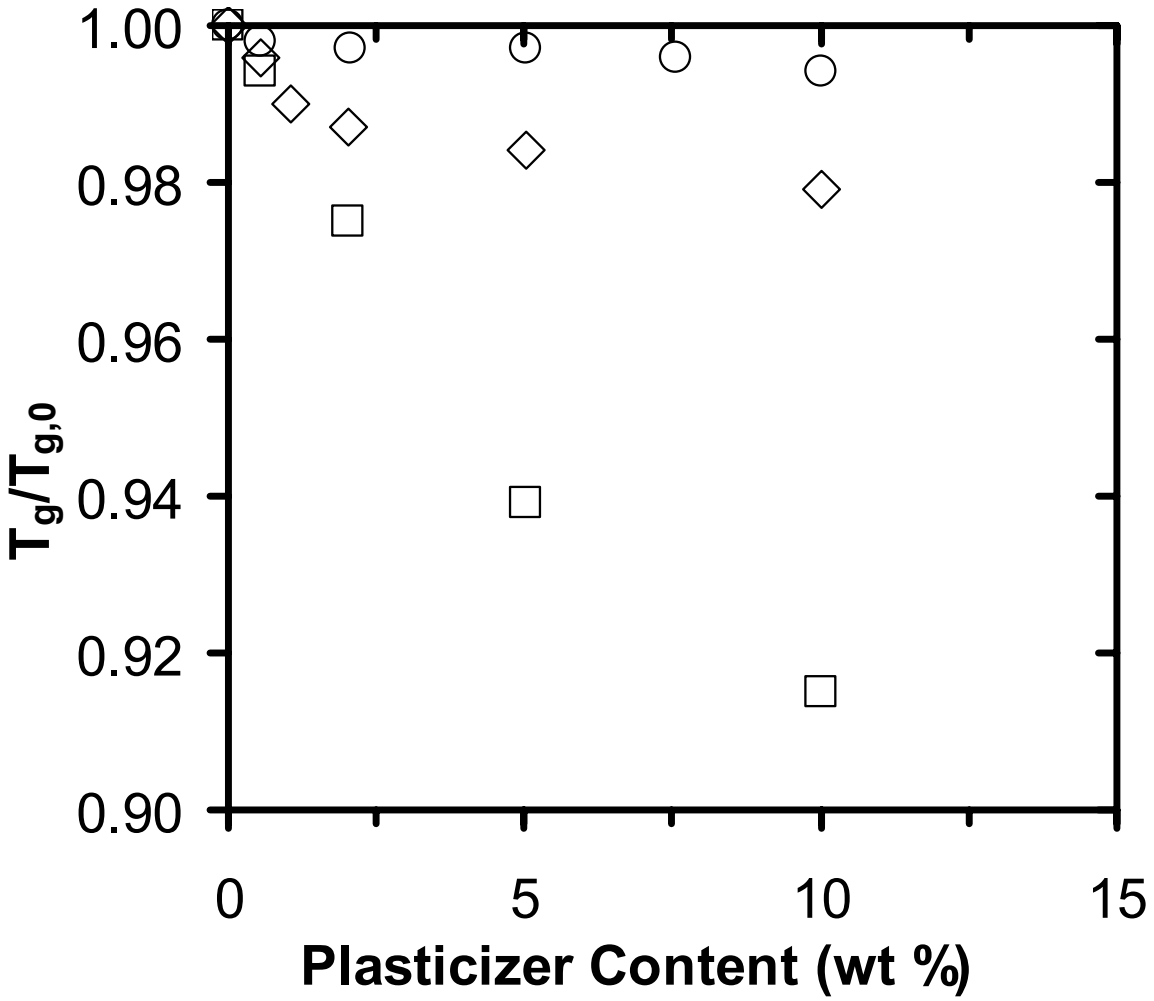

Figure 12-2: Plasticization of BPAPC (□), PS (◊), and PiBMA (○) by DR1. Data normalized to the *Tg* of the neat polymer. Both *Tg* and *Tg,0* measured on an absolute temperature scale (K).

related to the exponent βw in the KWW equation and the length scale of cooperatively rearranging regions.

The average relaxation times of the probe rotation for the nearly unplasticized case (0.5 wt% DR1) in BPAPC have been compared to the dielectric relaxation measurements of neat BPAPC (Ishida 1961) and the temperature dependence of viscosity for neat BPAPC system (Mercier 1965). Qualitatively there is a good agreement between the dielectric measurements and SHG rotational times. The temperature dependence of the viscosity measurements also agrees well with the temperature dependence of the rotational correlation times of DR1 in BPAPC, and these data may be fitted to a WLF expression with reasonable C_1 and C_2 values. Moreover, the glassy regime can be fitted to an apparent Arrhenius temperature dependence with reasonable activation energy values. Therefore, it is possible to assert that rotational motions of DR1 are coupled to the segmental motions of the α-relaxation in BPAPC.

The direct comparison of typical SHG relaxation spectra indicate clearly that there are true differences in the width of the distribution of relaxation times as a function of diluent content, and these trends are not simply numerical artifacts of the fitting procedure. This is made obvious by examining a typical fit obtained by a direct comparison of the two spectra, with different diluent content, at the same Tg/T values. For instance, Figure 12-3 compares directly the relaxation spectrum of the 10 wt% DR1/BPAPC to the 0.5 wt% DR1 plasticized BPAPC system best fit to the KWW curve. This comparison distinctly shows the differences in the breadth of the distribution of relaxation times exist at temperatures above, below, and at Tg. In each case the relaxation spectra of the heavily plasticized systems are narrower than relaxation spectra for the nearly unplasticized systems.

Figure 12-4 shows that the plot of average relaxation times as a function of reciprocal temperature and diluent content provides an excellent indication of the degree

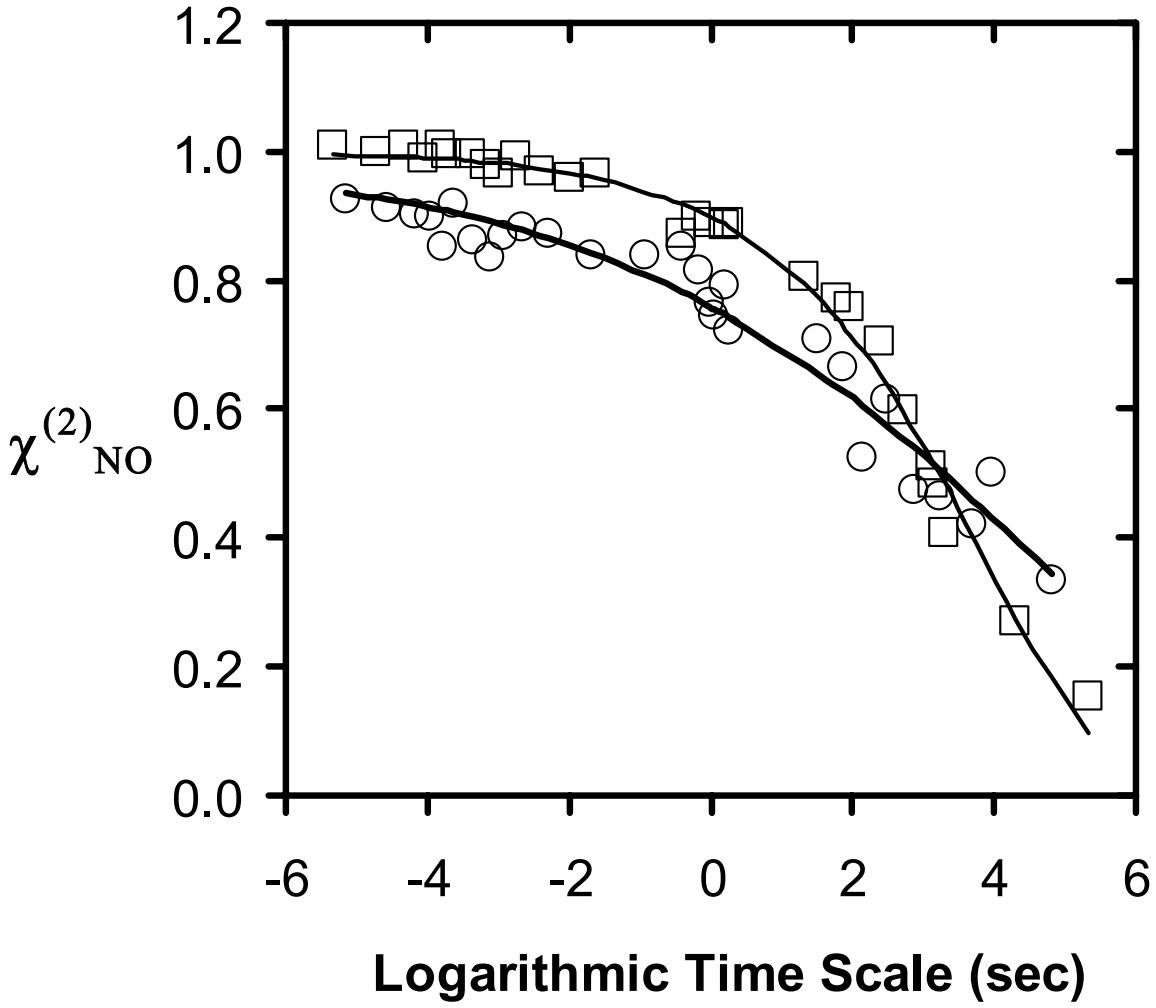

Figure 12-3: Comparison of SHG decay curves for 10 wt % DR1 (□) and 0.5 wt % DR1 (○) plasticized BPAPC in the glassy regime (at Tg/T = .1.05 to 1.06). Bold and thin curves represent Kohlrausch-Williams-Watts (KWW) best fits for 10 wt % and 0.5 wt % DR1 in BPAPC, respectively.

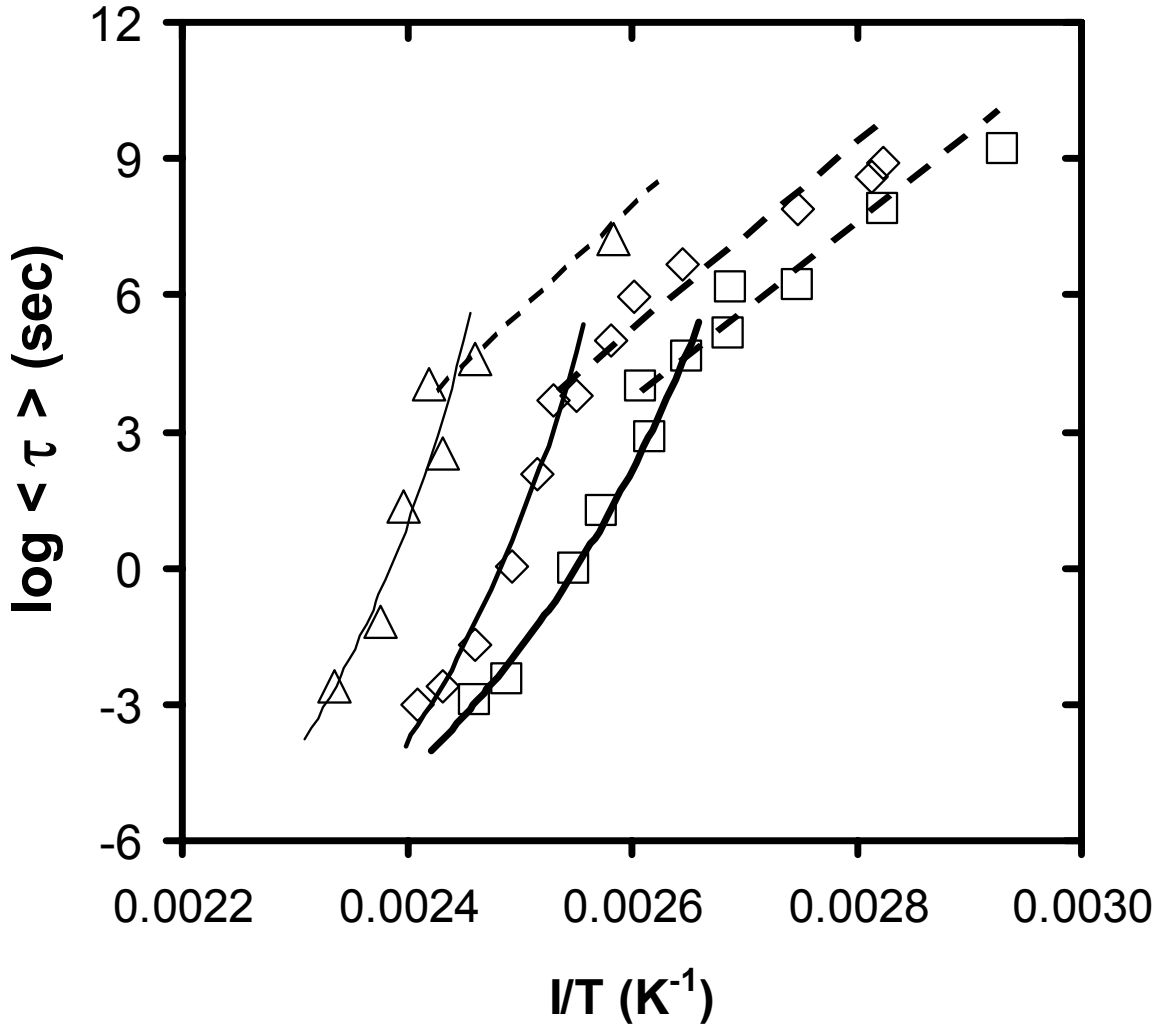

Figure 12-4: The average rotational relaxation times as a function of reciprocal temperature scale for 10 wt % DR1 (□), 5 wt % DR1 (◊), and 2 - 0.5 wt % DR1 (Δ) in BPAPC. The straight lines represents apparent Arrhenius curve fits. The curved lines represents WLF curve fits.

of plasticization and large differences in relaxation behavior. For instance, at 403 K, the average relaxation times for 10 wt% and 0.5 wt% DR1 in BPAPC differ by approximately seven orders or magnitude in time. Upon close examination of the data on the reciprocal temperature plot and with the limited data available, it is possible to assert that there are differences in the temperature dependence of the α-relaxation in the plasticized systems. Each of the plasticized systems may be fitted to separate WLF curves indicating that there is weaker temperature dependence in the heavily plasticized cases in comparison to the weakly plasticized systems. A lower temperature dependence would imply that there is a corresponding reduction in the amount of polymer segmental cooperativity.

Changes in the fragility of DR1/BPAPC systems can be observed once the relaxation data for varying degrees of chromophore content are rescaled on a Tg/T plot. This suggests that the diluent molecules present at the levels studied reduce the ability of the chain segments to interact and couple intermolecularly. This behavior is consistent with what one would expect for significant changes in the size of the CRRs. Hence, we believe the differences in temperature dependencies for the systems with various diluent contents are real, and they agree with the finding regarding the width in the relaxation distribution for these systems. In addition to the findings in the current SHG study, a selected number of studies have indicated that there are different temperature dependencies for the average α-relaxation times of a system with diluent relative to a system without diluent (Morris 1989; Saito 1963; Schausberger 1995). Similar to average α-relaxation times, changes in the temperature dependence of bulk resistivity have also been observed for polymeric materials by addition of diluents (van Turnhout 1975). The temperature dependence and corresponding local apparent Arrhenius activation energies were reduced with increasing amount of low molecular additives (such as di-n-butylphthalate).

Up to this point, the question of whether a diluent is capable of increasing or decreasing the width of the distribution of relaxation times has not been studied systematically. An increase in the distribution width indicates that the local chemical environment surrounding individual probe molecules has become less homogeneous yielding relaxation at an enhanced range of times; in contrast, a decrease indicates that fewer relaxation modes are available to the local segmental motion. A reasonably effective measure of this phenomenon is the comparison of the KWW βw parameter.

Figure 12-5 displays a normalized Tg/T plot of βw obtained over a range of temperatures for the 0.5, 2, 5 and 10 wt% DR1/BPAPC systems. From this, it is clear that different degrees of diluent addition show substantial and systematic differences. As the diluent loading increases, at a given Tg/T value, the βw parameter systematically increases indicating a corresponding decrease in the width of the distribution of relaxation times. This must be due to the differences in the local/microscopic environment surrounding the chromophore; 10 wt% DR1/BPAPC is approximately equivalent to one DR1 molecule for every 20 BPAPC chain segments while 0.5 wt% DR1/BPAPC converts approximately to 1 DR1 molecule for every 250 BPAPC chain segments. The presence of diluent in the higher concentration case is such that it is capable of affecting the characteristic length scale of the α-relaxation, which was evident from Figure 12-4. Therefore, the differences in the relaxation time distribution breadth are not startling.

Direct comparison of the KWW βw parameters for various plasticized systems as a function of ξ_{CRR}, N_{CRR} and V_{CRR} is shown in Figure 12-6. (See Table 12-1 for the values of the parameters used in equation 12-1 and 12.2 for estimating ξ_{CRR}, N_{CRR} and V_{CRR} values. Also see the experimental section (section 12.5) for details regarding how the values of some of the parameters were obtained.) No direct correlation between the breadth of the relaxation time distribution and the size scale of cooperatively rearranging

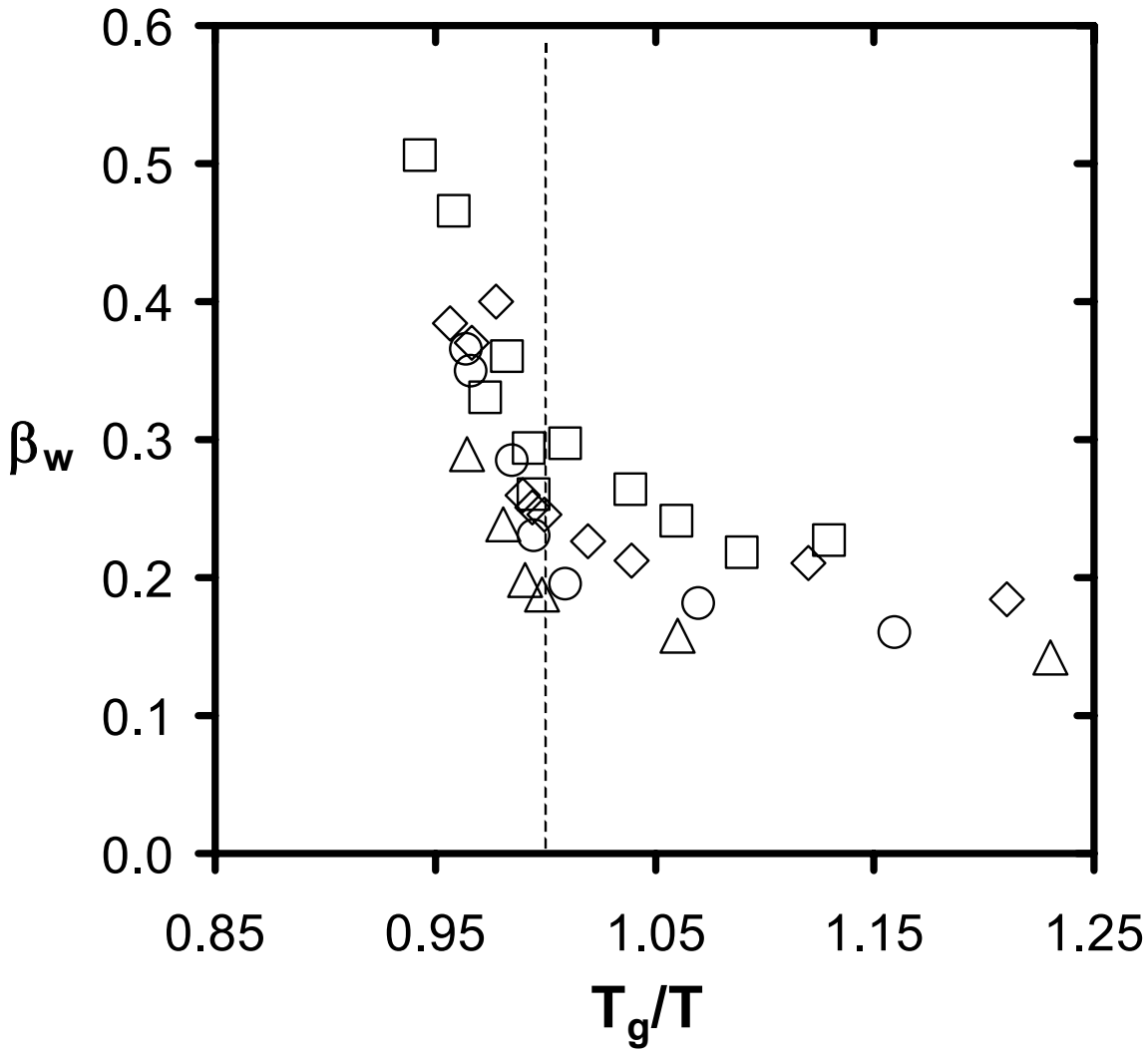

Figure 12-5: The β_W parameters for KWW stretched exponential best fit of SHG decay curve for 10 wt % DR1 (□), 5 wt % DR1 (◊), 2 wt % DR1 (○), and 0.5 wt % DR1 (Δ) in BPAPC on a normalized scale to compensate for the differences in *Tg* for varying degrees of plasticization.

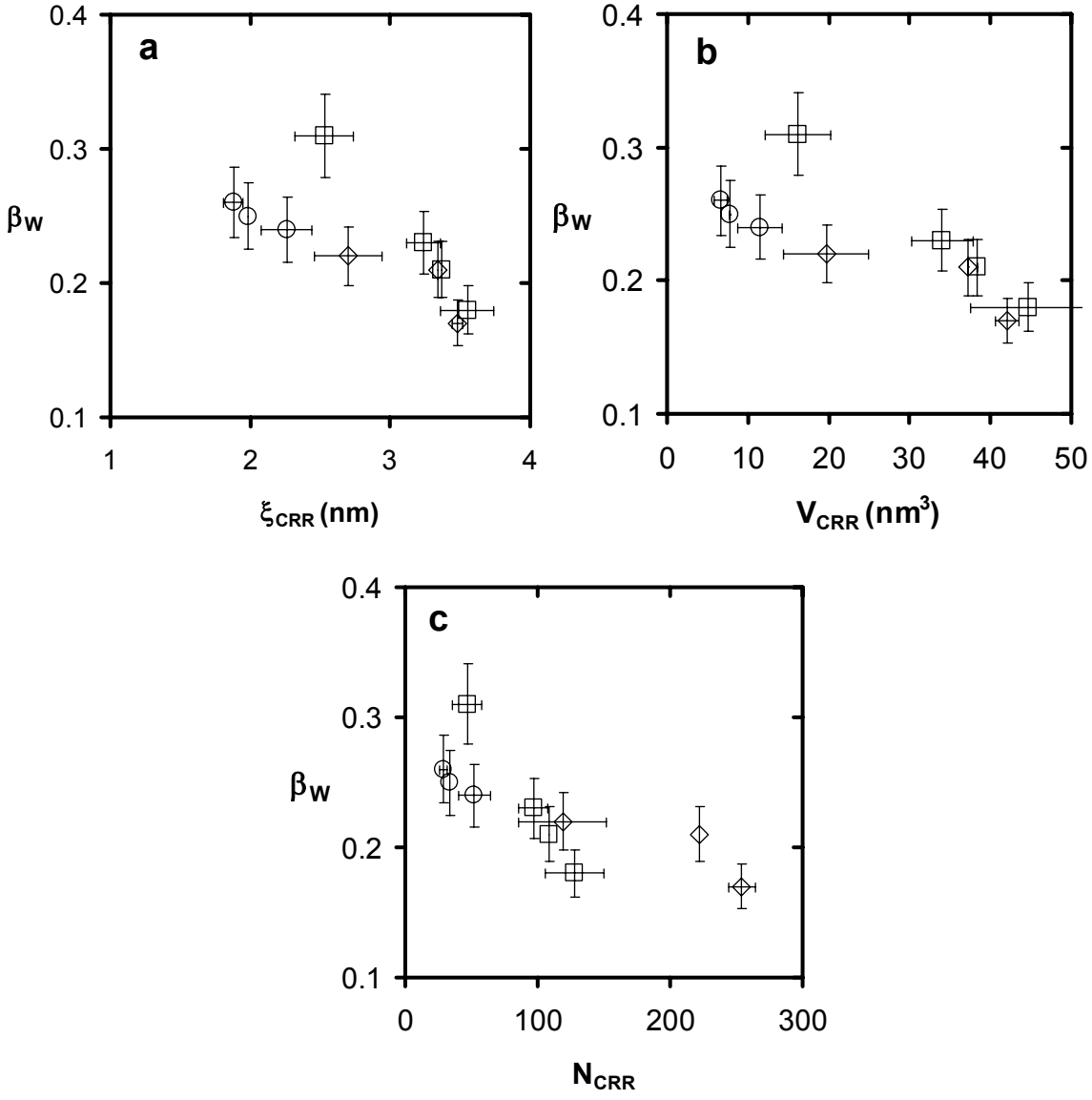

Figure 12-6: **(a-c)** The β_W parameters for KWW stretched exponential best fit of SHG decay curve for BPAPC (□), PS (◊), and PiBMA (○) plasticized with DR1, as a function of length scale of cooperativity (ξ_{CRR}), volume of cooperatively rearranging regions (V_{CRR}), and number of repeat units in one cooperatively rearranging region (N_{CRR}) for varying plasticizer contents. Error bars indicate the standard deviation about the mean of the measured values for a particular polymer and plasticizer composition.

Table 12-1: Sample Parameter Values Leading to the Calculation of ξ_{CRR}[66] and N_{CRR}

System[a]	ΔCp (J/gK)	Cp (J/gK)	δT (K)	*Tg(mid)* (K)	ξ_{CRR}[b] (nm)	N_{CRR}[c]
BPAPC (0-0.5)	0.266	1.444	2.20	415	3.6	128
BPAPC (2)	0.219	1.718	1.92	407	3.4	109
BPAPC (5)	0.231	1.492	2.36	391	3.2	97
BPAPC (10)	0.205	1.605	2.97	390	2.6	47
PS (0-0.5)	0.261	1.741	1.98	377	3.5	249
PS (2)	0.266	1.652	2.20	372	3.3	222
PS (5)	0.331	1.653	3.42	366	2.7	120
PiBMA (0-0.5)	0.189	1.881	2.67	335	2.3	52
PiBMA (2)	0.211	2.641	2.44	334	2.0	34
PiBMA (5)	0.256	1.635	4.57	329	1.9	29

[a] Parenthesis indicates percentage of DR1 added as a plasticizer.

[b] ξ_{CRR} values have been truncated to one digit after the decimal place.

[c] N_{CRR} values have been rounded to the nearest digit.

regions was observed across all the systems. However, a systematic reduction in the breath of α-relaxation time distribution was seen with a reduction in the size scale of the CRRs as well as the number of repeat units involved in the α-relaxation at *Tg*, with varying diluent content within each system. The effect was much stronger in the BPAPC system, which was more effectively plasticized by DR1 as compared with both PS and PiBMA systems.

The fragility index, *m*, or simply fragility can be described as the slope at *Tg* of the curve representing the rubbery-state temperature dependence of log $<\tau>$ on a *Tg*/*T* plot, i.e.,

$$m \equiv \left(\frac{d \log < \tau >}{dT_g / T} \right) = \left(\frac{- d \log < \tau >}{dT_g \diagup T} \right) @ T = T_g \qquad 12.5$$

However, here the fragility is determined solely from the glass transition temperature and WLF parameters, C_1 and C_2 on a *Tg*/*T* scale. We start with the WLF temperature dependence:

$$\log(a_T) = \log\left(\frac{< \tau >}{< \tau >_{T_g}} \right) = \frac{- C_1 (T - T_g)}{C_2 + T - T_g} \qquad 12.6$$

Dividing the numerator and denominator in the final term by *T*, we obtain

$$\log(< \tau >) - \log(< \tau > T_g) = \frac{- C_1 \left(\frac{T_g}{T} - 1 \right)}{\frac{C_2}{T_g} \left(\frac{T_g}{T} \right) + 1 - \frac{T_g}{T}} \qquad 12.7$$

Since, log $<\tau>_{Tg}$ is constant, we can write the following expression by taking the first derivative with respect to Tg/T:

$$\left(\frac{d\log<\tau>}{dT_g/T}\right)=\frac{C_1\left(\frac{T_g}{T}-1\right)}{\frac{C_2}{T_g}\left(\frac{T_g}{T}\right)+1-\frac{T_g}{T}}+\frac{1-\frac{T_g}{T}}{\left[\frac{C_2}{T_g}-1\right]^2} \qquad 12.8$$

By evaluating this expression at $T = Tg$, equation 12.5 simplifies significantly to an expression that is equivalent to the fragility index:

$$m\equiv\left(\frac{d\log<\tau>}{dT_g/T}\right)@T=T_g=\frac{C_1T_g}{C_2} \qquad 12.9$$

This offers a simple comparison of fragility when the WLF parameters already have been obtained. With this alternate definition of fragility, the inverse relationship between m and the breadth of the distribution of relaxation times, associated with βw at Tg, is clear. Apparently, this is due to the fact that both measurements are dependent on polymer chain cooperativity (Bohmer 1993a; Sauer 1992). However, this also allows us to directly compare the m values to the length scales of CRRs for varying diluent content across different polymer systems.

Figure 12-7 compares m for various plasticized system as a function of ξ_{CRR}, N_{CRR} and V_{CRR}. Figure 12-7c demonstrates no systematic correlation between the fragility and the number of repeat units involved in the α-relaxation at Tg, with varying diluent content within each system. However, m decreases with a decrease in the number of repeat units involved in the α-relaxation at Tg across all systems. Figures 12-7a and 12-7b shows the direct correlation between the fragility index and the size scale of cooperatively rearranging regions across all systems with varying diluent contents. All data points across various systems fall onto a linear fit depicting a direct linear

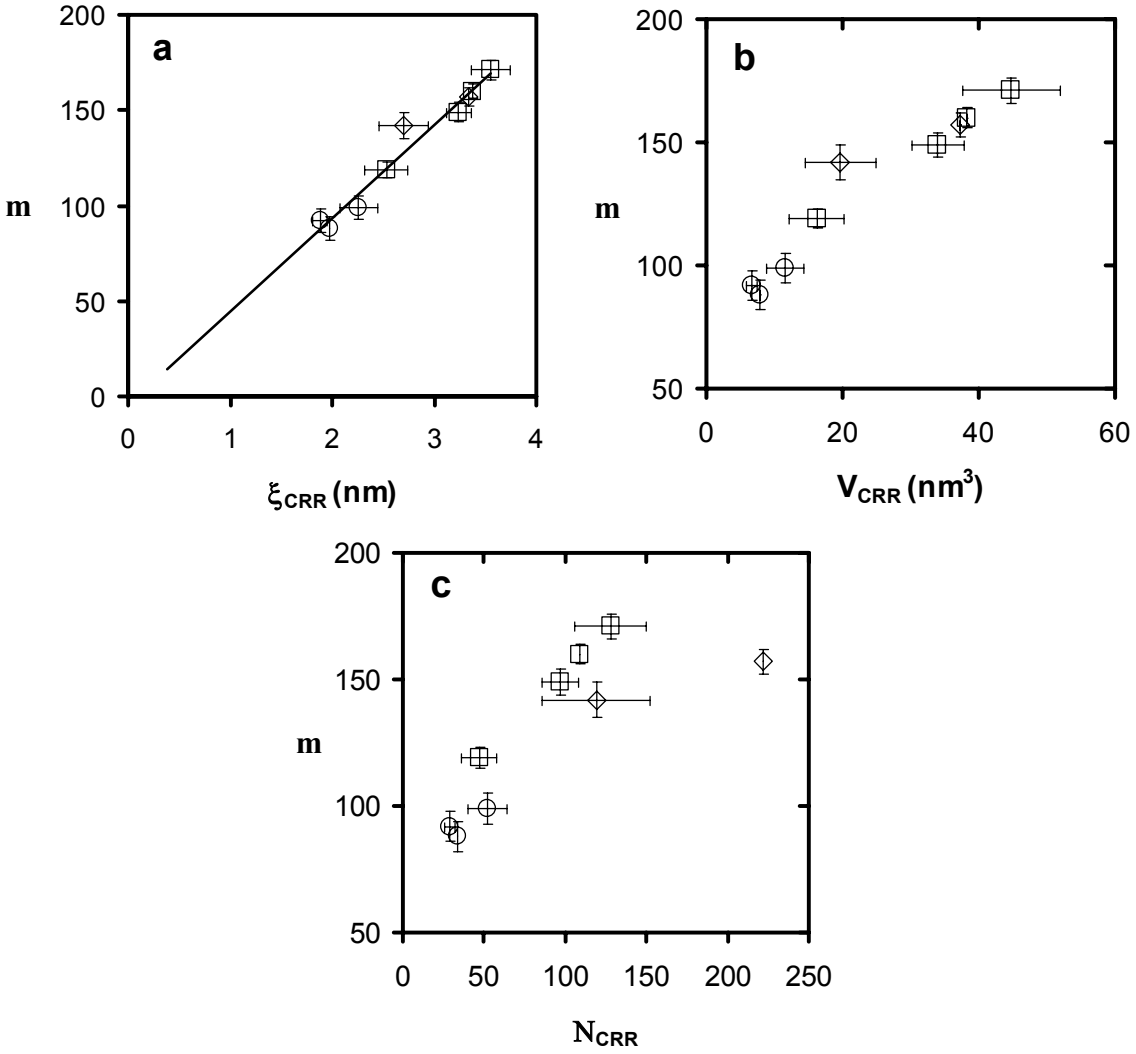

Figure 12-7: **(a-c)** The fragility index (m) for BPAPC (□), PS (◊), and PiBMA (○) plasticized with DR1, as a function of length scale of cooperativity (ξ_{CRR}), volume of cooperatively rearranging regions (V_{CRR}) and number of repeat units in one cooperatively rearranging region (N_{CRR}), for varying plasticizer contents. Error bars indicate the standard deviation about the mean of the measured values for a particular polymer and plasticizer composition. Solid line in plot (a) is the best-fit line to the data.

association between m and ξ_{CRR}.

In a recent study, Erwin and Colby (Erwin 2002), based on limited data from literature, demonstrated a power law relation between m and the cooperative length scale at the Tg. However it is worth mentioning that some of the data obtained by them from the literature have rather large values of CRRs ranging as high as 7.1 to 18 nm for various systems, much bigger than the generally accepted values of 1 - 5 nm (Donth 1979, 1982, 1999, 1984, 1996, 2000, 2001a; Tran 2004; Korus 1997; Robertson 2004; Mitteilungen 1982; Khale 1999; Ellison 2005a; Hempel 2000; Vyazovkin 2004; Hong 2002; Barut 1998; Qin 2003; Reinsberg 2001; Tracht 1998; Arndt 1996, 1997; Richert 1996). These relatively large values for the length scale of CRRs may result in a fit that needs a power law relation between m and ξ_{CRR}. Hence, in this study their data were reanalyzed using a linear fit to draw a meaningful comparison. It is noteworthy that their data fit fairly accurately to a linear fit with correlation coefficient (R^2) value better than 0.86 across fifteen different systems, ranging from low molecular weight organics to polymers and inorganics. This was also true for the data reported at Tg + 10 K in their study. Therefore, when analyzed in a different manner the results by Erwin and Colby (Erwin 2002) can be seen as complementing the results from this study.

By definition, the lower limit of ξ_{CRR} corresponds to roughly 1 ~ 3 repeat units per CRR. If the number of repeat units becomes smaller than that, then each CRR essentially behaves like an independent repeat unit with no need for a cooperative motion. The lower limit for m using the lower limit for ξ_{CRR} from Figure 12-7a generates a value fairly close to the predicted theoretical lower limit of m (Hodge 1996). Thus, even though the linear fit in Figure 12-7a is very simple, it does a good job capturing various aspects of m and ξ_{CRR} and does a good job connecting the two.

So far, it was shown how changing the diluent composition may affect the relaxation processes of various polymers. One can also investigate the effect of varying

the polymer matrices while maintaining a constant probe concentration. Figure 12-8 shows the average rotational reorientation times, $<\tau>$, for freely doped chromophores in five amorphous matrices: PMA, PiBMA, PS, BPAPC and BPAPS. The BPAPS was doped with 5 wt% DRDR4 whereas others were doped with 5 wt% DR1. Due to probe thermal stability/decomposition and probe sublimation, it was not possible to use DR1 in BPAPS and therefore DPDR4 was used in BPAPS. To ensure that DPDR4 is coupled with the α-relaxation for the BPAPS system, SHG relaxation data were compared to the mechanical relaxation data (David 1994) for the BPAPS system, and acceptable agreement was found between the two studies.

From the WLF values of the systems examined here, it is possible to suggest a trend in which the fractional free volume at *Tg* decreases as the polymer *Tg* increases; this would result in an increased amount of cooperativity. Also, as the *Tg* increases from PMA to BPAPS, the temperature dependence of the α-relaxation times in the rubbery region also increases, resulting in a increasing fragility index in going from PMA to BPAPS. It is also noteworthy that addition of these values in Figure 12-7a still results in a linear dependence between m and ξ_{CRR}. Clearly, the polymer chains with higher degrees of aromaticity, chain rigidity and correspondingly higher *Tg* also have higher degrees of cooperativity and fragility.

12.7 Conclusions

The impact of diluent content in modifying the distribution of relaxation times, fragility and the cooperative length scale dynamics has been reported in BPAPC, PiBMA and PS systems. Key questions about the correlation between the size scale of cooperatively rearranging regions (CRRs) to the width or distribution in the relaxation spectrum and fragility have been addressed in a systematic study of DR1 plasticization of these system at various concentrations. A best fit to the KWW curve reveals large changes in the relaxation spectrum of the 10 wt% plasticized DR1/BPAPC system as

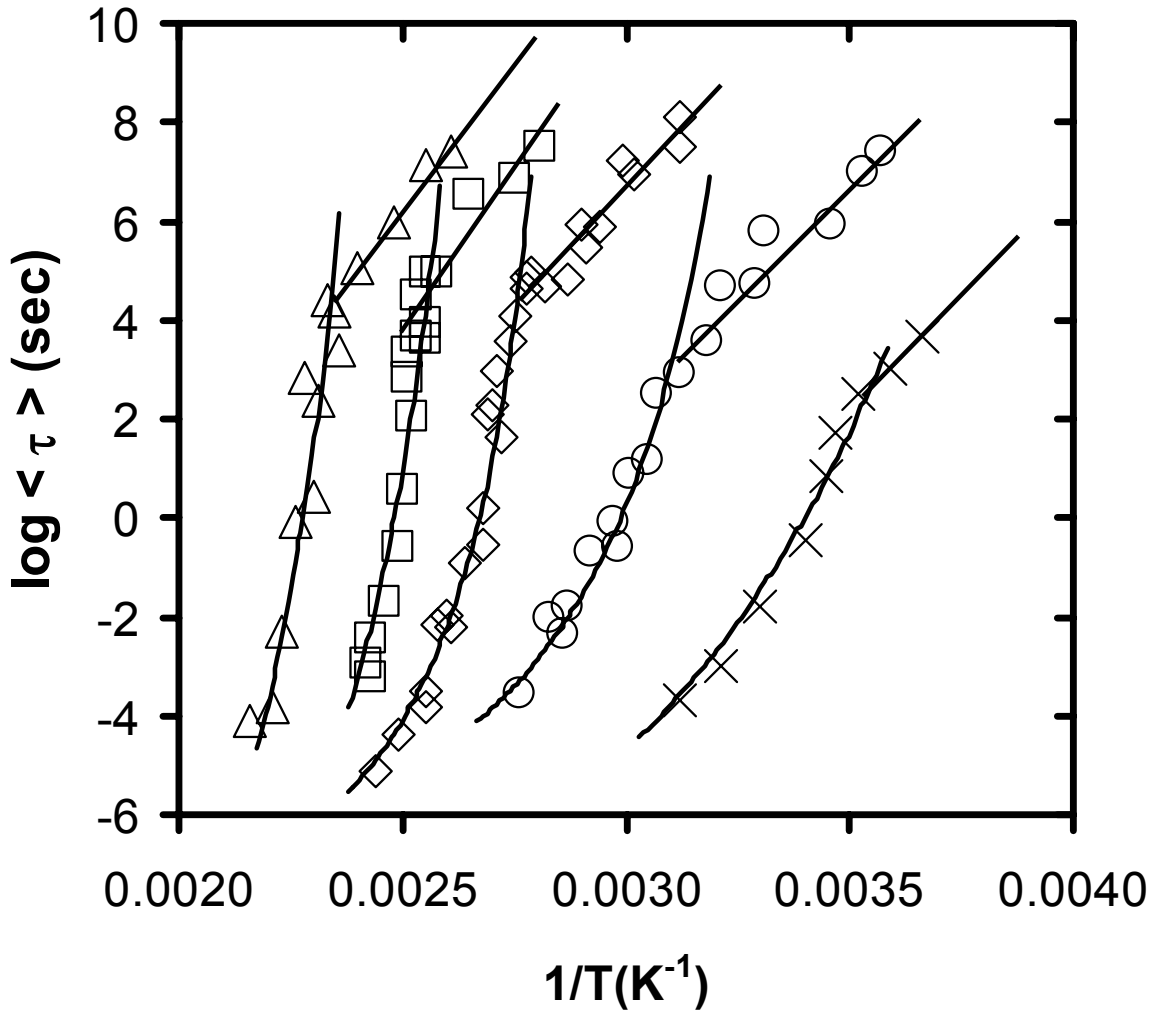

Figure 12-8: The average rotational relaxation times for 5 wt % DR1 in PMA (×), PiBMA (○), PS (◊), BPAPC (□), and 5 wt % DPDR4 in BPAPS (Δ). The solid curves represents WLF curve fits. Dashes lines represent Arrhenius fits.

compared with the 0.5 wt% DR1 plasticized BPAPC system. The relaxation spectrum of the heavily plasticized system was narrower than relaxation spectra for the nearly unplasticized system. Large changes in the average relaxation times as a function diluent content provided an excellent indication of the degree of plasticization and large differences in relaxation behavior. A weaker temperature dependence of WLF curves in the heavily plasticized cases in comparison to the weakly plasticized systems was seen. A systematic increase in the βw parameter was seen with increasing concentration of DR1 from 0.5 to 10 wt%, indicating decrease in the width of the distribution of relaxation times in BPAPS system.

With varying diluent content within each system a reduction in the βw parameter was seen with reduction in ξ_{CRR} as well as the number of repeat units involved in the α-relaxation at *Tg*. A direct linear correlation between *m* and ξ_{CRR} was seen across all systems for all diluent concentrations. The linear fit connecting the size scale and the fragility also does a good job capturing the fundamental theoretical limits of CRRs and fragility. The study of BPAPS and PMA along with BPAPC, PS and PiBMA, with varying chain stiffness and repeat unit structure, also shows that systems with higher degrees of aromaticity, chain rigidity and correspondingly higher *Tg* have higher degrees of cooperativity and fragility, further confirming the direct correlation between the two.

CHAPTER 13

CONCLUSIONS AND RECOMMENDATIONS FOR FUTURE WORK

13.1 Conclusions

Applications of nanoconfined amorphous materials range from diffusion-controlled separation and sensors to microelectronics and nanocomposites. However, when small molecule and polymeric glass formers are confined to the nanoscale, deviations from bulk properties are observed in the glass transition temperature (*Tg*), physical aging, viscosity, etc. With many technologies under development relying on nanoconfined polymers, it is not only scientifically but also technologically important to understand how confinement modifies properties. In this dissertation, I have studied in detail the *Tg* behavior of nanoconfined polymer films and 1-dimensional (1-D) patterned polymer nanostructures.

Confinement effects in thin and ultrathin polymer films are studied by novel fluorescence techniques in Chapter 3. The ability to employ an intensive measurable, the excited-state fluorescence lifetime, in defining the *Tg* of polymers is demonstrated and compared to the use of an extensive measurable, fluorescence intensity. Besides pyrene, other chromophores are also studied for their sensitivity to the *Tg* of the polymer in which they are present. In some cases, the chromophore may naturally be a part of the polymer, such as the phenyl ring on each repeat unit of polystyrene (PS). In other cases, the dye may be an external dopant, as in the case of decacyclene. In yet other cases, the dye may be covalently attached at low levels to the polymer, as in the case of TC1-labeled poly(methyl methacrylate) (PMMA). In addition, intrinsic fluorescence from the phenyl groups in PS is used to determine the *Tg*-nanoconfinement effect in films as thin as ~ 15 nm. The decrease in *Tg* with decreasing film thickness (below ~ 60 nm) agrees well with results obtained by extrinsic pyrene fluorescence (Ellison 2003).

Chapter 4 describes the effect of nanoconfinement on the *Tg* of PS films, which is investigated in neat PS over the broadest *MW* range ever reported in a single study (5,000-3,000,000 g/mol). In contrast to two recent reports (Singh 2004; Miyazaki 2004), here it is observed that PS *MW* has no significant impact on the film thickness dependence of *Tg* - *Tg*,bulk. This result is consistent with the substantial evidence in the literature indicating that *Tg*-nanoconfinement effects originate from interfaces and surfaces which impact the cooperative segmental mobility associated with *Tg* and are not due to other factors which may depend on *MW* such as degree of chain end segregation, entanglement density, etc.

The characteristic dynamics of the cooperative motion associated with *Tg* is also examined in Chapter 4 via the size of a CRR at *Tg*, ξ_{CRR}. The value of ξ_{CRR} is approximately independent of PS *MW* over the same range of *MW*s for which the *Tg*-nanoconfinement effect is *MW* invariant. However, other system variations such as modification of repeat unit structure yield changes in ξ_{CRR} values of bulk polymer systems that do not correlate in an obvious manner with the strength of the *Tg*-nanoconfinement effect. For example, both the PS + 4 wt % dioctyl phthalate (DOP) system and poly(4-tertbutyl styrene) (PTBS) exhibit reduced values of ξ_{CRR} relative to PS; however, PS + 4 wt % DOP exhibits no *Tg*-nanoconfinement effect down to a film thickness of 14 nm (Ellison 2004a), while PTBS exhibits the onset of the effect at a thickness of 300-400 nm in supported films. Future studies related to how free surfaces and interfaces impact cooperative segmental dynamics as a function of polymer repeat unit structure and diluent addition are warranted.

Chapter 5 describes an innovative fluorescence/multilayer technique which is exploited to determine the influence of confinement and interfacial effects on the glass transition temperature (*Tg*) of PMMA films supported on silica. With single-layer PMMA films that are less than 90-nm-thick, *Tg* increases roughly linearly with

decreasing logarithmic thickness. The use of bilayer films reveals that compared to *Tg*(bulk), *Tg* is reduced at the free surface by 7-8 K for a 12-nm-thick free-surface layer and increased at the substrate interface by 10 K for a 12-nm-thick substrate layer of a bulk film, resulting in a *Tg*-gradient across the film. Measurements of confined bilayer films reveal that the stronger substrate effects percolate across the film to modify the *Tg* dynamics at the free surface. Thus, with nanoconfinement, the stronger substrate effects dominate the free-surface effects, providing an explanation for the increase in average *Tg* with decreasing single-layer PMMA film thickness. With extreme confinement, the *Tg*-gradient across the film thickness is suppressed, with both substrate layer and free-surface layer *Tg*s exceeding *Tg*(bulk). These results demonstrate that strongly perturbed *Tg* dynamics at the interfaces propagate across many layers of CRRs within the films, meaning that configurational changes associated with cooperative segmental dynamics within a CRR do not occur independently of neighboring CRRs. Thus, insight into the fundamental nature of the glass transition may be gained by measuring the nanoscale distributions of *Tg*s in confined polymers.

Chapter 6 describes the development and use of a novel intrinsic fluorescence technique, which is used to characterize intensity ratios in dilute solutions and the *Tg* in thin and ultrathin films of PS and styrene (S)/methyl methacrylate (MMA) random copolymers. Dilute solution fluorescence is characterized by a ratio of excimer to monomer fluorescence intensity. This ratio increases dramatically with increasing S-content in the copolymer and varies linearly with the S-S dyad fraction in the copolymer. This result is consistent with the notion that excimer fluorescence in dilute solution results from nearest neighbor S units with negligible impact of energy migration. Thin and ultrathin film fluorescence is characterized via integrated fluorescence intensity. The *Tg* is determined from the intersection of the rubbery- and glassy-state temperature dependences of integrated intensity measured upon cooling from an equilibrated state.

The *Tg*-nanoconfinement effect measured by intrinsic fluorescence in supported PS films agrees well with results from studies using extrinsic probe fluorescence (Ellison 2003, 2005a) and ellipsometry (Keddie 1994b). The nanoconfinement effect may be tuned using copolymer composition. As S-content decreases in S/MMA copolymers, the nanoconfinement effect changes from a decrease to an increase in *Tg* relative to bulk *Tg*, with an intermediate S-content copolymer exhibiting a nearly thickness-invariant *Tg*. The latter effect occurs because of a balance of the effects associated with the free surface, leading to a reduction in *Tg* with nanoconfinement, and attractive polymer-substrate interactions involving hydrogen-bonds between the hydroxyl groups on the surface of the substrate and the ester groups in the MMA repeat units, leading to an enhancement of *Tg*.

In Chapter 7, the impact of various parameters that can potentially modify or "tune" the *Tg*-nanoconfinement effect is explored in detail. Among the parameters investigated are molecular weight (covered in Chapter 4; see conclusions earlier in this chapter), composition of a random copolymer (covered in Chapter 6; see conclusions earlier in this chapter), slight modification to the repeat unit structure, changes in polymer chain stiffness or backbone rigidity, and addition of low molecular weight diluents.

In contrast to the absence of an effect of *MW* on the *Tg*-nanoconfinement effect in PS, small modifications to the repeat unit structure of PS have a dramatic impact on the *Tg*-nanoconfinement effect. A stronger film thickness dependence of *Tg* is observed for poly(4-methyl styrene) (P4MS) compared to PS, while PTBS exhibits a stronger dependence than both PS and P4MS. The *Tg* reduction for a 21-nm-thick PTBS film is 47 K relative to *Tg*,bulk, which is the largest deviation from *Tg*,bulk ever observed for supported polymer films. Furthermore, the onset thickness for the *Tg*-nanoconfinement effect is 300-400 nm in PTBS, the largest thickness for which such a *Tg*-nanoconfinement effect has been reported.

Small modifications to the side group of PMMA are also observed to have dramatic impact on the *Tg*-nanoconfinement effect of PMMA films. The average *Tg* across a film of poly(isobutyl methacrylate) (PiBMA) is invariant with nanoconfinement. In contrast, the *Tg* of PMMA increases with nanoconfinement while those of poly(ethyl methacrylate) (PEMA) and poly(propyl methacrylate) (PPMA) decrease with nanoconfinement.

The *Tg*-nanoconfinement effect is also "tuned" by the change in the backbone rigidity of the repeat unit structure. The strength of the thickness dependence of *Tg* is greater for bisphenol-A-polycarbonate (BPAPC) than for PS, while bisphenol-A-polysulfone (BPAPS) exhibits even stronger dependence than both PS and BPAPC. Thus, the strength of the thickness dependence of *Tg* follows the order of the rigidity of the polymer backbone structure. In particular, for a 34-nm-thick film of BPAPS, *Tg* is reduced by 24 K relative to *Tg*,bulk, while BPAPC and PS films of the same thickness exhibit *Tg* values which are reduced by 12 K and 8 K, respectively. The onset thickness for *Tg* reduction in BPAPS (~ 130 nm) is almost three times the onset thickness for PS (~ 40-50 nm).

Finally, the addition of small molecule diluents has a significant impact on the tunability of *Tg*-nanoconfinement effects in polymer films. The *Tg*-nanoconfinement effect is eliminated down to a film thickness of 20 nm in PMMA films by addition of small molecule diluents such as DOP. In PVAc, the *Tg*-nanoconfinement effect is eliminated down to a film thickness of 6 nm when water is sorbed from the atmosphere, resulting in a small percent of water dispersed naturally in the polymer matrix.

Chapter 8 describes the first study of the determination of *Tg* as a function of confinement in 1-D polymer nanostructures. With PMMA nanolines supported on silica, the important roles of the ratio of free-surface area to polymer-substrate interface area and the attractive polymer-substrate interactions in defining the nanostructure *Tg* are

demonstrated. Attractive polymer-substrate interactions result in a substantial increase of *Tg* with decreasing thickness in ultrathin PMMA films. However, when such attractive polymer-substrate interactions are present in nanopatterned polymers, an increase in the ratio of free-surface area to the polymer-substrate interfacial area can substantially reduce the *Tg* of 1-D nanostructures supported on a substrate, even to temperatures below the *Tg* of the bulk polymer, thereby "tuning" the *Tg*-nanoconfinement effect.

Chapter 9 explores in detail the strength of *Tg* (related to the difference in the rubbery and glassy state measurables defining *Tg*) as a function of PS *MW* and with slight modification to the PS repeat unit structure in thin and ultrathin films. For both PS *MW*s the strength of *Tg* is decreased with decreasing logarithmic film thickness in a nearly identical manner. No correlation between the film thickness dependence of *Tg* (refer to Figure 4-4, Chapter 4) and the film thickness dependence of the strength of *Tg* is observed. Similar to the PS case, no correlation between the thickness dependence of *Tg* and the thickness dependence of the strength of *Tg* for P4MS or PTBS (refer to Chapter 7, Section 7.2.3) is observed. However, examination of glassy state temperature dependence of integrated intensity (*Sg*) and rubbery state temperature dependence of integrated intensity (*Sr*) individually revealed that both *Sg* and *Sr* increase approximately with decreasing film thickness for PS films. However, *Sr* undergoes much larger increase (to smaller negative values) than *Sg* as film thickness decreases indicating that the reduced strength of *Tg* in thinner PS films appears to be a result of *Sr*, which approaches *Sg*. Similar effects for P4MS and PTBS are also seen.

The translational diffusion coefficients of decacyclene and Disperse Red 1 (DR1) in PS thin and ultrathin films are characterized using a novel multilayer fluorescence technique in Chapter 10. The diffusion coefficient is determined by measuring the break-through time, which is the time taken by the non-radiative energy transfer (NRET)

acceptor probe to diffuse towards the NRET donor probe. Probe diffusion in substrate-supported PS films is reduced as the film thickness is decreased below approximately 125 nm for decacyclene and 300 nm for DR1, respectively. For a 93-nm-thick PS film, the diffusion coefficient of decacyclene was reduced to approximately one-third of its value in bulk PS. In contrast, DR1 diffusion for a 125-nm-thick PS is reduced by an order of magnitude from its value in bulk PS.

In Chapter 11, it is shown that intrinsic fluorescence is a powerful tool for determining the annealing conditions needed to relax the unequilibrated local conformational populations that result in spin-coated PS and S/MMA copolymer films. The residual stresses induced by spin coating affect the conformational populations in the polymers; those populations affect excimer and monomer fluorescence, which in turn affect the integrated fluorescence intensity. Partial stress relaxation occurs during heating in the glassy state of thin and ultrathin films. However, with the heating protocol used here and as characterized by intrinsic fluorescence, full relaxation of the stresses induced by spin coating does not generally occur until the films, both thin and ultrathin, are heated to ~ 15-20 K above *Tg*. (In contrast, extrinsic probe fluorescence yields little sensitivity to residual stresses and their relaxation.) It is also demonstrated that many tens of minutes are required to achieve or nearly achieve a steady-state local conformational population in films when annealed at *Tg* + 10 K, with no impact of molecular weight. Finally, it is also shown that stresses associated with local chain conformations may be relaxed to a certain extent for samples stored or aged below *Tg*. These results, coupled with the characterization of the *Tg*-nanoconfinement effect, indicate that many observations of modified *Tg*-behavior in confined films are not caused by spin-coating induced stresses. Instead, the *Tg*-nanoconfinement effect is present in many polymers with well-equilibrated local conformational populations.

Chapter 12 describes the impact of diluent content in modifying the distribution of

relaxation times, fragility and the cooperative length scale dynamics in BPAPC, PiBMA and PS systems. Key questions about the correlation between the size scale of cooperatively rearranging regions (CRRs) to the width or distribution in the relaxation spectrum and fragility are addressed in a systematic study of addition of DR1 into these systems. Best fits of the relaxation data to the Kohlrausch-Williams-Watts (KWW) curve show large changes in the relaxation spectrum of the 10 wt% Disperse Red 1 (DR1)/BPAPC system as compared to the 0.5 wt% DR1/BPAPC system. The relaxation spectra of systems with a high diluent content are narrower than relaxation spectra for the nearly neat systems, i.e., systems with low loading of diluent. A weaker temperature dependence of Williams-Landel-Ferry (WLF) curves in systems with high diluent content is seen in comparison to the nearly neat systems. A systematic increase in the stretching exponent (βw) is seen with increasing concentration of DR1 from 0.5 to 10 wt%, indicating decrease in the width of the distribution of relaxation times in BPAPS system.

A reduction in the βw parameter is seen to correlate with reductions in the size scale of cooperatively rearranging regions (ξ_{CRR}) and the number of repeat units in one CRR (N_{CRR}), with varying diluent content within each system. However, no one single correlation was evident across all the systems. Direct linear correlation between the fragility index (m) and ξ_{CRR} is seen across all systems for all diluent concentrations. Study of BPAPS and poly(methyl acrylate) (PMA) along with BPAPC, PS and PiBMA, with varying chain stiffness and repeat unit structure, also shows that systems with higher degrees of aromaticity, chain rigidity and correspondingly higher *Tg* have higher degrees of cooperativity and fragility, further confirming the direct correlation between the two.

13.2 Recommendations for Future Work

Chapter 3 described the use of a novel fluorescence technique to study the nanoconfinement effects in various polymeric films. The ability to employ an intensive measurable, the excited-state fluorescence lifetime, in defining the *Tg* of polymers is

demonstrated and compared to the use of an extensive measurable, fluorescence intensity, in a bulk film. However, the sensitivity of excited-state fluorescence lifetime in defining the *Tg* in confined geometry is yet to be studied (Ellison 1996). Ellison *et al.* (Ellison 2005c) studied several fluorescence dyes (e.g. pyrene, anthracene, phenanthrene, decacyclene), for their ability to report *Tg* in thin and ultrathin films. However, there are numerous other dyes that may be potentially used for probe-based fluorescence measurement for characterizing *Tg* in various polymeric systems. These include coronene, dibenzo(b,def)chrysene, benzo(b)chrysene, picene, pentacene, dibenz(a,f)anthracene, dibenz(a,h)anthracene, benzo(a)pyrene, perylene, benzo(e)pyrene, napthacene, benz(a)anthracene, chrysene, triphenylene, benzo(c)phenanthrene, etc., among others (Fujimoto 2002).

Chapter 4 described the effect of nanoconfinement on the *Tg* of PS films over the broadest *MW* range ever reported in a single study (5,000-3,000,000 g/mol). It was observed that PS *MW* has no significant impact on the film thickness dependence of *Tg* - *Tg*,bulk. Similar studies in other systems such as PMMA and P2VP, in which *Tg* increases with decreasing film thickness in contrast to that of PS, remain to be undertaken. Effects of branching on the *Tg*-nanoconfinement effects in nonlinear polymers also deserve to be studied.

Chapter 5 described a fluorescence/multilayer technique which was exploited to determine the influence of nanoconfinement and interfacial effects on the *Tg* of PMMA films supported on silica. The results in Chapter 5 indicated that the strongly perturbed *Tg* dynamics at an interface can propagate over many layers of cooperatively rearranging regions (CRRs). It will be extremely useful to study other systems which shows more dramatic *Tg*-nanoconfinement effect than seen in PMMA system. Poly(2-vinyl pyridine) (P2VP) exhibits large *Tg* increases relative to *Tg*,bulk of 40-50 K upon nanoscale confinement (vanZanten 1996; Roth 2007a). Many experiments were attempted with

P2VP by Ellison *et al.* (Ellison 2005c) by employing a variety of dopants and labels but were unsuccessful for a variety of different reasons. However, a polymer with similar molecular structure as that of P2VP such as poly (4-vinyl pyridine) (P4VP) may prove successful in the future. Poly(tert-butyl styrene) stands out as other system that has shown huge reduction in *Tg* as a function of film thickness (Chapter 7). Clearly, there are many polymer systems that would be good targets for future multilayer/fluorescence studies.

As part of this thesis research, various attempts were made to synthesis PTBS using solution and bulk free-radical polymerization, employing azobisisobutyronitrile (AIBN) or benzoyl peroxide (BPO) as initiator. However, most of these attempts resulted in a cross-linked polymer due to the presence of large number of acidic hydrogens on the tert-butyl group causing excessive chain transfer. A very small numbers of attempts resulted in an un-crosslinked polymer, but the yield was extremely low (less than 5 mg of polymer was produced for 15 ml of monomer used). Future attempts should be aimed at increasing the yield as well as the *MW* of the polymerized sample. One way to do this is to pursue nitroxide-mediated controlled free-radical polymerization technique also commonly known as NM-CRP used previously by Jousset *et al.* to synthesize PTBS (Jousset 1997).

A novel intrinsic fluorescence technique was described in Chapter 6 to measure the *Tg* of thin and ultrathin films of PS and S/MMA random copolymers. The *Tg*-nanoconfinement effect measured by intrinsic fluorescence in supported PS films was seen to agree well with results from studies using extrinsic probe fluorescence (Ellison 2003, 2005a) and ellipsometry (Keddie 1994b). It may be possible to extend this approach to other random copolymer systems that could exhibit even greater tunability of *Tg* with comonomer content.

Chapter 7 explored in detail the impacts of various parameters that can potentially "tune" the *Tg*-nanoconfinement effect. Even though Chapter 7 answered a number of

questions, it simultaneously raised many more. For instance, how is the distribution of *Tg*s affected in various systems as the *Tg*-nanoconfinement effects are tuned, and how does it compare to the distribution of *Tg*s in neat PS and PMMA systems? Is the tunability a result of a modification of the degree of cooperativity of the polymer or due to a modification in the magnitude of the perturbation on *Tg* at interfaces or a combination of the two? These questions may potentially be addressed by investigating the distribution in *Tg* values for various systems such as P2VP, PVAc, and PTBS and comparing that to already characterized PS, PMMA systems. Studies of the *Tg*-nanoconfinement effect in other systems other complex systems such as poly (cyclohexyl methacrylate) (PcHMA), etc. are also warranted to fully understand the tunability aspect of *Tg*-nanoconfinement effect and to comprehend the fundamental nature of the glass transition itself.

Chapter 10 described the development of novel fluorescence multilayer technique by which mobility associated with diffusion may be determined in thin and ultrathin polymer films. This technique was used for the first study of the translational diffusion of DR1 in PS thin and ultrathin films. It was also used to study decacyclene diffusion in PS films. The study of these two systems revealed the effect of nanoconfinement on mobility associated with diffusion in thin and ultrathin films. The effects observed in this study have been hypothesized to result from confinement resulting in a narrowing of the alpha-relaxation distribution (a narrowing of the dynamic heterogeneity) in the middle layer of trilayer polymer films. Further investigation of this hypothesis can be undertaken with additional studies of dyes of variable sizes (such as 4-(dimethylamino)-4'-nitrostilbene (DANS), 4-tricyanovinyl-[N-(2-hydroxyethyl)-N-ethyl]aniline (TC1), rubrene, 4-(dimethylamino) benzylidenemalonitrile (DMN), lophine 1, diphenyl Disperse Red 4 (DPDR4), and 9,10-bis-phenyl ethynyl anthracene (BPEA)) and fluorescence studies especially those allowing for measurement of the effect of confinement on dye

diffusion as a function of temperature. Additionally, dielectric spectroscopy studies may also be useful in directly measuring how the short-time side of the alpha-relaxation distribution is altered by confinement.

The simple, novel approach that was used to characterize diffusion coefficients in bulk and confined trilayer films can be extended to study many other important systems and problems. For example, using this approach, the effect of attractive polymer-substrate interactions in altering dye translational diffusion can be studied as a function of distance from the polymer-substrate interface. Poly(methyl methacrylate) on silica allows for such a study. Similarly, the approach described here can be modified by covalently attaching DR1 to low molecular weight polymer that can be added to a high molecular weight polymer matrix, thereby allowing for the determination of how confinement affect the out-of-plane diffusion of polymers. Such a study would complement the first study of the effect of confinement on translational diffusion in polymers done a little more than a decade ago by Frank *et al.* (Frank 1996a), who observed a small reduction in the in-plane translational diffusion of polymer with confinement.

Chapter 11 described the use of intrinsic fluorescence as a powerful tool for determining the annealing conditions needed to fully relax the unequilibrated local conformational populations that result in spin-coated PS and S/MMA copolymer films. Similar studies may be possible for other systems capable of showing intrinsic fluorescence such as BPAPC, BPAPS, polymer blends, as well as polymer nanocomposites and gradient copolymers. Even though I do not have any conclusive results, a couple of measurements have suggested that intrinsic fluorescence may also be sensitive to physical aging response in bulk or ultrathin films of BPAPS. In the future, intrinsic fluorescence may prove to be a powerful tool for all other sorts of studies ranging from crystallization to micellization formation.

Lastly, only two research groups (Lenhart 2002, 2003; Grohens 2001) have studied the impact of cross-linking density on the properties of polymers in nanoconfined geometry. Grohens *et al.* (Grohens 2001) did the first study investigating the impact of cross-linking density on *Tg*-nanoconfinement effect. In their study, supported poly(vinyl chloride) (PVC) thin films were chemically cross-linked in solution by terephthaloyl chloride. The *Tg* of the polymer layer was seen to increase with increasing the cross-linking time, but no effect of film thickness was seen. Clearly, more efforts are required in this area to further advance our understanding of the *Tg*-nanoconfinement effect in thin and ultrathin films.

REFERENCES

Adam, G.; Gibbs, J.H. *J. Chem. Phys.* **1965**, 43, 139.

Agbor, N.E.; Cresswell, J.P.; Petty, M.C.; Monkman, A.P. *Sensors and Actuators B* **1997**, 41, 137.

Agbor, N.E.; Petty, M.C.; Monkman, A.P. *Sensors and Actuators B* **1995**, 28, 173.

Albala, R.; Olmos, D.; Aznar, A.J.; Baselga, J.; Gonzalez-Benito, J. *J. Coll. Int. Sci.* **2004**, 277, 71.

Alberty, K.A.; Hogen-Esch, T.E.; Carlotti, S. *Macromol. Chem. Phys.* **2005**, 206, 1035.

Alcoutlabi, M.; McKenna, G.B. *J. Phys.: Condens. Matter* **2005**, 17, R461.

Alivisatos, A.P. *Science* **1996**, 271, 933.

Anastasiadis, S.H.; Karatasos, K.; Vlachos, G.; Manias, E.; Giannelis, E.P. *Physical Review Letters* **2000**, 84, 915.

Anderson, P.W. *Science* **1995**, 267, 1615.

Andreozzi, L.; Di Schino, A.; Giordano, M.; Leporini, D. *J. Phys.: Condens. Matter* **1996**, 8, 3795.

Andreozzi, L.; Giordano, M.; Leporini, D. *J. Phys. Chem.* **1999**, 103, 4097.

Angell, C.A. *J. Non-Cryst. Solids* **1991**, 131-133, 13.

Angell, C.A. *Polymer* **1997**, 38, 6261.

Angell, C.A. *Proc. Natl. Acad. Sci. USA* **1995b**, 92, 6675.

Angell, C.A. *Science* **1995a**, 267, 1924.

Angell, C.A.; Ngai, K.L.; McKenna, G.B.; McMillan, P.F.; Martin, S.W. *Applied Physics Letters* **2000**, 88, 3113.

Anwand, D.; Muller, F.W.; Strehmel, B.; Schiller, K. *Makromol. Chem.* **1991**, 192, 1981.

Arkhipov, V.I.; Bassler, H. *J. Non-Cryst. Solids* **1994b**, 172, 396.

Arkhipov, V.I.; Bassler, H. *J. Phys. Chem.* **1994a**, 98, 662.

Arndt, M.; Stannarius, R.; Gorbatschow, W.; Kremer, F. *Physical Review E* **1996**, 54, 5377.

Arndt, M.; Stannarius, R.; Groothues, H.; Hempel, E.; Kremer, F. *Phys. Rev. Lett.* **1997**, 79, 2077.

Ash, B.J.; Siegel, R.W.; Schadler, C.S. *J. Polym. Sci. Part B Polym. Phys.* **2004**, 42, 4371.

Bair, H.E.; Johnson, G.E.; Anderson, E.W.; Matusoka, S. *Polm. Sci. Engg.* **1981**, 21, 930.

Baljon, A.R.C.; Billen, J.; Khare, R. *Phys. Rev. Lett.* **2004**, 93, 255701-1.

Baljon, A.R.C.; Van Weert, M.H.M.; DeGraaff, R.B.; Khare, R. *Macromolecules* **2005**, 38, 2391.

Barkley, M.D.; Kowelcyzk, A.A.; Brand, L. *Journal of Chemical Physics* **1981**, 75, 3581.

Barrer, R.M. "*Diffusion In and Through Solids*" Cambridge University Press, London, **1951**.

Bartos, J.; Kristiak, J. *J. Non-Cryst. Solids* **1998**, 235-237, 293.

Barut, G.; Pississ, P.; Pelster, R.; Nimtz, G. *Phys. Rev. Lett.* **1998**, 80, 3543.

Baschnagel, J., Meyer, H., Varnik, F., Metzger, S., Aichele, M., Muller, M., Binder, K. *Interf. Sci*. **2003**, 11, 159.

Baschnagel, J.; Binder, K. *J. de Physique I* **1996**, 6, 1271.

Baschnagel, J.; Varnik, F. *J. Phys.: Condens. Matter* **2005**, 17, R851.

Basile, L.J. *J. Chem. Phys.* **1962**, 36, 2204.

Bauer, C.; Bohmer, R.; Moreno-Flores, S.; Richert, R.; Sillescu, H. *Phys. Rev. E* **1999**, 61, 1755.

Bazuin, C.G.; Eisenberg, A. *J. Polym. Sci. Part B Polym. Phys.* **1986**, 24, 1155.

Beaucage, G.; Composto, R.; Stein, R.S. *J. Polym. Sci. Part B Polym. Phys.* **1993**, 31, 319.

Bernazzani, P.; Simon, S.L.; Plazek, D.J.; Ngai, K.L. *Eur. Phys. J. E* **2002**, 8, 201.

Berriot, J.; Montes, H.; Lequeux, F.; Long, D.; Sotta, P. *Europhys. Lett*. **2003**, 64, 50.

Berriot, J.; Montes, H.; Lequeux, F.; Long, D.; Sotta, P. *Macromolecules* **2002**, 35, 9756.

Berthier, L.; Biroli, G.; Bouchaud, J.-P.; Cipelletti, L.; Masri, E.El.; L'Hote, D.; Ladieu, F.; Pierno, M. *Science* **2005**, 310, 1797.

Birge, N.O.; Nagel, S.R. *Phys. Rev. Lett.* **1985**, 54, 2674.

Bitsanis, I.; Hadziioannou, G. *J. Chem. Phys.* **1990**, 92, 3827.

Blum, F.D.; Young, E.N.; Smith, G.; Sitton, O.C. *Langmuir* **2006**, 22, 4741.

Bohmer, R.; Angell, C.A. *Phys. Rev. B* **1993b**, 48, 5857.

Bohmer, R.; Ngai, K.L.; Angell, C.A.; Plazek, D.J. *J. Chem. Phys.* **1993a**, 99, 4201.

Boiko, Y.M.; Prud'homme, R.E. *J. Polym. Sci. Part B Polym. Phys.* **1998**, 36, 567.

Bokobza, L.; Jasse, B.; Monnerie, L. *Eur. Polym. J.* **1977**, 13, 921.

Bower, D.I. *"An Introduction to Polymer Physics*", Cambridge University Press: Cambridge, U.K., **2002**.

Boyd, R.W. *"Nonlinear Optics, Academic Press Inc."*, San Diego, **1992**.

Brady, R.F.; Charlesworth, J.M. *J. of Coat. Tech.* **1993**, 65, 81.

Brandrup, J.; Immergut, E.H.; Grulke, E.A. editors. *"Polymer Handbook"*, 4th Ed. New York, Wiley, **1999**.

Bratton, D.; Yang, D.; Dai, J.Y.; Ober, C. K. *Polym. Adv. Technol.* **2006**, *17*, 94.

Breslow, R.; Tirrell, M.V. *"Beyond the Molecular Frontier: Challenges for Chemistry and Chemical Engineering"*, National Academies Press: Washington, D.C., **2003**, p. 146.

Brown, G.O.; Atvars, T.D.Z.; Guardala, N.A.; Price, J.L.; Weiss, R.G. *J. Polym. Sci. Part B Polym. Phys.* **2004**, 42, 2957.

Brown, H.R.; Russell, T.P. *Macromolecules* **1996**, 29, 798.

Bullock, A.T.; Cameron, C.G.; Miles, I.S. Polymer **1986**, 27, 191.

Campoy-Quiles, M.; Sims, M.; Etchegoin, P. G.; Bradley, D. D. C. *Macromolecules* **2006**, 39, 7673.

Casalini, R.; Ngai; Robertson, C.G.; Roland, C.M. *J. Polym. Sci. Part B Polym. Phys.* **2000**, 1841.

Chang, I.; Fujara, F.; Geil, B.; Heuberger, G.; Mangel, T.; Sillescu, H. *J. Non-Cryst. Solids* **1994**, 172-174, 248.

Chen, M.; Dalton, L.R.; Yu, L.P.; Shi, Y.Q.; Steier, W.H. *Macromolecules* **1992**, 25, 4032.

Chen, W.; Ahmed, H. *Appl. Phys. Lett.* **1993**, 62, 1993.

Chipalkatti, M.H.; Laski, J.J. *Polym. Mat. Sci. Engg.* **1991**, 64, 131.

Chou, S.Y.; Krauss, P.R.; Renstrom, P.J. *Science* **1996**, 272, 85.

Cicerone, M.T.; Blackburn, F.R.; Ediger, M.D. *Macromolecules* **1995**, 28, 8224.

Cicerone, M.T.; Wagner, P.A.; Ediger, M.D. *J. Phys. Chem. B* **1997**, 101, 8727.

Clauss, B.; Salem, D.R. *Macromolecules* **1995**, 28, 8328.

Cohen, M.H.; Turnbull, D. *J. Chem. Phys.* **1959**, 31, 1164.

Cohen, Y.; Reich, S. *J. Polym. Sci. Part B Polym. Phys.* **1981**, 19, 599.

Corrales, T.; Peinado, C.; Bosch, P.; Catalina, F. *Polymer* **2004**, 45, 1545.

Crank, J.; Park, G.S. *"Diffusion in Polymers"*; Academic Press Inc.: Bristol, **1967**.

D'Amour, J.N.; Okoroanyanwu, U.; Frank, C.W. *Microelect. Eng.* **2004**, 45, 4507.

Dalnoki-Veress, K.; Forrest, J.A.; de Gennes, P.G.; Dutcher, J.R. *J. Phys. IV* **2000**, 10, 221.

Dalnoki-Veress, K.; Forrest, J.A.; Murray, C.; Gigault, C.; Dutcher, J.R. *Phys. Rev. E* **2001**, 63, 031801-1.

Dalnoki-Veress, K; Nickel, B.G.; Roth, C.; Dutcher, J.R. *Phys. Rev. E* **1999**, 59, 2153.

David, C. ; Lempereur, M. ; Geuskens, G. *Eur. Polym. J.* **1973**, 9, 1315.

David, L.; Sekkat, A.; Etienne, S. *J. Non-Cryst. Solids* **1994**, 172-174, 214.

De Deus, J.F.; Souza, G.P.; Corradini, W.A.; Atvars, T.D.Z.; Akcelrud, L. *Macromolecules* **2004**, 37, 6938.

de Gennes, P.G. *Eur. Phys. J. E* **2000**, 2, 201.

Debenedetti, P.G.; Stillinger, F.H. *Nature* **2001**, 410, 259.

DeMaggio, G.B.; Frieze, W.E.; Gidley, D.W.; Zhu, M.; Hristov, H.A., Yee, A.F. *Phys. Rev. Lett.* **1997**, 78, 1524.

Deppe, D.D. *"Ph.D. Thesis"*, Northwestern University, **1996c**.

Deppe, D.D.; Dhinojwala, A.; Torkelson, J.M. *Macromolecules* **1996a**, 29, 3898.

Deppe, D.D.; Miller, R.D.; Torkelson, J.M. *J. Polym. Sci. Part B Polym. Phys.* **1996b**, 34, 2987.

Deschenes, L.A.; Vanden Bout, D.A. *Science* **2001**, 292, 255.

Despotopoulou, M.M.; Frank, C.W.; Miller, R.D.; Rabolt, J.F. *Macromolecules* **1996**, 29, 5797.

Despotopoulou, M.M.; Frank, C.W.; Miller, R.D.; Rabolt, J.F. *Macromolecules* **1995**, 28, 6687.

Dhinojwala, A.; Torkelson, J.M. *Macromolecules* **1994a**, 27, 4817.

Dhinojwala, A.; Wong, G.K.; Torkelson, J.M. *J. Chem. Phys.* **1994b**, 15, 6046.

Dhinojwala, A.; Wong, G.K.; Torkelson, J.M. *Macromolecules* **1993**, 26, 5943.

DiMarzio, E.A.; Gibbs, J.H. *J. Polym. Sci.* **1959**, 40, 121.

DiMarzio, E.A.; Gibbs, J.H. *J. Polym. Sci. Part A* **1963**, 1, 1417.

Dionisio, M.; Ramos, J.J.M.; Williams, G. *Polymer International* **1993**, 32, 145.

Dixon, P.K.; Wu, L.; Nagel, S.R.; Williams, B.D.; Carini, J.P. *Phys. Rev. Lett.* **1990**, 65, 1108.

Dobisz, E.A.; Brandow, S.L.; Bass, R.; Mitterender, J. *J. Vac. Sci. Technol.* **2000**, 18, 107.

Donati, C.; Douglas, J.F.; Kob, W.; Plimpton, S.J.; Poole, P.H.; Glotzer, S.C. *Phys. Rev.*

Lett. **1998**, 80, 2338.

Donth E. *J. Non-Cryst. Solids* **1982**, *53*, 325.

Donth, E. *"The Glass Transition"*, Springer, Berlin, **2001b**.

Donth, E. *Acta Polym.* **1979**, 30, 481.

Donth, E. *Acta Polym.* **1999**, 50, 240.

Donth, E. *Acta Polym.* **1984**, 35, 120.

Donth, E. *J. Polym. Sci. Part B Polym. Phys.* **1996**, 34, 2881.

Donth, E.; Hempel, E.; Schick, C. *J. Phys.: Condens. Matter* **2000**, 12, L281.

Donth, E.; Huth, H.; Beiner, M. *J. Phys.: Condens. Matter* **2001a**, 13, L451.

Donthu, S.; Pan, Z.X.; Myers, B.; Shekhawat, G.; Wu, N.G.; Dravid, V. *Nano Lett.* **2005b**, 5, 1710.

Donthu, S.K.; Pan, Z.; Shekhawat, G.S.; Dravid, V.P.; Balakrisnan, B.; Tripathy, S. *J. Appl. Phys.* **2005a**, 98, 024304.

Doolittle, A.K.; Doolittle, D.B. *J. Appl. Phys.* **1957**, 28, 901.

Dorkenoo, K.D.; Pfromm, P.H. *J. Polym. Sci. Part B Polym. Phys.* **1999**, 37, 2239.

Dorkenoo, K.D.; Pfromm, P.H. *Macromolecules* **2000**, 33 3747.

Doruker, P.; Mattice, W.L. *Macromolecules* **1999**, 32, 194.

Duvvuri, K.; Richert, R. *J. Phys. Chem.* **2002**, 117, 4414.

Duvvuri, K.; Richert, R. *J. Phys. Chem. B* **2004**, 108, 10451.

Ediger, M.D. *Annu. Rev. Phys. Chem.* **2000**, 51, 99.

Ediger, M.D.; Angell, C.A.; Nagel, S.R. *J. Phys. Chem.* **1996**, 100, 13200.

Efremov, M.Y.; Olson, E.A.; Zhang, M.; Zhang, Z.; Allen, L.H. *Macromolecules* **2004a**, 37, 4607.

Efremov, M.Y.; Olson, E.A.; Zhang, M.; Zhang, Z.S.; Allen, L.H. *Phys. Rev. Lett.* **2004b**, 91, 085703.

Ellison, C.J. *"Ph.D. Thesis"*, Northwestern University, **2005c**.

Ellison, C.J.; Kim, S.D.; Hall, D.B.; Torkelson, J.M. *Eur. Phys. J. E* **2002a**, 8, 155.

Ellison, C.J.; Miller, K.E.; Torkelson, J.M. *Polymer* **2004b**, 45, 2623.

Ellison, C.J.; Mundra, M.K.; Torkelson, J.M. *Macromolecules* **2005a**, 38, 1767.

Ellison, C.J.; Priestley, R.D.; Broadbelt, L.J.; Mundra, M.K.; Rittigstein, P.; Torkelson, J.M. *SPE ANTEC* **2005b**, 63, 2350.

Ellison, C.J.; Ruszkowski, R.L.; Fredin, N.J.; Torkelson, J.M. *Phys. Rev. Lett.* **2004a**, 92, 095702-1.

Ellison, C.J.; Torkelson, J.M. *J. Polym. Sci. Part B Polym. Phys.* **2002b**, 40, 2745.

Ellison, C.J.; Torkelson, J.M. *Nature Mater.* **2003**, 2, 695.

Ellison, E.H.; Thomas, J.K. *Langmuir* **1996**, 12, 1870.

Erwin, B.M.; Colby, R.H. *J. Non-cryst. Sol.* **2002**, 307-310, 225.

Fakhraai, Z.; Sharp, J.S.; Forrest, J.A. *J. Polym. Sci. Part B Polym. Phys.* **2004**, 42, 4503.

Ferry, J.D. *"Viscoelastic Properties of Polymers"*, 3rd ed., Wiley: New York, **1980**.

Fitz, B.D.; Mijovic, J. *Macromolecules* **1999**, 32, 3518.

Flory, P.J. *"Statistical Mechanics of Chain Molecules"*, Hanser: New York, **1989**.

Forrest, J.A. *Eur. Phys. J. E* **2002**, 8, 261.

Forrest, J.A.; Dalnoki-Veress, K. *Adv. Coll. Interf. Sci.* **2001**, 94, 167.

Forrest, J.A.; Dalnoki-Veress, K.; Dutcher, J.R. *Phys. Rev. E* **1997**, 56, 5705.

Forrest, J.A.; Dalnoki-Veress, K.; Dutcher, J.R. *Phys. Rev. E* **1998**, 58, 6109.

Forrest, J.A.; Dalnoki-Veress, K.; Stevens, J.R.; Dutcher, J.R. *Phys. Rev. Lett.* **1996**, 77, 2002.

Forrest, J.A.; Mattsson, J. *Phys. Rev. E* **2000**, 61, R53.

Frank, B.; Gast, A.P.; Russell, T.P.; Brown, H.R.; Hawker, C. *Macromolecules* **1996a**, 29, 6531.

Frank, C.W. *Macromolecules* **1975**, 8, 305.

Frank, C.W.; Rao, V.; Despotopoulou, M.M.; Pease, R.F.W.; Hinsberg, W.D.; Miller, R.D.; Rabolt, J.F. *Science* **1996b**, 273, 912.

Fryer, D.S.; Bollepali, S.; de Pablo, J.J.; Nealey, P.F. *J. Vac. Sci. Tech. B* **1999**, 17, 3351.

Fryer, D.S.; Nealey, P.F.; de Pablo, J.J. *Macromolecules* **2000**, 33, 6439.

Fryer, D.S.; Peters, R.D.; Kim, E.J.; Tomaszewski, J.E.; de Pablo, J.J.; Nealey, P.F.; White, C.C.; Wu, W.L. *Macromolecules* **2001**, 34, 5627.

Fuchs, K.; Friedrich, C.; Weese, J. *Macromolecules* **1996**, 29, 5893.

Fujimoto, C.; Maekawa, A.; Murao, Y.; Jinno, K.; Takeichi, T. *Analytical Sciences* **2002**, 18, 65.

Fukao, K. *Eur. Phys. J. E* **2003**, 12, 119.

Fukao, K.; Miyamoto, Y. *Europhys. Lett.* **1999**, 46, 649.

Fukao, K.; Miyamoto, Y. *Phys. Rev. E* **2000**, 61, 1743.

Fukao, K.; Sakamoto. A. *Phys. Rev. E* **2005**, 71, 041803.

Fukao, K.; Uno, S.; Miyamoto, Y.; Hoshino, A.; Miyaji, H. *J. Non-cryst. Sol.* **2002**, 307, 517.

Fukao, K.; Uno, S.; Miyamoto, Y.; Hoshino, A.; Miyaji, H. *Phys. Rev. Lett.* **2001**, 64, 051807.

Fulcher, G.S. *J. Am. Ceram. Soc.* **1923**, 8, 339.

Gapinski, J.; Paluch, M.; Patkowski, A. *Phys. Rev. E* **2002**, 66, 011501.

Ge, S.; Pu, Y.; Zhang, W.; Rafailovich, M.; Sokolov, J.; Buenviaje, C.; Buckmaster, R.; Overney, R.M. *Phys. Rev. Lett.* **2000**, 85, 2340.

Gelles, R.M.; Frank, C.W. *Macromolecules* **1982a**, 15, 747.

Gelles, R.M.; Frank, C.W. *Macromolecules* **1982b**, 15, 1486.

Gibbs, J.H.; DiMarzio, E.A. *J. Chem. Phys.* **1958**, 28, 373.

Glotzer, S.C. *J. Non-cryst. Sol.* **2000**, 274, 342.

Goodson, T.; Wang, C.H. *Macromolecules* **1993**, 26, 1837.

Gotze, W.; Sjogren, L. *Rep. Prog. Phys.* **1992**, 55, 241.

Granick, S.; Hu, H.W. *Langmuir* **1994**, 10, 3857.

Greiner, R.; Schwarzl, F.R. *Rheol. Acta* **1984**, 23, 378.

Griffith, L.G.; Naughton, G. *Science* **2002**, 295, 1009.

Grohens, Y.; Brogly, M.; Labbe, C.; David, M.O.; Schultz, J. *Langmuir* **1998**, 14, 2929.

Grohens, Y.; Brogly, M.; Labbe, C.; Schultz, J. *Polymer* **1997**, 38, 5913.

Grohens, Y.; Hamon, L.; Reiter, G.; Soldera, A.; Holl, Y. *Eur. Phys. J. E* **2002**, 8, 217.

Grohens, Y.; Sacristan, J.; Hamon, L.; Reinecke, H.; Mijangos, C.; Guenet, J.M. *Polymer* **2001**, 42, 6419.

Guilbault, G.G. *"Practical Fluorescence: Theory, Methods and Techniques"*, Marcel Dekker Inc.: New York, **1973**.

Gupta, M.C.; Gupta A. *Polym. Photochem.* **1983**, 3, 211.

Hains, P.J.; Williams, G. *Polymer* **1975**, 16, 725.

Hall, D.B.; Deppe, D.D.; Hamilton, K.E.; Dhinojwala, A.; Torkelson, J.M. *J. Non-Cryst. Solids* **1998c**, 235-237, 48.

Hall, D.B.; Dhinojwala, A.; Torkelson, J.M. *Phys. Rev. Lett.* **1997c**, 79, 103.

Hall, D.B.; Hamilton, K.E.; Miller, R.D.; Torkelson, J.M. *Macromolecules* **1999**, 32, 8052.

Hall, D.B.; Hooker, J.C.; Torkelson, J.M. *Macromolecules* **1997a**, 30, 667.

Hall, D.B.; Miller, R.D.; Torkelson, J.M. *J. Polym. Sci. Part B Polym. Phys.* **1997b**, 35, 2795.

Hall, D.B.; Torkelson, J.M. *Macromolecuules* **1998b**, 31, 8817.

Hall, D.B.; Underhill, P.; Torkelson, J.M. *Polym. Eng. Sci.* **1998a**, 38, 2039.

Hamilton, K. *"Ph.D. Thesis"*, Northwestern University, **1996**.

Hartmann, L.; Gorbatschow, W.; Hauwede, J.; Kremer, F. *Eur. Phys. J E* **2002**, 8, 145.

Hartschuh, R.; Ding, Y.; Roh, J.H.; Kisliuk, A.; Sokolov, A.P.; Soles, C.L.; Jones, R.L.; Hu, T.J.; Wu, W.L.; Mahorowala, A.P. *J. Polym. Sci.*, *Part B: Polym. Phys.* **2004**, 42, 1106.

Hartschuh, R.D.; Kisliuk, A.; Novikov, V.; Sokolov, A.P.; Heyliger, P.R.; Flannery, C.M.; Johnson, W.L.; Soles, C.L.; Wu, W.L. *Appl. Phys. Lett.* **2005,** 87, 173121.

Hempel, E.; Hempel, H.; Hensel, A.; Schick, C.; Donth, E. *J. Chem. Phys. B* **2000**, 104, 2460.

Herminghaus, S.; Seeman, R.; Landfester, K. *Phys. Rev. Lett.* **2004**, 93, 017801-1.

Hirayama, F.; Lipsky, S. *J. Chem. Phys.* **1969**, 51, 1939.

Hodge, I. M. *J. Non-Cryst. Solids* **1997**, 212, 77.

Hodge, I.M. *J. Non-Cryst. Solids* **1996**, 202, 164.

Hodge. I.A. *Science* **1995**, 267, 1945.

Hofstraat, J.W.; Veurnick, J.; Gebben, B.; Verheij, H.J.; Verhoeven, J.W. *J.Fluor.* **1998**, 8, 1998.

Höhne, G.W.H; Hemminger, W.; Flammersheim, H.-J. *"Differential Scanning Calorimetry"*, New York , **2003**.

Hong, P.D.; Chuang, W.T.; Yeh, W.J.; Lin, J.L. *Polymer* **2002**, 43, 6879.

Hooker, J.C.; Torkelson, J.M. *Macromolecules* **1995**, 28, 7683.

Hoyle, C.E.; Zhao, J.; Orler, B.; Kuang; McDonald, C.W. *J. Macromol. Sci. Pure Appl. Chem.* **2001**, 38, 527.

Hu, H.W.; Granick, S. *Science* **1992**, 258, 1339.

Huang, D.; Colucci, D.M.; McKenna, G.B. *J. Chem. Phys.* **2002**, 116, 3925.

Huang, D.; McKenna, G.B. *J. Chem. Phys.* **2001b**, 114, 5621.

Huang, Y.; Duan, X.F.; Wei, Q.Q.; Lieber, C.M. *Science* **2001a**, 291, 630.

Huang, Y.; Paul, D.R. *Macromolecules* **2006**, 39, 1554.

Huang, Y.; Paul, D.R. *Polymer* **2004**, 45, 8377.

Hutchinson, J.M. *Prog. Polym. Sci.* **1995**, 20, 703.

Hwang, Y.; Inoue, T.; Wagner, P.A.; Ediger, M.D. *J. Polym. Sci.* **2000**, 38, 68.

Ishida, Y.; Yamafuji, K. *Kolloid Z.* **1961**, 177, 97.

Itagaki, H.; Horie, K.; Mita, I. *Prog. Polym. Sci.* **1990**, 15, 361.

Itagaki, H.; Inagaki, Y.; Kobayashi, N. *Polymer* **1996**, 37, 3553.

Jackson, C.L.; McKenna, G.B. *Chem. Mater.* **1996**, 8, 2128.

Jackson, C.L.; McKenna, G.B. *J. Non-cryst. Solids* **1991**, 131, 221.

Jacques, P.P.L.; Poller, R.C. *Eur. Polym. J.* **1993**, 29, 83.

Jager, W.F.; van den Berg, O.; Picken, S. *J. Macromol. Symp.* **2005**, 230, 11.

Jain, T.S.; de Pablo, J.J. *Phys. Rev. Lett.* **2004**, 92, 155505-1.

Jean, Y.C.; Zhang, R.; Cao, H.; Yuan, J.P.; Huang, C.M. *Phys. Rev. B* **1997**, 56, R8459.

Jensen, R.E.; O'Brien, E.; Wang, J.; Bryant, J.; Ward, T.C.; James, L.T.; Lewis, D.A. *J. Polym. Sci. Part B Polym. Phys.* **1998**, 36, 2781.

Jiang, Q.; Shi, H.X.; Li, J.C. *Thin Solid Films* **1999**, 354, 283.

Jones, B.A.; Torkelson, J.M. *J. Polym. Sci. Part B Polym. Phys.* **2004**, 42, 3470.

Jones, R.A.L.; Richards, R.W. *"Polymers at Surfaces and Interfaces"*; Cambridge University Press: Cambridge, **1999a**.

Jones, R.L.; Hu, T.; Soles, C.L.; Lin, E.K.; Reano, R.M.; Pang, S.W.; Casa, D.M. *Nano Lett.* **2006**, 6, 1723.

Jones, R.L.; Kumar, S.K.; Ho, D.L.; Briber, R.M.; Russell, T.P. *Nature* **1999b**, 400, 146.

Kajiyama, T.; Tanaka, K.; Takahara, A. *Macromolecules* **1997**, 30, 280.

Kalyanasundaram, K.; Thomas, J.K. *J. Am. Chem. Soc.* **1977**, 10, 133.

Kanaya, T.; Miyazaki, T.; Watanabe, H.; Nishida, K.; Yamano, H.; Tasaki, S.; Bucknall, D.B. *Polymer* **2003**, 44, 3769.

Kawaguchi, D.; Tanaka, K.; Kajiyama, T.; Takahara, A.; Tasaki, S. *Macromolecules* **2003**, 36, 1235.

Kawaguchi, D.; Tanaka, K.; Takahara, A.; Kajiyama, T. *Macromolecules* **2001**, 34, 6164.

Kawana, S.; Jones, R.A.L. *Eur. Phys. J. E* **2003**, 10, 223.

Kawana, S.; Jones, R.A.L. *Phys. Rev. E* **2001**, 63, 021501-1.

Keddie, J.L.; Jones, R.A.L. *Israel J. Chem.* **1995**, 35, 21.

Keddie, J.L.; Jones, R.A.L.; Cory, R.A. *Europhys. Lett.* **1994b**, 27, 59.

Keddie, J.L.; Jones, R.A.L.; Cory, R.A. *Faraday Discuss.* **1994a**, 98, 219.

Kerle, T.; Lin, Z.Q.; Kim, H.C.; Russell, T.P. *Macromolecules* **2001**, 34, 3484.

Khale, S.; Schroter, K.; Hempel, E.; Donth, E. *J. Chem. Phys.* **1999**, 111, 6462.

Kim, J.H.; Jang, J. *Macromolecules* **2002a**, 35, 311.

Kim, J.H.; Jang, J.; Zin, W.C. *Langmuir* **2000**, 16, 4064.

Kim, J.H.; Jang, J.; Zin, W.C. *Langmuir* **2001**, 17, 2703.

Kim, S.D.; Torkelson, J.M. *Macromolecules* **2002b**, 35, 5943.

Kohler, W.; Robello, D.R.; Dao, P.T.; Willand, C.S.; Williams, D.J. *J. Chem. Phys.* **1990**, 93, 9157.

Kohlrausch, R. *Ann. Phys. (Leipzig)* **1847**, 72, 353.

Korus, J.; Hempel, E.; Beiner, M.; Khale, S.; Donth, E. *Acta. Polymer.* **1997**, 48, 369.

Kosbar, L.L.; Kuan, S.W.J.; Frank, C.W.; Pease, R.F.W. *ACS Symp. Ser.* **1989**, 381, 95.

Kovacs, A.J. *"A Multiparameter Approach for Structural Recovery of Glasses and Its Implication for Their Physical Properties. Structure and Mobility in Molecular and Atomic Glasses"*, ed. J.M. O'Reilly and M. Goldstein, Vol. 371, The New York Academy of Sciences: New York, **1981**.

Kovacs, A.J. *J. Polym. Sci.* **1958**, 30, 131.

Kraus, J.; Muller-Buschbaum, P.; Kuhlmann, T.; Schubert, D.W.; Stamm, M. *Europhys. Lett.* **2000**, 49, 210.

Krausch, G.; Dai, C.A.; Kramer, E.J.; Marko, J.F.; Bates, F.S. *Macromolecules* **1993**, 25, 5566.

Kuhlmann, T.; Kraus, J.; Muller-Buschbaum, P.; Schubert, D.W.; Stamm, M. *J. Non-cryt. Sol.* **1998**, 235-237, 457.

Lakowicz, J.R. *"Principles of Fluorescence Spectroscopy"*, Plenum: New York, **1999**.

Lamarre, L.; Sung, C.S.P. *Macromolecules* **1983**, 16, 1729.

Law, K.Y.; Loutfy, R.O. *Polymer* **1983**, 24, 439.

Lenhart, J.L.; van Zanten, J.H.; Dunkers, J.P.; Parnas, R.S. *Langmuir* **2000**, 16, 8145.

Lenhart, J.L.; van Zanten, J.H.; Dunkers, J.P.; Parnas, R.S. *Macromolecules* **2001**, 34, 2225.

Lenhart, J.L.; Wu, W.L. *Langmuir* **2003**, 19, 4863.

Lenhart, J.L.; Wu, W.L. *Macromolecules* **2002**, 35, 5145.

Levine, B.F. *Chem. Phys. Lett.* **1976**, 37, 576.

Li, G.; Du, W. M.; Sakai, A.; Cummins, H. Z. *Phys. Rev. A* **1992**, 46, 3343.

Li, L.; Hu, J.; Yang, W.; Alivisatos, A.P. *Nano Lett.* **2001,** 1, 349.

Li, L.; Li, B.; Chen, J.L.; Zhou, D.S.; Xue, G.; Liu, X.N. *Polymer* **2004**, 45, 2813.

Lin, E.K.; Wu, W-L.; Satija, S.K. *Macromolecules* **1997**, 30, 7224.

Lin, L. ; Bidstrup, S.A. *J. Appl. Polym. Sci.* **1993**, 49, 1277.

Lin, S.Y.; Fleming, J.G.; Hetherington, D.L.; Smith, B.K.; Biswas, R.; Ho, K.M.; Sigalas, M.M.; Zubrzycki, W.; Kurtz, S.R.; Bur, J. *Nature* **1998**, 394, 251.

Lin, W.Y.; Blum, F.D. *J. Am. Chem. Soc.* **2001**, 123, 2032.

Liu, Y.; Roy, A.K.; Jones, A.A.; Inglefield, P.T.; Ogden, P. *Macromolecules* **1990**, 23, 968.

Liu, Y.; Russell, T.P.; Samant, M.G.; Stohr, J.; Brown, H.R.; Cossy-Favre, A.; Diaz, J. *Macromolecules* **1997**, 30, 7768.

Ljungberg, N.; Colombini, D.; Wesslen, B. *J. Appl. Polym. Sci.* **2005**, 96, 992.

Long, D.; Lequeux, F. *Eur. Phys. J. E* **2001**, 4, 371.

Loo, L.Y.; Register, R.A.; Ryan, A.J. *Phys. Rev. Lett.* **2000**, 84, 4120.

Loutfy, L.O. *Macromolecules* **1983a**, 16, 678.

Loutfy, R.O. *Macromolecules* **1981**, 14, 271.

Loutfy, R.O. *Pure Appl. Chem.* **1986**, 58, 1239.

Loutfy, R.O.; Arnold, B.A. *J. Phys. Chem.* **1982**, 86, 4205.

Loutfy, R.O.; Teegarden, D.M. *Macromolecules* **1983b**, 16, 452.

Lu H.; Nutt, S. *Macromolecules* **2003**, 36**,** 4010.

Lyuksyutov, S.F.; Vaia, R.A.; Paramonov, P.B.; Juhl, S.; Waterhouse, L.; Ralich, R.M.; Sigalov, G.; Sancaktar, E. *Nat. Mater.* **2003**, 2, 468.

Majeste, J.C.; Montfort, J.P.; Allal, A.; Marin, G. *Rheol. Acta* **1998**, 37, 486.

Major, M.D.; Torkelson, J.M. *Macromolecules* **1986**, 19, 2801.

Mansfield, K.F.; Theodorou, D.N. *Macromolecules* **1989**, 22, 3143.

Marceau, S.; Tortai, J.-H.; Tillier, J.; Vourdas, N.; Gogolides, E.; Raptis, I.; Beltsios, K.; van Werden, K. *Microelectr. Eng.* **2006**, 83, 1073.

Mark, J; Ngai, K.; Graessley, W.; Mandelkern, L.; Samulski, E.; Koenig, J.; Wignall, G. *"Physical Properties of Polymers"*, 3rd ed., Cambridge University Press: Cambridge, **2004**.

Martins, T.D.; Yamaki, S.B.; Prado, E.A.; Atvars, T.D.Z. *J. Photochem. And Photobiol.* **2003**, 156, 91.

Masson, J.L.; Green, P.F. *Phys. Rev. E* **2002**, 65, 031806-1.

Mattsson, J.; Forrest, J.A.; Borjesson, L. *Phys. Rev. E* **2000**, 62, 5187.

Mayes, A.M. *Macromolecules* **1994**, 27, 3114, and references therein.

McCafferty, E.; Wightman, J.P. *Surf. Interf. Anal.* **1998**, 26, 549.

McCaig, M.S.; Paul, D.R. *Polymer* **2000b**, 41, 629.

McCaig, M.S.; Paul, D.R.; Barlow, J.W. *Polymer* **2000a,** 41, 639.

McCoy, J.D.; Curro, J.G. *J. Chem. Phys.* **2002**, 116, 9154.

McCrum, N.G.; Read, B.E.; Williams, G. *"Anelastic and Dielectric Effects in Polymeric Solids"*, Dover Publications, Inc.: New York, **1991**.

McKenna, G.B. *Eur. Phys. J. E* **2003**, 12, 191.

McKenna, G.B. *"Glass Formation and Glassy Behavior"*, Chapter 10, Comprehensive Polymer Science: Vol. 2 Polymer Properties, Pergamon Press: Oxford, **1989**.

McKenna, G.B. *J. Phys. IV* **2000**, 10, 53.

Melnichenko, Y.B.; Schuller, J.; Richert, R.; Ewen, B.; Loong, C.K. *J. Chem. Phys.* **1995**, 103, 2016.

Menon, N.; Nagel, S.R.; Veneros, D.C. *Phys. Rev. Lett.* **1994**, 73, 963.

Menon, N.; O'Brien, K.P.; Dixon, P.K.; Wu, L.; Nagel, S.R.; Williams, B.D.; Carini, J.P. *J. Non-Cryst. Solids* **1992**, 141, 61.

Merabia, S.; Sotta, P.; Long, D. *Eur. Phys. J. E* **2004**, 15, 189.

Mercier, J.P.; Aklonis, J.J.; Litt, M.; Tobololsky, A.V. *J. Appl. Poly. Sci.* **1965**, 9, 447.

Merolle, M.; Garrahan, J.P.; Chandler, D. *Proc. Natl. Acad. Sci. USA* **2005**, 102, 10837.

Meyer, E.F.; Jamieson, A.M.; Simha, R.; Palmen, J.H.M.; Booji, H.C.; Maurer, F.H.J. *Polymer* **1990**, 31, 243.

Mezei, F.; Knaak, W.; Farrago, B. *Phys. Rev. Lett.* **1987**, 58, 571.

Mitteilungen, K. *Acta Polymerica* **1982**, 33, 741.

Miyazaki, T.; Inoue, R.; Nishida, K.; Kanaya, T. *Eur. Phys. J. Special Topics* **2007**, 141, 203.

Miyazaki, T.; Nishida, K.; Kanaya, T. *Phys. Rev. E* **2004**, 69, 061803-1.

Monnerie, L. *J. Non-Cryst. Solids* **1991**, 170, 315.

Morris, J.F.; Gelerinter, E. *Polymer* **1989**, 30, 165.

Mukherjee, M.; Bhattacharya, M.; Sanyal, M.K.; Geue, T.; Grenzer, J.; Pietsch, U. *Phys. Rev. E* **2002**, 66, 061801.

Muller, M. *J. Chem. Phys.* **2002**, 116, 9930.

Mundra, M.K.; Donthu, S.K.; Dravid, V.P.; Torkelson, J.M. *Nano Letters* **2007a**, 7, 713.

Mundra, M.K.; Ellison, C.J.; Behling, R.E.; Torkelson, J.M. *Polymer* **2006**, 47, 7747.

Mundra, M.K.; Ellison, C.J.; Rittigstein, P.; Torkelson, J.M. *Eur. Phys. J. Special Topics* **2007b**, 141, 143.

Nakatsuka, H.; Ye, J.Y.; Hattori, T.; Maruyama, Y.; Ishikawa, M. *Prog. Theor. Phys. Supp.* **1997**, 126, 433.

Ngai, K.L. *J. Chem. Phys.* **1998a**, 109, 6982.

Ngai, K.L. *J. Polym. Sci. Part B Polym. Phys.* **2006**, 44**,** 2980.

Ngai, K.L. *J. Phys. IV* **2000**, 10, Pr7.

Ngai, K.L.; Rizos, A.K.; Plazek, D.J. *J. Non-Cryst. Solids* **1998b**, 235-237, 435.

Ngai, K.L.; Roland, C.M. *Macromolecules* **1993**, 26, 6824.

Noy, A.; Miller, A.E.; Klare, J.E.; Weeks, B.L.; Woods, B.W.; DeYoreo, J.J. *Nano Lett.* **2002**, 2, 109.

O'Connell, P.A.; McKenna, G.B. *Eur. Phys. J. E* **2006**, 20, 143.

O'Connell, P.A.; McKenna, G.B. *Science* **2005**, 307, 1760.

O'Reilly, J.M. *J. Appl. Phys.* **1977a**, 48, 4043.

O'Reilly, J.M. *J. Appl. Polym. Sci. Part C Polym. Symp.* **1977b**, 63, 165.

O'Reilly, J.M. *J. Polym. Sci.* **1962**, 57, 429.

Oh, W.T.; Ree, M.H. *Langmuir* **2004**, 20, 6932.

Orts, W.J.; van Zanten, J.H.; Wu, W.L.; Satija, S.K. *Phys. Rev. Lett.* **1993**, 71, 867.

Park, C.H.; Kim, J.H.; Ree, M.; Sohn, B.H.; Jung, J.C.; Zin, W.C. *Polymer* **2004**, 45, 4507.

Peter, S.; Meyer, H.; Baschnagel, J. *J. Polym. Sci. Part B Polym. Phys.* **2006**, 44**,** 2951.

Petrie, S.E.B.; Moore, R.S.; Flick, J.R. *J. Appl. Phys.* **1972**, 42, 4318.

Pfromm, P.H.; Koros, W.J. *Polymer* **1995**, 36, 2379.

Pham, J.Q.; Green, P.F. *J. Chem. Phys.* **2002**, 116, 5801.

Pham, J.Q.; Green, P.F. *Macromolecules* **2003**, 36, 1665.

Piner, R.D.; Zhu, J.; Xu, F.; Hong, S.H.; Mirkin, C.A. *Science* **1999**, 283, 661.

Pissis, P.; Daoukaki-Diamanti, D.; Apekis, L.; Christodoulides, C. *J. Phys.: Condens. Matter* **1994**, 6, L325.

Plazek, D. J.; Bero, C. A.; Chay, I. C. *J. Non-Cryst. Solids* **1994**, 172–174, 181.

Plazek, D.J.; Ngai, K.L. *Macromolecules* **1991**, 24, 1222.

Pochan, D.J.; Lin, E.K.; Satija, S.K.; Wu, W.L. *Macromolecules* **2001**, 34, 3041.

Pottinger, M.T.; Coburn, J.C.; Edman, J.R. *J. Polym. Sci. Part B Polym. Phys.* **1994**, 32, 825.

Prasad, P.N.; Williams, D.J. *"Introduction to Nonlinear Optics in Molecular and Polymeric Materials"*, John Wiley: New York, **1990**.

Pratt, F.L.; Lancaster, T.; Brooks, M.L.; Blundell, S.J.; Prokscha, T.; Morenzoni, E. *et al. Phys. Rev. B* **2005**, 72, 121401.

Prest, W.M.; Luca, D.J. *J. Appl. Phys.* **1980a**, 50, 6067.

Prest, W.M.; Luca, D.J. *J. Appl. Phys.* **1980b**, 51, 5170.

Priestley, R.D.; Mundra, M.K.; Rittigstein, P.; Broadbelt, L.J.; Torkelson, J.M. **2007a**, submitted.

Priestley, R.D.; Broadbelt, L.J.; Torkelson, J.M. *Macromoecules* **2005a**, 38, 654.

Priestley, R.D.; Broadbelt, L.J.; Torkelson, J.M.; Fukao, K. *Phys. Rev. E* **2007b**, in press.

Priestley, R.D.; Ellison, C.J.; Broadbelt, L.J.; Torkelson, J.M. *Science* **2005b**, 309, 456.

Priestley, R.D.; Rittigstein P.; Broadbelt, L.J.; Fukao, K.; Torkelson, J.M. *J. Phys.: Condens. Matter* **2007c**, in press.

Prucker, O.; Christian, S.; Bock, H.; Ruhe, J.; Frank, C.W.; Knoll, W. *Macromol. Chem. Phys.* **1998**, 199, 1435.

Przhonska, O.; Slominsky, Y.; Stahl, U.; Daehne, S. *J. Lumin.* **1996**, 69, 105.

Pu, Y.; Rafailovich, M.H.; Sokolov, J.; Gersappe, D.; Peterson, T.; Wu, W.L.; Schwarz, S.A. *Phys. Rev. Lett*. **2001a**, 87, 206101-1.

Pu, Y.; White, H.; Rafailovich, M.H.; Sokolov, J.; Patel, A.; White, C.; Wu, W.L.; Zaitsev, V.; Schwarz, S.A. *Macromolecules* **2001b**, 34, 8518.

Qin, X.; Ediger, M.D. *J. Phy. Chem. B* **2003**, 107, 459.

Quake, S.R.; Scherer, A. *Science* **2000**, 290, 1536.

Quirin, J.C.; Bartko, A.P.; Dickson, R.M.; Torkelson, J.M. *Polym. Preprints* **2001**, 42, 174.

Ray, P.; Binder, K. *Europhys. Lett.* **1994**, 27, 53.

Ree, M.; Park, Y.H.; Kim, K.; Kim, S.I.; Cho, C.K.; Park, C.E. *Polymer* **1997**, 38, 6333.

Reid, R.F.; Soutar, I. *J. Polym. Sci. Part B Polym. Phys.* **1978**, 16, 231.

Reinsberg, S.A.; Heuer, A.; Doliwa, B.; Zimmermann, H.; Spiess, H.W. *J. Non-cryst. Sol.* **2002**, 307, 208.

Reinsberg, S.A.; Qui, X.H.; Wilhelm, M.; Spiess, H.W.; Ediger, M.D. *J. Chem. Phys.* **2001**, 114, 7299.

Reiter, G. *Europhys. Lett.* **1993**, 23, 579.

Reiter, G. *Phys. Rev. Lett.* **1992**, 68, 75.

Reiter, G.; Castelein, G.; Sommer, J.U.; Rottele, A.; Thurn-Albrecht, T. *Phys. Rev. Lett.* **2001a**, 87, 226101.

Reiter, G.; de Gennes, P.G. *Eur. Phys. J. E* **2001b**, 6, 25.

Reiter, G.; Hamieh, M.; Damman, P.; Scalvons, S.; Gabriele; Vilmin, R.; Raphael, E. *Nat Mater* **2005**, 4, 754.

Remillard, J.T.; Jones, J.R.; Poindexter, B.D.; Helms, J.H.; Weber, W.H. *Appl. Spectroscopy* **1998**, 52, 1369.

Resnick, D.J.; Dauksher, W.J.; Mancini, D.; Nordquist, K.J.; Bailey, T.C.; Johnson, S.; Stacey, N.; Ekerdt, J.G.; Willson, C.G.; Sreenivasan, S.V.; Schumaker, N. *J. Vac. Sci. Technol. B* **2003**, 21, 2624.

Richardson, H.; Lopez-Garcia, I.; Sferrazza, M.; Keddie, J.L. *Phys. Rev. E* **2004**, 70, 051805.

Richardson, M.J.; Savill, N.G. *Polymer* **1977**, 18, 3.

Richert, R. *J. Chem. Phys.* **2000**, 113, 8404.

Richert, R. *J. Phys.: Condens. Matter* **2002**, 14, R703.

Richert, R. *Phys. Rev. B* **1996**, 54, 15762.

Riggleman, R.A.; Yoshimoto, K.; Douglas, J.F.; de Pablo, J.J. *Phys. Rev. Letts.* **2006**, 97, 045502.

Rittigstein P.; Priestley, R.D.; Broadbelt, L.J.; Torkelson, J.M. *Nat. Mater.* **2007**, 6, 278.

Rittigstein, P.; Torkelson, J.M. *J. Polym. Sci. Part B Polym. Phys.* **2006**, 44, 2935.

Rizos, A.K.; Ngai, K.L. *Macromolecules* **1998**, 31, 6217.

Rizos, A.K.; Ngai, K.L. *Phys. Rev. E* **1999**, 59, 612.

Robertson, C.G.; Santangelo, P.G.; Roland, C.M. *J. Non-Cryst. Solids* **2000**, 275, 153.

Robertson, C.G.; Wang, X.R. *Mcromolecules* **2004**, 37, 4266.

Roland, C.M.; Ngai, K.L. *J. Non-Cryst. Solids* **1997**, 212, 74.

Roland, C.M.; Casalini, R. *J. Chem. Phys.* **2003a**, 119, 1838.

Roland, C.M.; Casalini, R.; Santangelo, P.; Sekula, M.; Ziolo, J.; Paluch, M. *Macromolecules* **2003b**, 36, 4954.

Roland, C.M.; Ngai, K.L. *J. Non-cryst. Solids* **1994**, 172, 868.

Roland, C.M.; Ngai, K.L. *Macromolecules* **1992**, 25, 5765.

Roland, C.M.; Santangelo, P.G.; Ngai, K.L.; Meier, G. *Macromolecules* **1993**, 26, 6164.

Roth C.B.; McNerny, K.L.; Jager, W.F.; Torkelson, J.M. *Macromolecules* **2007a**, 40, 2568.

Roth C.B.; Torkelson, J.M. *Macromolecules* **2007b**, 40, 3328.

Roth, C.B.; Dutcher, J.R. *Eur. Phys. J. E* **2003**, 12, 103.

Roth, C.B.; Dutcher, J.R. *J. Electroanal. Chem.* **2005**, 584, 13.

Royal, J.S.; Torkelson, J.M. *Macromolecules* **1990**, 23, 3536.

Royal, J.S.; Torkelson, J.M. *Macromolecules* **1992a**, 25, 1705.

Royal, J.S.; Torkelson, J.M. *Macromolecules* **1992**b, 25, 4792.

Royal, J.S.; Torkelson, J.M. *Macromolecules* **1993**, 26, 5331.

Russell, E.; Israeloff, N.E. *Nature* **2000**, 408, 695.

Saiter, A.; Bureau, E.; Zapolsky, H.; Saiter, J. M. *J. Non-Cryst. Solids* **2004**, 345-346, 556.

Saito, S. *Coll. Polym. Sci.* **1963**, 189, 116.

Santangelo, P.G.; Ngai, K.L.; Roland, C.M. *Macromolecules* **1994b**, 27, 3859.

Santangelo, P.G.; Roland, C.M. *Macromolecules* **1998**, 31, 4581.

Santangelo, P.G.; Roland, C.M.; Ngai, K.L.; Rizos, A.K.; Katerinopoulos, H. *J. Non-cryst. Sol.* **1994a**, 172-174, 1084.

Sanz, A.; Mendicuti, F. *Polymer* **2002**, 43, 6123.

Sasaki, T.; Shimizu, A.; Mourey, T.H.; Thurau, C.T., Ediger, M.D. *J. Chem. Phys.* **2003**, 119, 8730.

Sauer, B.B.; Avakian, P. *Polymer* **1992**, 33, 5128.

Schausberger, A.; Ahrer, I. *Macromol. Chem. Phys.* **1995**, 196, 2161.

Schiener, B.; Bhmer, R.; Loidl, A.; Chamberlin, R.V. *Science* **1996**, 274, 752.

Schmidt-Rohr, K.; Spiess, H.W. *Phys. Rev. Lett.* **1991**, 66, 3020.

Schonals, A.; Goering, H.; Schick, C. *J. Non-cryst. Solids* **2002**, 305, 140.

Schott Glass © - http://www.us.schott.com, **2007**.

Schulman, S.G. *"Fluorescence and Phosphorescence Spectroscopy: Physicochemical Principles and Practice"*, Pergamon Press: New York, **1977**.

Schurr, O.; Yamaki, S.B.; Wang, C.; Atvars, T.D.Z.; Weiss, R.G. *Macromolecules* **2003**, 36, 3485.

Schwab, A.D.; Agra, D.M.G.; Kim, J.H.; Kumar, S.; Dhinojwala, A. *Macromolecules* **2000,** 33, 4903.

Schwab, S.D.; Levy, R.L. *Advances in Chemistry Series* **1990**, 227, 397.

Sears, R.; Darby, S. *"Encyclopedia of Polymer Science"*, Plasticizers - Supplementary Vol., 2nd ed., **1989**.

Serghei, A.; Mikhailova, Y.; Huth, H.; Schick, C.; Eichhorn, K.J.; Voit, B.; Kremer, F. *Eur. Phys. J. E* **2005**, 17, 199.

Serrano, B.; Baselga, J.; Pierola, I.F. *Polm. J.* **2002**, 34, 905.

Sharp, J.S.; Forrest, J.A. *Eur. Phys. J. E* **2003c**, 12, S97.

Sharp, J.S.; Forrest, J.A. *Phys. Rev. E* **2003b**, 67, 031805.

Sharp, J.S.; Forrest, J.A. *Phys. Rev. Lett.* **2003a**, 91, 235701-1.

Shearmur, T.E.; Clough, A.S.; Drew, D.W.; van der Grinten, M.G.D.; Jones, R.A.L. *Polymer* **1998**, 39, 2155.

Shen, Y.R. *"The Principles of Nonlinear Optics"*, John Wiley: New York, **1984**.

Shmorhun, M.; Jamieson, A.M.; Simha, R. *Polymer* **1990**, 31, 812.

Sidebottom, D.; Torell, L. *Phys.Rev. Lett.* **1993**, 71, 2260.

Sillescu, H. *J. Non-Cryst. Solids* **1999**, 243, 81.

Singh, L.; Ludovice, P.J.; Henderson, C.L. *Thin Solid Films* **2004**, 449, 231.

Soles, C.L.; Douglas, J.F.; Jones, R.L.; Wu, W.L. *Macromolecules* **2004b**, 37, 2901.

Soles, C.L.; Douglas, J.F.; Wu, W.L.; Peng, H.; Gidley, D.W. *Macromolecules* **2004a**, 37, 2890.

Solunov, C.A. *Eur. Polym. J.* **1999**, 35, 1543.

Spangler, L.L. *"PhD Thesis"*, Northwestern University, **1992**.

Spangler, L.L.; Royal, J.S.; Torkelson, J.M. *Polym. Eng. Sci.* **1990**, 30, 644.

Sperling, L.H. *"Introduction to Physical Polymer Science"*, Wiley-Interscience: New York, **1992**.

Spiess, H.W. *Coll. Polym. Sci.* **1983**, 261, 193.

Srinivas, S.; Babu, J.R.; Riffle, J.S.; Wilkes, G.L.; *J. Macromol. Sci.Phys.* **1997**, B36, 455.

Stafford, C.M.; Harrison, C.; Beers, K.L.; Karim, A.; Amis, E.J.; Vanlandingham, M.R.; Kim, H.C.; Volksen, W.; Miller, R.D.; Simonyi, E.E. *Nat. Mater.* **2004**, 3, 545.

Stafford, C.M.; Vogt, B.D.; Harrison, C.; Julthongpiput, D.; Huang, R. *Macromolecules* **2006**, 39, 5095.

Stahelin, M.; Walsh, C.A.; Burland, D.M.; Miller, R.D.; Twieg, R.J.; Volksen, W. *J. Appl.Phys.***1993**, 73, 8471.

Stebbins, J.F.; Farnan, I. *Science* **1992**, 255, 586.

Stevenson, J.D.;Schmalian, J.;Wolynes, P.G. *Nature Phys*. **2006**, 2, 268.

Stickel, F. *"PhD Thesis"*, Mainz University, Germany, **1995**.

Stickel, F.; Fischer, E.W.; Richert, R. *J. Chem. Phys.* **1996**, 104, 2043.

Struik, L.C.E. *"Physical Aging in Amorphous Polymers and Other Materials"*, Elsevier: Amsterdam, **1978**.

Sung, C.S.; Lamarre, L.; Chung, K.H. *Macromolecules* **1981**, 14, 1839.

Sung, L; Karim, A.; Douglas, J.F.; Han, C.C. *Phys. Rev. Lett.* **1996**, 76, 4368.

Sutton, S.J.; Izumi, K.; Miyaji, H.; Miyamoto, Y.; Miyashita, S. *J. Mat. Sci.* **1997**, 32, 5621.

Svanberg, C. *Macromolecules* **2007**, 40**,** 312.

Tanaka, K.; Arjura, F.; Nagamura, T.; Kajiyama, T. *Polym. J.* **2004**, 36, 498.

Tanaka, K.; Yoon, J.S.; Takahara, A.; Kajiyama, T. *Macromolecules* **1995**, 28, 934.

Tant, M.R.; Wilkes, G.L. *Polym. Eng. Sci.* **1981**, 21, 874.

Tate, R.S.; Fryer, D.S.; Pasqualini, S.; Montague, M.F.; de Pablo, J.J.; Nealey, P.F. *J. Chem. Phys.* **2001**, 115, 9982.

Therriault, D.; White, S.R.; Lewis, J.A. *Nat. Mater.* **2003**, 2, 265.

Thomas, T.L.; Sivakumar, N.; Gurunathan, L.; Mishra, A.K. *Poly. Test.* **2003**, 22, 143.

Thurau, C.T.; Ediger, M.D. *J. Chem. Phys.* **2002**, 116, 9089.

Tomczak, N.; Vallee, R.A.L.; van Dijk, E.M.H.P.; Garcia-Parajo, M.; Kuipers, L.; van Hulst, N.F.; Vancso, G.J. *Eur. Polym. J.* **2004**, 40, 1001.

Torell, L.M.; Aronsson, R. *J. Chem. Phys.* **1983**, 78, 1121.

Torkelson, J.M.; Lipsky, S.; Tirrell, M. *Macromolecules* **1981**, 14, 1601.

Torkelson, J.M.; Lipsky, S.; Tirrell, M.; Tirrell, D.A. *Macromolecules* **1983**, 16, 326.

Torkelson, J.M.; Tirrell, M.; Frank, C.W. *Macromolecules* **1984,** 17, 1505.

Torres, J.A.; Nealey, P.F.; de Pablo, J.J. *Phys. Rev. Lett.* **2000**, 85, 3221.

Tracht, U.; Wilhelm, M.; Heuer, A.; Feng, H.; Schmidt-Rohr, K.; Spiess, H.W. *Phys. Rev. Lett.* **1998**, 81, 2727.

Tran, T.A.; Said, S.; Grohens, Y. *Polym. Mater. Sci. Eng.* **2004**, 91, 677.

Tsai, F.J.; Torkelson, J.M. *Macromolecules* **1988b**, 21, 1026.

Tsai, F.J.; Torkelson, J.M. *Polymer* **1988a**, 29, 1004.

Tseng, K.C.; Turro, N.J.; Durning, C.J. *Phys. Rev. E* **2000a**, 61, 1800.

Tseng, K.C.; Turro, N.J.; Durning, C.J. *Polymer* **2000b**, 41, 4751.

Tsui, O.K.C.; Russell, T.P.; Hawker, C.J. *Macromolecules* **2001a**, 34, 5535.

Tsui, O.K.C.; Zhang, H.F. *Macromolecules* **2001b**, 34, 9139.

Turrion, S.G., Olmos, D., Ekizoglou, N., Gonzalez-Benito, J. *Polymer* **2005**, 46**,** 4023.

Tyndall, G.W.; Leezenberg, P.B.; Waltman, R.J.; Castenada, J. *Tribol. Lett.* **1998**, 4, 103.

Vala, M.T.; Haebig, J.; Rice, S.A. *J. Chem. Phys.* **1965**, 43, 886.

Valeur, B. *"Molecular Fluorescence"*, Wiley-VCH: Weinheim, **2002**.

Vallee, R.A.L.; Tomczak, N.; Kuipers, L.; Vancso, G.J.; van Hulst, N.F. *Chem. Phys. Lett.* **2004**, 384, 5.

Valley, J.F.; Wu, J.F.; Valencia, C.L. *Appl. Phys. Lett.* **1990**, 57, 1084.

van den Berg, O.; Cangialosi, D.; Jager, W.F.; van Veen, A.; Picken, S.J. *Polym. Mater. Sci. Engg.* **2004b**, 90, 611.

van den Berg, O.; Jager, W.; Cangialosi, D.; van Turnhout, J.; Verhiejen, P.J.T.; Wubbenhorst, M.; Picken, S.J. *Macromolecules* **2006a**, 39, 224.

van den Berg, O.; Jager, W.F.; Picken, S.J. *J. Org. Chem.* **2006b**, 71, 2666.

van den Berg, O.; Sengers, W.G.F.; Jager, W.F.; Picken, S.J.; Wubbenhorst, M. *Macromolecules* **2004a**, 37, 2560.

van Turnhout, J. *"Thermally Stimulated Discharge of Polymer Electrets"*, Elsevier: Amsterdam, **1975**.

Van Workum, K.; de Pablo, J.J. *Nano Lett.* **2003**, 3, 1405.

van Zanten, J.H.; Wallace, W.E.; Wu, W.L. *Phys. Rev. E* **1996**, 53, R2053.

Varnik, F.; Baschnagel, J.; Binder, K. *J. Non-Cryst. Solids* **2002**, 307, 524.

Vigil, M.R.; Bravo, J.; Atvars, T.D.Z.; Baselga, J. *Macromolecules* **1997**, 30, 4871.

Viot, P.; Targus, G.; Kivelson, D. *J. Chem. Phys.* **2000**, 112, 10368.

Vogel, H. *Phys. Z.* **1921**, 22, 645.

Vrentas, J.S.; Duda, J.L. *J. Polym. Sci., Part B: Polym. Phys.* **1977**, 15, 403.

Vyazovkin, S.; Dranca, I. *J. Phys. Chem. B* **2004**, 108, 11981.

Wallace, W.E.; Tan, N.C.B.; Wu, W.L.; Satija, S. *J. Chem. Phys.* **1998**, 108, 3798.

Wallraff, G.M.; Hinsberg, W.D. *Chem. Rev.* **1999**, 99, 1801.

Wang, C.-Y.; Ediger, M.D. *J. Chem. Phys.* **2000**, 112, 6933.

Wang, C.-Y.; Ediger, M.D. *J. Phys. Chem. B* **1999**, 103, 4177.

Wang, C.-Y.; Ediger, M.D. *Macromolecules* **1997**, 30, 4770.

Wang, L.M.; He, F.; Richert R. *Phys. Rev. Lett.* **2004**, 92, 095701-1.

Weeks, E.R.; Crocker, J.C.; Levitt, A.C.; Schofield, A.; Weitz, A.D. *Science* **2000**, 287, 627.

Weldon, M.K.; Marisco, V.E.; Chabal, Y.J.; Hamann, D.R.; Christman, S.B.; Chaban, E.E. *Surf. Sci.* **1996**, 368, 163.

Wendt, H.; Richert, R. *J. Phys. Chem. A* **1998**, 102, 5775.

White, C.C.; Migler, K.B.; Wu, W.L. *Polym. Eng. Sci.* **2001**, 41, 1497.

Whitlow, S.J.; Wool, R.P. *Macromolecules* **1991**, 24, 5926.

Williams, G.; Watts, D.C. *Trans. Faraday Soc.* **1970**, 66, 80.

Williams, G.; Watts, D.C.; Dev S.B.; North, A.M. *Trans. Faraday Soc.* **1971**, 67, 1323.

Williams, M.L.; Landel, R.F.; Ferry, J.D. *J. Am. Chem. Soc.* **1955**, 77, 3701.

Wubbenhorst, M.; Murray, C.A.; Dutcher, J.R. *Eur. Phys. J. E* **2003**, 12, S109.

Xia, Y.N.; Rogers, J.A.; Paul, K.E.; Whitesides, G.M. *Chem. Rev.* **1999**, 99, 1823.

Xie, R.; Yang, B.X.; Jiang, B.Z. *Polymer* **1993**, 34, 5016.

Xu, J.; Xia, H.P.; Zhang, Y.P.; Zhang, J.L.; Wang, J.H. *J. Inorg. Mater.* **2005**, 20, 193.

Yamaki, S.B.; Prado, E.A.; Atvars, T.D.Z. *Eur. Polym. J.* **2002**, 38, 1811.

Yamamoto, S.; Tsujii, Y.; Fukuda, T. *Macromolecules* **2002**, 35, 6077.

Ye, J.Y.; Hattori, T.; Inouye, H.; Ueta, H.; Nakatsuka, H. *Phys. Rev. B* **1996**, 53, 8349.

Ye, J.Y.; Hattori, T.; Nakatsuka, H.; Maruyama, Y.; Ishikawa, M. *Phys. Rev. B* **1997**, 56, 5286.

Ye, J.Y.; Ishikawa, M.; Yogi, O.; Okada, T.; Maruyama, Y. *Chem. Phys. Lett.* **1998**, 288, 885.

Yilmaz, Y.; Kaya, D.; Pekcan, O. *Eur. Phys. J. E* **2004**, 15, 19.

Ylitalo, D.A.; Frank, C.W. *Polymer* **1996**, 37, 4969.

Yoshimoto, K.; Jain, T.S.; Nealey, P.F.; de Pablo, J.J. *J. Chem. Phys.* **2005**, 122, 144712.

Zhang, J.; Chen, H.; Li, Y.; Suzuki, R.; Ohdaira, T.; Jean, Y.C. *Radiation Physics and Chemistry* **2007**, 76, 172.

Zhang, J.; Wang, C.H. *Macromolecules* **1988**, 21, 1811.

Zhang, S.H.; Jin, X.; Painter, P.C.; Runt, J. *Macromolecules* **2003**, 36, 7179.

Zheng, X.; Rafailovich, M.H.; Sokolov, J.; Strzhemechny, Y.; Schwarz, S.A.; Sauer, B.B.; Rubenstein, M. *Phys. Rev. Lett.* **1997**, 79, 241.

Zhou, C.; Chung, T.-S.; Wang, R.; Goh, S.H. *J. Appl. Polym. Sci.* **2004**, 92, 1758.

Zhu, J.; Somorjai, G.A. *Nano Lett.* **2001,** 1, 8.

VITA

MANISH KUMAR MUNDRA

Birthdate

March 1, 1980, Bhilwara, R.J., India

Education

B.S. in Materials Science
Indian Institute of Technology, Bombay – India, May 2002
M.S. in Metallurgical Process Engineering
Indian Institute of Technology, Bombay – India, June 2003

Publications

Impact of Polystyrene Molecular Weight and Modification to the Repeat Unit Structure on the Glass Transition Temperature - Nanoconfinement Effect and the Cooperativity Length Scale - C.J. Ellison, M.K. Mundra, & J.M. Torkelson, Macromolecules 38, 1767-1778 (2005).

Confinement, Composition and Spin-Coating Effects on the Glass Transition and Stress Relaxation of Thin Films of Polystyrene and Styrene - Containing Random Copolymers: Sensing by Intrinsic Fluorescence - M.K. Mundra, C.J. Ellison, R.E. Behling, & J.M. Torkelson, Polymer, 47, 7747-7759 (2006).

Fluorescence Studies of Confinement in Polymer Films and Nanocomposites: Glass Transition Temperature, Plasticizer Effects, and Sensitivity to Stress Relaxation and Local Polarity - M.K. Mundra, C.J. Ellison, P. Rittigstein, & J.M. Torkelson, Euro. Phys. J. - Special Topics, 141, 143-151 (2007).

Effect of Spatial Confinement on the Glass Transition Temperature of Patterned Polymer Nanostructures - M.K. Mundra, S.K. Donthu, V.P. Dravid, & J.M. Torkelson, Nano Letters, 7, 713-718 (2007).

Direct Measurements of Interfacial and Nanoconfinement Effects on the Glass Transition Temperature of Polymeric Glass Formers - R.D. Priestley, M.K. Mundra, P. Rittigstein, L.J. Broadbelt, and J.M. Torkelson, submitted to Proceeding at National Academy of Science Foundation (PNAS), 2007.

Confinement and Interfacial Effects on the Glass Transition of a Series of Poly(n-methacrylate) Films - R.D.Priestley, M.K. Mundra, N. Barnett, L.J. Broadbelt, and J.M. Torkelson, submitted to Australian Journal of Chemistry, 2007.